Adsorption of Antibiotics and Nickel from Aqueous Solutions on Heterogeneous Adsorbents Based on Barley Straw

A Thesis Submitted to the College of Graduate and Postdoctoral Studies

in Partial Fulfillment of the Requirements

for the Degree of Doctor of Philosophy

Bei Yan

School of Environment and Sustainability

University of Saskatchewan

Saskatoon, Canada

PERMISSION TO USE

In presenting this thesis in partial fulfillment of the requirements for a Postgraduate degree from the University of Saskatchewan, I agree that the Libraries of this University may make it freely available for inspection. I further agree that permission for copying of this thesis in any manner, in whole or in part, for scholarly purposes may be granted by Dr. Catherine Hui Niu, who supervised my thesis work or, in her absence, by the Executive Director of the School of Environment and Sustainability in which my thesis work was done. It is understood that any copying or publication or use of this thesis or parts thereof for financial gain shall not be allowed without my written permission. It is also understood that due recognition shall be given to me and to the University of Saskatchewan in any scholarly use which may be made of any material in my thesis.

Requests for permission to copy or to make other use of material in this thesis in whole or part should be addressed to:

Executive Director of the School of Environment and Sustainability

University of Saskatchewan

Saskatoon, Saskatchewan, S7N 5C8, Canada

OR

Dean of the College of Graduate and Postdoctoral Studies

University of Saskatchewan

107 Administration Place

Saskatoon, Saskatchewan S7N 5A2 Canada

ABSTRACT

Water security is essential in order to achieve sustainability. Concerns of antibiotic-contaminated water bodies have prompted research of effective water treatment technologies. Researchers are particularly concerned about two commonly prescribed fluoroquinolones antibiotics with broad-spectrum activity and good oral absorption: levofloxacin (LEV) and norfloxacin (NOR). However, these drugs cannot be completely metabolized in humans or animals, nor can they be effectively removed using current wastewater treatment technologies such as activated sludge. As a result, they are discharged into the environment and become emerging environmental contaminants, which coexist with metals such as nickel ions in diverse aquatic systems. Consequently, they may threaten human health.

Adsorption, the partitioning of a target compound between the fluid and adsorbent phase, is an alternative technology for pollutant removal. In this work, raw barley straw (RBS)--an abundantly generated agricultural byproduct mainly composed of cellulose, hemicellulose, and lignin--was pretreated by H_3PO_4 impregnation and microwave heating. This pretreated barley straw (PBS) was used as an adsorbent for the removal of LEV, NOR, and nickel ions, which are representatives of antibiotics and heavy metals, from artificial wastewater. The research included the following phases:

1. Phase I: Pretreatment and characterization of adsorbents based on barley straw. PBS that had a high surface area (1314 ± 10 m^2/g) was obtained at conditions of 5% (*w/v*) H_3PO_4 impregnation concentration and 9 min 700 W microwave heating. The total organic carbon (TOC) released into suspensions from the adsorbents significantly reduced from 34.4 ± 0.9 mg/g (RBS) to 0.9 ± 0.2 mg/g (PBS) indicating the enhanced stability of PBS. Barley straw adsorbents were characterized by particle size distribution, elemental compositions, scanning electron microscopy, and thermogravimetric analysis.

2. Phase II: Adsorption of LEV on PBS. PBS demonstrated high LEV adsorption capacities in a wide range of solution pH (2.47-9.60). The experimental maximum LEV adsorption capacity of PBS (408 ± 5 mg LEV/g at pH 6.88 and 298.15 K) was much higher than that of RBS and the reported adsorbents. The adsorption kinetics and equilibrium at different temperatures were investigated, and the kinetic and isotherm data were well-fitted by the pseudo-second-order kinetic model and *Langmuir-Freundlich* model, revealing that the adsorption of LEV on PBS was an endothermic process. The activation energy was determined to be 45.9 kJ/mol. The desorption of LEV loaded on PBS was examined, and the site energy and its distribution of PBS for LEV adsorption were estimated. The weighted mean and standard deviation of the distribution were employed to depict the interaction strength between the adsorbent and adsorbate, and adsorption heterogeneity. The π-π electron-donor-acceptor (EDA) interaction between the π^* aromatic C=C of PBS and the π^* carbon atom in the benzene ring attached to fluorine of LEV was proposed as one of the major adsorption mechanisms. Such interaction was investigated by C *K*-edge X-ray absorption near-edge structure (XANES) spectroscopy.
3. Phase III: Adsorption of NOR on PBS. High NOR adsorption capacities of PBS were also obtained in a wide pH range (2.67-10.50). The experimental maximum NOR adsorption capacity of PBS (396 ± 14 mg NOR/g at pH 6.96 and 298.15 K) was much higher than that of RBS and the reported adsorbents. The adsorption kinetics and equilibrium with respect to temperature were evaluated using the pseudo-second-order kinetic model and *Langmuir-Freundlich* model, respectively. The adsorption of NOR on PBS was an endothermic processes with an activation energy of 22.2 kJ/mol. The desorption of NOR loaded on PBS was also examined. The adsorption site energy and its distribution were also determined to exhibit the adsorption mechanism. At the tested

temperatures of 298.15-318.15 K, the higher the temperature, the higher the weighted mean (therefore the stronger the adsorption affinity), and the slightly weaker the heterogeneity. The percentage of adsorption sites, whose site energy is greater than or equal to a specific E^* value, was estimated. The proposed dominant forces, EDA interactions (n-π and π-π), were investigated by the C and O *K*-edge XANES spectroscopy.

4. Phase IV: Adsorption of nickel on PBS and impact of nickel on LEV adsorption. The adsorption isotherms of nickel on PBS and RBS were well-fitted using the *Langmuir-Freundlich* model. Solution pH played an important role during the nickel adsorption process. Results of XANES and extended X-ray absorption fine structure spectroscopy indicated that the adsorbed Ni remained the same oxidation state (II) as $NiSO_4$ and was associated with 6 oxygen atoms from water or the functional groups of PBS (e.g., carboxyl group) at an atomic distance of 2.043 ± 0.013 Å. The site energy and its distributions of PBS and RBS for nickel adsorption were determined and demonstrated that the adsorption affinity between PBS and nickel was stronger than that of RBS. Ni(II) slightly suppressed the LEV adsorption on PBS at the tested pH values (4.0, 7.0, and 9.0) since the cationic Ni(II) competed with LEV for the negatively charged adsorption sites of PBS.
5. Phase V: The extended application of PBS in selective water removal from water-ethanol mixture was investigated to produce fuel grade ethanol. PBS demonstrated a higher water adsorption capacity (0.63 ± 0.02 mol/g) and a close water to ethanol adsorption ratio (4.85) compared with RBS (0.50 ± 0.01 mol/g and 5.00). Utilization of PBS in ethanol concentration can be optimized by a dynamic system control in order to achieve a higher concentration of ethanol.

DEDICATION

To my parents for their unconditional love and sacrifices for me to achieve my goals.

To my dear wife, Mrs. Xiaowei Ma, for her constant support and encouragement along the way.

ACKNOWLEDGEMENTS

I would like to express my heartfelt gratitude to my supervisor, Dr. Catherine Hui Niu, for the motivations, kindness, patience, and all the valuable advices that she provided through the time of research and writing the thesis.

I would also thank Drs. Renfei Feng and Jian Wang for their support in the X-ray measurements and analysis. A special gratitude is given to the committee members, Drs. Jafar Soltan, Paul Jones, and Saman Razavi, for their support and advices in this work. I also greatly appreciate the great help and friendship from all my colleagues. I sincerely thank Mr. Richard Blondin of the Department of Chemical and Biological Engineering for his technical support.

Financial support for this work was provided by the China Scholarship Council, the University of Saskatchewan, the Natural Science and Engineering Research Council of Canada, the Canada Foundation for Innovation, the Saskatchewan Ministry of Agriculture and the Canada-Saskatchewan Growing Forward 2-bilateral agreement. The synchrotron X-ray measurements were performed at the Canadian Light Source, Saskatoon, Saskatchewan. All the supports are highly appreciated.

Finally, but not least, my thanks go to all the members in the School of Environment and Sustainability and the Department of Chemical and Biological Engineering for making the work environment pleasant, friendly, and productive.

TABLE OF CONTENTS

LIST OF TABLES

LIST OF FIGURES

CHAPTER 1 INTRODUCTION AND LITERATURE REVIEW

1.1 Introduction

1.1.1 Research Motivation

Pharmaceuticals in water bodies and water streams have been reported globally (Luo et al. 2014, Petrie et al. 2015). In a wide variety of pharmaceutical compounds, antibiotics have raised increasing worries about the potential risks to human health and ecosystems. Antibiotics are a cause for concern for the following reasons: 1) their extensive use, e.g., 17061 tons of antibiotics used in both human and veterinary medicine in the U.S. in 2011 (Food and Drug Administration 2012, 2013); 2) their diverse sources, e.g., waste streams originating from residential areas, sewage treatment plants, hospitals, and animal farms; 3) antibiotic resistance, e.g., exposure to a relatively low fluoroquinolone concentration (4 mg/L) in facilitating the evolution of fluoroquinolone-resistant *Campylobacter jejuni* (Gaunt and Piddock 1996); and 4) ineffective water treatment technologies, e.g. activated sludge (Zorita et al. 2009), biological degradation (Martínez-Alcalá et al. 2017), and photolytic and photocatalytic decomposition (Sturini et al. 2012).

Among antibiotics, fluoroquinolones (FQs) are a class of broad-spectrum antibiotics commonly used in both human and veterinary medicine. Despite their effectiveness, these drugs cannot be completely metabolized in humans and animals, nor can they be effectively removed using current wastewater treatment technologies such as activated sludge. As a result, they are discharged into the environment and become emerging environmental contaminants. FQs have been detected in diverse aquatic systems. For example, the concentration of levofloxacin (LEV, a widely used third-generation FQ) in one of the downstream rivers close to a drug formulation facility in Pakistan was found to be up to 8000 ng/L (Khan et al. 2013). Norfloxacin (NOR, a popularly used second-generation FQ) was detected in Bohai Bay, and

the concentration was reported to be 6.8 μg/L (Bu et al. 2013). Furthermore, FQs can accumulate to a very high level in soils through the land application of fertilizers, sewage sludge, and wastewater irrigation (Wang and Wang 2015).

In addition to pharmaceuticals, nickel has also been found in water bodies and streams (Malamis and Katsou 2013). Nickel is used in many industries, such as mineral processing, electroplating, production of paints and batteries, manufacturing of sulfate, and porcelain enameling. When nickel makes its way into wastewater, it is associated with several diseases (e.g., dermatitis, nausea, chronic bronchitis, gastrointestinal distress, and lung cancer) and thus threatens human health (Flores-Garnica et al. 2013, Sharma and Singh 2013). Furthermore, the discharged nickel ions may pose another health threat as they coexist with antibiotics (e.g., LEV and NOR) in diverse aquatic systems.

As a branch of sustainability, water security is crucial. Water pollution and water scarcity are thorny issues that people face. It is obvious that the reuse of treated antibiotic/heavy metal containing wastewater not only benefits the environment and human health, but also greatly improves social and economic justice, and decreases the cost of water due to the increase in water supply, which is good practice of sustainability. Importantly, the research of sustainability in wastewater treatment has gained momentum in the past decades, which involves the creation of new concepts, methodologies, and approaches. An effective method for removing pollutants from aquatic systems has been found to be adsorption that is the partitioning of a compound between the fluid and solid phase. In previous research, barley straw--an abundantly generated agricultural byproduct mainly composed of cellulose, hemicellulose and lignin--has been used in the adsorption of nickel from aqueous solution, showing its potential for selective removal of contaminants (Ou et al. 2015, Thevannan et al. 2010). However, the removal capacity needs to be improved, and the secondary pollution caused by the release of organic compounds (measured as total organic carbon, TOC) from

adsorbents into aqueous solution needs to be addressed. It has been reported that H_3PO_4 impregnation with heating increased the percentage of acidic groups on wood's surface and enhanced the porous structures favorable for adsorption (Jagtoyen and Derbyshire 1998). A microwave radiation method is a possible way to solve the problems of thermal gradient and high cost of heating preparation (Hoseinzadeh Hesas et al. 2013).

In this work, it was hypothesized that the aforementioned issues (i.e., low adsorption capacity and TOC release) could be addressed through the modification of barley straw by H_3PO_4 impregnation and microwave heating, and that the pretreated barley straw (PBS) can be used as an adsorbent for the removal of LEV, NOR (representatives of antibiotics), and nickel (representative of heavy metals) from aqueous solution.

1.1.2 Knowledge Gaps

The following knowledge gaps were identified:

- Raw barley straw has the potential to be an adsorbent for removing pollutants. This application is important so that the agricultural byproducts can be reused and agricultural industries can benefit. However, prior to this thesis work, no research results have been reported on the pretreatment of raw barley straw (RBS) and on the characterization of PBS, such as particle size distribution, elemental composition, *Fourier* transform infrared spectroscopy (FTIR), scanning electron microscopy (SEM), thermogravimetric analysis (TGA), and *Brunauer-Emmett-Teller* (BET) surface area.
- Adsorption of antibiotics (e.g., LEV and NOR) using adsorbents based on barley straw is promising and may provide an alternate technology for removal of pharmaceutical pollutants. However, the corresponding adsorption kinetics, equilibrium, and site energy distribution (including the strength of adsorption affinity and the energetical heterogeneity of the adsorbents) have not been systematically investigated.

- Adsorption of nickel by adsorbents based on barley straw would benefit nickel industries. However, as noted above, the adsorption equilibrium and site energy distribution have not yet been investigated.
- Adsorption of LEV by adsorbents made from barley straw or similar lignocellulosic biomass in the presence of Ni(II) ions that may co-exist in water is critical for a better understanding of the environmental fate and transport of emerging pharmaceutical contaminants in aquatic systems. However, this has not been previously researched.
- Reusability of adsorbents based on barley straw is important to reduce the cost of material processing. RBS and PBS loaded with LEV, NOR or Ni need to be recycled. This work has not yet been explored.

1.1.3 Objectives

To address the knowledge gaps, the following objectives were created,

1 Pretreatment and characterizations of adsorbents based on barley straw

1.1 Develop PBS from RBS by H_3PO_4 impregnation and microwave heating;

1.2 Reduce the release of organic compounds (measured as TOC) from RBS;

1.3 Characterize the physical and chemical properties of PBS (e.g., particle size, point of zero net charge, elemental composition, porous structure, and functional groups).

2 Adsorption of LEV on adsorbents based on barley straw

2.1 Investigate the adsorption kinetics of LEV on PBS;

2.2 Determine the adsorption isotherm of LEV on PBS;

2.3 Desorb LEV loaded on PBS;

2.4 Determine the adsorption site energy and its distribution of PBS for LEV adsorption;

2.5 Explore the interactions between PBS and LEV by X-ray absorption spectroscopy.

3 Adsorption of NOR on adsorbents based on barley straw

3.1 Investigate the adsorption kinetics of NOR on PBS;

3.2 Determine the adsorption isotherm of NOR on PBS;

3.3 Desorb NOR loaded on PBS;

3.4 Determine the adsorption site energy and its distribution of PBS for NOR adsorption;

3.5 Explore the interactions between PBS and NOR by X-ray absorption spectroscopy.

4 Adsorption of nickel on adsorbents based on barley straw and impact of nickel on LEV adsorption

4.1 Determine the adsorption isotherms of nickel on PBS and RBS;

4.2 Desorb nickel loaded on PBS;

4.3 Determine the adsorption site energy and its distributions of PBS and RBS for nickel adsorption;

4.4 Explore the effect of nickel on LEV adsorption by PBS at different solution pH.

1.2 Occurrence of Antibiotics in Aquatic Environments

1.2.1 Fluoroquinolones

Fluoroquinolone antibiotics (FQs) are an important class of antibiotic compounds commonly used in human and veterinary medicine. They inhibit key bacterial enzymes (e.g., DNA gyrase and topoisomerase IV) involved in unwinding the DNA helix for replication and transcription (Owens Jr and Ambrose 2000). However, FQs may be problematic as cannot be completely metabolized in humans or animals, thus are discharged into environment. A series of recent studies focused on their prevalence, fate, and environmental risks (Bouyarmane et al. 2015, Gao et al. 2015, Leal et al. 2013). For example, FQs up to 0.40 mg/kg were reported in agricultural soil worldwide, and FQs degraded slowly in soil (half-lives > 60 d) (Gao et al. 2015). Guangzhou and Macao of China also reported four FQs (norfloxacin, ciprofloxacin, lomefloxacin, and enrofloxacin) in tap water ranging from 1.0 to 679.7 ng/L (Yiruhan et al. 2010).

1.2.1.1 Classification and Properties

Flumequine was the first FQ which was patented in 1973, after that many FQs have been patented and used today, such as norfloxacin (1978), pefloxacin (1979), enoxacin (1980), fleroxacin (1981), ciprofloxacin (1981), ofloxacin (1982), and levofloxacin (1987) (Appelbaum and Hunter 2000). The typical molecular structure of FQs is displayed in Figure 1.1.

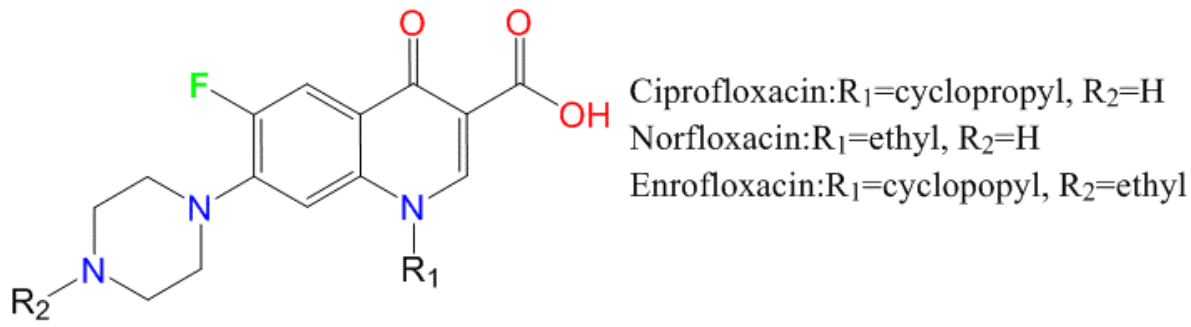

Figure 1.1 Typical molecular structure of FQs.

FQs can be classified into four generations based on antimicrobial activity (Table 1.1). First-generation agents have moderate Gram-negative activity and minimal systemic distribution, which are used less often today. Second-generation FQs have expanded Gram-negative activity and atypical pathogen coverage but limited Gram-positive activity. These agents are the most active against aerobic Gram-negative bacilli. Third-generation FQs, such as levofloxacin (LEV), achieve expanded Gram-negative and atypical intracellular activity, and improved Gram-positive coverage. Finally, fourth-generation agents further improve Gram-positive coverage, maintain Gram-negative coverage, and gain anaerobic coverage (Ambrose et al. 1997).

Table 1.1 Comparison of FQs generation (Owens Jr and Ambrose 2000)**.**

FQs generations	Microbiological activity	Administration and characteristics	Indications
First-generation			
Nalidixic acid	Enterobacteriaceae	Oral administration	Uncomplicated urinary tract infections
Cinoxacin		Low serum and tissue drug concentrations	Not for use in systemic infections
		Narrow gram-negative coverage	
Second-generation			
Class I	Enterobacteriaceae	Oral administration	Uncomplicated urinary tract infections
Lomefloxacin		Low serum and tissue drug concentrations	Not for use in systemic infections
Norfloxacin		Improved gram-negative coverage with the	
Enoxacin		first-generation quinolones	
		Limited gram-positive coverage	
Class II		Oral and intravenous administration	Complicated urinary tract and catheter-related
Ofloxacin	Enterobacteriaceae,	Higher serum, tissue and intracellular drug	infections
Ciprofloxacin	atypical pathogens;	concentration compared with class I agents	Gastroenteritis with severe diarrhea
	Pseudomonas aeruginosa	Coverage of atypical pathogens	Prostatitis
	(ciprofloxacin only)		Nosocomial infections

Table 1.1 Continued.

Third-generation			
Levofloxacin Sparfloxacin Gatifloxacin Moxifloxacin	Enterobacteriaceae, atypical pathogens, streptococci	Oral and intravenous administration Similar to class II second-generation quinolones but with modest streptococcal coverage Increased hepatic metabolism (sparfloxacin and moxifloxacin)	Similar indications as for second-generation FQs Community-acquired pneumonia in hospitalized patients or if atypical pathogens are strongly suspected; in non-hospitalized patients with risk factors for resistant pneumococcal infection
Fourth-generation			
Trovafloxacin	Enterobacteriaceae, atypical pathogens, methicillin-susceptible	Oral and intravenous administration Similar to third-generation quinolones but with improved gram-positive coverage and added anaerobic coverage	Consider for treatment of intra-abdominal infections

The status of selected FQs used for respiratory infections is given in Table 1.2. Among the FQs, levofloxacin (LEV) is a new but already widely used broad-spectrum FQ antibiotic (Yamashita et al. 2006). In 2011, more than 55 tons of LEV were used in human medicine in the U.S., ranking second in FQs consumption (Food and Drug Administration 2012). Norfloxacin (1-Ethyl-6-fluoro-4-oxo-7-(1-piperazinyl)-1,4-dihydro-3-quinolinecarboxylic acid, NOR) is a so-called second-generation FQ, which acts by inhibiting bacterial DNA gyrase enzyme for DNA replication (Jia et al. 2012). In this work, LEV and NOR were chosen as the model antibiotics.

Table 1.2 Current status of FQs used for respiratory infections (Zhanel et al. 2012).

Fluoroquinolone	Current market status (no prescriptions dispensed)
Ciproflocaxin (NO.1)	Marketed (>150 million)
Clinafloxacin	Withdrawn because of adverse effects
Gatifloxacin	Marketed (>4 million)
Gemifloxacin	Awaiting regulatory approval
Grepafloxacin	Withdrawn because of adverse effects
Levofloxacin (NO.2)	Marketed (>150 million)
Moxifloxacin	Marketed (>6 million)
Sitafloxacin	Phase III
Trovafloxacin	Use restricted because of adverse effects

FQs contain amine and carboxyl groups (Figure 1.1), thus, FQs can be neutral (zwitterion), cationic, or anionic; also, their physicochemical and biological properties may change at various pH conditions. For example, LEV had two values of dissociation constant via its tertiary amine group (pK_{a2} = 8.15) and carboxyl group (pK_{a1} = 6.02), and it can be positively charged (pH < 6.02), negatively charged (pH > 8.15), or zwitterionic (pH 6.02-8.15) (Sousa et

al. 2012). NOR also had two values of dissociation constant: pK_{a2} = 8.51 and pK_{a1} = 6.22, and can be positively charged (pH < 6.22), negatively charged (pH > 8.51), or zwitterionic (pH 6.22-8.51) (Pei et al. 2011).

1.2.1.2 Fluoroquinolones as Pollutants

FQs cannot be completely metabolized in humans or animals, nor can they be effectively removed using current wastewater treatment technologies such as activated sludge. As a result, FQs are discharged into the environment and become emerging environmental contaminants. These drugs may present a risk to human health and ecosystem, e.g., antibiotic resistance: exposure to a relatively low FQ concentration (4 mg/L) in facilitating the evolution of FQ-resistant *Campylobacter jejuni* (Gaunt and Piddock 1996). A series of recent studies have focused on their prevalence, fate, and environmental risks (Bouyarmane et al. 2015, Gao et al. 2015, Leal et al. 2013).

Surface water plays an important role in the occurrence and spread of FQs, so development of strategies to improve water quality becomes a permanent necessity. Some published works evaluated different approaches and could be applied in assessing the potential health risks associated with indirect exposure to pharmaceuticals, metabolites, and degradation products in drinking water. The pharmaceutical industry is a big consumer of various raw materials and provides large amounts of residuals containing wastewaters at the same time. For example, the level of LEV of one of the downstream rivers close to a drug formulation facility in Pakistan was up to 8000 ng/L (Khan et al. 2013). At the moment, there are a lot of production units that do not function according to environmental regulations, and that expel the untreated wastewaters to the surface waters and sewage networks. According to a case study in Japan, the concentration of LEV presented in sources of sewage before treatment was 552 ng/L, though it was treated by the process of activated sludge, only 49% of LEV was removed (Yasojima et al. 2006). As such, LEV is discharged into the environment. In addition, due to

the high use of NOR and ineffective wastewater treatment technologies, NOR are also being discharged and detected in diverse aquatic systems. For example, the NOR concentration in Bohai Bay was reported to be 6.8 μg/L (Bu et al. 2013), and can accumulate to a very high level in soils through the land application of fertilizers, sewage sludge, and wastewater irrigation (Wang and Wang 2015). The occurrence of FQs may result in questions regarding the unknown healthy effects even in very small concentrations (Jones et al. 2001).

As an important function of the ecosystem, degradation of polycyclic aromatic hydrocarbons by natural bacterial communities has been a natural remedy of pollutant sediments. An experimental study investigated whether exposure to the antibiotic ciprofloxacin affected this function of an aquatic ecosystem. The results demonstrated that degradation of pyrene that a parameter of this function was negatively affected by the presence of ciprofloxacin, and showed a clear dose-effect dependence (Näslund et al. 2008). Thus, FQs from industrial and medical sources dissolve in surface waters and may affect various environmental patterns. There is a need to effectively remove FQs from aquatic environment to protect water security

Furthermore, a very unique property of FQ antibiotics in comparison to commonly studied hydrophobic organic contaminants is their various functional groups, such as keto and carboxyl groups (Gu and Karthikeyan 2005). These functional groups enabled FQs to interact with other chemicals such as heavy metal ions (Pan et al. 2012). Because the presence of various contaminants in one system is common in the environment, research on the adsorption of antibiotics in the presence of heavy metal ions could greatly improve the knowledge to assess antibiotic risks. The further discussions were given in the Section of 1.4.2.4.

1.2.2 *β*-Lactams

Different from FQ antibiotics, *β*-lactams are narrow-spectrum antibiotics and work as bacteriostatic via inhibiting the synthesis of bacterial peptidoglycan cell wall, which are highly

effective for the Gram-positive genera *Streptococcus*, *Gonococcus*, and *Staphylococcus* (Donowitz and Mandell 1988). The *β*-lactam antibiotics mainly include penicillin and cephalosporin antibiotics. The penicillin antibiotics were the first medication to be effective against bacterial infections. Although many types of bacteria have developed resistance to such antibiotics due to the long-term use, 1460.42 tons of penicillin antibiotics were consumed in human medicine in the U.S. in 2011, and penicillins still ranked first in the antibiotic consumption (Food and Drug Administration 2012, 2013). Among the penicillin antibiotics, amoxicillin, piperacillin, and penicillin V are the most commonly used. Compared with penicillins, cephalosporin antibiotics are derived from 7-amino-cephalosporanic acid, which condensed with a six-membered heterocycle. In 2011, 496.91 tons of cephalosporins were used in human medicine in the U.S., and such antibiotics ranked second in the antibiotic consumption (Food and Drug Administration 2012, 2013).

However, *β*-lactams also cannot be completely metabolized by humans or animals, and are then discharged into the aquatic systems, such as municipal swages, rivers, streams, lakes, and seawater. For example, penicillin G has been detected in the raw sewage before entering a wastewater treatment plant (WWTP), and the concentration was determined to be 153 ± 4 μg/L (Li et al. 2008). Importantly, the occurrence of *β*-lactam antibiotics has contributed to the increasing serious antibiotic resistance. Uwaydah et al. studied the penicillin-resistant *Streptococcus pneumoniae* in Lebanon. Among the tested 123 clinical isolates of *Streptococcus pneumoniae*, 17 isolates have resistance at a penicillin level of 1.0 μg/L (Uwaydah et al. 2006).

1.2.3 Sulfonamides

Sulfonamide-containing compounds have been widely used as antibiotics in human and veterinary medicine due to the low cost. Such antibiotics are characterized by a sulfonyl group connected to an amine group, and their typical structure are displayed in Figure 1.2.

Sulfonamides inhibit the development of bacterial by competition with para-aminobenzoic acid that works for the synthesis of folic acid (Wormser and Keusch 1979). It has been reported that more than 10000 sulfonamide derivatives were synthesized, but only about 40 of them are used as antibiotics, such as sulfamethoxazole, sulfanilamide, sulfadimethoxine, N^4-acetylsulfamethazien, and sulfapyridine.

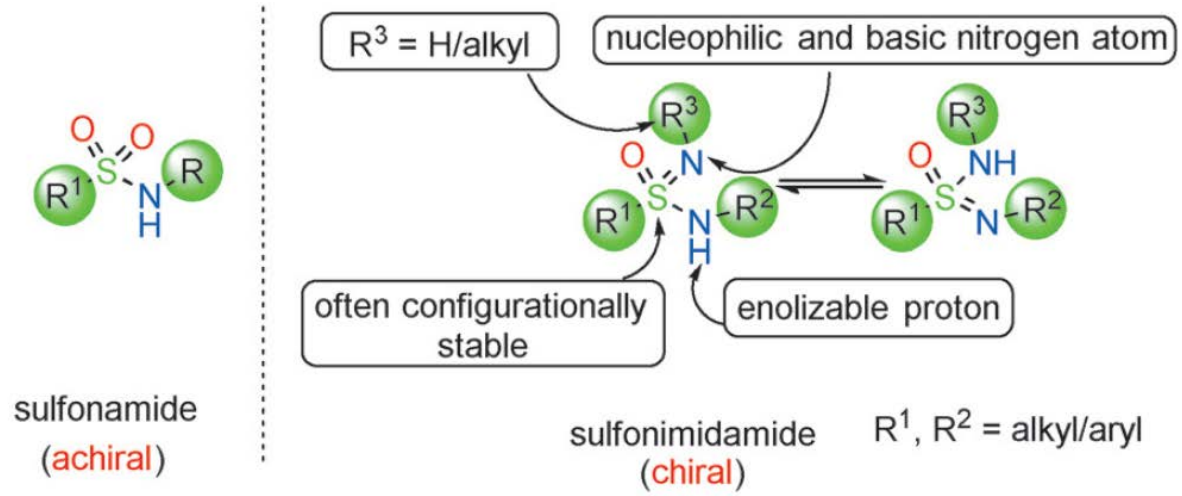

Figure 1.2 Typical structure of sulfonamide antibiotics (Ait Lahcen and Amine 2017).

In 2011, 864.77 tons of sulfonamide antibiotics have been used in the U.S. for human and veterinary medicine (Food and Drug Administration 2012, 2013). However, sulfonamide antibiotics cannot be completely metabolized by humans or animals as well, and are excreted via urine into water bodies and water streams. For example, sulfamethoxazole has been detected in the sewage influent of a WWTP in Guangzhou, China, and the concentration was determined to be 7.91 μg/L (Peng et al. 2006). Moreover, sulfamethoxazole was also reported in urban water with a concentration of 5.60 μg/L (Peng et al. 2008). The long-time exposure of sulfonamide antibiotics even in a low concentration could lead to a sulfonamide antibiotics resistance that have occurred in bacterial strains (Dmitrienko et al. 2014), which eventually risks human health. There is a need to remove sulfonamide antibiotics from water bodies and

water streams to ensure the adequately treated effluent quality for various uses and to protect human health.

1.2.4 Tetracyclines

Tetracyclines are broad-spectrum antibiotics and being used in both human and veterinary medicine, which act against Gam-positive and Gram-negative by binding to the 30 S ribosome and preventing the access of aminoacyl tRNA to the acceptor site on the mRNA-ribosome complex (Marzo and Dal Bo 1998). Figure 1.3 illustrates the worldwide usage of tetracycline antibiotics (Daghrir and Drogui 2013). Similar to the FQ antibiotics, tetracycline antibiotics cannot be completely metabolized by human or animals, nor can they be effectively removed during wastewater treatment using current technologies, and are eventually discharged in active form into environment. For example, Miao et al. reported the occurrence of tetracycline (0.15-0.97 μg/L) in the final effluent from a WWTP in Canada (Miao et al. 2004). A higher residual concentration was also reported by Deblonde et al. in the effluent from a WWTP (Deblonde et al. 2011). Concerns of water resources contaminated by antibiotics (e.g., FQs, β-lactams, sulfonamides, and tetracyclines) have prompted research of effective and efficient water treatment technologies. As the newest class of antibiotics and broad-spectrum antibiotics that are commonly used in human and veterinary medicine, FQ antibiotics such as levofloxacin and norfloxacin were chosen as the target contaminants in this work.

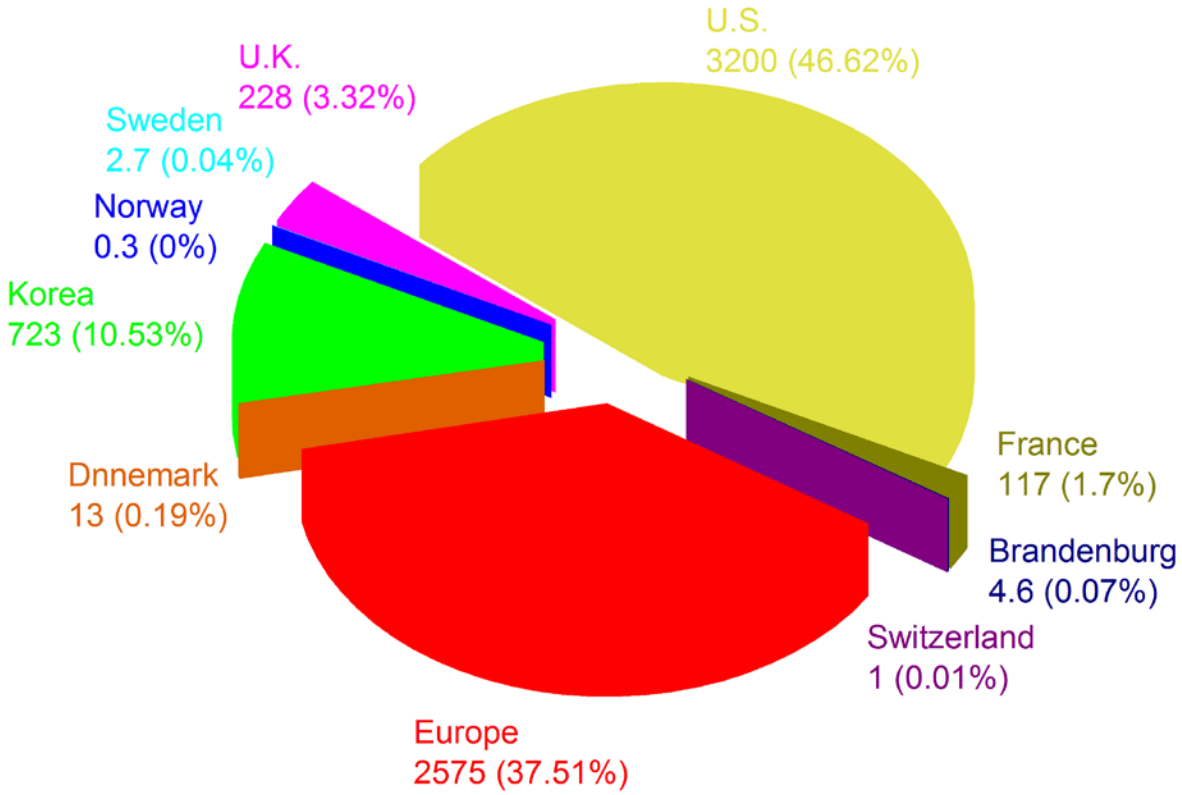

Figure 1.3 Worldwide usage of tetracycline antibiotics (unit ton) (Daghrir and Drogui 2013).

1.3 Treatment Technologies for Removal of Antibiotics

Right now, there is not one specific treatment technology that can completely remove various antibiotics from aquatic system due to their diverse physical, chemical, and biological properties. In a wastewater treatment plant (WWTP), antibiotic-containing wastewater generally undergoes mechanical, chemical, and biological processes. The removal efficiencies (i.e., the ratio of the amount of antibiotic removed by a WWTP to the initial amount of antibiotic that entered the plant) of antibiotics by the conventional sewage treatment are far from satisfactory level since these plants were not designed for antibiotic-containing wastewater. For example, the average removal efficiency of NOR obtained from 52 wastewater treatment plants, which utilized a variety of removal processes such as a two activated sludge process with a nitrification tank, an extended aeration tank, rotating biological contactors, and a pure oxygen activated sludge reactor, was only 68% (Van Doorslaer et al. 2014). It has been

reported that membrane bioreactor systems had a slightly higher removal efficiency than conventional activated sludge treatment, but the construction and operating of membrane technologies costed more due to the expensive membrane materials. A general review of current treatment technologies is presented in the following subsections to compare their performance in removal of antibiotics.

1.3.1 Coagulation-flocculation

As a chemical water treatment technology, coagulation-flocculation is applied prior to sedimentation and filtration to remove particles and some dissolved substances. Coagulation is used to neutralize charges and form a gelatinous mass to trap (or bridge) particles, and flocculation is gentle stirring or agitation to facilitate the formation of large enough particles, both coagulation and flocculation are employed to promote the particles to be filtered from liquid phase. In the process of coagulation-flocculation, chemicals (such as lime, alum, iron salts, and polymers) are used, (Homem and Santos 2011). As mentioned above, such technology needs a subsequent treatment to remove the antibiotic contaminants in a coagulated form.

Over the last decade, coagulation-flocculation was applied to remove antibiotics from effluent, but the removal efficiencies were low. Suarez et al. reported the removal of ibuprofen, diclofenac, naproxen, and sulfamethoxazole by $FeCl_3$ and $Al_2(SO_4)_3$, the corresponding removal efficiencies were (12.0 ± 4.8)%, (21.6 ± 19.4)%, (31.8 ± 10.2)%, and (6.0 ± 9.5)%, respectively (Suarez et al. 2009). The removal of fluoroquinolones, quinoxaline derivatives, and trimethoprim by coagulation-flocculation have also been investigated, while the removal efficiencies were lower than 30% (Stackelberg et al. 2007, Vieno et al. 2007). The low removal efficiencies of this technology have prompted research on effective and efficient water treatment technologies.

1.3.2 Biodegradation

According to the “Glossary of Environment Statistics” by United Nations, biodegradation is the process by which organic substances are decomposed by micro-organisms (mainly aerobic bacteria) into simple substances, such as carbon dioxide, water, and ammonia (United Nations. Statistical Division and United Nations. Deparment for Economic Social Information and Policy Analysis 1997). Application of biodegradation in antibiotics-containing water systems has been investigated in the past decades. Most of the study results demonstrated that the biodegradability of antibiotics at aerobic conditions by bacteria was low. For example, the biodegradation of 18 antibiotics has been tested by Alexy et al. based on the guidelines of the Organization of the Economic Cooperation and Development (OECD) “301 D”. Only benzylpenicillin sodium salt (27%), amoxicillin (5%), nystatin (4%), and trimethoprim naphthoate (4%) were slightly degraded in 28 days, and the degradation of the rest antibiotics were less than 4% (Alexy et al. 2004). Pérez et al. reported relative high removal efficiencies of three antibiotics (sulfamethazine 50%, sulfamethoxazole 75%, and sulfathiazole 93%) at a low concentration level (20 μg/L) in activated sludge process after 10 days, while the pathway (biodegradation and/or adsorption) to remove the antibiotics was still not clear (Pérez et al. 2005). The biodegradation of FQs (e.g., ciprofloxacin and ofloxacin) was also studied, and the results demonstrated that there was no reduction of ciprofloxacin and only 5% ofloxacin was degraded even after 40 days (Kümmerer et al. 2000). Moreover, Jia et al. also reported extremely low removal efficiencies (< 2%) of FQs (e.g., norfloxacin, ciprofloxacin, enrofloxacin, moxifloxacin, and lomefloxacin) during biodegradation in a municipal sewage treatment plant (Jia et al. 2012), which again demonstrated the ineffectiveness of biodegradation particular for FQ antibiotics.

1.3.3 Advanced Oxidation Processes

Higher degradation efficiencies of antibiotics were obtained by advanced oxidation processes (AOPs) that can be defined as aqueous phase oxidation methods based on highly reactive oxygen species such as hydroxyl radicals (Fink et al. 2012). As a widely used oxidation agent, hydrogen peroxide is not strong enough to oxidize organic compounds such as antibiotics, therefore, it usually combines with other reagents, catalysts, and ultraviolet (UV) irradiation to induce the formation of hydroxyl radicals. The commonly used AOPs include UV/H_2O_2, Fenton ($Fe^{2+,3+}$/H_2O_2), and photo-Fenton ($Fe^{2+,3+}$/H_2O_2/UV and $Fe^{2+,3+}$/H_2O_2 simulated sunlight), and heterogeneous catalysis (Petrovic et al. 2011). The selected applications of such methods are given as follows.

UV/H_2O_2 has been proposed as an effective treatment method for organic contaminants in drinking water and reclaimed water. In this process, pollutants are degraded in two ways. Some organic chemicals directly absorb UV light, which then causes the destruction of chemical bonds and the subsequent breakdown of the contaminants. Other organic species do not degrade quickly or efficiently by direct UV photolysis. Therefore, the addition of H_2O_2 is necessary to more efficiently degrade contaminants. However, the presence of hydroxyl radical scavengers in natural water systems (e.g., carbonate species (HCO_3^- and CO_3^{2-}), natural organic matter, and other organic compounds) could have a negative influence on the efficiency of UV/H_2O_2. Keen and Linden investigated the effectiveness of UV/H_2O_2 and direct photolysis by low-pressure and medium-pressure mercury vapor UV sources for degradation of six antibiotics (i.e., clindamycin, ciprofloxacin, penicillin-G, trimethoprim, erythromycin, and doxycycline), and the results demonstrated that all of the antibiotics lost activity when the UV dose was over 500 mJ/cm^2 (Keen and Linden 2013). Furthermore, an interesting phenomenon has been reported that specific transformation reactions (fluoroquinolone-to-fluoroquinolone) occurred during the UV-C irradiation processes. Three transformations (i.e., enrofloxacin-to-

ciprofloxacin, difloxacin-to-sarafloxacin, and pefloxacin-to-norfloxacin) were observed with a direct UV photolysis at 253.7 nm (Snowberger et al. 2016). Importantly, these transformations do not degrade the three parent FQs (i.e., enrofloxacin, difloxacin, and pefloxacin), but form equivalent or more potent (difloxacin-to-sarafloxacin) FQ antibiotics. Thus, transformations of antibiotics should be considered in the applications of UV based treatment technologies.

Among AOPs, Fenton and photo-Fenton technologies have been studied for few decades and applied before or after a biological treatment, particularly the synthetic pharmaceuticals such as antibiotics (Bandara et al. 1997, Oller et al. 2011). In most cases, the photo-Fenton applications were operated at an acidic pH (i.e., 2.5 < pH < 3-4), since iron should be soluble and the Fe^{3+}-hydroxyl complexes exist in an acidic pH. For example, photo-Fenton as a tertiary treatment of antibiotic-containing sewage (e.g., ibuprofen, ofloxacin, sulfamethoxazole, and triclosan) was studied by Klamerth et al., and the results demonstrated that all antibiotics were successfully degraded below their limit of detection at conditions of solar light, 20 mg/L Fe, pH = 3, and 50 mg/L initial H_2O_2 (Klamerth et al. 2010). However, such conditions lead to additional costs (e.g., pH adjustment) and secondary pollutants (e.g., acidic wastewater) which limit its application. De la Cruz et al. reported the degradation of 25 pharmaceuticals by Fenton at a neutral pH in a WWTP of Vidy, Lausanne (Switzerland), and photo-Fenton with $UV_{254\ nm}$ and H_2O_2 (50 mg/L) achieved the best result that over 97% of pharmaceuticals were degraded, particularly 100% for norfloxacin and ofloxacin (De la Cruz et al. 2012). Such photo-Fenton process that was operated at a neutral pH can wide the feasibility of Fenton like AOP technologies at large commercial scale.

Heterogeneous catalysis by semiconductors (usually metal oxides) is also a commonly used AOP. Exposed to light such as UV, the semiconductor works as a sensitizer for light-induced redox reactions. Metal oxides (e.g., ZnO, ZnS, Fe_3O_4, CuO, and TiO_2) with UV irradiation have been applied in this technology and been found to be effective for the

degradation of antibiotics (Vijaikumar et al. 2008, Zelmanov and Semiat 2008). Fink et al. reported the high activity of nanoparticles (CuO and TiC) for the oxidative degradation of enrofloxacin, a common veterinary FQ. Within a contact time of 12 h, 90% enrofloxacin was degraded under sunlight (Fink et al. 2012). However, the reaction mechanism needs to be further investigated.

1.3.4 Membrane Processes

Compared with conventional sewage treatments such as activated sludge, membrane systems (membrane filtration processes and membrane bioreactor) have been reported to be more efficient to remove pharmaceutical contaminants and have many advantages, e.g., operation at a high concentration, less sludge production, and a significant reduction of suspended solid (Sipma et al. 2010). Membrane filtration processes contain microfiltration (MF), ultrafiltration (UF), reverse osmosis (RO), and nanofiltration (NF). The major mechanism of membrane processes to retain contaminants could be size exclusion, adsorption onto membrane, and charge repulsion. Among these methods, MF (pore size 0.1-10 μm) and UF are generally low efficiency in removal of antibiotics because their much larger pore size than antibiotics, and NF (pore size 1-10 nm) and RO have been proposed as the most promising membrane processes to remove antibiotics (Luo et al. 2014). Koyuncu et al. reported the application of NF in removal of four tetracycline and seven sulfonamide antibiotics, and the results demonstrated that the removal efficiencies increased with increase in molecular weight of such antibiotics (may have larger molecular size), more than 95% removal efficiencies were achieved as the molecular weight was higher than 300 g/mol, and complete removals were observed when the molecular weight of tetracycline was higher than 450 g/mol (Koyuncu et al. 2008). Effective removal (98.9%) of tetracycline antibiotics from water using hybrid carbon membrane has been reported (Liu et al. 2017). Removal of FQ antibiotic (i.e., enrofloxacin) was also investigated by RO and NF membranes, the removal efficiencies of enrofloxacin by

RO and NF membranes were higher than 97.2% and 99.1%, respectively (Košutić et al. 2007). However, the antibiotics were still retained in the wastewater and concentrated in the sludge rather than degraded in the membrane processes.

Membrane bioreactor (MBR) combines conventional activated sludge (CAS) treatment and membrane filtration technology, and is considered as a good option for upgrading the existing WWTP and serving small communities with a high quality outlet effluent. It has been reported that MBR process was able to remove antibiotics that may resist the activated sludge treatment (Radjenović et al. 2009), because MBR had a higher concentration of sludge to which antibiotics were adhered, the longer sludge retention time (SRT) in MBR may facilitate the microbial degradation of antibiotics, and the membrane can also block antibiotics (Radjenović et al. 2009). Sipma et al. investigated the removal of antibiotics by MBR in comparison with CAS, the removal efficiencies of erythromycin, ofloxacin, sulfamethoxazole, and trimethoprim were 45% (MBR) and 2% (CAS), 93.5% and 75%, 73% and 33%, and 57% and 11%, respectively (Sipma et al. 2010). Nguyen et al. compared the hollow fiber and flat sheet MBR systems for removal of FQ antibiotics, and achieved high removal of norfloxacin (hollow fiber 62-86% and flat sheet 93-99%), ofloxacin (68-93% and 73-93%), and ciprofloxacin (54-70% and 76-93%) (Nguyen et al. 2017). Although MBR systems had higher removal efficiencies than CAS systems, the high cost of membrane materials and high energy consumption limit the wide application of such technology. There is a need to develop a cost effective and high efficient technology to remove antibiotics from aquatic systems.

1.4 Adsorption

The aforementioned technologies are either low cost low efficiency or high cost high efficiency. There is a need to develop an alternative technology that is low cost but high efficiency for pollutant removal. Adsorption has been reported to be one of the most effective methods for the removal of contaminants from liquid phase (Boparai et al. 2011, Kovalova et

al. 2013, Sun et al. 2015). Adsorption is the partitioning of a compound between the fluid (gas or liquid) and solid phase, and has been known to mankind for more than 100 years. Right now adsorption has been widely applied for the purpose of desired bulk separation or purification. The fundamental elements in adsorption theory is illustrated in Figure 1.4. The solid phase is named as adsorbent; the substance adsorbed on adsorbent is referred to as adsorbate. The release of adsorbed substance into fluid phase is called desorption, which could be achieved by changing the properties of the fluid phase, e.g., temperature, pressure, solution pH, and concentration of adsorbate.

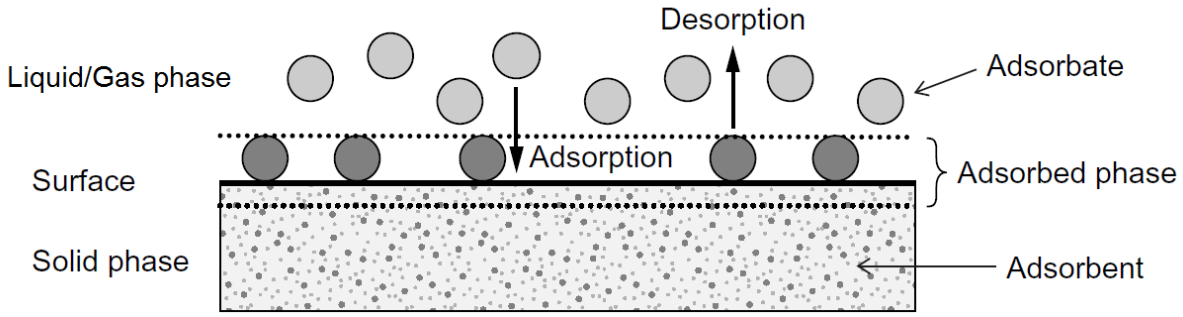

Figure 1.4 Fundamental elements of adsorption process (Worch 2012).

The adsorption mechanisms can be mainly classified as: steric mechanism, the pores of porous materials such as molecular sieve allow small molecules to enter while exclude large molecules from entry; equilibrium mechanism, the solid (adsorbent) is able to accommodate different adsorbates, and the adsorbate that has stronger adsorption affinity with the adsorbent is preferentially adsorbed by the adsorbent; and kinetic mechanism, different adsorbates have different diffusion rates into the pore of adsorbent, thus adsorption of an adsorbate that has faster diffusion rate could be achieved by controlling the time of exposure (Do 1998). Therefore, choosing a proper adsorbent for a given adsorption system is critical. Generally, a good adsorbent must retain a reasonably high surface area or micropore volume and a relatively larger porous network for the transport of adsorbate, which means the adsorbent must have a

suitable combination of micropores and macropores. In 1985, based on the adsorption of nitrogen on a wide range of adsorbents at 77.35 K (boiling point of nitrogen), the pore of a solid material was classified as: micropore (<2 nm), mesopore (2-50 nm), and macropore (>50 nm) (International Union of Pure and Applied Chemistry 1991, Sing 1985). The adsorbents that satisfy the aforementioned criteria include activated carbon, zeolite, alumina, and silica gel, which are commonly used in chemical, biological, and biochemical industries (Yang 2003).

Adsorption technology has been applied in water and wastewater treatment for decades. The typical applications of adsorption technology are listed in Table 1.3. Both organic and inorganic substances can be removed from the aquatic systems. Activated carbon is the most commonly used adsorbent in water treatment, and it could be divided into powdered activated carbon (PAC) and granular activated carbon (GAC). PAC can continuously provide fresh carbon, and be seasonally or occasionally used when target adsorbates present at high concentrations (Snyder et al. 2007). Controlling of tastes and odors such as geosmin and 2-methylisoborneol is one of the common uses of PAC. The full-scale GAC is widely applied in WWTPs as a replacement for anthracite media in traditional filter or as an adsorption bed after conventional filtration (Moore et al. 2003, Moore et al. 2001).

Table 1.3 Adsorption process in water treatment.

Application	Objectives	Adsorbent
Drinking water treatment	Removal of dissolved organic matter, organic micropollutants, and arsenic	Activated carbon, aluminum oxide, and iron hydroxide
Urban wastewater treatment	Removal of phosphate and micropollutants	Activated carbon, aluminum oxide, and iron hydroxide
Industrial wastewater treatment	Removal or recycling of specific chemicals	Activated carbon and polymeric adsorbents
Groundwater remediation	Removal of organic substances	Activated carbon
Treatment of landfill leachate	Removal of organic matters	Activated carbon

1.4.1 Achievements over the Past Decade

Concerns about water resources contaminated by antibiotics and heavy metals have prompted research on effective and efficient water treatment technologies. Adsorption has been claimed as an effective and efficient technology for removal of antibiotics and heavy metals from liquid phases (Bunmahotama et al. 2015). Among the adsorbents, activated carbon has been employed to remove antibiotics, such as tetracyclines, penicillins, and FQs. Rivera-Utrilla et al. reported the adsorption behavior of tetracycline and oxytetracycline on commercial activated carbon, the maximum tetracycline and oxytetracycline adsorption capacities were 471 and 413 mg/g at 298 K and pH 7, respectively (Rivera-Utrilla et al. 2013). The activated

carbon made from vine wood by NaOH impregnation was applied to remove amoxicillin, penicillin G, and tetracycline, and the corresponding maximum adsorption capacities were determined to be 2.69, 8.41, and 1.98 mg/g at pH 2 (Pouretedal and Sadegh 2014). Furthermore, as emerging contaminants, the adsorption behaviors of FQ antibiotics by activated carbons attracted increasing attentions. Ahmed and Theydan explored the adsorption of ciprofloxacin and norfloxacin by activated carbon made form *Albizia lebbeck* seed pods by KOH chemical activation, and the corresponding maximum adsorption capacities were determined to be 131 mg/g at 298 K and pH 9, and 167 mg/g at 298 K and pH 5 (Ahmed and Theydan, 2014). The adsorption of ciprofloxacin on activated carbon was reported to be an endothermic process, in which the maximum adsorption capacities increased from 109 mg/g to 118 and 131 mg/g as the solution temperature was increased from 303 K to 313 and 323 K (Conkle et al. 2010).

Except for activated carbon, other adsorbents, such as alumina, montmorillonite, goethite, and graphene oxide, were also used to remove antibiotics from aquatic systems. Graphene oxide has been used to remove tetracycline, the maximum adsorption capacity was determined to be 313 mg/g, and π-π interaction and cation-π bonding were proposed as the major mechanisms (Gao et al. 2012). The adsorption of levofloxacin (a third generation FQ antibiotic) on graphene oxide was also investigated, and the maximum adsorption capacity was determined to be 257 mg/g (Dong et al. 2016). Liu et al. reported the adsorption of levofloxacin on iron-pillared montmorillonite (48.6 mg/g, 298 K and pH = 7.00), and the kinetic analysis suggested a chemical adsorption (Liu et al. 2015). The adsorption of norfloxacin on carbon nanotubes (<150 mg/g, 298 K and pH 6.8-7.2) (Peng et al. 2012, Wang et al. 2010c), iron-doped activated alumina (7 mg/g, 298 K and pH 6.5) (Liu et al. 2011) were also investigated. However, different to the adsorption of tetracycline antibiotics, the FQ antibiotics adsorption capacities of aforementioned adsorbents are low. As such, there is need to develop a new adsorbent that has high adsorption capacity for FQ antibiotics.

In addition, removal of heavy metals such as nickel by adsorption technology was also studied. The nickel adsorption capacities of activated carbons made from lignin and sugarcane bagasse pith were determined to be 14 (298 K and pH 7) (Gao et al. 2013) and 141 mg/g (298 K and pH 6.5) (Krishnan et al. 2011). Some researchers investigated the removal of nickel by biosorption. Biosorption is a process that uses inexpensive biomass materials to sequester target substance from liquid or gas phase, and the biomaterials used in this process are termed as biosorbents (Volesky 2007). For example, Krishnani et al. used lignocellulosic bagasse as a biosorbent to remove nickel from wastewater, and the maximum adsorption capacity was determined to be 2.8 mg/g (Krishnani et al. 2009).

According to the previously reported work (Ou et al. 2015, Thevannan et al. 2010), barley straw, an abundantly generated agricultural byproduct mainly composed of cellulose, hemicellulose, and lignin, can be used as a biosorbent in the adsorption of nickel from aqueous solution and shows its potential for removing contaminants. The electrostatic attraction between the negatively charged barley straw surface and positively charged nickel ions was suggested as the dominant interaction. However, the removal capacity needs to be improved and the secondary pollution caused by organic compounds release from adsorbents into aqueous solution needs to be addressed. To achieve the optimum adsorption conditions, the major factors affecting the adsorption process were discussed in the following subsections.

1.4.2 Factors Affecting the Adsorption Process

1.4.2.1 Effect of Solution pH

It is well known that solution pH affects charge state of adsorbent and speciation of adsorbate, and therefore the adsorption process. The adsorption of tetracycline and oxytetracycline on commercial activated carbon was investigated at different pH, both the highest adsorption capacities were observed at pH 7, the corresponding adsorption at pH 2 were 65% (tetracycline) and 57% (oxytetracycline) of those at pH 7, and the adsorption at pH 10

were 50% and 56% of those at pH 7, respectively. Such results were explained by the progressive ionization of the oxygen-containing functional groups of the commercial activated carbon, which led to a more negative charged surface as the solution pH was increased (Rivera-Utrilla et al. 2013). However, the maximum ciprofloxacin and norfloxacin adsorption capacities of activated carbon made form *Albizia lebbeck* seed pods by KOH chemical activation were achieved at pH 9 (131 mg/g at 298 K) and 5 (167 mg/g at 298 K), respectively (Ahmed and Theydan 2014).

Wang et al. investigated the adsorption of norfloxacin on surface-modified carbon nanotubes at different solution pH (Wang et al. 2010c). As solution pH was lower than 4.00 (point zero charge), the surface of surface-modified carbon nanotubes was positively charged, otherwise negatively charged (pH > 4.00). In addition, as mentioned in the Section of 1.2.1.1, norfloxacin had two values of dissociation constant via its tertiary amine group (pK_{a2} = 8.51) and carboxyl group (pK_{a1} = 6.22), and it can be positively charged (pH < 6.22), negatively charged (pH > 8.51), and zwitterionic (pH 6.22-8.51) (Pei et al. 2011). As solution pH was increased from 2.00 to 7.20, the norfloxacin adsorption capacity increased (carbon nanotubes and norfloxacin had opposite charges), and then decreased when solution pH was further increased to 10.50 (carbon nanotubes and norfloxacin had the same charge state and could repel each other). The highest NOR adsorption of surface-modified carbon nanotubes was achieved at pH 7.20. Thus, the pH-dependent electrostatic attraction was first expected to be the major driving force by the authors. However, further analysis of the results demonstrated that the variation of NOR adsorption capacity of surface-modified carbon nanotubes in the pH range (2.00-10.50) was low, therefore, electrostatic attraction between carbon nanotubes and norfloxacin influenced the adsorption process of norfloxacin on carbon nanotubes, but it may not be the principal mechanism. Consequently, the π-π electron-donor-acceptor interactions (not significantly affected by solution pH) between carbon nanotubes (π-electron-donors) and

benzenes ring of norfloxacin molecules (π-electron-acceptors, due to the strong electron withdrawing ability of the fluorine group) were proposed as the dominant mechanism (Wang et al. 2010c). Such electron-donor-acceptor interactions were further discussed in the Section of 1.4.3.

1.4.2.2 Effect of Temperature

As a critical environment parameter, temperature influences the adsorption kinetics and equilibrium. Boparai et al. reported the adsorption of cadmium ion on nano zerovalent iron particles (770 mg/g at 297 K), and the adsorption kinetics with respect to temperature was investigated. The obtained kinetic data were well fitted by the pseudo-second-order kinetic model. As the solution temperature was increased, the rate constant and initial adsorption rate increased. Based on the *Arrhenius* equation, the activation energy was determined to be 54.8 kJ/mol, which suggested a chemical adsorption (Boparai et al. 2011).

In addition, the adsorption of norfloxacin on graphitized carbon nanotubes at different temperatures were studied by Wang et al. As the solution temperature was increased from 288 K to 298 and 310 K, the norfloxacin adsorption capacity of graphitized carbon nanotubes increased from 66 mg/g to 77 and 98 mg/g, which revealed an endothermic process. As a result, the π-π electron-donor-acceptor interaction was considered as the predominant mechanism (Wang et al. 2010c). Liu et al. also studied the adsorption of levofloxacin (a third generation FQ antibiotic) on iron-pillared montmorillonite (clay mineral) at various temperatures, the results also indicated an endothermic process, and the adsorption was classified as a chemical adsorption (Liu et al. 2015).

1.4.2.3 Effect of Ionic Strength

Wastewater contains various cations (e.g. Na^+, K^+, Ca^{2+}, Mg^{2+}, and NH_4^+) and anions (e.g. Cl^-, SO_4^{2-}, PO_4^{3-}, and HCO_3^-). Such ions may affect the adsorption process via influencing the competition among cations, metal's activity, interface potential, solution pH, and particularly

the property of the electrical double layer. During the adsorption process, an electrical double layer may be formed in the surrounding of the adsorbed cations (antibiotic^{+} and heavy metal^{+}) due to the electrostatic interactions. As the solution ionic strength is improved, the thickness of aforementioned electrical double layer decreases, which results in a decrease of surface charge of the adsorbent. Most studies show that an increase in ionic strength decreases the adsorption capacity of the adsorbent (Białk-Bielińska et al. 2012, Graouer-Bacart et al. 2013, Thevannan et al. 2010).

1.4.2.4 Presence of Heavy Metals

A very unique property of antibiotics in comparison to commonly studied hydrophobic organic contaminants is their various functional groups, such as tricarbonylamide, phenolic diketone, and dimethylamine groups of tetracycline antibiotics (Wan et al. 2010), keto and carboxyl groups of FQ antibiotics (Turel 2002), and amino group and N-heteroaromatic rings of sulfonamide antibiotics (Wu et al. 2012). These functional groups enable antibiotics to interact with other chemicals such as metal ions. Complexation of antibiotics with metals is a well-known phenomenon and has been proposed as the major mechanism for interaction of metals and antibiotics (Pulicharla et al. 2015). For example, Cu^{2+} could have six vacancies of electronic orbital by d^2sp^3 hybrid orbital, all of which are possible to be filled with a pair of lone-pair electrons (Wu et al. 2012). The lone-pair electrons are usually supplied by oxygen, sulfur, and nitrogen. The complexation of antibiotics with Cu^{2+} indicated that coordination sites of Cu^{2+} can be occupied by ligands (e.g., carboxyl and hydroxyl groups of antibiotics) to form a stable structure (Chen et al. 2009).

FQ antibiotics can complex with heavy metal cations via the 4-oxo and adjacent carboxyl groups (Figure 1.1), although there may be difference among FQs (such as ciprofloxacin, enrofloxacin, and norfloxacin) and heavy metals in the extent of interaction (Polk 1989). Ftouni et al. studied the structure of copper(II)-enrofloxacin complex using Cu *K*-edge X-ray

absorption near edge structure (XANES) spectroscopy (Ftouni et al. 2012). It has been proposed that two carboxylate and two pyridine oxygen atoms from two enrofloxacin molecules coordinated in Cu^{2+} equatorial plane, whereas two water molecules weakly interact in the axial positions to form the CuO4···O2 chromophore. The Cu *K*-edge XANES spectrum of [Cu(enrofloxacin)$_2$(H_2O)$_2$] exhibited a very weak pre-edge feature at 8977.4 eV that corresponds to the 1s→3d transition. The very weak intensity of this pre-edge was consistent with an octahedral symmetry. In addition, there was a shoulder in the low energy side of the edge (8984.0 eV) due to 1s→4p_z and shakedown electron transitions. Such result revealed a tetragonal distortion, since Cu^{2+} cannot be bonded to enrofloxacin in the equatorial plane with the same degree of angular overlap as water molecule. The steric hindrance would affect the ability of the ligand to transfer charge to the metal when core electrons are removed in 1s→4p_z transition.

Moreover, extended X-ray absorption fine structure (EXAFS) spectroscopy was used to study the ternary complexes of norfloxacin adsorption on montmorillonite in the presence of Cu(II) at different pH (Pei et al. 2011). The analysis of spectra indicated that: norfloxacin$^+$ was adsorbed on montmorillonite by the formation of outer-sphere montmorillonite-norfloxacin-Cu(II) ternary surface complex at pH 4.5, and Cu(II) suppressed the adsorption of norfloxacin on montmorillonite; montmorillonite-norfloxacin-Cu(II) and montmorillonite-Cu(II)-norfloxacin ternary surface complexes co-existed at pH 7.0, and the presence of Cu(II) increased the norfloxacin adsorption capacity of montmorillonite; montmorillonite-Cu(II)-norfloxacin ternary surface complex was likely formed at pH 9.0, which was different to Cu(II)(norfloxacin)$_2$ precipitate of the solution, and the norfloxacin adsorption capacity of montmorillonite was again increased.

As introduced before, LEV is a zwitterionic molecule and can complex with heavy metals strongly via its carboxyl and keto groups (Wallis et al. 1996), consequently affecting the

adsorption behavior of both LEV and heavy metals. As a representative of heavy metals, nickel is one of the concerns in the water sources. Nickel wastewater is abundantly generated from industries (e.g., mineral processing, electroplating, production of paints and batteries, and manufacturing of sulfate and porcelain enameling) and is associated with dermatitis, nausea, coughing, chronic bronchitis, gastrointestinal distress, and lung cancer, which threatens human health (Flores-Garnica et al. 2013, Sharma and Singh 2013). Furthermore, it has been reported that Ni(II) may complex with FQs and change their physical, chemical, and biological properties (Uivarosi 2013). LEV and nickel in aquatic environment may affect each other. These may present a risk to human health through contaminated drinking water. Therefore, removal of nickel and investigating its effect on adsorption of LEV are essential.

To the best knowledge of the author of this work, there is no investigation on adsorption of LEV in the presence of Ni(II) in environment.

1.4.3 Electron-Donor-Acceptor Interactions

Nonbonding electrons (*n*) of surface-associated functional groups, e.g., carboxyl groups (-COO^-) and hydroxyl groups (-O^-), have been considered to be strong *n*-electron-donors (Chen et al. 2008). The aromatic rings on adsorbent surface, particularly as the number of associated rings increases, could be strong π-electron-donors due to the occurrence of quadrupole moment (Keiluweit and Kleber 2009). On the other hand, the benzene ring of norfloxacin has been proposed as a π-electron-acceptor due to the strong electron withdrawing ability of the fluorine group and nitrogen-containing groups (Keiluweit and Kleber 2009, Wang et al. 2010c). As a result, the *n*-π and π-π electron-donor-acceptor pairs could be formed between the carboxyl (-COO^-), hydroxyl (-O^-), and aromatic groups of the adsorbent and the benzene ring of FQ antibiotics such as norfloxacin and levofloxacin. The π-π electron-donor-acceptor interactions have been suggested as the major mechanism for the adsorption of antibiotics (e.g., ofloxacin, norfloxacin, sulfadiazine, sulfamethoxazole, sulfamethazine, cephalexin, amoxicillin, and

tetracycline) on graphene oxides (Liu et al. 2016), biochar (Peng et al. 2016), and carbon nanotubes (Wang et al. 2010c).

Furthermore, the electron-donor-acceptor interactions are polar interactions (Foster and Fyfe 1966, Keiluweit and Kleber 2009). As temperature is increased, the static dipole polarizability increases (Adam et al. 2013, Blundell et al. 2000), and the strength of electron-donor and -acceptor increases. Consequently, the electron-rich functional groups of adsorbent (e.g., $-COO^-$, $-O^-$ and aromatic groups) and the benzene rings attached to fluorine of FQ antibiotics become stronger electron-donors and electron-acceptors, and the *n*-π and π-π electron-donor-acceptor interactions could be enhanced at a higher temperature.

CHAPTER 2 THEORY

2.1 Adsorption Kinetics

Kinetic models based on chemical reaction have been used to describe the adsorption process. Among these models, the pseudo-second-order kinetic model assumes that adsorption capacity is proportional to the number of active sites occupied on the adsorbent (Ho 2006), and has been employed to describe the adsorption of FQs, such as ofloxacin and oxolinic acid (Tan et al. 2013). In the current work, it was also used to simulate the adsorption data, as presented below:

$$\frac{dq_t}{dt} = k(q_e - q_t)^2 \tag{2.1}$$

Integration with the initial condition $q_t = 0$ at $t = 0$ gave

$$\frac{t}{q_t} = \frac{1}{kq_e^2} + \frac{t}{q_e} \tag{2.2}$$

where k is the pseudo-second-order rate constant (g/(mg·h)), q_t and q_e denote the adsorption at time t and the equilibrium adsorption capacity (mg/g), respectively.

Once the rate constant was obtained, the activation energy of adsorption could be determined based on the *Arrhenius* equation (Eq. (2.3)) by plotting *lnk* against *1/T* (in Kelvin),

$$lnk = -\frac{E_a}{R}\left(\frac{1}{T}\right) + lnA \tag{2.3}$$

where E_a is the activation energy of adsorption (kJ/mol) and R is the universal gas constant 8.314 J/(mol·K). A is the so-called frequency factor or pre-exponential factor that includes factors like the frequency of collisions and their orientation, and is often taken as a constant across small temperature ranges. The value of activation energy can be used to differentiate the type of adsorption: physisorption or chemisorption. Physical adsorption is readily reversible and attains equilibrium rapidly, therefore, it requires less energy than chemical adsorption. The energy of activation for physical adsorption is usually no more than 1 kcal/mol (equivalent to

4.2 kJ/mol). However, chemical adsorption is specific and involves stronger forces, thus requiring larger activation energies (Smith 1970, Unuabonah et al. 2007).

2.2 Adsorption Equilibrium Modeling

The *Langmuir-Freundlich* model has been commonly and successfully applied to describe the adsorption phenomena involved in *Langmuir* type isotherms and heterogeneous surfaces, such as the adsorption of NOR on reduced graphene oxide (Tang et al. 2013), adsorption of enrofloxacin and ofloxacin on bamboo biochar (Wang et al. 2015), adsorption of sulfamethoxazole on carboxylic-functionalized carbon nanotubes (Lan et al. 2016), and adsorption of ciprofloxacin on activated carbon and carbon xerogel (Carabineiro et al. 2012). Considering that PBS is a modified lignocellulosic biomass and contains various components demonstrating the heterogeneity, and each of the experimentally obtained FQs adsorption isotherms has a saturation capacity demonstrating a *Langmuir* type property, the *Langmuir-Freundlich* model was used to fit the experimental data in this work and given below (Sips 1948):

$$q_e = \frac{q_m b C_e^n}{1 + b C_e^n} \tag{2.4}$$

where C_e is the equilibrium concentration of adsorbate in liquid phase (mg/L), q_m is the maximum adsorption capacity of the adsorbent (mg/g), b is the adsorption equilibrium constant (L/mg), and n is indicative of the surface site heterogeneity of the adsorbent.

2.3 Approximate Site Energy and Its Distribution

The site energy distribution of the adsorbent relates to the adsorption isotherm. In a heterogeneous adsorption system, such distribution was determined by the following integral equation (Carter et al. 1995, Shen et al. 2015):

$$q_e(C_e) = \int_0^\infty q_h(E, C_e) F(E) \mathrm{d}E \tag{2.5}$$

This equation defined the total adsorption q_e of an adsorbate by a heterogeneous surface as the integral of an energetically homogeneous isotherm $q_h(E, C_e)$ multiplied by the site energy frequency distribution $F(E)$ over a range of local adsorption sites with a homogeneous energy E. Adsorption energy E is the adsorption energy difference between the solute (adsorbate, i.e., LEV, NOR, and nickel in this work) and solvent (water) for a given adsorption site.

The above integral was solved with the import of the *Cerofolini* approximation (Cerofolini 1974, Seidel and Carl 1989), in which the equilibrium adsorbate concentration (C_e) was associated with the adsorption energy (E),

$$C_e = C_s exp[-\left(\frac{E-E_S}{RT}\right)] \tag{2.6}$$

$$C_e = C_s exp\left(-\frac{E^*}{RT}\right) \tag{2.7}$$

$$E^* = E - E_s \tag{2.8}$$

$$E^* = -RTln(C_e/C_s) \tag{2.9}$$

where C_s is the maximum solubility of adsorbate at the given conditions and E_s is the adsorption energy corresponding to $C_e = C_s$ (Derylo-Marczewska et al. 1984). The C_s value of LEV in water at 298.15 K and pH 6.88 is 50000 mg/L (Food and Drug Administration 2008), and these values at 308.15 and 318.15 K are estimated to be 57594 and 65754 mg/L. The C_s value of NOR in water is 400 mg/L at 298.15 K and pH 7, and such values at 308.15 and 318.15 K are estimated to be 677.7 and 1111 mg/L (Blokhina et al. 2016, Ross and Riley 1990). The maximum solubility of $NiSO_4$ in water at 298.15 K is 6.25×10^5 mg/L. E^*, referring to the difference of adsorption energies between the adsorbate and solvent to the adsorbent surface based on the reference point E_s, was calculated by incorporating the known values of C_s and C_e into Eq. (2.9). Eq. (2.9) may also be obtained from the Polanyi adsorption potential theory, and therefore the adsorption energy could be associated with the adsorption potential that is proportional to the polarizability (Manes and Hofer 1969).

Assuming that the *Langmuir-Freundlich* model (Eq. (2.4)) is applicable to the PBS-adsorbate (i.e., LEV, NOR, and nickel) adsorption system, when Eq. (2.7) is incorporated into Eq. (2.4), the isotherm $q_e(C_e)$ can be presented as a function of E^* and given below:

$$q_e(E^*) = \frac{q_m b C_s^n e^{\frac{-nE^*}{RT}}}{1+bC_s^n e^{\frac{-nE^*}{RT}}} \tag{2.10}$$

$q_e(E^*)$ represents the adsorption capacity with a specific site energy E^* and above. Then, differentiating the isotherm, an approximate site energy distribution $F(E^*)$ was determined as follows (Carter et al. 1995):

$$F(E^*) = \frac{-dq_e(E^*)}{dE^*} \tag{2.11}$$

$$F(E^*) = \frac{q_m nb C_s^n e^{\frac{-nE^*}{RT}}}{RT(1+bC_s^n e^{\frac{-nE^*}{RT}})^2} \tag{2.12}$$

Since the derived site energy distribution was not normalized, the area under the distribution curve equaled the maximum adsorption capacity q_m (Carter et al. 1995):

$$\int_0^{+\infty} F(E^*)dE^* = q_m \tag{2.13}$$

The position of the mode of site energy distribution curve, E_m^* (value of E^* at the maximum of distribution) was determined from the derivative of Eq. (2.12) (i.e., when $\frac{dF(E^*)}{dE^*}$ =0),

$$E_m^* = \frac{RT}{n}\ln(bC_s^n) \tag{2.14}$$

It has been reported that the interaction strength between the adsorbate and adsorbent can be depicted by the weighted mean of site energy distribution (Carter et al. 1995, Shen et al. 2015). The value of weighted mean was calculated as follows:

$$\mu(E^*) = \frac{\int_0^{+\infty} E^* \cdot F(E^*)dE^*}{\int_0^{+\infty} F(E^*)dE^*} \tag{2.15}$$

By incorporating Eq. (2.12) and Eq. (2.13) into the above equation and integrating them, the weighted mean can be determined,

$$\mu(E^*) = \frac{RT}{n} \ln(1 + bC_s^n) \tag{2.16}$$

Revealed by the width of site energy distribution, the site energy heterogeneity of the adsorbent for adsorbate can be quantified by the standard deviation σ_e^* of the distribution (Shen et al. 2015). The value of σ_e^* was determined by the following equations:

$$\mu(E^{*2}) = \frac{\int_0^{+\infty} E^{*2} \cdot F(E^*) dE^*}{\int_0^{+\infty} F(E^*) dE^*} \tag{2.17}$$

Again, incorporating Eq. (2.12) and Eq. (2.13) into Eq. (2.17) and integrating them gave,

$$\mu(E^{*2}) = \frac{2(RT)^2}{n^2} \int_0^{bC_s^n} \frac{1}{bC_e^n} ln(1 + bC_e^n) d(bC_e^n) \tag{2.18}$$

Then, the standard deviation was calculated,

$$\sigma_e^* = \sqrt{\mu(E^{*2}) - \mu(E^*)^2} \tag{2.19}$$

Furthermore, according to the site energy distribution $F(E^*)$, the percentage (P) of binding sites, the site energy of which are above E^*, was determined,

$$P(E^*) = \frac{\int_{E^*}^{+\infty} F(E^*) dE^*}{\int_0^{+\infty} F(E^*) dE^*} \tag{2.20}$$

The substitution of Eq. (2.10), Eq. (2.12) and Eq. (2.13) into Eq. (2.20) resulted in,

$$P(E^*) = \frac{bC_S^n e^{\frac{-nE^*}{RT}}}{1 + bC_S^n e^{\frac{-nE^*}{RT}}} \tag{2.21}$$

CHAPTER 3 MATERIALS AND METHODS

3.1 Materials

The raw barley straw (RBS) was supplied by the Poultry Center of the University of Saskatchewan, Saskatoon, Canada. It was sun dried, then crushed and sieved to achieve the sizes of 0.425-1.18 mm. After that, the straw was dried in an oven at 378.15 K and kept in desiccators.

LEV, NOR, and nickel solutions were prepared by dissolving levofloxacin ($C_{18}H_{20}FN_3O_4$, ≥ 98 *wt*%, 361.37 g/mol, Sigma-Aldrich), norfloxacin ($C_{16}H_{18}FN_3O_3$, ≥ 99 *wt*%, 319.33 g/mol, Northernchem Inc.), and hydrated nickel sulfate ($NiSO_4 \cdot 6H_2O$, > 98.9 *wt*%, Fisher Scientific) in deionized water, respectively. 0.1 M sulfuric acid (H_2SO_4, > 98.0% (*w/v*), E.M Science) and 0.1 M sodium hydroxide (NaOH, > 98.3 *wt*%, Fisher Scientific) solutions were prepared for pH adjustment. Three purchases were made from Fisher Scientific: 99.8% (*w/v*) acetonitrile anhydrous and 88% (*w/v*) formic acid as the mobile phase in high performance liquid chromatography (HPLC) analysis, $Ni(CH_3COO)_2$ (> 99 *wt*%) as a reference to the nickel crystal structure, and 85% (*w/v*) H_3PO_4. Ethylenediaminetetraacetic acid disodium salt dihydrate (EDTA, 99 *wt*%) used in desorption experiments as a chelating agent was obtained from Sigma-Aldrich. Deionized water was used in all procedures.

3.2 Pretreatment Method

20 g dried raw barley straws (0.425-1.18 mm) were mixed with a 400 mL 0-25% (*w/v*) H_3PO_4 solution. The mixture was magnetically stirred at 100 rpm for 24 h. Then, it was filtered to obtain the impregnated barley straw. The wet impregnated barley straw was heated in a 700 W Rival microwave for 8-10 min, and the maximum value of heating temperature was 844.15 K. After that, the samples were mixed with deionized water, and the mixture was heated to 353.15-363.15 K for 30 min. The mixture was then filtered by deionized water for 5-6 times to

remove the residual H_3PO_4 and other salts until the filtrate pH became constant at about 4. Finally, the obtained wet particles were dried at 378.15 K.

In regards to consideration of sustainability, H_3PO_4 solution used in the impregnation of raw barley straw could be recycled and reused in the pretreatment of barley straw. In addition, continuing reducing the MW energy used in the pretreatment process should be investigated. These two aspects could form areas of future research.

3.3 Determination of Point of Zero Net Charge

To assess the optimal pH for adsorption, it would be important to determine the point of zero net charge (PZNC) value of adsorbent as it provides with information on the charge state of the surface of adsorbent at a specific pH. The PZNC was determined by a salt titration method (Davis and Leckie 1978). The titration was conducted by monitoring the change in pH upon addition of salt such as sodium sulfate to a PBS or RBS suspension. In this work, 20.0 mg PBS or RBS particles were mixed with a 20 mL 0.2 M sodium sulfate aqueous solution or deionized water. The contact time of 6 h was confirmed to be sufficient for reaching equilibrium at 298.15 ± 0.50 K. The solution pH was adjusted using 0.1 M H_2SO_4 or 0.1 M NaOH, and was measured by a pH meter (ISTEK, MODEL 915 PDC). Then the equilibrium pH of each sample was plotted against the added amount of acid or base. Once the two curves (i.e., adsorbent in salt solution and adsorbent in deionized water) were obtained, the PZNC value of PBS or RBS could be determined by the intersection of the two curves. Because the electrical charge density on the surface of adsorbent is zero at PZNC, and the solution pH of suspension was not changed at the elevated salt concentration, which means that the two PBS or RBS suspensions (in sodium sulfate aqueous solution or deionized water) have same pH value as adding a same amount of acid or base. All titration experiments were run in duplicate. This method has been used in the previous studies to determine the PZNC of biomass materials (Thevannan et al. 2010).

3.4 Adsorption and Desorption of Levofloxacin or Norfloxacin on Adsorbents Based on Barley Straw

All adsorption experiments were carried out using a batch mode. The initial concentrations of LEV/NOR ranged from 10 mg/L to 100 mg/L. In the kinetic experiments, 5.0 ± 0.1 mg PBS (made from RBS by 5% (*w/v*) H_3PO_4 impregnation and 9 min MW heating) particles were mixed with a 50.0 mL LEV/NOR solution at different temperatures (298.15, 308.15, and 318.15 K) for 1, 2, 4, 6, 12, 24, 30, 36, 48, 72, 96, 120, 144, and 168 h. The initial solution pH was adjusted using 0.1 M H_2SO_4 or 0.1 M NaOH to the desired values. During the adsorption process, no significant change of pH was observed; therefore, no acid or base solution was added. In the adsorption equilibrium experiments, the contact time of PBS particles with the LEV/NOR solution was set as 168 h to reach equilibrium.

To avoid light, all suspensions were shaken at 150 rpm in the dark. 0.2 mL supernatant was taken out by a 1 mL syringe (B-D Syringes), the supernatant was then filtered by a 0.20 μm Acrodisc Syringe Filter (Pall Corporation, no LEV/NOR adsorption by the syringe filter was observed). The LEV/NOR concentration in the filtrate was determined by a high performance liquid chromatography (HPLC). All experiments were conducted in triplicate. The same concentration series of LEV/NOR solutions without PBS was conducted at the same controlled conditions. The results showed that the initially added amounts of LEV/NOR remained unchanged (no degradation). Thus, the amount of LEV/NOR adsorbed per unit mass of adsorbents was calculated by the LEV/NOR mass difference at the initial and final stage of adsorption divided by the dry net weight of PBS. The results were presented in average values with the corresponding standard deviations.

Desorption experiments were conducted immediately after adsorption at the same temperature and in the same vials as those for the adsorption experiments. The LEV/NOR solution was removed from the vials by a SOCOREX Acura 835 micropipette (1-10 mL). Then,

the same volume of deionized water was added. The pH of each sample was re-adjusted to the desired values. Next, the vials were shaken at 150 rpm for 168 h in the dark. The desorption efficiency was determined by the ratio of the amount of LEV/NOR released from the adsorbent at desorption equilibrium to the initially adsorbed LEV/NOR.

3.5 Adsorption and Desorption of Nickel on Adsorbents Based on Barley Straw

Adsorption experiments were performed in a titrator (SCHOTT Instruments TITRONIC universal) in which the solution pH was auto-adjusted to the desired values and kept constant. 600 ± 0.1 mg PBS (made from RBS by 5% (*w/v*) H_3PO_4 impregnation and 9 min MW heating) was added to a 300 mL nickel sulfate solution, and the mixture was magnetically stirred at a speed of 200 rpm. The initial concentrations of nickel (Ni^{2+}) ranged from 25 mg/L to 1000 mg/L. Adsorption experiments were run at 298.15 ± 0.50 K for 5 hours to ensure that the adsorption equilibrium was reached. Nickel concentration was measured by an instrument of atomic absorption spectroscopy (AAS, Aurora Instruments Ltd., AI 1200), which is similar to the previous research (Thevannan et al. 2010). Nickel adsorption capacity per unit dry mass of adsorbents was calculated by nickel mass balance in the adsorption samples. Each of the experiments was performed in duplicate.

To perform the desorption experiments, PBS was first loaded with nickel, then separated using a filter, and dried in an oven at 378.15 K for 24 h. Next, 600 mg PBS loaded with nickel was added into 300 mL deionized water. The pH was adjusted to 2.0 by 2 M H_2SO_4. The mixture was shaken at a speed of 200 rpm for 24 h.

3.6 Adsorption of Levofloxacin on Pretreated Barley Straw in the Presence of Nickel Ions

The adsorption experiments of LEV on PBS (made from RBS by 5% (*w/v*) H_3PO_4 impregnation and 9 min MW heating) in the presence of Ni(II) were done in a batch mode by mixing 5.0 ± 0.1 mg PBS with a 50.0 mL LEV-nickel solution. The initial LEV concentrations ranged from 10 mg/L to 100 mg/L with the addition of Ni (11.74 mg Ni/L equivalent to 0.2 mmol/L prepared using $NiSO_4 \cdot 6H_2O$). The solution pH was adjusted to 4.0, 7.0, and 9.0, and was kept constant by adding acid (0.1 M H_2SO_4) or base (0.1 M NaOH) during the adsorption process. Then, the mixtures were shaken at 150 rpm and 298.15 K in the dark for 168 h to reach adsorption equilibrium. Other conditions were controlled as the same way as those described in the Section of 3.4. The equilibrium concentrations of LEV and Ni were determined by HPLC and AAS, respectively.

3.7 Adsorption of Water or Ethanol by Adsorbents Based on Barley Straw

0.2 g dry RBS or PBS (made from RBS by 5% (*w/v*) H_3PO_4 impregnation and 9 min MW heating) was mixed with a 30 g water or ethanol solution, and the mixture was shaken at 150 rpm for 0.5 -20 h at 298.15 ± 0.5 K.

In addition, to examine the capability of PBS to selectively remove water from ethanol-water mixture at 298.15 ± 0.5 K, batch adsorption experiments were done in ethanol-water mixtures initially containing 78 *wt*% ethanol. 0.2 g dry PBS was mixed with a 30 g 78 *wt*% ethanol solution, and the mixture was shaken at 150 rpm for 2.0 h. All the adsorption experiments were run in triplicate with a blank undergoing the same treatment, and the data were presented in average values with the corresponding standard deviations.

Adsorption of pure water and pure ethanol by RBS and PBS were determined by weighing the difference of the dry and wet weight of PBS and RBS, then divided by the dry weight of

the respective dry materials. Water concentration in the ethanol-water mixture was analyzed by a Karl Fischer coulometer (Mettler Toledo DL 32). The ethanol content was calculated by subtracting the mass of water from the total mass of the sample.

3.8 Analyses

3.8.1 Determination of Levofloxacin Concentration

Six standard solutions (10, 20, 40, 60, 80, and 100 mg/L) of LEV were prepared by dissolving LEV powder (≥ 98 *wt*%, 361.37 g/mol, Sigma-Aldrich) into deionized water. Such solutions were then analyzed by a HPLC (Agilent Technologies 1260 Infinity Quaternary LC) equipped with a Poroshell 120, EC-C18 column (2.7 μm, 4.6×100 mm) and a UV detector at 293 nm. The mobile phase was 60:40 (v/v) of acetonitrile anhydrous and 0.1% formic acid in deionized water with a flow rate of 0.75 mL/min. The UV spectra of six standard LEV solutions are displayed in Figure 3.1. The retention time of LEV in the HPLC was 1.21 ± 0.02 min, similar to that in the literature (Dafale et al. 2015, Locatelli et al. 2015). All the measurements were done in triplicate. The obtained LEV calibration curve is illustrated in Figure 3.2, and the corresponding values of Pearson correlation coefficient and coefficient of determination R^2 were determined to be 0.999 and 0.999, respectively.

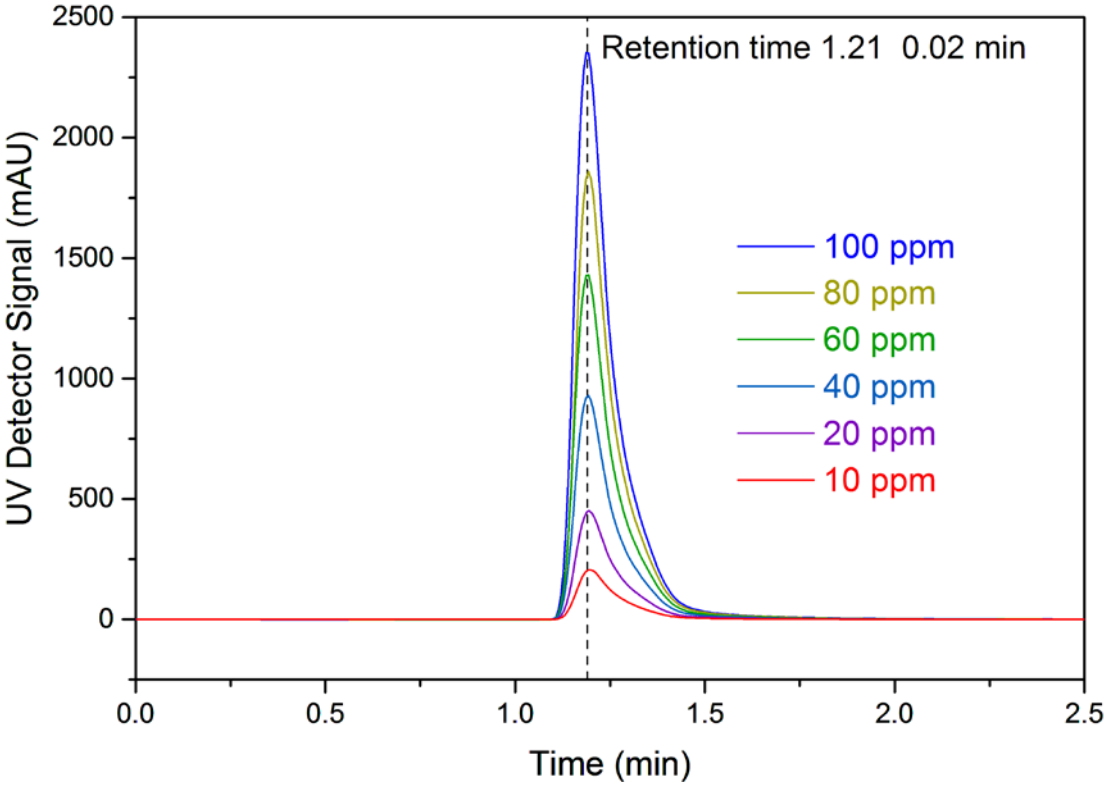

Figure 3.1 UV spectra of six standard LEV solutions by Agilent 1260 HPLC.

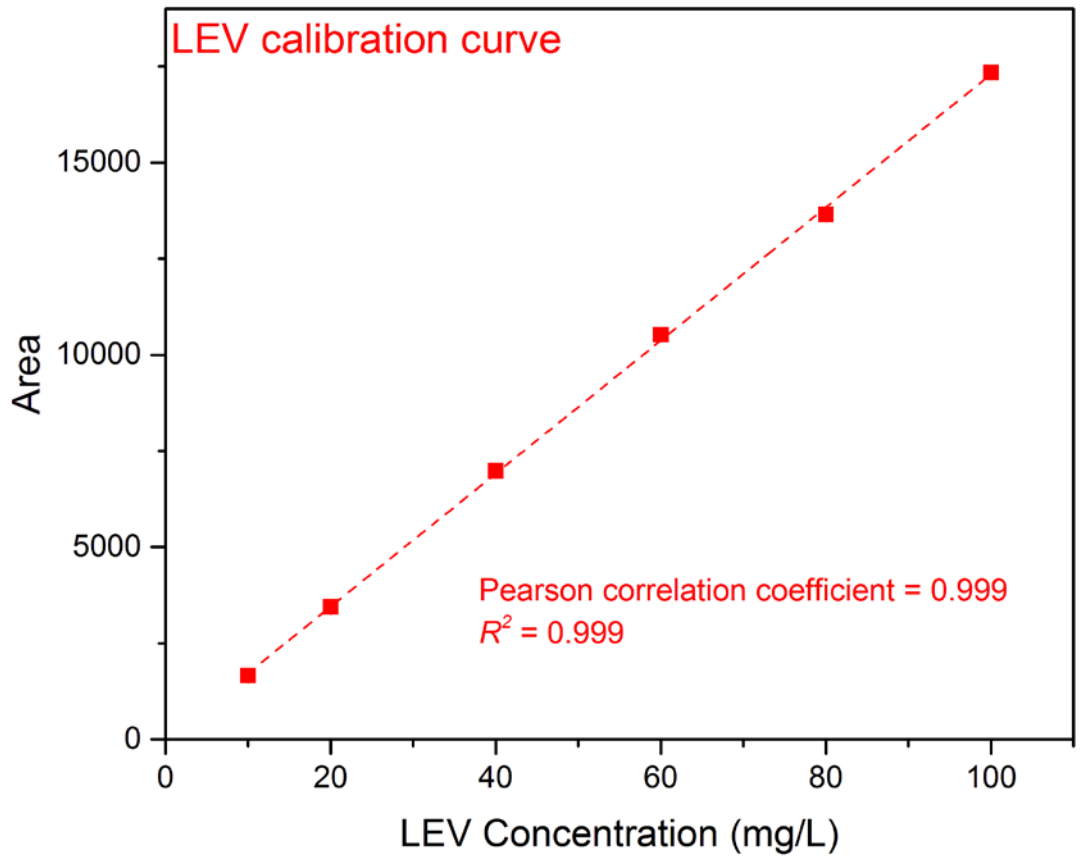

Figure 3.2 LEV calibration curve used in this work.

3.8.2 Determination of Norfloxacin Concentration

Similar to the aforementioned steps of LEV, six standard solutions (10, 20, 40, 60, 80, and 100 mg/L) of NOR were prepared by dissolving NOR powder (≥ 99 *wt*%, 319.33 g/mol, Northernchem Inc.) into deionized water. Such solutions were then analyzed by a HPLC (Agilent Technologies 1260 Infinity Quaternary LC) equipped with a Poroshell 120, EC-C18 column (2.7 µm, 4.6×100 mm) and a UV detector at 280 nm. The mobile phase was 60:40 (v/v) of acetonitrile anhydrous and 0.1% formic acid in deionized water with a flow rate of 0.75 mL/min. The UV spectra of six standard NOR solutions are illustrated in Figure 3.3. The retention time of NOR in the HPLC was 1.20 ± 0.02 min, similar to that in the literature (Liu et al. 2011, Peng et al. 2012). All the measurements were done in triplicate. With high values of Pearson correlation coefficient (0.999) and R^2 (0.999), the obtained calibration curve (Figure 3.4) was applied for the NOR adsorption experiments.

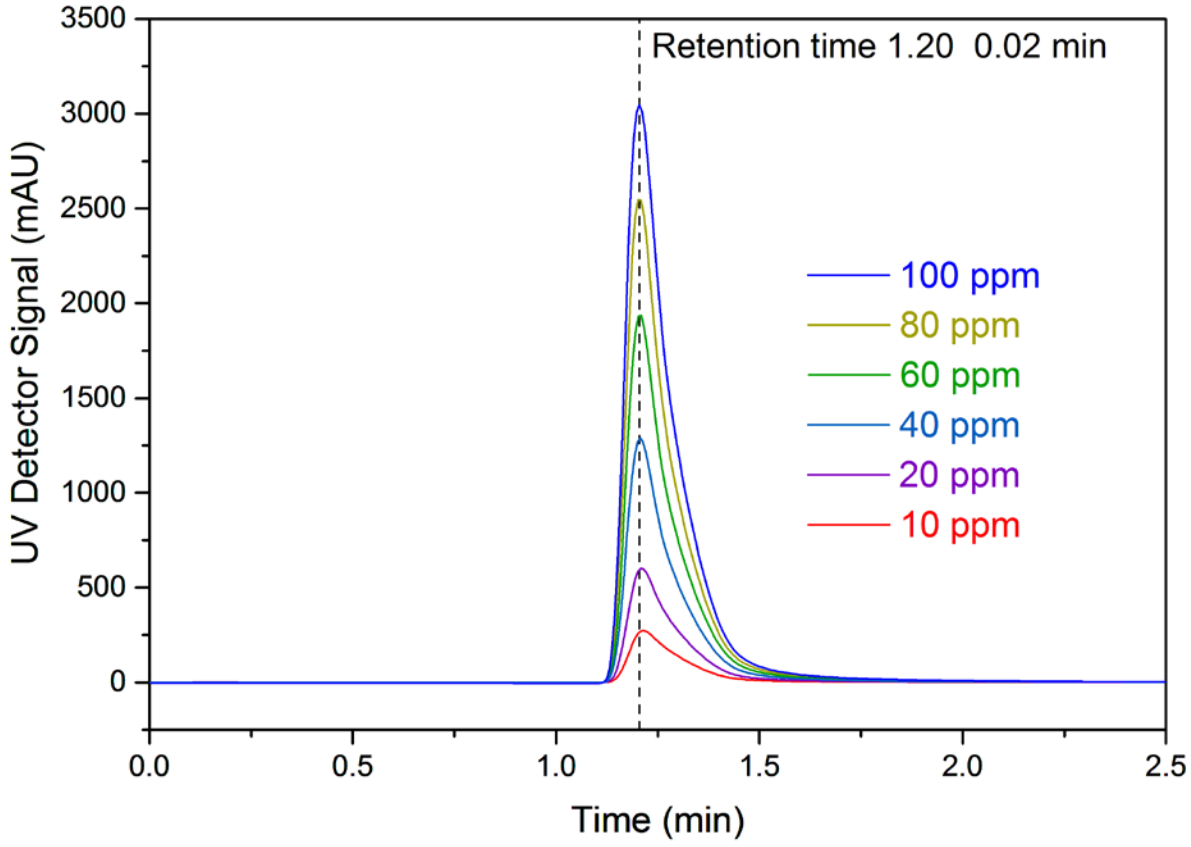

Figure 3.3 UV spectra of six standard NOR solutions by Agilent 1260 HPLC.

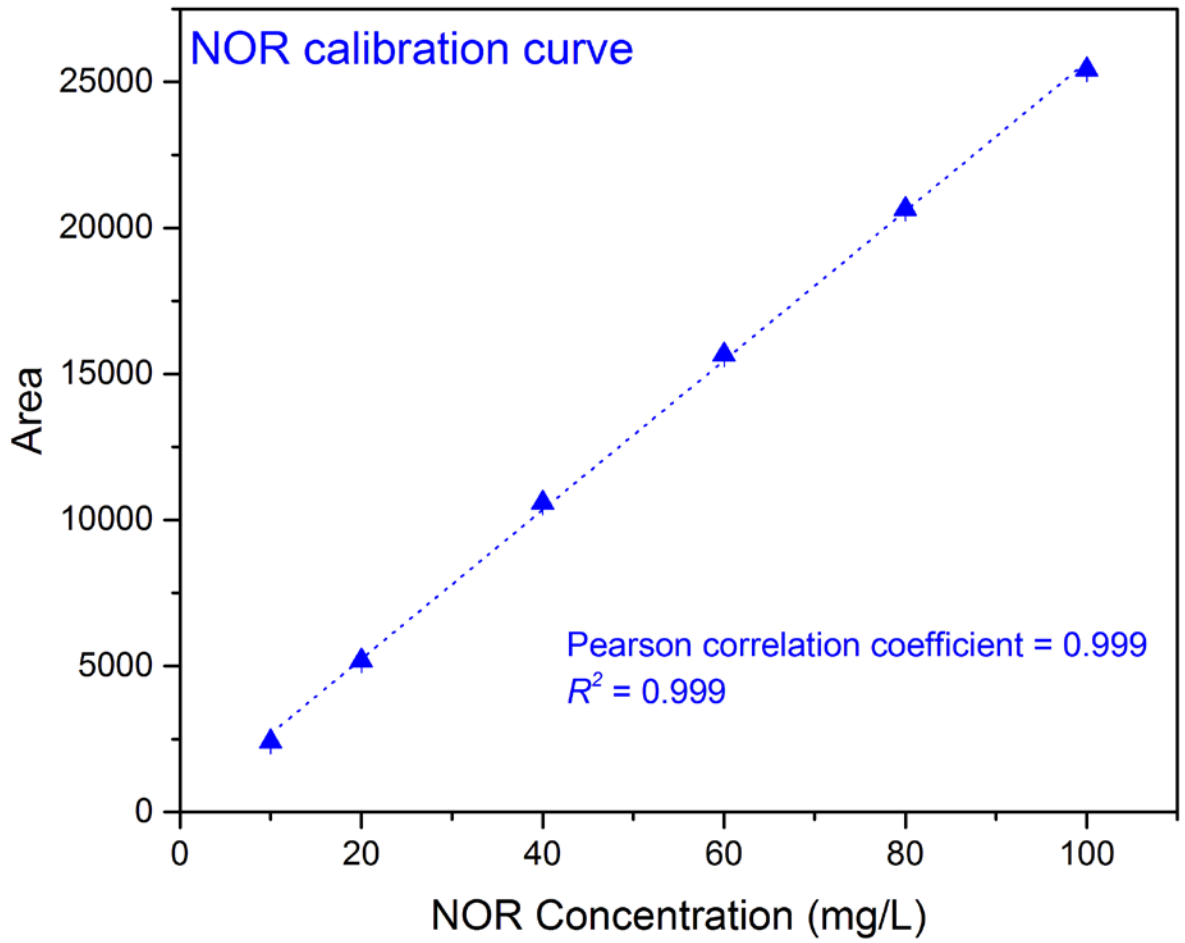

Figure 3.4 NOR calibration curve used in this work.

3.8.3 Determination of Nickel Concentration

Five Ni standard solutions (0, 1, 2, 5, and 10 mg/L) were prepared by dissolving hydrated nickel sulfate ($NiSO_4 \cdot 6H_2O$, > 98.9 *wt*%, Fisher Scientific) into deionized water. Such solutions were then analyzed by an instrument of atomic absorption spectroscopy (AAS, Aurora Instruments Ltd., AI 1200). All the measurements were done in duplicate, which is similar to the previous research (Thevannan et al. 2010). With high values of Pearson correlation coefficient (0.996) and R^2 (0.993), the obtained calibration curve (Figure 3.5) was applied for the nickel adsorption experiments.

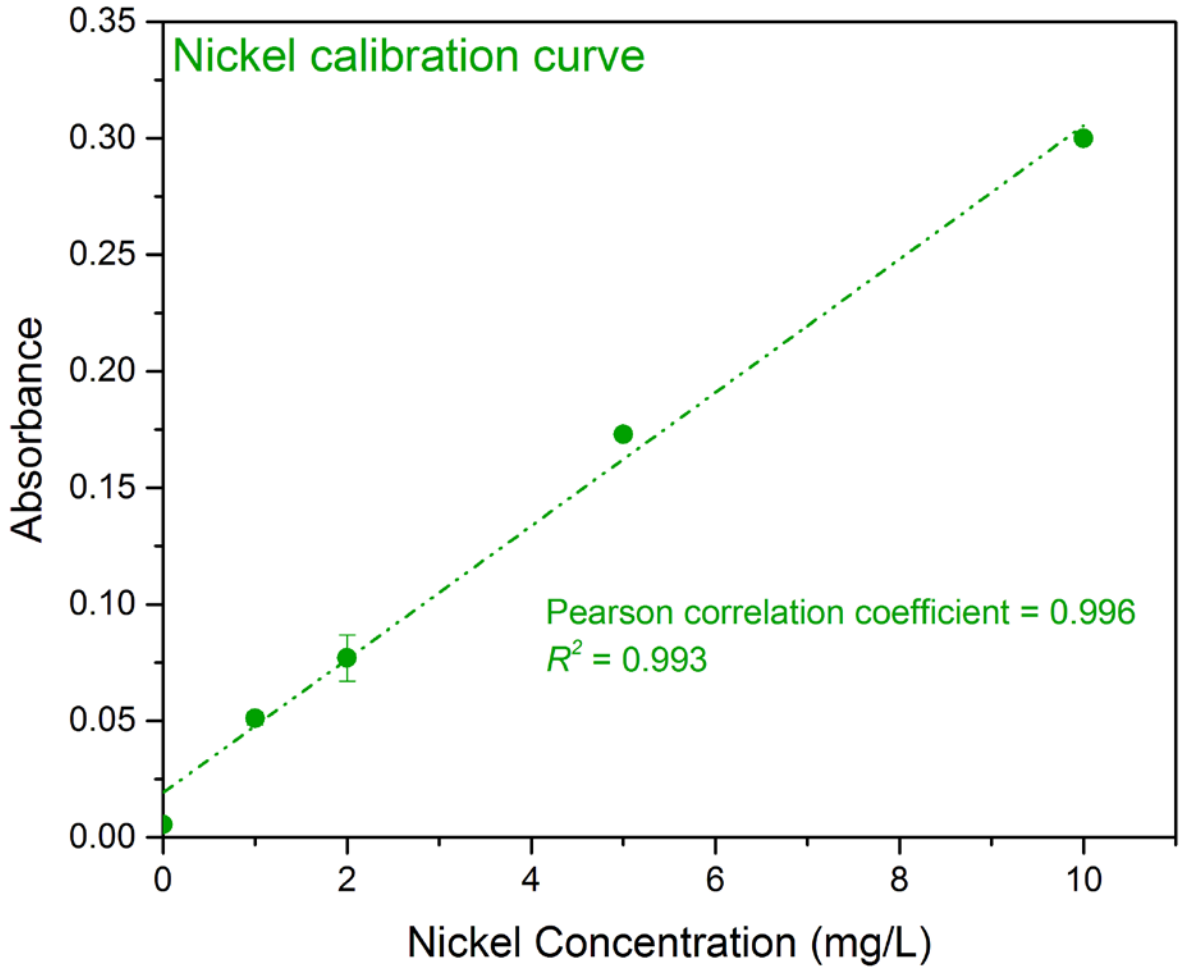

Figure 3.5 Nickel calibration curve used in this work.

3.8.4 Determination of Total Organic Carbon (TOC)

Based on the report of "Analysis of Total Organic Carbon" (University of Massachusetts 2012), six total organic carbon (TOC) standard solutions (0, 100, 200, 300, 400, and 500 mg/L) were prepared by dissolving potassium hydrogen phthalate ($HOOCC_6H_4COOK$, 204.22 g/mol, ≥ 99.95 *wt*%, Sigma-Aldrich) into deionized water. Such solutions were then analyzed by the SHIMADZU TOC-V_{CSH} analyzer combing with the ASI-V automatic sampler. All the measurements were done in duplicate. The obtained calibration curve is displayed in Figure 3.6, and the corresponding values of Pearson correlation coefficient and R^2 were determined to be 0.999 and 0.999, respectively. Therefore, the calibration curve was employed to determine the TOC concentration in the suspensions.

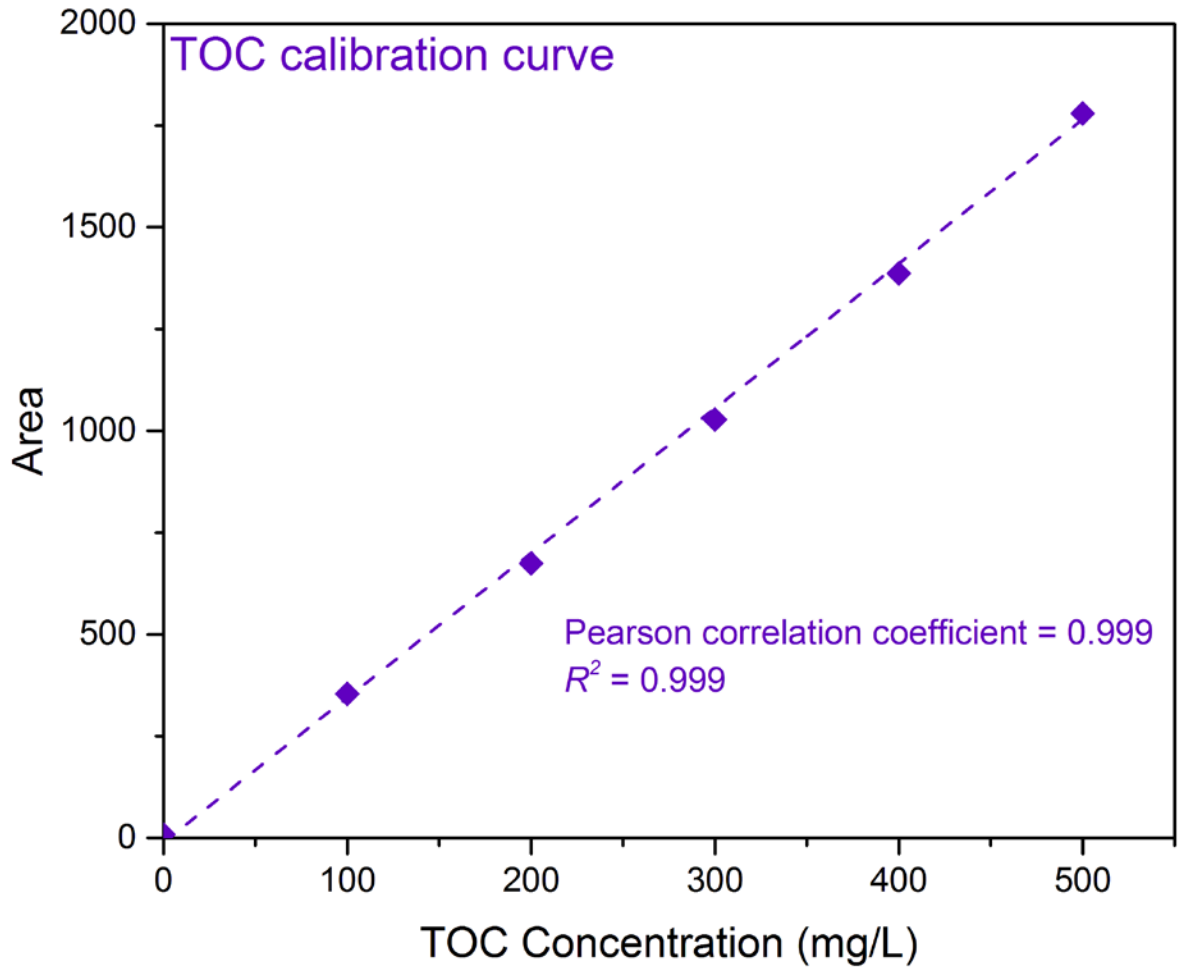

Figure 3.6 TOC calibration curve used in this work.

3.9 Characterizations of Adsorbents Based on Barley Straw

The adsorbents based on barley straw were characterized by multiple methods, such as particle size distribution, surface area, elemental compositions, scanning electron microscopy, and thermogravimetric analysis. To investigate the adsorption mechanisms, the *Fourier* transform infrared spectroscopy (FTIR), the X-ray fluorescence (XRF), and the X-ray absorption spectroscopy (XAS) including X-ray absorption near-edge structure (XANES) and extended X-ray absorption fine structure (EXAFS) spectroscopy were also performed, and the details of sample preparations and measurements were given in the following subsections.

3.9.1 Particle Size Distribution

Pretreated barley straw (PBS, 5% (*w/v*) H_3PO_4 impregnation and 9 min 700 W microwave heating) was first produced according to the method mentioned in the Section of 3.2. The particle size distribution of PBS was measured by the Mastersizer 2000 (Malvern Instruments) via a laser diffraction method. The samples (~ 5g) were first dispersed in water and then delivered to the optical bench. Many individual detectors were arrayed within the optical bench, and each detector captured the light scattering from a particular range of angles. Large particles scatter light at small angles relative to the laser beam and small particles scatter light at large angles. Once the angular scattering intensity data were obtained, the Mie theory of light scattering was used to calculate the size of the particles. The particle size was reported as a volume equivalent sphere diameter.

3.9.2 *Brunauer-Emmett-Teller* (BET) Surface Area

The surface area of adsorbents were analyzed by the Micromeritics ASAP 2020 using liquid nitrogen at 77 K. The samples (adsorbents based on barley straw, ~0.15 g) were first degassed at 383.15 K under vacuum for 6 h. The BET surface area was determined from the relative pressure (P/P_0) ranged from 0.001 to 0.21. The micropore area and mesopore area were calculated by the *t*-plot method and *Barrett-Joyner-Halenda* (BJH) method, respectively.

3.9.3 Scanning Electron Microscopy (SEM)

A Hitachi ultra-high resolution field emission SEM SU8010 was used to investigate the surface topography of adsorbents based on barley straw. PBS (5% (*w/v*) H_3PO_4 impregnation and 9 min 700 W microwave heating) was produced according to the method mentioned in the section of 3.2. The cold field emission gun with small energy spread emitted electrons that interact with atoms in the sample surface. Various signals were then derived from such electron-sample interaction. Received by the detector, these signals containing sample information (e.g., external morphology, crystalline structure, chemical information, and

orientation of materials) were consequently converted to ultra-high resolution images. In this work, the measurements of PBS and RBS were carried on at 3.3 kV with magnification from 6000 to 100000 times.

3.9.4 Elemental Compositions

The elemental compositions (i.e., carbon, hydrogen, nitrogen, and sulfur) of adsorbents based on barley straw were determined through the CHN Analyzer (Elemantar Americas vario ELIII). 4-6 mg of sample was put in a tin boat which was placed in the analyzer after being fold properly. Sample was burnt in an excess of oxygen in the analyzer, and the combustion products were collected in several traps and used to estimate the composition of the sample. The results were given in percentage by weight, i.e., *wt*%.

3.9.5 Thermogravimetric Analysis (TGA)

In order to study the influence of 5% (*w/v*) H_3PO_4 impregnation on the devolatilization characteristics of barley straw at different temperatures, the thermogravimetric analysis (TGA) of adsorbents were performed from 298.15 K to 1073.15 K using the TGA 5500 (TA Instruments). The sample was continuously weighed by the TGA instrument as it was heated with a constant heating rate. Finally, the total weight was plotted against temperature, which reveals the physical and chemical properties of the sample.

3.9.6 *Fourier* Transform Infrared Spectroscopy

A PerkinElmer Spectrum 100 FTIR spectrometer using an ATR mode was employed to obtain the FTIR data of the finely ground particles of RBS, PBS, PBS loaded with LEV, PBS loaded with NOR, and the powder of pure LEV and NOR. The sample of PBS loaded with LEV or NOR was prepared by the following steps: 5.0 ± 0.1 mg PBS was mixed with a 50.0 ± 0.5 mL LEV solution (C_0 = 40 mg/L and pH 6.88 ± 0.03) or NOR solution (C_0 = 73 mg/L and pH 6.96 ± 0.07), and the mixture was then shaken at 150 rpm in the dark for 168 h. The

adsorbents loaded with antibiotics were collected by filtration, washed with deionized water for three times, and then freeze-dried. The amount of LEV and NOR loaded on PBS was determined to be 347 ± 12 LEV mg/g PBS and 396 ± 19 mg NOR/g PBS, respectively. To ensure the quality of the data, the experiments were repeated six times. The FTIR spectra were recorded from 500 to 4000 cm^{-1} over 256 scans.

3.9.7 X-ray Spectroscopy

3.9.7.1 XANES Analysis for the Adsorption of Levofloxacin and Norfloxacin on Pretreated Barley Straw

Similar to the Section of 3.9.6, the sample of PBS loaded with LEV or NOR was prepared: 5.0 ± 0.1 mg PBS was mixed with a 50.0 ± 0.5 mL LEV solution (C_0 = 100 mg/L and pH 6.88 ± 0.03) or NOR solution (C_0 = 100 mg/L and pH 6.96 ± 0.07), and the mixture was then shaken at 150 rpm in the dark for 168 h. The adsorbents loaded with antibiotics were collected by filtration, washed with deionized water for three times, and then freeze-dried. There were 408 ± 4 mg LEV or 349 ± 17 mg NOR adsorbed per gram of dry fresh PBS.

The XANES measurements of adsorption of LEV and NOR on PBS at scanning transmission X-ray microscopy (STXM) beamline were conducted at the soft X-ray beamline 10ID-1 of the Canadian Light Source, which is a 2.9 GeV third-generation synchrotron facility, to probe the chemical bonding/interactions between the adsorbate and adsorbent. The selected samples (PBS, pure LEV, PBS loaded with LEV, pure NOR, and PBS loaded with NOR) were first dispersed in a 95% (*w/v*) alcohol solution, and were then suspension casted on a Si_3N_4 window. To provide with a spatial resolution of 30 nm, a 25 nm outermost-zone plate (CXRO, Berkeley Lab) was used. The in-plane polarization dependence of the sample was averaged out by a circularly polarized soft X-ray beam generated from the SM elliptically polarized undulator (EPU). Over a range of photon energies across the elemental edges of interest, the samples were raster-scanned with the synchronized detection of transmitted X-rays to generate

the image sequences (stacks). The C *K*-edge image stacks covered an energy range of 280-310 eV, with energy steps as fine as 0.15 eV around the XANES peaks and 0.5 eV in the pre-edge and the continuum. The energy of O *K*-edge spectrum ranged from 525 to 560 eV, and the energy steps around the XANES peaks and in the pre-edge and the continuum were 0.2 eV and 0.5 eV, respectively. The XANES spectra of PBS, pure LEV, PBS loaded with LEV, pure NOR, and PBS loaded with NOR can be extracted from each pure region in the C and O *K*-edge image stacks. More details on the XANES experimental and data analysis can be found in the publications (Chen et al. 2014a, Chen et al. 2014b, Sun et al. 2011).

3.9.7.2 XRF and XANES Analysis for the Adsorption of Nickel on Pretreated Barley Straw

The samples of PBS loaded with nickel was prepared according to the description in the Section of 3.5. The adsorbent (PBS loaded with nickel) was collected by filtration and washed by deionized water for 3 times, then freeze-dried. The amount of nickel loaded on PBS varied from 0 mg/g to 57.0 mg/g.

XRF and XAS measurements of the adsorption of nickel on PBS were carried on the Very Sensitive Elemental and Structural Probe Employing Radiation from a Synchrotron (VESPERS) beamline at the Canadian Light Source in Saskatoon, Saskatchewan, Canada (Feng et al. 2010, Feng et al. 2007). For XRF measurements, the X-ray beam with an incident energy of 10 keV was employed to excite the sample. The emitted XRF spectrum was recorded by a 4-element Vortex® silicon drift detector, which mainly contains Ni K_α and K_β characteristic emission lines. Ni *K*-edge X-ray absorption near edge structure (XANES) and extended X-ray absorption fine structure (EXAFS) spectroscopy were measured using fluorescence mode with a double crystal Si (111) monochromator. Energy calibration was performed with a nickel metal foil (*K*-edge at 8333 eV). All experiments were carried out under ambient conditions. The obtained XANES and EXAFS data were analyzed by the free software IFEFFIT, which is a suite of interactive programs for XAS analysis (Newville 2001). IFEFFIT combines high-quality and well-tested

XAS analysis algorithms, tools for general data manipulation, and graphical display of data (Ravel and Newville 2005). The collected data were *Fourier* transformed over the *k*-region of 3-12 $Å^{-1}$ with k^2 weighting. The fitting was performed in *k*-space yielding optimal values for the coordination numbers (*CN*), atomic distance (*r*), *Debye-Waller* factors (σ^2), and *R*-factor that represents the relative error of the crystallographic model fitting results to the experimental data.

CHAPTER 4 PREPARATION AND CHARCTERIZATIONS OF ADSORBENTS BASED ON BARLEY STRAW

In this chapter, pretreated barley straw (PBS) was made from raw barley straw (RBS) by H_3PO_4 impregnation and microwave (MW) heating. Because H_3PO_4 impregnation concentration and MW radiation time in the pretreatment are the most important factors, the influence of these parameters on the PBS pore size distribution and surface area were investigated. Furthermore, using the quantitative data (H_3PO_4 impregnation concentration, MW radiation time, and *Brunauer-Emmett-Teller* (BET) surface area of PBS) obtained from the designed experiments, the response surface methodology (RSM) was used for multiple regression analysis (MRA) to further evaluate the correlation between the BET surface area (Y) and the H_3PO_4 impregnation concentration (X_1) and MW radiation time (X_2), and to optimize the preparation process. In addition, the adsorbents based on barley straw were characterized by multiple methods, such as particle size distribution, elemental compositions, scanning electron microscopy (SEM), and thermogravimetric analysis (TGA).

4.1 Preparation of Adsorbents Based on Barley Straw

Generally, a good adsorbent must have a reasonably high surface area and a relatively larger porous network for the transport of adsorbate, which means the adsorbent must have a suitable combination of micropores and macropores. According to the IUPAC (International Union of Pure and Applied Chemistry 1991), the pore of a solid material can be divided into three groups: micropore (< 2 nm), mesopore (2-50 nm), and macropore (> 50 nm). As such, the high value of BET surface area and suitable pore surface area distribution were set as the major criteria to optimize the preparation conditions, i.e., the concentration of H_3PO_4 impregnation and MW radiation time.

4.1.1 Effect of H_3PO_4 Impregnation Concentration and Microwave Radiation Time on Surface Area and Pore Size Distribution

The pore surface area distribution (determined by the *t*-plot method and *Barrett-Joyner-Halenda* (BJH) adsorption method) of PBS prepared at different H_3PO_4 impregnation concentrations are presented in Figure 4.1. The results showed that PBS made from RBS contained micropores, mesopores, and macropores, and that the concentration of H_3PO_4 significantly affected the surface area distribution of PBS.

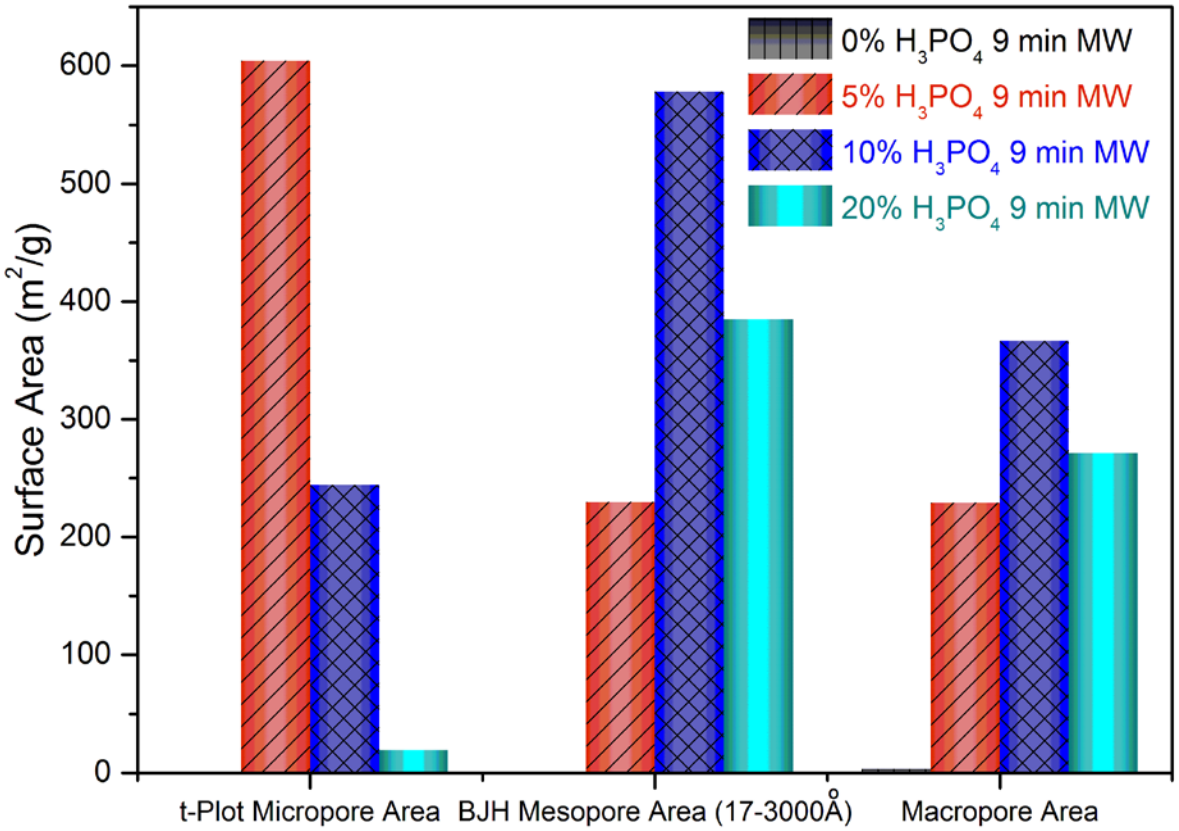

Figure 4.1 Effect of H_3PO_4 impregnation concentration on the surface area distribution of PBS.

Without H_3PO_4 impregnation, the BET surface area of PBS heated in the MW for 9 min was just 4 m^2/g including 1.0 m^2/g micropore, 0.2 m^2/g mesopore, and 2.8 m^2/g macropore, which are almost invisible in Figure 4.1 because of the low values. The micropore, mesopore, and macropore volume of RBS was not given in Figure 4.1 since the surface area of RBS (2

m^2/g) was too small to detect these data. When RBS was impregnated by the 5% (*w/v*) H_3PO_4 solution, the micropore surface area of PBS significantly increased followed by mesopore and macropore area. The results demonstrated that H_3PO_4 played a significant role on improving the porosity of RBS, which led to the largely increased surface area. Xie and Jagtoyen's work also proved that H_3PO_4 facilitated the development of new micropores and enlarged the existing micropores to mesopores via promoting the release of volatiles (Jagtoyen and Derbyshire 1998, Xie et al. 2013). However, when the H_3PO_4 impregnation concentration was continuously increased to 10% (*w/v*) H_3PO_4, the micropore area decreased, mesopore and macropore areas increased, and mesopore consequently became the dominant pore. As the H_3PO_4 impregnation concentration was further increased to 20% (*w/v*), micropore, mesopore, and macropore areas dramatically decreased. The porous structure of PBS may be destroyed at the high H_3PO_4 concentrations. Such results indicated that higher portion of micropores and higher porosity of PBS were achieved by impregnating RBS at 5% (*w/v*) H_3PO_4. Table 4.1 further presents the effect of H_3PO_4 impregnation concentration on the total BET surface area of PBS. As given in Table 4.1, RBS had a total BET surface area of 2 m^2/g. Although RBS was heated for 9 min (but without H_3PO_4 impregnation), the total BET surface area was just 4 m^2/g. However, with 5% (*w/v*) H_3PO_4 impregnation, the surface area was significantly increased to 1314 ± 10 m^2/g. When the concentration of H_3PO_4 was further increased to 25% (*w/v*), the surface area decreased from 1314 m^2/g to 105 m^2/g. Because a higher surface area was preferred, impregnating RBS in a 5% (*w/v*) H_3PO_4 solution was favored.

Table 4.1 BET surface area values of PBS prepared at different H_3PO_4 impregnation concentrations.

H_3PO_4 impregnation		MW		BET surface
Concentration, % (*w/v*)	Time, h	Power, W	Radiation time, min	area, m^2/g
0	0	0	0	2
0	24	700	9	4
5	24	700	9	1314 ± 10
10	24	700	9	1231
15	24	700	9	1144
20	24	700	9	934
25	24	700	9	105

Note: Coefficient of variation of the BET surface area measurement is less than 1%.

Apart from H_3PO_4 impregnation concentration, MW radiation time is another important factor affecting surface area development of PBS. Compared with a traditional furnace, using a MW to heat saved energy and time (Waheed ul Hasan and Ani 2014). In this experiment, the radiation time in a MW of 700 W was varied from 2 min to 10 min while the impregnation concentration of H_3PO_4 was kept at 5% (*w/v*). Due to unsatisfactory results of the samples obtained at heating time less than 8 min in terms of BET surface area, only results achieved at 8 min and above are listed in Table 4.2. The results revealed that as the MW radiation time was increased from 8 min to 9 min, the BET surface area increased from 1167 m^2/g to 1314 m^2/g, then decreased to 1189 m^2/g when the MW radiation time was further increased to 10 min. Similar change of surface area was also observed in the case of 10% (*w/v*) H_3PO_4 impregnation concentration. Thus, 9 min resulting in a higher BET surface area was chosen as the optimal MW radiation time at the tested conditions.

Table 4.2 BET surface area values of PBS at different MW radiation times.

MW		H_3PO_4 impregnation		BET surface area, m^2/g
Power, W	Radiation time, min	Concentration, % (*w/v*)	Time, h	
700	8	5	24	1167
700	9	5	24	1314 ± 10
700	10	5	24	1063
700	8	10	24	909
700	9	10	24	1231
700	10	10	24	1189

Note: Coefficient of variation of the BET surface area measurement is less than 1%.

SEM images of PBS (5% (*w/v*) H_3PO_4 impregnation with 9 min MW heating) and RBS were taken to compare their external morphology. Figure 4.2 reveals that PBS had a highly porous surface with cracks, channels, and large holes in comparison with RBS. PBS may possess a potentially high adsorption capacity due to the well-developed porous structure. Consequently, at the tested experimental conditions, 5% (*w/v*) H_3PO_4 impregnation concentration and 9 min MW radiation time were more appropriate to produce PBS with a higher surface area and an enhanced porous structure.

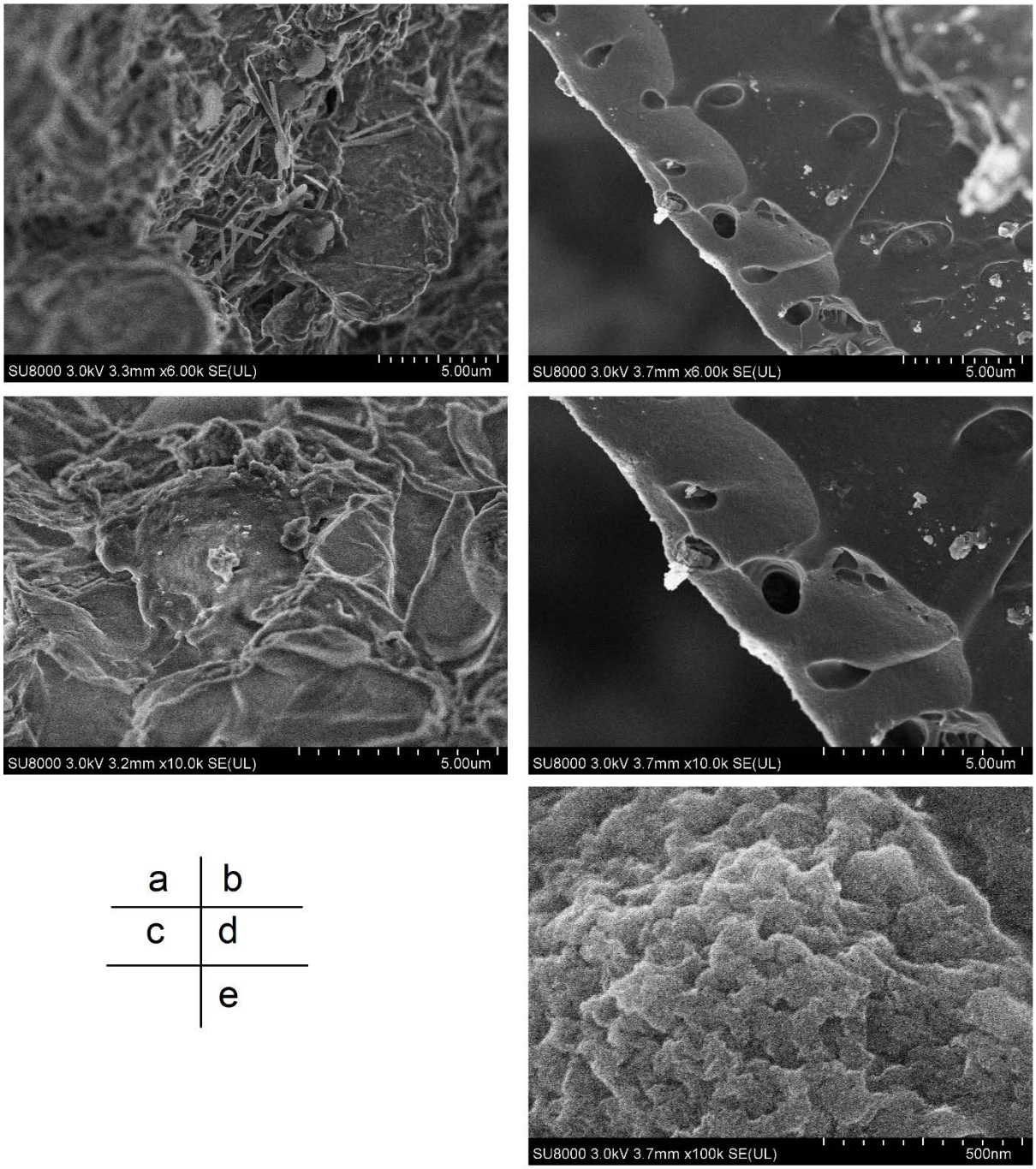

Figure 4.2 SEM images of PBS and RBS: a) RBS, magnification time 6000; b) PBS, magnification time 6000; c) RBS, magnification time 10000; d) PBS, magnification time 10000; e) PBS, magnification time 100000.

4.1.2 Multiple Regression Analysis

Based on the above mentioned results, the BET surface area of the developed adsorbent as a function of impregnation concentration of H_3PO_4 and MW radiation time was modeled by a

statistical modeling technique called multiple regression analysis (MRA). In this study, using quantitative data obtained from the designed experiments, the response surface methodology (RSM) was used for MRA to simultaneously evaluate multivariate equations. This method was firstly introduced by *G. E. P. Box* and *K. B. Wilson* in 1951 (Box and Wilson 1951). RSM was used to investigate the relationship between the independent variables and dependent variables (responses variables) and to determine the most critical factors by a polynomial model (Murphey and Pardalos 2002).

A second-degree polynomial model is presented in Eq. (4.1):

$$Y = B_0 + \sum_{i=1}^{f} B_i X_i + \sum_{i=1}^{f} B_{ii} X_i^2 + \sum_{i=1}^{f-1} \sum_{j=2}^{f} B_{ij} X_i X_j \quad (4.1)$$

where Y is the predicted response, X_i, X_j are the real value of the independent variable, B_0 is a constant, B_i is the linear coefficient, B_{ii} is the quadratic coefficient, B_{ij} is the interaction coefficient, and f is the number of factors (Sahu et al. 2010).

In this work, Eq. (4.1) was used to model the predicted response BET surface area (Y) of PBS as a function of the independent variables impregnation concentration of H_3PO_4 (X_1) and MW radiation time (X_2). MATLAB was used for the regression analysis, such as analysis of variance (ANOVA) and model fitting.

As listed in Table 4.3, the F Statistic values of H_3PO_4 impregnation concentration, MW radiation time and interaction were 51317, 6763, and 1111 that were far greater than 1. Moreover, the p-values of H_3PO_4 impregnation concentration and MW radiation time were far less than 0.05. Such results indicated that both H_3PO_4 impregnation concentration and MW radiation time had significant effect on the BET surface area of PBS. In addition, the p-value of interaction was far less than 0.05, which meant that the interaction between H_3PO_4 impregnation concentration and MW radiation time was significant, too.

Table 4.3 ANOVA analysis of the effect of H_3PO_4 impregnation concentration and MW radiation time on BET surface area.

	H_3PO_4 impregnation concentration	MW radiation time	Interaction
*SS**	4775871	314698.95	206761.35
F	51317	6763	1111
p	8.08E-31	6.81E-23	2.23E-19

* *SS* the sum of the squared deviations

The modeling results of BET surface area (*Y*) versus H_3PO_4 impregnation concentration (X_1) and MW radiation time (X_2) are illustrated in Figure 4.3. The values of coefficient of determination (R^2) and root-mean-square error (*RMSE*) were determined and presented in Table 4.4. The cubic polynomial model that is a third order response model and considers interaction of the two parameters demonstrated a better correlation with the experimental data. With a higher value of R^2 (0.998), the cubic polynomial model might be applied to predict the BET surface area of PBS at a specific H_3PO_4 impregnation concentration and MW radiation time.

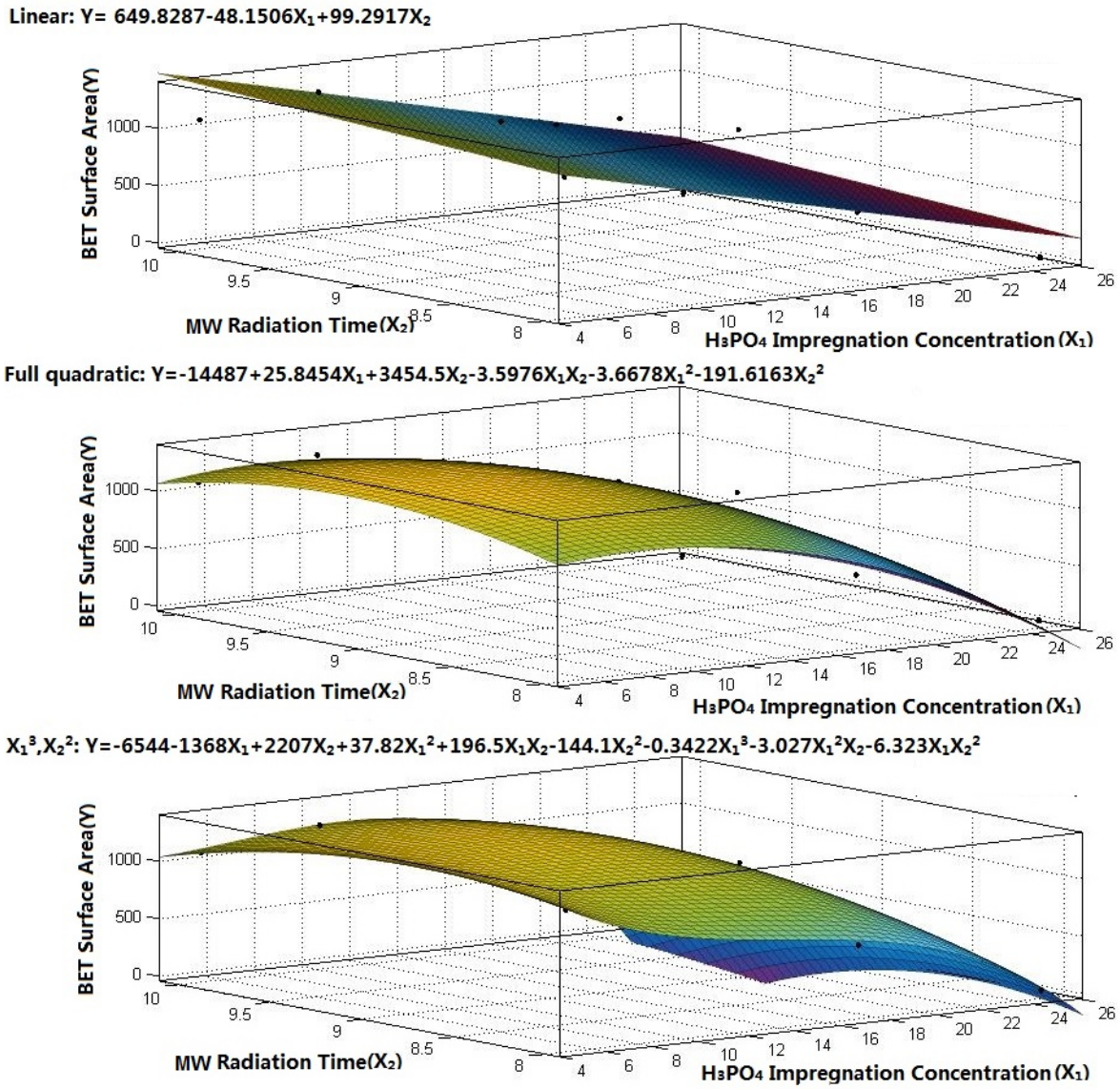

Figure 4.3 Modeling of BET surface area (*Y*) versus H_3PO_4 impregnation concentration (X_1) and MW radiation time (X_2).

Table 4.4 Modeling results of BET surface area (*Y*) versus H_3PO_4 impregnation concentration (X_1) and MW radiation time (X_2).

Regression model	Equation	R^2	*RMSE*
Linear polynomial	$Y = 649.8287-48.1506X_1+99.2917X_2$	0.757	245
Full quadratic polynomial	$Y = -14487+25.8454X_1+3454.5X_2-3.5976X_1X_2-3.6678X_1^2-191.6163X_2^2$	0.954	135
Cubic polynomial	$Y = -6544-1368X_1+2207X_2+37.82X_1^2+196.5X_1X_2-144.1X_2^2-0.3422X^3-3.027X_1^2X_2-6.323X_1X_2^3$	0.998	48

Among the tested conditions, PBS made from RBS at 5% (*w/v*) H_3PO_4 impregnation and 9 min MW (700 W) heating demonstrated the highest surface area (1314 ± 10 m^2/g) and a well-developed porous structure. Moreover, the total organic carbon (TOC) released into suspensions from the adsorbents significantly reduced from 34.4 ± 0.9 mg/g (RBS) to 0.9 ± 0.2 mg/g (PBS, 5% (*w/v*) H_3PO_4 impregnation and 9 min MW heating) indicating enhanced stability of PBS. Thus PBS made from RBS at 5% (*w/v*) H_3PO_4 impregnation and 9 min MW (700 W) heating was chosen for further characterizations as follows.

4.2 Characterizations of Adsorbents Based on Barley Straw

4.2.1 Particle Size Distribution

The particle size distribution of PBS (5% (*w/v*) H_3PO_4 impregnation and 9 min MW heating) was measured and presented in Figure 4.4. The volume mean diameter was 316 μm, and the median was 251 μm. 10% of the population have a diameter smaller than 83 μm, and 90% have a diameter smaller than 651 μm.

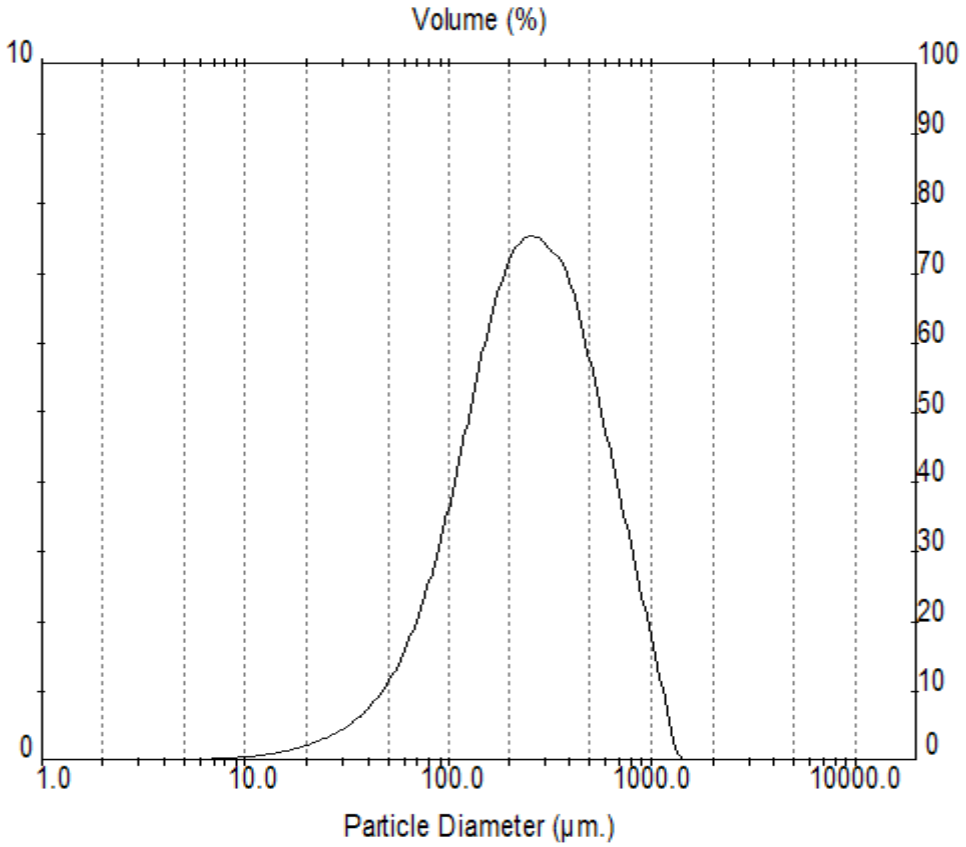

Figure 4.4 Particle size distribution of PBS made from RBS (0.425-1.18 mm) at 5% (*w/v*) H_3PO_4 impregnation and 9 min MW heating.

4.2.2 Elemental Analysis

The major elements of PBS compared with RBS were analyzed by a CHN Analyzer, and the results are given in Table 4.5. It showed that the weight percentage (*wt*%) of carbon (C), hydrogen (H), nitrogen (N), and sulfur (S) of RBS were 42.0, 5.9, 1.5, and 0.2, respectively. It has been reported that cellulose (31-34 *wt*%), hemicelluloses (24-29 *wt*%), and lignin (14-15 *wt*%) were the main organic constitutes that were nearly 78 *wt*% of the total weight of RBS (Ch. Teas et al. 2001), and that the ash content was found to be 9.8% (P, 1.7%; Mg, 1.6%; Fe, 0.3%; Al, 0.3%) (Thevannan et al. 2010). C, H, N, and S determined in this work were the major elements of the aforementioned organic components.

Table 4.5 The elemental analysis and BET surface area of RBS and PBS.

Adsorbent	H_3PO_4, (*w/v*)	MV time, min	Elemental analysis, *wt*%				BET surfaces area, m^2/g
			C	H	N	S	
RBS	0	0	42.0 ± 0.2	5.9 ± 0.3	1.5 ± 0.1	0.2 ± 0.1	2
PBS1	5%	8	68.1 ± 0.2	1.9 ± 0.2	1.9 ± 0.0	0.1 ± 0.0	1166
PBS2	5%	9	68.9 ± 0.4	1.7 ± 0.2	2.1 ± 0.0	0.1 ± 0.0	1314 ± 10
PBS3	5%	10	65.0 ± 0.0	1.9 ± 0.1	2.2 ± 0.0	0.1 ± 0.0	1189
PBS4	15%	9	63.8 ± 1.0	2.4 ± 0.1	1.0 ± 0.0	0.1 ± 0.0	1145
PBS5	25%	9	60.5 ± 0.2	3.3 ± 0.0	0.6 ± 0.4	0.0 ± 0.0	105

Compared with RBS, the carbon content of PBS increased as impregnated by a 5% (*w/v*) H_3PO_4 solution. However, further increase of H_3PO_4 concentration decreased the carbon content of PBS from (68.9 ± 0.4)% to (60.5 ± 0.2)%. In addition, the MW radiation time slightly affected the carbon contents of PBS in the tested range. The carbon content slightly increased from (68.1 ± 0.2)% to (68.9 ± 0.4)% as the MW radiation time was increased from 8 min to 9 min, then decreased to (65.0 ± 0.0)% with increase in the MW radiation time to 10 min. Thus heating time over 10 min is not favored. Moreover, the carbon content of PBS was found to be associated with the BET surface area: the higher the carbon content, the higher the BET surface area. As discussed before, the main organic constitutes of RBS were cellulose, hemicelluloses, and lignin, which are nearly 78% of the total weight of RBS and contain function groups such as -C=C-, $-CH_2OH$, and -OH. It has been considered that H_3PO_4 may promote dehydration and condensation reactions in celluloses, hemicelluloses, and lignin (Jagtoyen and Derbyshire 1998).

4.2.3 Thermogravimetric Analysis

To investigate the effect of H_3PO_4 on devolatilizing barley straw, thermogravimetric analysis (TGA) was done on barley straw with and without 5% (*w/v*) H_3PO_4 impregnation. The results are illustrated in Figure 4.5. It's obvious that with the addition of H_3PO_4, the devolatilization temperature of barley straw greatly decreased compared with that of barley straw without H_3PO_4 impregnation. There were two steps observed in significant weight loss of barley straw impregnated by H_3PO_4. Step 1 was from 298.15 K to 523.15 K and step 2 was from 523.15 K to 723.15 K. The weight loss at 323.15 K can be explained by the loss of carboxyl and methyl groups from hemicelluloses as per the analysis of hardwoods by Jagtoyen, Derbyshire, and Solum (Jagtoyen and Derbyshire 1993, 1998, Solum et al. 1995). Substantial reactions of cellulose and formation of ketenes began at 373.15 K, which produced CO, CO_2, and CH_4 (as a result of the loss of aliphatic, carboxyl, and carbonyl groups). At higher temperatures (523.15-723.15 K), the weight of barley straw impregnated by H_3PO_4 sharply dropped. This could be attributed to that H_3PO_4 is an effective flame retardant for cellulose, and it can form ester linkage with -OH groups on cellulose (Katsuura and Inagaki 1975).

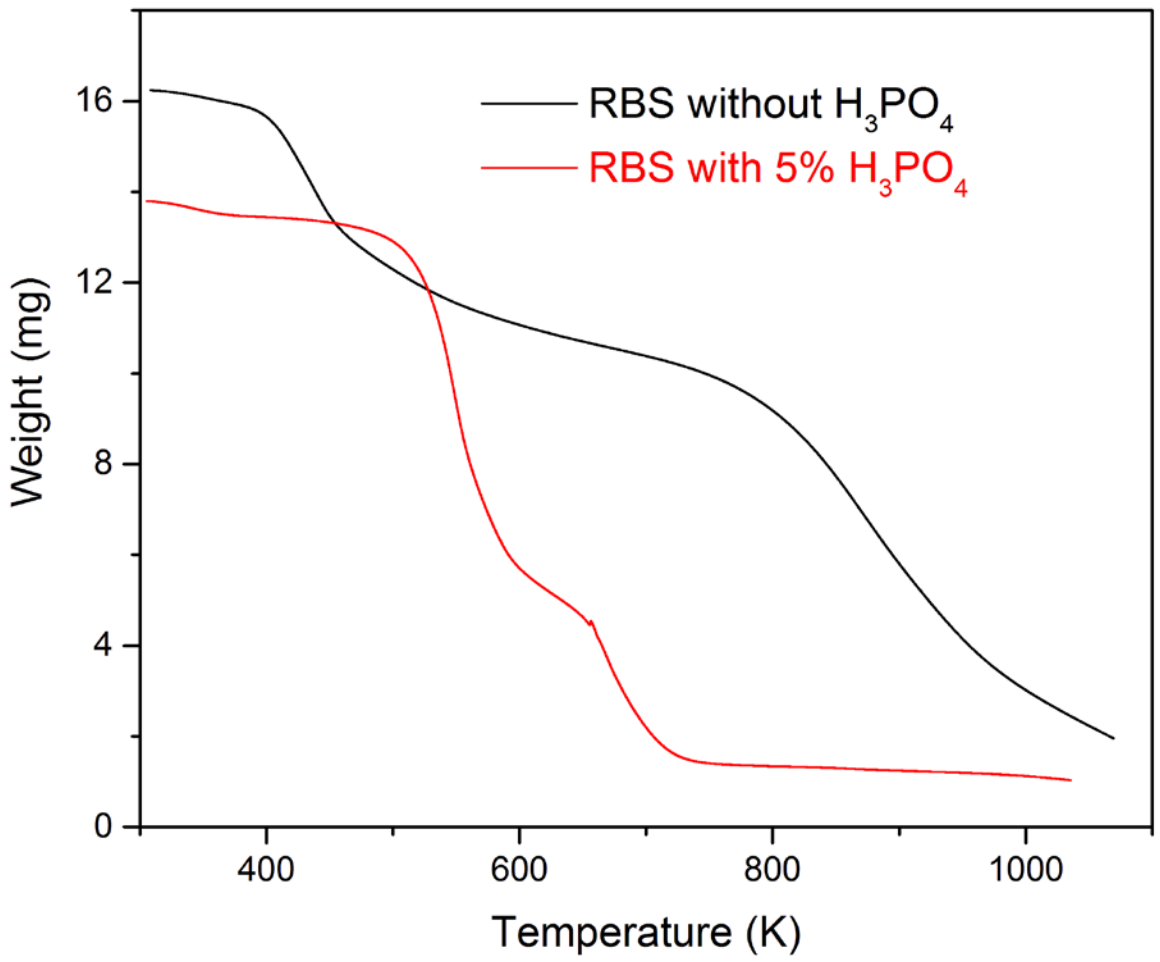

Figure 4.5 TGA analysis of barley straw with or without 5% (*w/v*) H_3PO_4 impregnation.

As these reactions proceeding, formation of micropore, mesopore, and macropore took place. An expansion process was driven by the formation of phosphate esters, which left the matrix in an expanded state with an accessible porous structure. H_3PO_4 may stabilize the structure of cellulose by inhibiting the formation of levoglucosan (Jagtoyen and Derbyshire 1998). In addition, the removal of carbon and light hydrocarbon gases (e.g., CO, CO_2, and CH_4) may also contribute the diverse porous structure of PBS.

4.3 Chapter Summary

PBS with a high surface area (1314 ± 10 m^2/g) and well-developed porous structure was made from RBS by 5% (*w/v*) H_3PO_4 impregnation and 9 min MW (700 W) heating. Moreover, the total organic carbon (TOC) released into suspensions from the adsorbents significantly

reduced from 34.4 ± 0.9 mg/g (RBS) to 0.9 ± 0.2 mg/g (PBS) indicating an enhanced stability of PBS. Both H_3PO_4 and MW radiation time played important roles on enhancing the surface area of PBS. The MRA modeling results demonstrated the high correlation between the surface area of PBS and the H_3PO_4 concentration and MW radiation time. The two factors also interacted with each other. With high value of R^2, the cubic polynomial model might be applied to predict the BET surface area of PBS at specific H_3PO_4 impregnation concentrations and MW radiation times. The obtained PBS was then characterized by multiple methods, such as particle size distribution, elemental compositions, SEM, and TGA analysis. The volume mean diameter of PBS was 316 μm, and the median was 251 μm. 10% of the population have a diameter smaller than 83 μm, and 90% have a diameter smaller than 651 μm. C 68.9%, H 1.7%, N 2.1%, and S 0.1% were the major elements of PBS. With the addition of H_3PO_4, the devolatilization temperature of barley straw greatly decreased compared with that of barley straw without H_3PO_4 impregnation.

In regards to consideration of sustainability, H_3PO_4 solution used in the impregnation of raw barley straw could be recycled and reused in the pretreatment of barley straw. In addition, continuing reducing the MW energy used in the pretreatment process could form an area of future research.

CHAPTER 5 ADSORPTION OF LEVOFLOXACIN ON PRETREATED BARLEY STRAW

Among the fluoroquinolone (FQ) antibiotics, levofloxacin (LEV) is a new kind but already widely used FQ antibiotic, which acts by inhibiting bacterial DNA gyrase enzyme required for DNA replication (Yamashita et al. 2006). Figure 5.1 shows the molecular structure and charge state of LEV (Sousa et al. 2012). In 2011, more than 55 tons of LEV were used for human medicine in the U.S., and it ranked second in the FQs' consumption (Food and Drug Administration 2012). However, LEV is not completely metabolized by humans and animals, nor can it be completely removed during wastewater treatment using current technologies, and eventually it is discharged into the environment. There is a need to effectively remove LEV from water bodies and streams to ensure the adequately treated effluent quality for various uses and to protect human health.

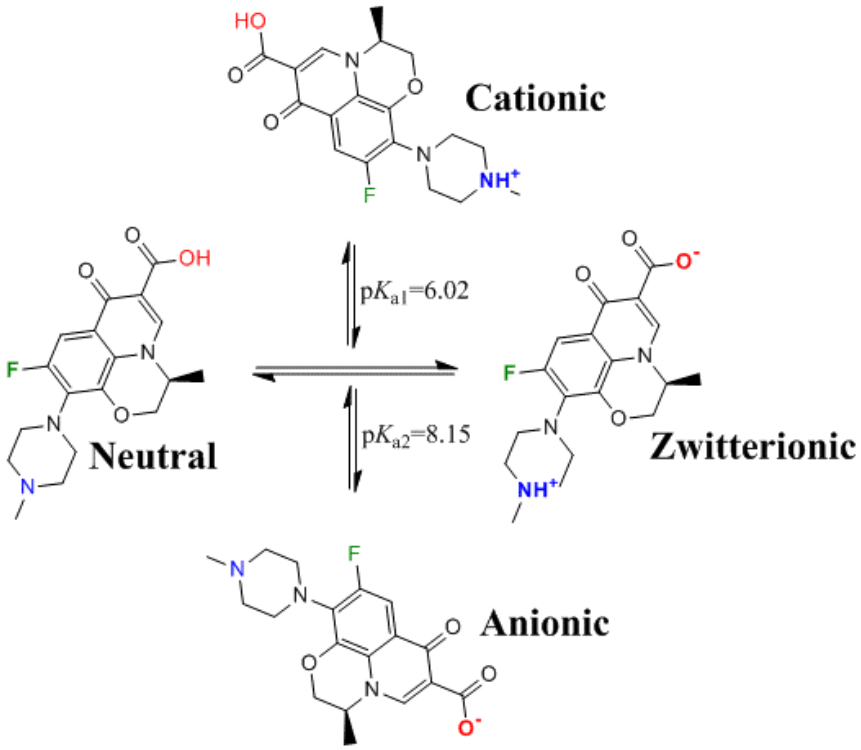

Figure 5.1 Molecular structure and pH-dependent speciation of LEV.

Adsorption has been proposed as one of the most effective technologies for removing contaminants from aquatic systems. In this chapter, the pretreated barley straw (PBS) was used as an adsorbent for LEV removal from the artificial wastewater at various solution pH and temperatures. The adsorption kinetics and equilibrium involved in the adsorption processes were investigated at different initial LEV concentrations, solution pH, and solution temperatures. The *Langmuir-Freundlich* model was applied to simulate the equilibrium LEV adsorption data. Site energy and its distribution function were determined to analyze the interaction strength between the adsorbent and adsorbate and to depict the adsorption site energetical heterogeneity. The electron-donor-acceptor (EDA) interactions between the aromatic groups (electron-donors) of PBS and the benzene rings (electron-acceptors) of LEV molecules were investigated with the aid of C *K*-edge X-ray absorption near-edge structure (XANES) spectroscopy.

5.1 Adsorption Kinetics

5.1.1 Effect of Contact Time

Adsorption kinetics is of importance to affect the adsorption. Figure 5.2 demonstrates the effect of contact time on LEV adsorption by PBS at different initial LEV concentrations. At all the tested conditions, a rapid adsorption of LEV was observed at the first 12 h, then a slower adsorption process followed until equilibrium was reached. The phenomenon was similar to that of LEV adsorption by iron-pillared montmorillonite (Liu et al. 2015). The initial rapid adsorption may be due to the fast surface adsorption, then followed by a slower internal diffusion. Moreover, at lower initial LEV concentrations of 10 mg/L and 20 mg/L, the equilibrium LEV adsorption capacities of PBS were achieved in 72 h, while at higher initial LEV concentrations of 40 mg/L and 100 mg/L, 168 h were required to reach the adsorption equilibrium. Therefore, 168 h was set as the contact time for isotherm studies.

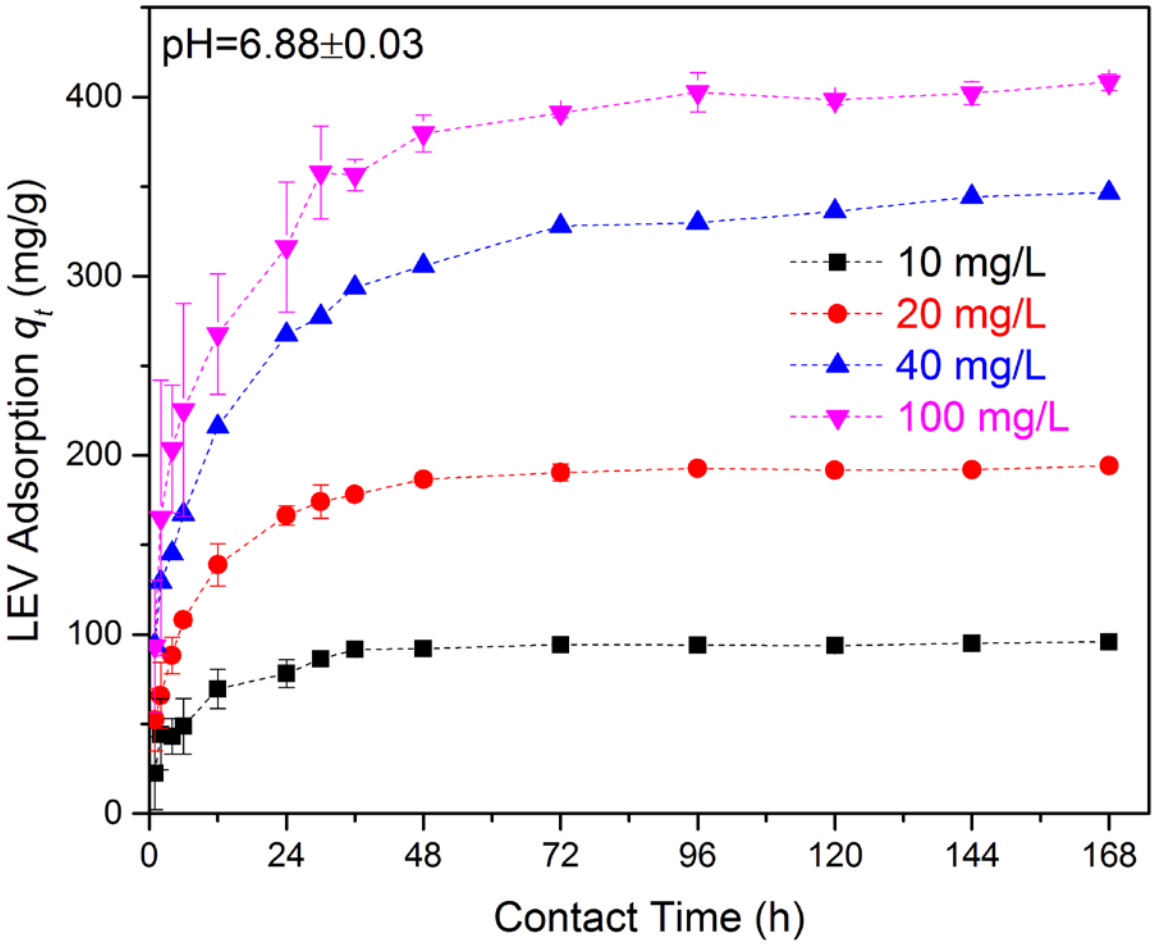

Figure 5.2 Effect of contact time on LEV adsorption by PBS.

50.0 ± 0.5 mL LEV solution, 5.0 ± 0.1 mg PBS, pH = 6.88 ± 0.03, and 298.15 ± 0.50 K. Error bars represent standard deviation.

In addition, as shown in Figure 5.3, at lower LEV concentrations of 10 mg/L and 20 mg/L (298.15 K), the values of removal ratio of LEV by PBS with reference to initial amount of LEV were determined to be 98% and 97%, respectively. When the LEV concentration was continuously increased to 40 mg/L and 100 mg/L, the values of removal ratio decreased to 88.68% (40 mg/L) and 40.13% (100 mg/L), while the equilibrium adsorption capacities (q_e) increased to 347 mg/g (40 mg/L) and 408 mg/g (100 mg/L). This indicated that the LEV removal efficiency highly depended on the initial LEV concentration if the rest conditions were kept constant.

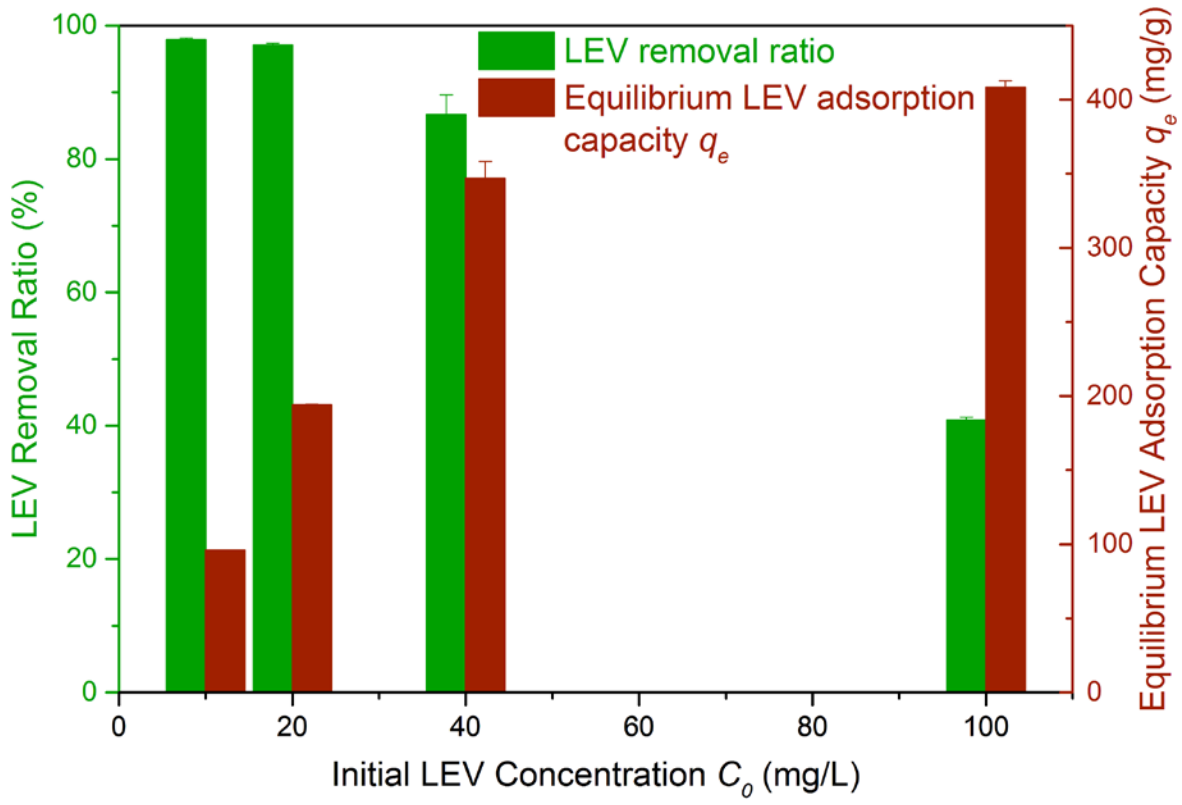

Figure 5.3 Equilibrium adsorption capacity q_e and removal ratio of LEV by PBS versus initial LEV concentration C_0.

50.0 ± 0.5 mL LEV solution, 5.0 ± 0.1 mg PBS, pH = 6.88 ± 0.03, and 298.15 ± 0.50 K. Error bars represent standard deviation.

5.1.2 Analysis of Activation Energy

To determine the activation energy of the adsorption of LEV on PBS, the adsorption kinetic experiments were conducted at different solution temperatures, and the kinetic data are plotted in Figure 5.4a. The results demonstrated that the adsorption rate of LEV on PBS and the equilibrium LEV adsorption capacity of PBS increased with increase in the temperature.

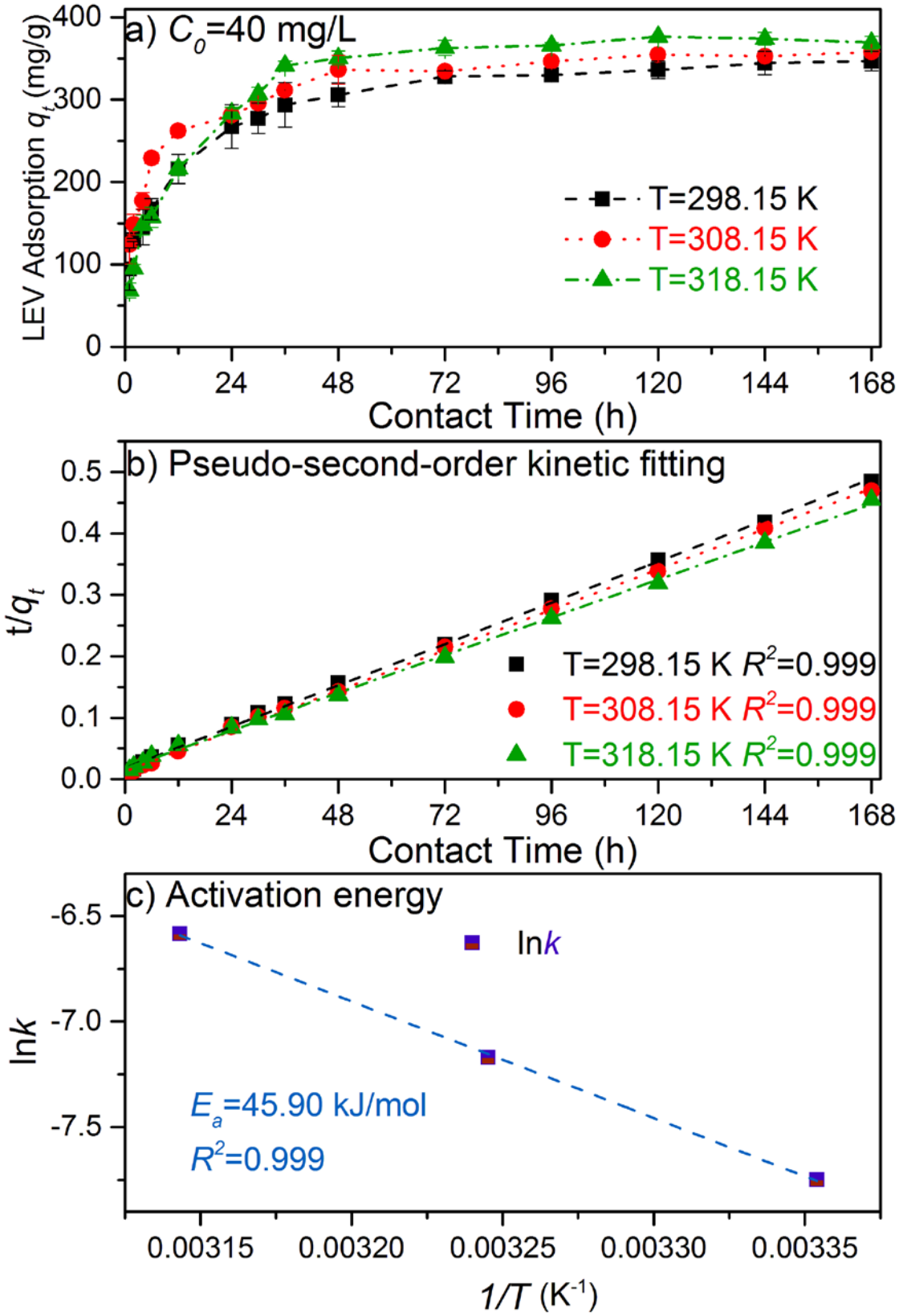

Figure 5.4 Kinetic analysis of LEV adsorption on PBS at different temperatures: a) effect of solution temperature; b) pseudo-second-order kinetic fitting; c) analysis of activation energy. 50.0 ± 0.5 mL LEV solution (C_0 = 40 mg/L), 5.0 ± 0.1 mg PBS, and pH 6.88 ± 0.03. Error bars represent standard deviation.

The pseudo-second-order kinetic model was used to fit the kinetic data obtained at different temperatures, and the corresponding fitting curves are displayed in Figure 5.4b. The fitting results along with corresponding values of coefficient of determination (R^2) and residual sum of square (*RSS*) were listed in Table 5.1. With high values of coefficient of determination (R^2>0.999), the obtained values of $q_{e,cal}$ and k at 298.15, 308.15, and 318.15 K were 357, 365, and 390 mg/g, and 4.31×10^{-4}, 7.70×10^{-4}, and 1.38×10^{-3} g/(mg·h), respectively. Furthermore, the initial rate of LEV adsorption on PBS (calculated from kq_e^2) was 55.04 mg/(g·h) (40 mg/L, pH 6.88, and 298.15 K). This may be due to the well-developed porous structure (revealed by the SEM image on page 59 and high specific surface area 1314 ± 10 m^2/g) and modified functional groups of PBS. Moreover, the initial rate of LEV adsorbed on PBS increased from 55.04 mg/(g·h) to 102.56 and 210.97 mg/(g·h) as the temperature was increased from 298.15 K to 308.15 and 318.15 K (40 mg/L and pH 6.88). Temperature may affect the adsorption kinetics: 1) the adsorption driving force $(q_e - q_t)$ increased due to the increase of equilibrium adsorption capacity q_e with increasing temperature; 2) the adsorption rate constant k increased as the temperature was increased. The influence of the temperature on adsorption rate constant k can be quantified by the *Arrhenius* equation.

Table 5.1 Kinetic parameters for the adsorption of LEV on PBS

Experimental			Pseudo-second-order kinetic model			
T, K	C_0, mg/L	q_e, mg/g	$q_{e,cal}$, mg/g	k, g/(mg·h)	R^2	*RSS**, $(mg/g)^2$
298.15	40	347	357	4.31×10^{-4}	0.999	5249
308.15	40	358	365	7.70×10^{-4}	0.999	5784
318.15	40	369	390	1.38×10^{-3}	0.999	77961

* *RSS* residual sum of squares, $(mg/g)^2$

The linearized *Arrhenius* equation (Eq. (2.3), Chapter 2, and page 33) was used to determine the activation energy (Figure 5.4c), which was 45.9 kJ/mol. The energy of activation for a physical adsorption is usually no more than 1 kcal/mol (equivalent to 4.2 kJ/mol). The obtained value of activation energy 45.9 kJ/mol in this work suggested that LEV was primarily adsorbed on PBS via chemical adsorption (Smith 1970, Unuabonah et al. 2007).

5.2 Adsorption Equilibrium

5.2.1 Effect of Solution pH

5.2.1.1 Levofloxacin Equilibrium Adsorption on Pretreated Barley Straw in a Wide Range of Solution pH

It is well known that solution pH affects the charge state of adsorbent and the speciation of adsorbate, therefore the adsorption process. The effect of solution pH on LEV adsorption was examined by varying the pH from 2.47 ± 0.05 to 9.60 ± 0.05 (final pH) at an initial LEV concentration 40 mg/L and 298.15 ± 0.50 K. Figure 5.5 shows that as solution pH was increased from 2.47 ± 0.05 to 6.88 ± 0.03, LEV adsorption increased, then decreased when solution pH was continuously increased to 9.60 ± 0.05. However, the difference of equilibrium LEV adsorption capacities of PBS at different pH was not significant, and all of the q_e values were above 294 mg/g (pH = 2.47 ± 0.05). The results demonstrated its broad applicability in a wide range of solution pH. Among the tested pH values, pH 6.88 ± 0.03 had the highest value of q_e (347 ± 12 mg/g). Thus, such pH value was chosen as the equilibrium solution pH for isotherm studies.

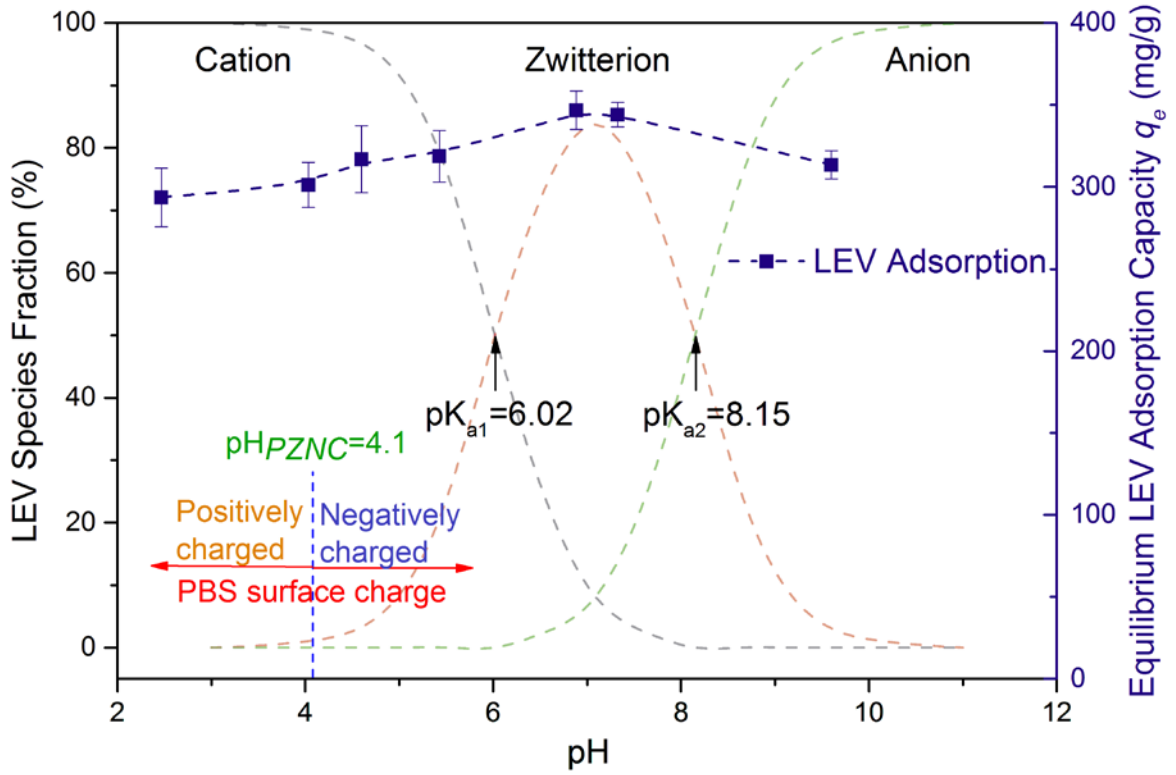

Figure 5.5 Effect of solution pH on LEV adsorption by PBS.

50.0 ± 0.5 mL, 40 mg/L LEV solution, 5.0 ± 0.1 mg PBS, contact time 168 h, and 298.15 ± 0.50 K. Error bars represent the standard deviation.

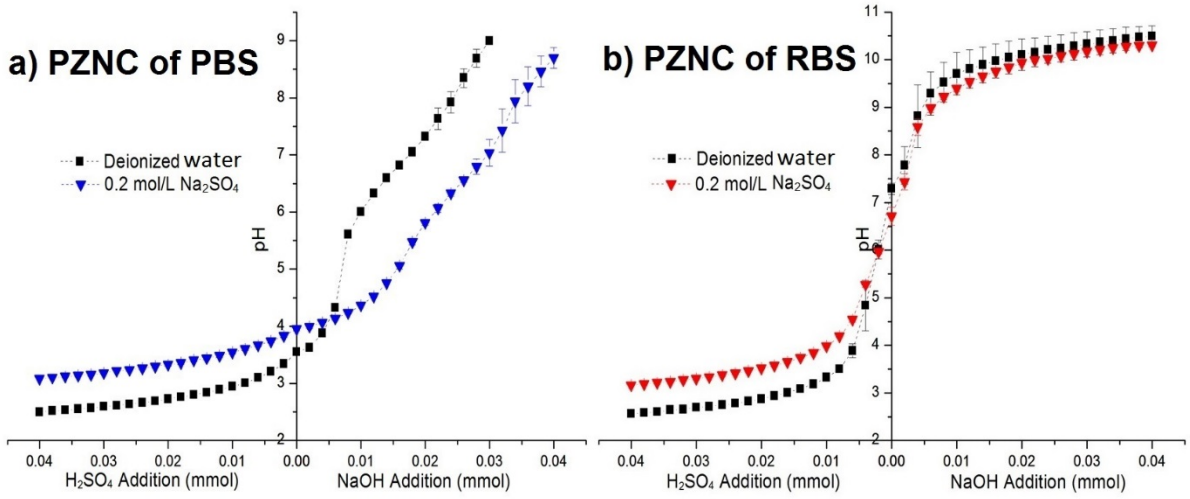

Figure 5.6 Determination of point of zero net charge of PBS and RBS.

20.0 ± 0.2 mL solution, 40 ± 2 mg PBS or RBS, contact time 24 h, and 298.15 ± 0.50 K. Error bars represent the standard deviation.

According to method mentioned in the Section of 3.3, the PZNC values of PBS and RBS were determined to be 4.10 and 5.90 (Figure 5.6), respectively. As solution pH was lower than

4.10, PBS was positively charged, otherwise negatively charged (pH > 4.10). In addition, LEV had two values of dissociation constant via its tertiary amine group (pK_{a2} = 8.15) and carboxyl group (pK_{a1} = 6.02), and it can be positively charged (pH < 6.02), negatively charged (pH > 8.15) and zwitterionic (pH 6.02-8.15) (Sousa et al. 2012). As shown in Figure 5.5, at pH 4.10-6.02, LEV had more positively charged groups than negatively charged groups, while PBS was negatively charged. LEV cations could be bonded to PBS via electrostatic attraction. As a result, LEV adsorption increased as solution pH was increased. Thus, electrostatic attraction was expected to play a role in the adsorption process.

LEV molecules and PBS surface had the same net charge and could repel each other at a pH < 4.10 and pH > 8.15. If the pH-dependent electrostatic attraction was the major mechanism, adsorption of LEV on PBS was expected to be significantly depressed. However, the q_e values at the acidic pH 2.47 and basic pH 9.60 were 294 mg/g and 314 mg/g, respectively, and the variation of LEV adsorption capacity in the pH range (2.47-9.60) was less than 15.3% using the highest q_e value achieved at pH 6.88 as a reference. It indicated that the pH-dependent electrostatic interaction between LEV and PBS influenced the adsorption process of LEV on PBS, but it may not be the principal mechanism. Other adsorption mechanism could be the dominant one.

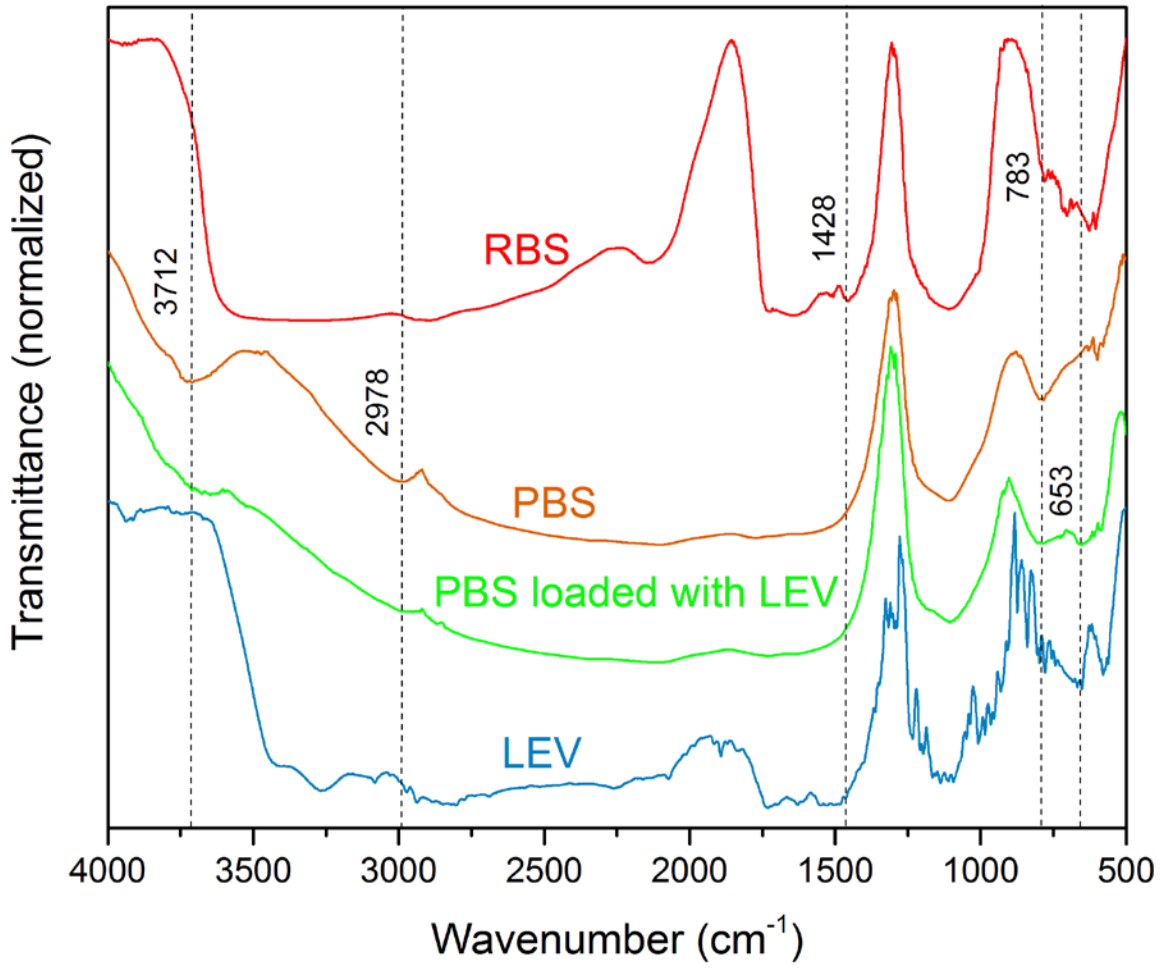

Figure 5.7 FTIR spectra of RBS, PBS, LEV, and PBS loaded with LEV (q_e = 347 ± 12 mg/g).

The FTIR measurements were performed for RBS, PBS, LEV, and PBS loaded with LEV, and the corresponding spectra are presented in Figure 5.7. The peak at 653 cm^{-1} on the spectrum of LEV could be attributed to the aromatic C-H bending of LEV, and it again appeared on the spectrum of PBS loaded with LEV, which indicated that LEV was successfully adsorbed by PBS. In addition, the peak at 783 cm^{-1} which can also be attributed to aromatic C-H bending (Pawlak and Pawlak 1997) appeared on the spectra of RBS, PBS, LEV, and PBS loaded with LEV. RBS contains lignin which has aromatic groups. After the pretreatment, such groups still existed. LEV also has a benzene ring as shown in Figure 5.1. Furthermore, the peak at 1428 cm^{-1} for C-H deformation on the spectrum of RBS disappeared on that of PBS and PBS loaded

with LEV. PBS was made from RBS by phosphoric acid impregnation with heating. Some of the C-H bond of RBS may be oxidized thus the peak was invisible on the spectrum of PBS.

It was also observed that a trough with an approximate centre at 2978 cm^{-1} for carboxylic O-H bond stretching appeared on the spectrum of PBS, which indicated that carboxyl groups were created on PBS. This may explain the decrease of PZNC from 5.9 (RBS) to 4.1 (PBS). Furthermore, a broad trough with an approximate centre at 3712 cm^{-1} for O-H stretching also appeared on the spectrum of PBS implying that hydroxyl groups existed on PBS. The intensity of the aforementioned two troughs representing carboxyl and hydroxyl groups reduced on the spectrum of PBS loaded with LEV, which indicated that these groups may participate in the binding of PBS and LEV.

The carboxyl groups ($-COO^-$) and hydroxyl groups ($-O^-$) on adsorbent surface have been considered to serve as strong *n*-electron-donors (Chen et al. 2008, Qu et al. 2008). In addition, the aromatic rings on adsorbent surface could also work as strong π-electron-donors as the number of associated rings increased (Keiluweit and Kleber 2009). The benzene ring of LEV can function as a π-electron-acceptor due to the strong electron withdrawing ability of the fluorine group (Keiluweit and Kleber 2009, Wang et al. 2010c). Thus, the benzene ring of LEV, and the carboxyl, hydroxyl, and aromatic groups of PBS revealed by the FTIR spectra may build the *n*-π and π-π electron-donor-acceptor (EDA) pairs. EDA interactions could be one of the predominant mechanisms for LEV adsorption on PBS. The type of bonds was not significantly affected by moderate solution pH, and may explain the significantly high LEV adsorption capacity of PBS in a wide range of solution pH (2.47-9.60). A similar mechanism has been reported in the analysis of NOR adsorption on carbon nanotubes (Wang et al. 2010c). The occurrence of EDA interactions was further investigated in the Section of 5.5.

Because of the existence of carboxyl and hydroxyl groups on PBS, PBS surface and LEV molecules may be charged dependent on the solution pH, as shown in Figure 5.5. As a result,

electrostatic attraction between the aforementioned functional groups on PBS and LEV molecules could be another adsorption mechanism, which was confirmed by the effect of pH on LEV adsorption capacity of PBS. However, the contribution of such mechanism may not be the major one since the effect of solution pH on LEV adsorption capacity was insignificant.

Furthermore, the surface oxygen-containing functional groups including -OH and -COOH of PBS might form hydrogen bonds (H-bonds) with C=O and O-H groups of LEV molecule (Hickey and Passino-Reader 1991), which might be supported by the fact that the intensity of the two troughs representing carboxyl and hydroxyl groups on the FTIR spectrum of PBS reduced after the adsorption of LEV. H-bonds have been reported in the adsorption of norfloxacin (Wang et al. 2010c) and substituted aromatics by carbon nanotube (Lin and Xing 2008) and the adsorption of aromatic compounds on soil (Zhu et al. 2004). In the study of aromatic compounds adsorption on soil, solution pH was found having more significant effect on adsorption of 2-nonanol and 2-nonanone on soil, the lower the value of solution pH, the lower the adsorption capacity (Zhu et al. 2004). Clearly, further study is required to evaluate the importance of hydrogen bond in the LEV-PBS adsorption process, although H-bond was reported as an insignificant role for the adsorption of substituted aromatics and carbon nanotubes (Lin and Xing 2008).

5.2.1.2 Levofloxacin Adsorption Isotherms at Various Solution pH

The experimentally obtained LEV adsorption isotherms of PBS at pH values of 4.03 ± 0.02, 6.88 ± 0.03, and 9.63 ± 0.09 are presented in Figure 5.8. Again, it was confirmed that the equilibrium capacity at pH 6.88 was superior to those achieved at acidic or basic pH values. The *Langmuir-Freundlich* model (Eq. (2.4), Chapter 2, and page 34) was used to simulate the adsorption isotherms, and the fitting results are given in Table 5.2. The *Langmuir-Freundlich* model successfully described the LEV equilibrium data with high values of coefficient of determination R^2. The obtained values of q_m, b, and n at pH 6.88, 4.03, and 9.63 were 417, 414,

and 384 mg/g, 1.10, 0.57, and 0.67 L/mg, and 1.04, 0.78, and 0.86, respectively. It has been reported that the *n* value is indicative of the surface site heterogeneity of the adsorbent, and the lower the value of "*n*", the stronger the heterogeneity (Cerofolini and Rudziński 1997). Therefore, such *n* values demonstrated a weaker heterogeneity at the neutral pH, which was further discussed in the later analysis of adsorption site energy distribution.

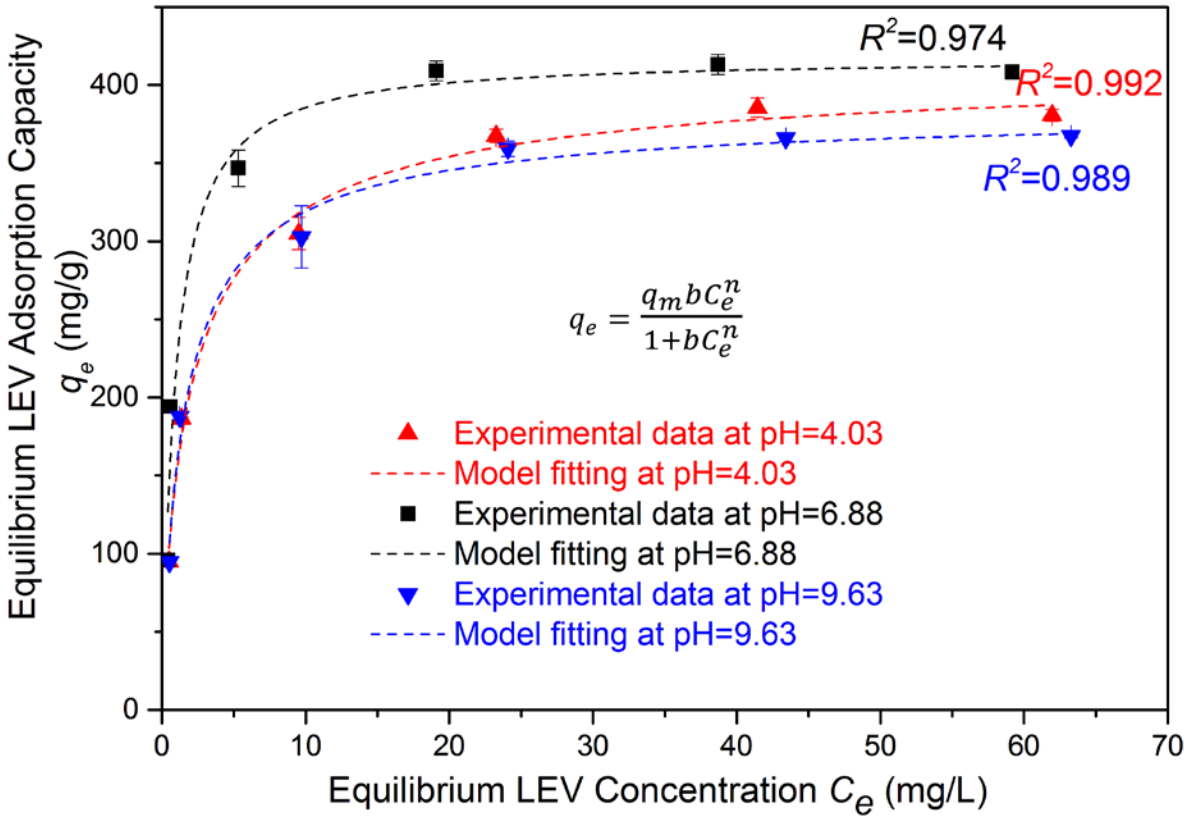

Figure 5.8 LEV adsorption isotherms of PBS at different solution pH.

50.0 ± 0.5 mL LEV solution, 5.0 ± 0.1 mg PBS, IS<0.02 M, and 298.15 ± 0.50 K. Error bars represent standard deviation.

Table 5.2 Fitting results of the LEV adsorption on PBS at different solution pH.

Temperature, K	pH	*Langmuir-Freundlich* model				
		q_m, mg/g	b, L/mg	n	R^2	RSS, $(mg/g)^2$
298.15 ± 0.50	4.03 ± 0.02	414 ± 24	0.57 ± 0.07	0.78 ± 0.13	0.992	548
298.15 ± 0.50	6.88 ± 0.03	417 ± 25	1.10 ± 0.36	1.04 ± 0.33	0.974	2525
298.15 ± 0.50	9.63 ± 0.09	384 ± 21	0.67 ± 0.11	0.86 ± 0.18	0.989	711

5.2.1.3 Approximate Site Energy and Its Distribution

The site energy E^* was calculated by Eq. (2.9) (Chapter 2 and page 35) and plotted as a function of the equilibrium LEV adsorption capacity in Figure 5.9. It can be seen that E^* dramatically decreased for all solution pH as LEV loading increased, revealing that LEV molecules first occupied the high-energy adsorption sites on PBS at low concentrations, then spread to the low-energy adsorption sites, which was similar to the adsorption of norfloxacin on carbon nanotubes (Wang et al. 2010c). Furthermore, the site energies of PBS obtained in this work were higher than those of the reported adsorbents for organic compounds such as norfloxacin (Wang et al. 2010c), naphthalene and lindane (Shen et al. 2015). Such results indicated that PBS might have a higher adsorption affinity for organic compounds than the reported adsorbents.

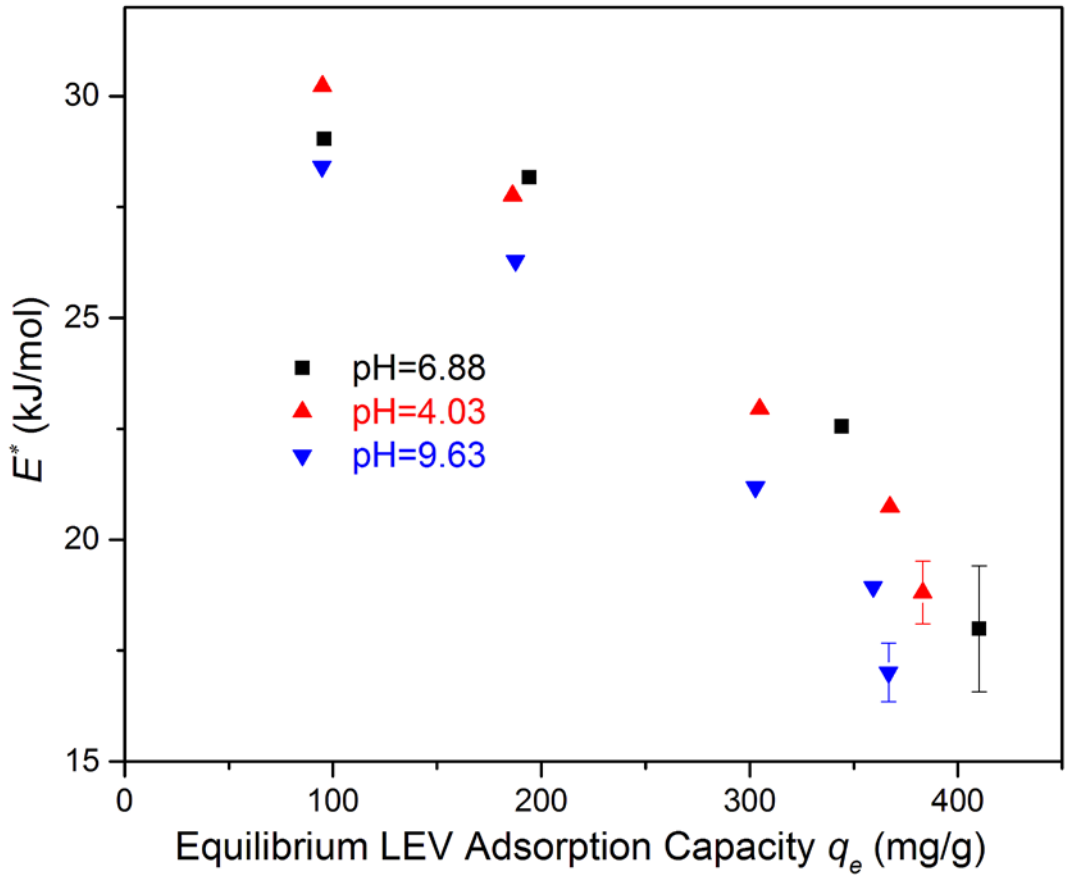

Figure 5.9 Dependence of site energy on LEV loading at different solution pH.
50.0 ± 0.5 mL LEV solution, 5.0 ± 0.1 mg PBS, and 298.15 ± 0.50 K. Error bars represent strand deviation.

The site energy distribution based on the *Langmuir-Freundlich* model (Eq. (2.4), Chapter 2, and page 34) of PBS for LEV adsorption at different pH values are illustrated in Figure 5.10. As given in Eq. (2.13) (Chapter 2 and page 36), the area under the site energy distribution curve can be interpreted as the maximum LEV adsorption capability. Thus, PBS demonstrated a higher LEV adsorption capacity at pH 6.88 than that at pH 4.03 and pH 9.63, which was confirmed by the experimental LEV adsorption data. In addition, the distributions at pH 4.03 and 9.63 were wider than that at pH 6.88.

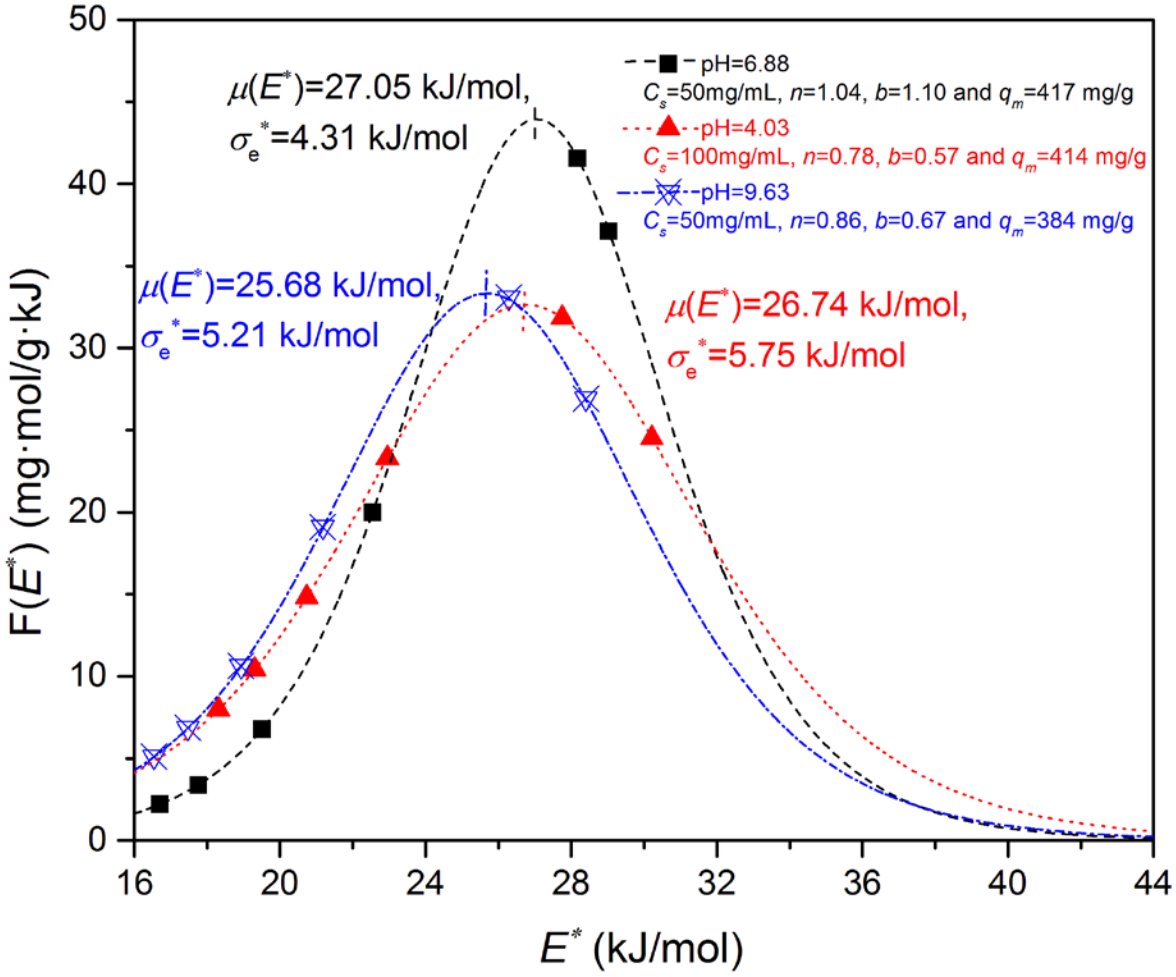

Figure 5.10 Site energy distributions of PBS for LEV adsorption at different solution pH. 50.0 ± 0.5 mL LEV solution, 5.0 ± 0.1 mg PBS, and 298.15 ± 0.50 K.

In order to make further analysis of the distribution, the weighted mean of site energy distribution and surface energy heterogeneity of PBS at the tested pH values were determined. It has been reported that the weighted mean of the distribution can be used to depict the interaction strength between the adsorbent (PBS) and adsorbate (LEV), and the width of the site energy distribution can be employed to describe the surface energetical heterogeneity of the adsorbent (Carter et al. 1995).

The value of weighted mean $\mu(E^*)$ of the distribution was calculated from Eq. (2.16) (Chapter 2 and page 36) and given in Figure 5.10 as well. Such value was used as a measure of the adsorption affinity of the adsorbent surface for the adsorbate. The higher the value of the

weighted mean, the stronger the adsorption affinity (Carter et al. 1995). The LEV adsorption on PBS at pH 6.88 had a slightly higher weighted mean (27.05 kJ/mol) than that at pH 4.03 (26.74 kJ/mol) and 9.63 (25.68 kJ/mol). Such higher weighted mean indicated the slightly stronger adsorption affinity, thus pH 6.88 was more favorable for LEV adsorption than pH 4.03 and 9.63. The slightly weighted mean reduction of PBS induced by the change of solution pH may result from the following mechanisms. The proposed electron-donor-acceptor (EDA) interactions between the benzene ring of LEV (electron-acceptor) and the aromatic, carboxyl and hydroxyl groups (electron-donors) of PBS may dominant the adsorption (Hunter et al. 2001, Hunter and Sanders 1990, Keiluweit and Kleber 2009, Shen et al. 2015). In spite of that, at pH < 4.10 and pH > 8.15, LEV molecules and PBS surface had the same sign of charge and could repel each other, which may slightly offset the EDA interactions. Furthermore, the adsorbed LEV molecules and free LEV molecules in solution also had the same sign of charge and could repel each other, which was slightly unfavorable for the adsorption of LEV on PBS. However, the effect of electric charge was not significant in the process because the values of weighted mean at the various pH were close.

Moreover, heterogeneous adsorption sites were formed on carbonaceous materials due to the diverse structure and chemical composition (Shi et al. 2011, Yoon et al. 2006). As the occurring frequency of the available adsorption sites with specific energies were described by the site energy distribution curve, the energetical heterogeneity of the adsorbent can be characterized by the standard deviation σ_e^* of site energy distribution (Shen et al. 2015). The values of standard deviation σ_e^* were calculated from Eq. (2.19) (Chapter 2 and page 37) and given in Figure 5.10. The adsorbent PBS demonstrated site energy heterogeneity for LEV adsorption at the tested three pH. PBS contained various functional groups such as aromatic, carboxyl, hydroxyl, and other oxygen-containing groups that may consequently contribute to the adsorption site energy heterogeneity. The results showed that σ_e^* increased from 4.31

kJ/mol to 5.21 and 5.75 kJ/mol when solution pH was changed from 6.88 to 4.03 and 9.63, respectively. The higher standard deviations at pH of 4.03 and 9.63 indicated higher degrees of heterogeneity, which were consistent to the *n* values from the *Langmuir-Freundlich* fitting. At the two pH values, functional groups on the adsorbent such as carboxyl and hydroxyl groups could be charged positively or negatively, which may vary the adsorption site energy. However, as mentioned before, the weighted mean of the distributions at either of the two pH values was slightly lower than that of pH 6.88, thus the LEV adsorption decreased. Clearly, the effect of solution pH on the adsorption site energy distribution needs to be further investigated.

5.2.2 Effect of Solution Temperature

As a critical environment parameter, temperature influences the adsorption process. Systematic study on the characteristics of LEV adsorption process including isotherms and adsorption energy with respect to temperature has been done in this section. The respective knowledge is important for understanding the mechanisms of LEV adsorption by PBS, and for the application of this technology in treating the water contaminated by LEV, FQs, or the like.

5.2.2.1 Levofloxacin Adsorption Isotherms at Different Solution Temperatures

The LEV adsorption isotherms of PBS at 298.15, 308.15, and 308.15 K are illustrated in Figure 5.11. The equilibrium LEV adsorption capacities of PBS increased as the temperature was increased, which revealed that the adsorption of LEV on PBS was an endothermic process. This was consistent with the adsorption of norfloxacin on carbon nanotubes (Wang et al. 2010c). The *Langmuir-Freundlich* isotherm model (Eq. (2.4), Chapter 2, and page 34) successfully fitted the LEV equilibrium data with high values of R^2, as given in Table 5.3. The obtained values of q_m, b, and n at 298.15, 308.15, and 318.15 K were 417, 437, and 448 mg/g, 1.10, 1.17, and 1.50 L/mg, and 1.04, 1.03, and 1.12, respectively. As mentioned in the Section of 5.2.1.2, the *n* value is indicative of the surface site heterogeneity of the adsorbent. The values of *n*

obtained at different temperatures were similar and therefore indicated the similar heterogeneity at the tested temperatures.

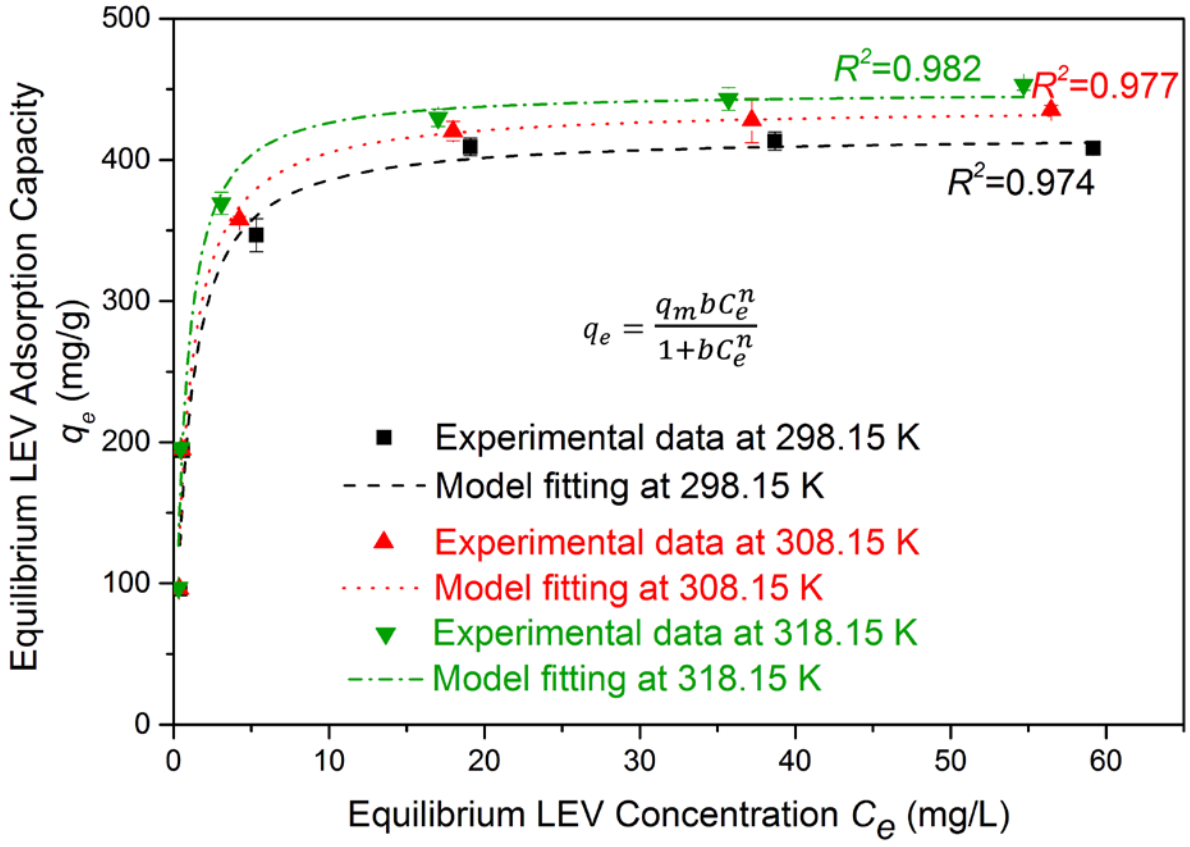

Figure 5.11 LEV adsorption isotherms of PBS at different temperatures.

50.0 ± 0.5 mL LEV solution, 5.0 ± 0.1 mg PBS, and pH 6.88 ± 0.03. Error bars represent standard deviation.

Table 5.3 Fitting results of the *Langmuir-Freundlich* model for LEV adsorption on PBS

Temperature, K	q_m, mg/g	b, L/mg	n	R^2	*RSS*, $(mg/g)^2$
298.15 ± 0.50	417 ± 25	1.10 ± 0.36	1.04 ± 0.33	0.974	2525
308.15 ± 0.50	437 ± 24	1.17 ± 0.36	1.03 ± 0.28	0.977	2351
318.15 ± 0.50	448 ± 20	1.50 ± 0.45	1.12 ± 0.25	0.982	1970

5.2.2.2 Approximate Site Energy and Its Distribution

Estimation of site energy and its distribution of the adsorbent for the target molecule is critical to elucidate the adsorption mechanism. Based on Eq. (2.9) (Chapter 2 and page 35), the site energy E^* was determined and plotted as a function of the equilibrium LEV adsorption capacity at different temperatures in Figure 5.12. As the amount of LEV adsorbed on PBS increased, the E^* dramatically decreased. This again indicated that the high-energy adsorption sites on PBS were first occupied by LEV molecules, and then the low-energy adsorption sites. The result was consistent to the adsorption of NOR on carbon nanotubes (Wang et al. 2010c).

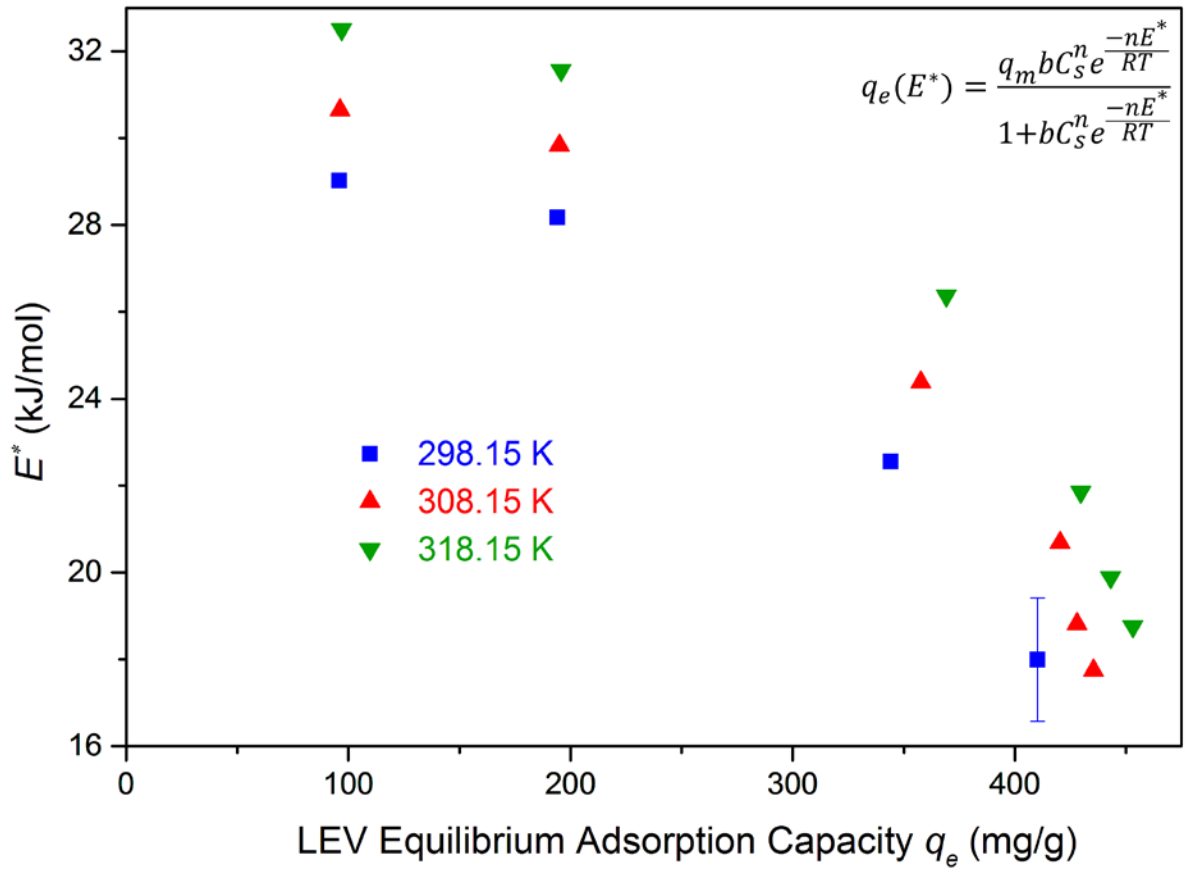

Figure 5.12 Dependence of site energy on LEV loading at different solution temperatures. 50.0 ± 0.5 mL LEV solution, 5.0 ± 0.1 mg PBS, and pH 6.88 ± 0.03. Error bars represent standard deviation.

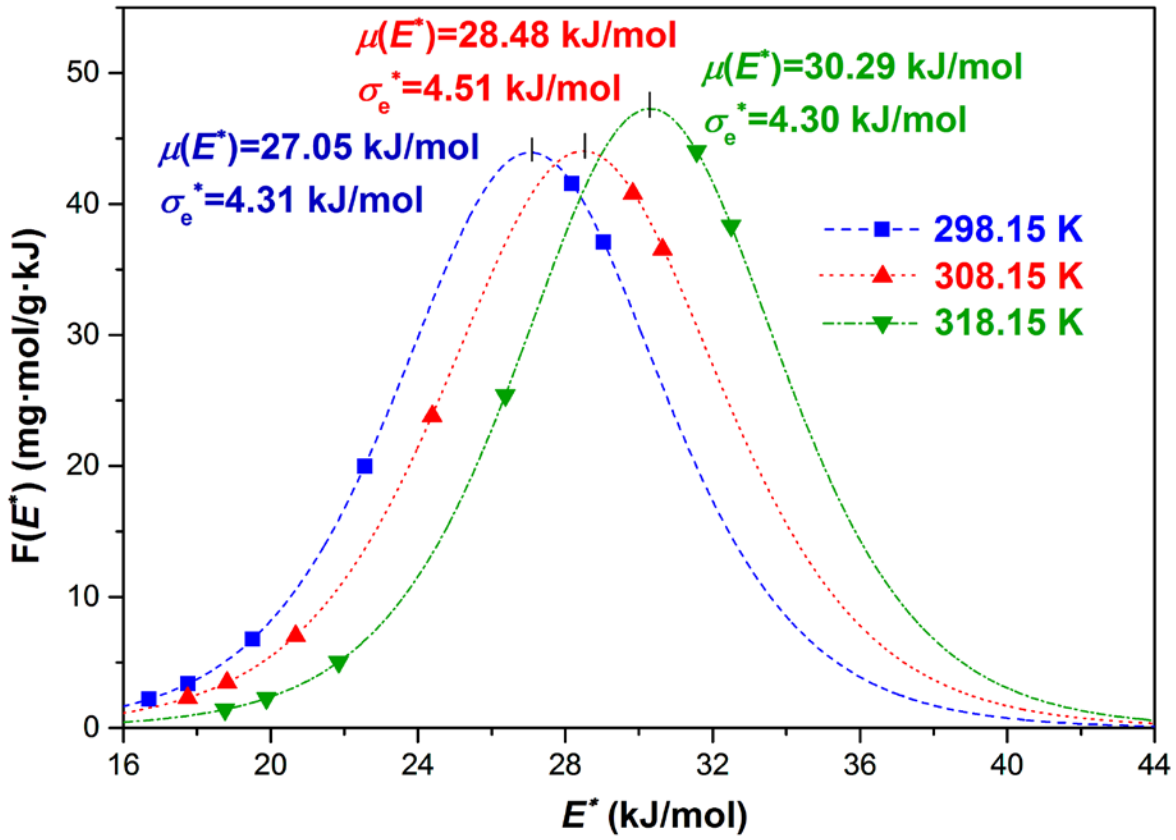

Figure 5.13 Site energy distributions of PBS for LEV adsorption at different solution temperatures.

50.0 ± 0.5 mL LEV solution, 5.0 ± 0.1 mg PBS, and pH 6.88 ± 0.03.

The site energy distributions of PBS for LEV adsorption based on the *Langmuir-Freundlich* model at different temperatures were determined and plotted in Figure 5.13. It has been reported that the higher the weighted mean of the distribution, the stronger the adsorption affinity (Carter et al. 1995). The LEV adsorption on PBS at 318.15 K had a slightly higher weighted mean $\mu(E^*)$ (30.29 kJ/mol) than that at 298.15 (27.05 kJ/mol) and 308.15 K (28.48 kJ/mol), which indicated a slightly stronger adsorption affinity, therefore, 318.15 K was more favorable for the adsorption reaction. The weighted mean diversification of PBS induced by the change of solution temperature can be explained as follows. EDA interaction was proposed as one of the major forces for LEV adsorption on PBS. They were polar interactions and based on the attractive force between electron-rich (donor) and electron-deficient (acceptor) entities. In this work, electron-rich aromatic π-system (PBS) served as π-electron-donor, and electron-

deficient π-system (LEV) worked as π-electron-acceptor. Increasing temperature increased the static dipole polarizability (Adam et al. 2013, Blundell et al. 2000), which led to the stronger EDA pair between the adsorbent (PBS) and adsorbate (LEV), therefore, the corresponding adsorption affinity (e.g., π-π EDA interaction) was enhanced. Such enhanced adsorption affinity was reflected by the slight increase in the weighted mean as the temperature was increased. The occurrence of EDA interactions was further discussed in the following Section of 5.5.

The energetical heterogeneity of PBS at 298.15, 308.15, and 318.15 K was evaluated by the standard deviation (σ_e^*) of site energy distribution, which were 4.31, 4.51, and 4.30 kJ/mol, respectively. Generally, the heterogeneity of adsorption sites for carbonaceous adsorbents originated from the defect structures, as well as the cross-linking and disordered arrangement of the diverse carbon structures. The heterogeneous adsorption sites of graphitized carbons for organic pollutants have been attributed to these aspects (McDermott and McCreery 1994, McDermott et al. 1993, Milewska-Duda and Duda 1997). The heterogeneity of adsorption sites could also be derived from the grafted functional groups (chemical composition heterogeneity), especially oxygen-containing functional groups (Yoon et al. 2006). In this work, PBS was made from RBS with H_3PO_4 impregnation and microwave heating. The oxygen-containing functional groups, such as -COOH and -OH, were induced to PBS (evidenced by the FTIR spectrum of PBS displayed in Figure 5.7). The BET surface area of PBS was measured to be 1314 ± 10 m^2/g, among which there were 750 ± 3 m^2 micropore/g, 284 ± 3 m^2 mesopore/g, and 280 ± 5 m^2 macropore/g (presented in the Chapter of 4 on page 55). The SEM results also revealed that PBS had a well-developed porous structure with cracks, channels, and holes (displayed in the Chapter of 4 on page 59). Thus, the specific structure and induced functional groups contributed to the energetical heterogeneity of PBS. The values of σ_e^* obtained at the tested three temperatures were very similar, so were the values of *n* obtained from the

Langmuir-Freundlich model. Both the values of n and σ_e^* demonstrated the consistent result that the heterogeneity of the PBS surface was similar in the tested temperature range.

5.3 Effect of Solution Ionic Strength

To investigate the effect of solution ionic strength (IS) on LEV adsorption by PBS, sodium chloride was added into the LEV solution at a pH of 6.88 ± 0.03 that was determined to be optimal as per the above results. As the background electrolyte, sodium widely existed in wastewater, and it is also an alkaline light metal with much low affinity for organic compounds (Muzzarelli 1973).

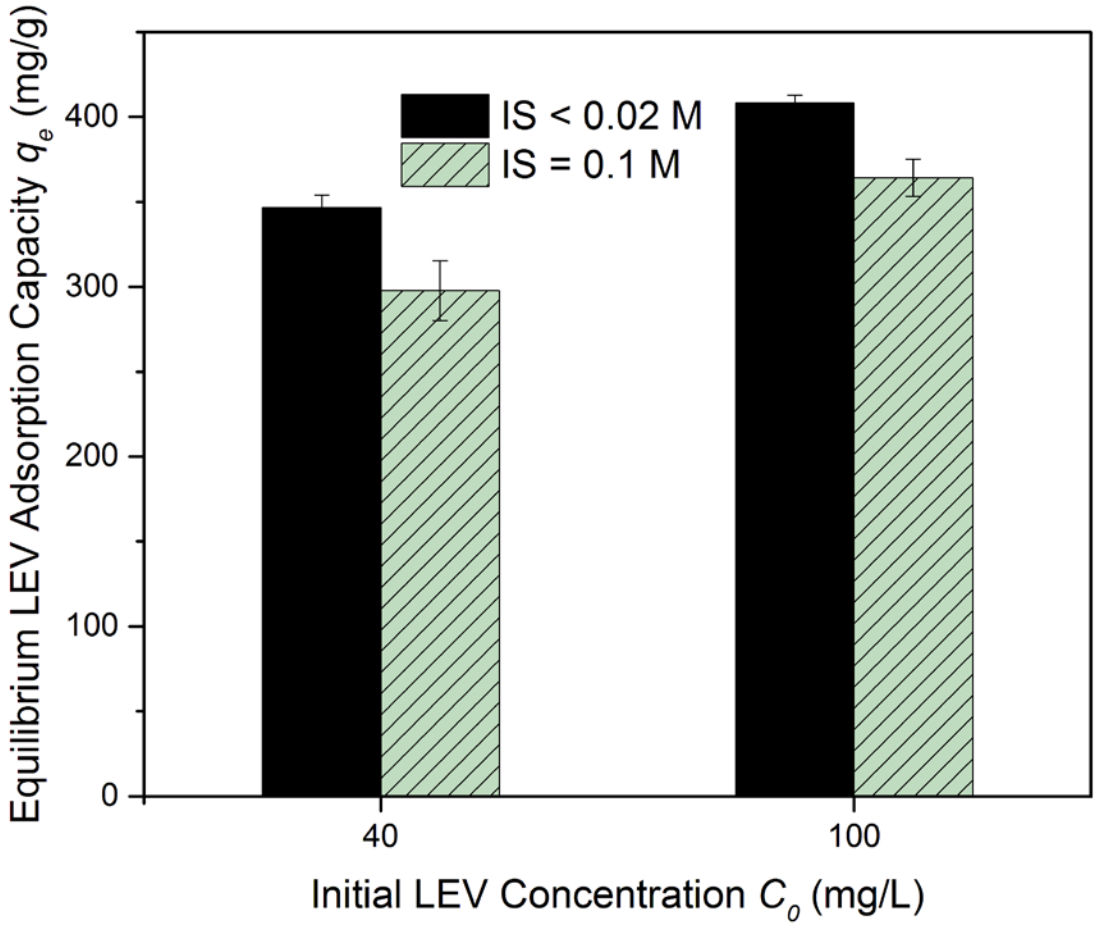

Figure 5.14 Effect of solution IS on LEV adsorption by PBS.

50.0 ± 0.5 mL LEV solution, 5.0 ± 0. 1 mg PBS, pH 6.88 ± 0.03, and 298.15 ± 0.50 K. Error bars represent standard deviation.

As illustrated in Figure 5.14, the LEV adsorption capacity achieved at initial LEV concentrations of 40 mg/L and 100 mg/L decreased from 347 ± 7 and 408 ± 4 mg/g to 298 ± 18 and 364 ± 11 mg/g, respectively, as the solution IS was increased from less than 0.02 M (no ionic strength control) to 0.1 M. The decreases were about 10%. This was in accordance with the adsorption of enrofloxacin on soil (Graouer-Bacart et al. 2013) and adsorption of sulfadimethoxine and sulfaguanidine on soil (Białk-Bielińska et al. 2012). It was suggested that the increase of solution IS induced a decreased thickness of the "electrical double layer" of the charged surface, and then led to a decreasing surface charge, as a result, the electrostatic attraction between the adsorbate and adsorbent was weakened (Białk-Bielińska et al. 2012). The change of IS may also influence the competition between the electrolyte ions and adsorbates for available adsorption sites (Tien 1994). The aforementioned reasons may consequently contribute the slightly decrease in LEV adsorption capacity of PBS with increase in solution IS. However, the effect of solution IS was insignificant compared with that in metal adsorption (Thevannan et al. 2010). This is favored because LEV is expected to be effectively adsorbed by PBS even in wastewater with elevated ionic strength.

5.4 Desorption of Levofloxacin Adsorbed on Pretreated Barley Straw

Desorption experiments were conducted immediately after adsorption at the same temperature and in the same vials as those for the adsorption experiments. The desorption results are illustrated in Figure 5.15. The black columns represent the LEV loaded on PBS at the specific pH values, and the red columns are the LEV desorbed from PBS at the same pH as that for adsorption. The desorption efficiencies shown in Figure 5.15 were lower than 10%. Such results indicated that only small percentage of LEV adsorption was reversible, and the binding between LEV molecules and PBS was strong.

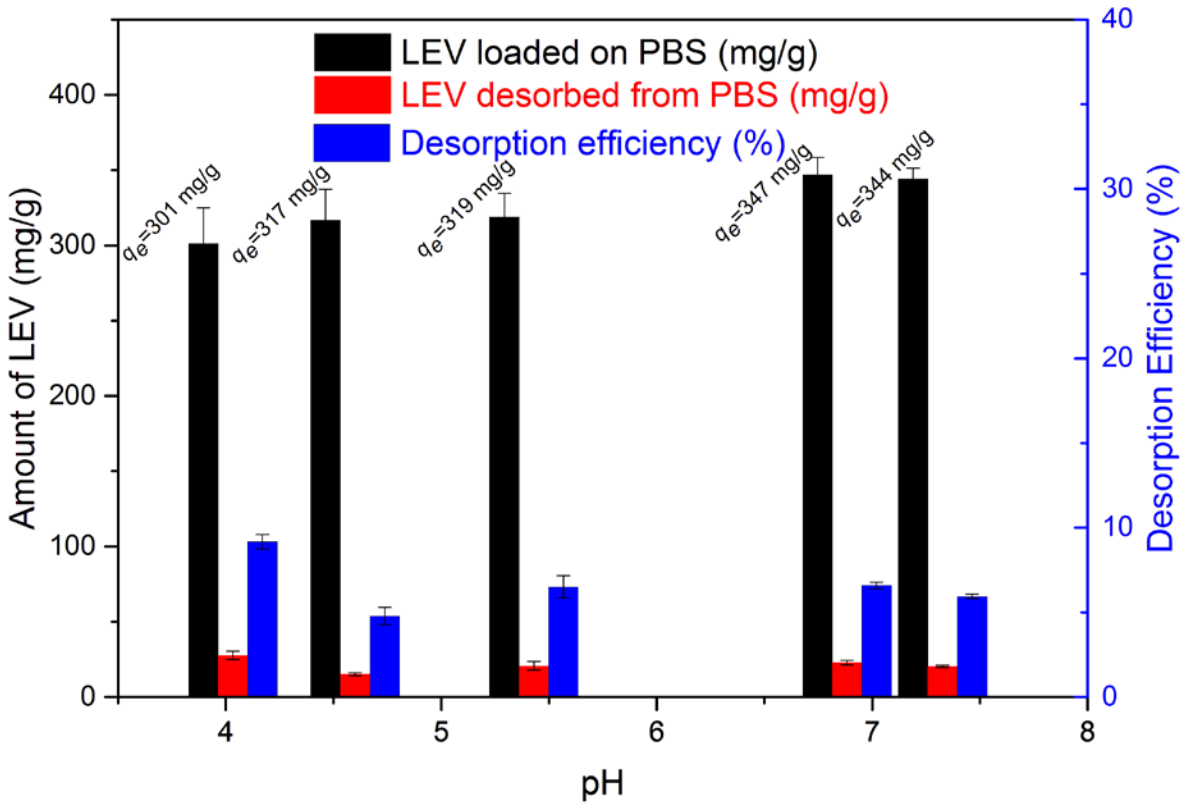

Figure 5.15 Effect of solution pH on LEV desorption by PBS.

50.0 ± 0.5 mL deionized water, 5.0 ± 0. 1 mg PBS, and 298.15 ± 0.50 K. Error bars represent standard deviation.

In addition, during desorption of LEV, solution pH slightly increased (Figure 5.16). Such results indicated that protons in the solution may exchange with positively charged groups such as tertiary amine of LEV adsorbed on PBS, which resulted in elution of LEV from PBS. LEV desorption was also examined at a more acidic condition with a solution pH of 2.0 using samples initially loaded 408 ± 4 mg LEV/g PBS achieved at pH 6.88. A slightly higher desorption efficiency of (20 ± 1)% was obtained. However, the desorption efficiency was still low.

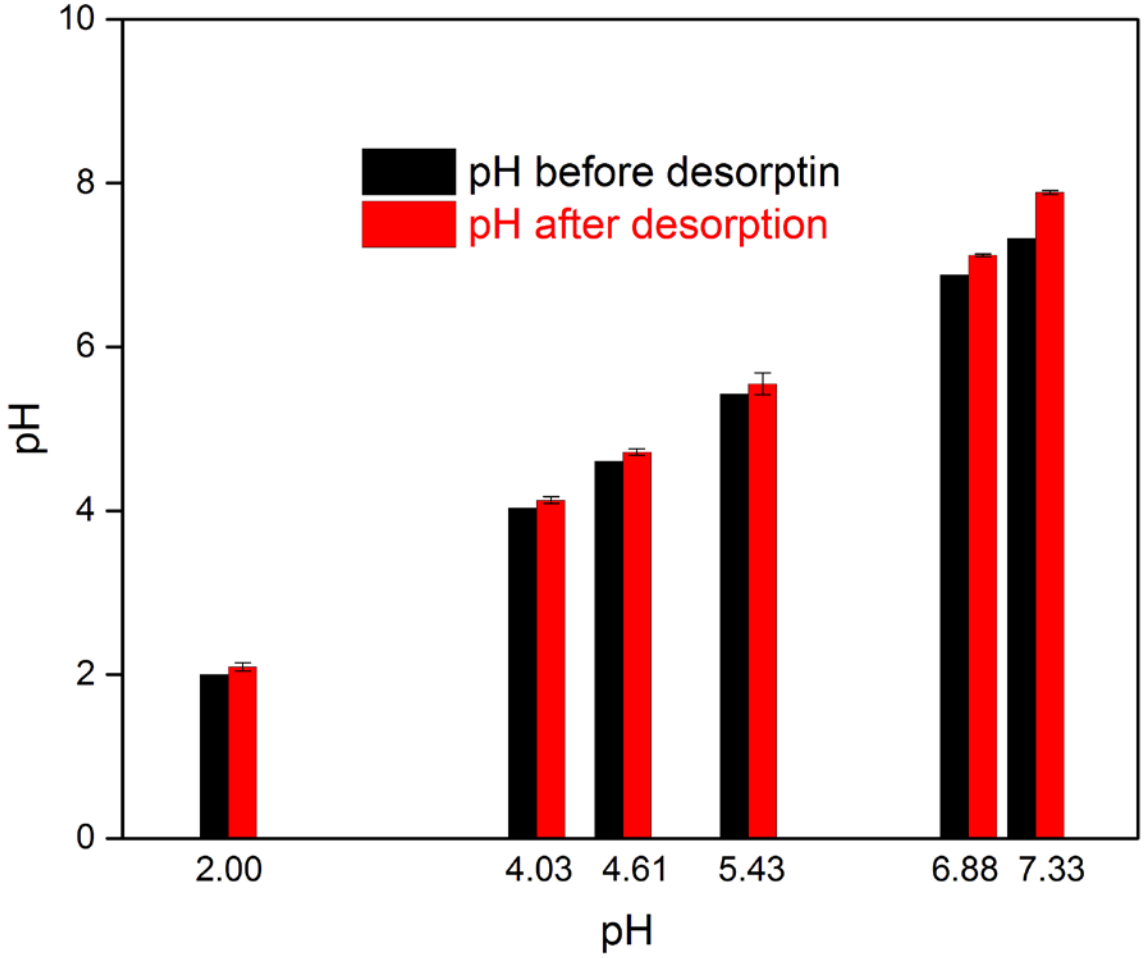

Figure 5.16 pH change after desorption.
50.0 ± 0.5 mL deionized water, 5.0 ± 0. 1 mg PBS, and 298.15 ± 0.50 K. Error bars represent standard deviation.

Further effort was made by using ethylenediaminetetraacetic acid disodium salt dihydrate (EDTA) in order to enhance the desorption efficiency. The desorption efficiency increased to 28.6% compared with that achieved without addition of EDTA, 20.4%. However, this is still far from satisfactory level. The results implied that pH-dependent ion exchange or electrostatic attraction may not be the major mechanisms of LEV adsorption, while they were predominant in nickel adsorption by RBS (Thevannan et al. 2010) and $Au(CN)_2$ adsorption by the crab shells (Niu 2002). Again, the results indicated that the adsorption of LEV on PBS may mainly through π-π electron-donor-acceptor interaction, the bonding strength of which could be larger than that of hydrogen bond, and comparable to inner-, and outer-sphere complex formation (Keiluweit

and Kleber 2009). Considering that the achieved desorption efficiency was low, other methods, such as oxidation and thermal treating in a microwave furnace, may be employed to improve the desorption efficiency. More in depth desorption studies would form an area of future research. In order to further elucidate the adsorption mechanism, X-ray absorption spectroscopy (XAS) analyses were done as follows.

5.5 π-π Electron-Donor-Acceptor Interactions Characterized by X-ray Absorption Near Edge Structure Spectroscopy

The C 1s *K*-edge X-ray absorption near edge structure (XANES) spectra of PBS, LEV, and PBS loaded with LEV are displayed in Figure 5.17. There was a resonance peak at an energy level of 285.52 eV observed on the spectrum of PBS. It represented 1s →π* C=C of aromatic C (Chen et al. 2014a). In addition, the peaks at 285.22, 285.98, and 286.73 eV observed on the LEV spectrum have been attributed to carbon atoms within a benzene ring that are bonded to hydrogen (C=C*-H) (Kuznetsova et al. 2001), nitrogen (C=C*-N) (Stöhr 1992), and fluorine (C=C*-F) (Brzhezinskaya et al. 2009, Plaschke et al. 2005), respectively. The strong peak at 288.54 eV of the LEV spectrum corresponded to 1s →π* C=O transition of carboxylic C (Chen et al. 2014a). Compared with the spectra of LEV and PBS loaded with LEV, the peak at 285.52 eV of the PBS spectrum blue shifted to 285.82 eV of the spectrum of PBS loaded with LEV. This blue shift indicated the higher energy value of photon resonance for excitation, and carbon atoms of aromatic π* C=C on PBS had partial-positive charges with less electron density and worked as π-electron-donors (Okbinoğlu 2014). On the other hand, there was a red shift from 286.73 eV of the LEV spectrum to 286.58 eV of the spectrum of PBS loaded with LEV. According to the research of NOR adsorption on surface-modified carbon nanotubes (Wang et al. 2010c), this phenomenon indicated that carbon atoms in the benzene ring attached to fluorine (C=C*-F) of LEV had partial-negative charges with more electron density and served as π-electron-acceptors due to the strong electron withdrawing

ability of F. The results of C *K*-edge XANES spectroscopy were in supportive of the occurrence of π-π EDA interaction between the aromatic π* C=C of PBS (as π-electron-donor) and π* carbon atom in benzene ring attached to fluorine of LEV molecules (as π-electron-acceptor).

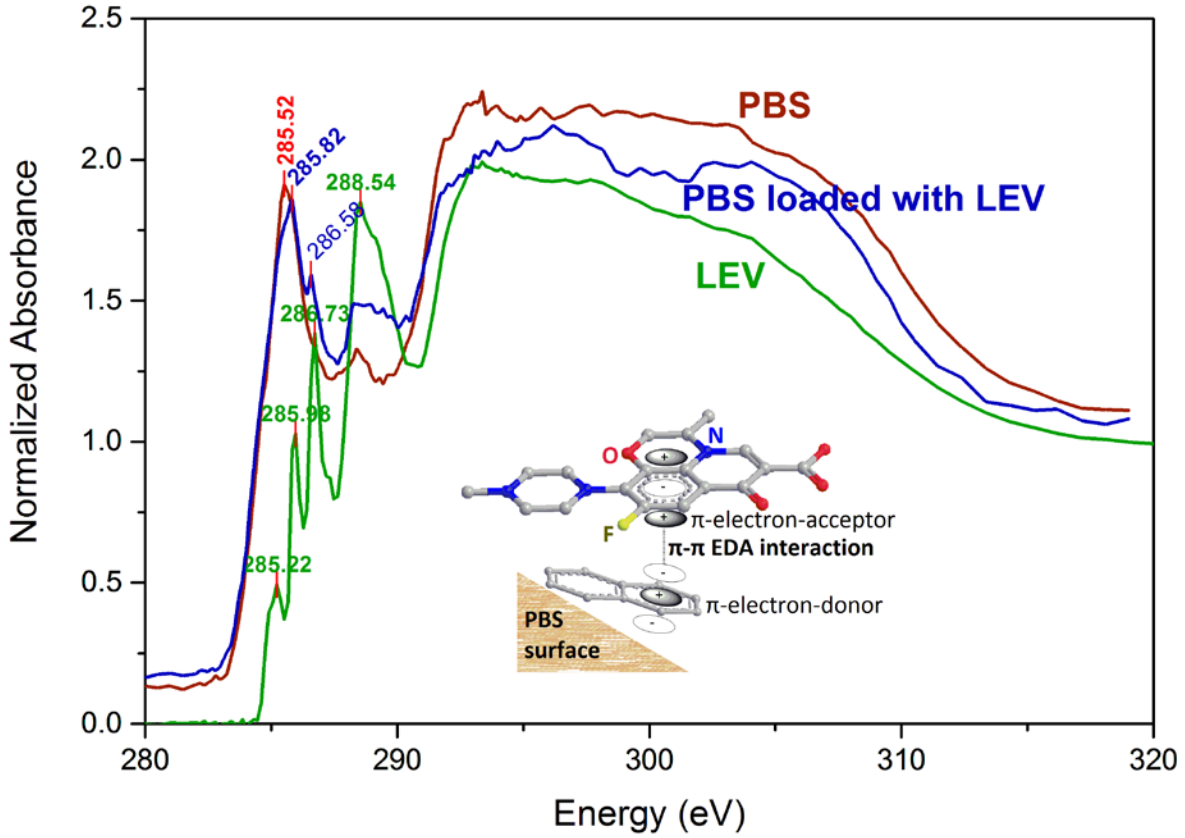

Figure 5.17 C *K*-edge XANES spectra of PBS, LEV, and PBS loaded with LEV (q_e = 408 ± 4 mg/g).
50.0 ± 0.5 mL LEV solution (C_0 = 100 mg/L), 5.0 ± 0.1 mg PBS, pH 6.88 ± 0.03, and 298.15 ± 0.50 K.

The π-π EDA interaction has been reported as the predominant mechanism in the adsorption of organic compounds (e.g. norfloxacin (Wang et al. 2010c), naphthalene and atrazine (Shen et al. 2015)) on heterogeneous adsorbents (e.g. lignin (Wang et al. 2007) and humic substances (Zhu et al. 2004)). PBS contained hydroxyl, carboxyl, and other polar groups, which tended to be polarizable. Surface sites close to polarized edge sites or defects of graphene sheets have been reported to be electron-rich-π-donors (McDermott and McCreery 1994, Zhu

and Pignatello 2005), as addressed in adsorption of aromatic compounds (e.g. benzene and polycyclic aromatic hydrocarbons) on black carbon (e.g. charcoal and soot) (Kubicki 2006, Zhu et al. 2005, Zhu and Pignatello 2005). As such, the proposed force, π-π EDA interaction between the polarizable PBS (aromatic groups, π-electron-donors) and LEV (benzene ring attached to F, π-electron-acceptor) became reasonable.

5.6 Comparison of Levofloxacin Adsorption Capacity of Pretreated Barley Straw with Other Adsorbents

The LEV adsorption capacity of PBS was first compared with raw barley straw (RBS) at an equilibrium pH 6.80 ± 0.15 in the 50.0 mL solutions initially containing 40 mg/L LEV and 5.0 mg PBS or RBS. The results demonstrated that PBS had a much higher LEV adsorption capacity (347 ± 12 mg/g) than RBS (6.2 ± 0.5 mg/g). Although RBS contained cellulose (31-34 *wt*%), hemicelluloses (24-29 *wt*%), and lignin (14-15 *wt*%) (Teas et al. 2001), RBS had a low surface area and was lack of adequate porous structure that are important for the adsorption of organic compounds. It has been reported that surface area and porosity were of importance for the adsorption of FQs by the carbonaceous materials such as carbon nanotubes (Yang and Xing 2010) and activated carbon (Liu et al. 2011). The BET surface area of PBS was 1314 ± 10 m^2/g, among which there were 750 ± 3 m^2 micropore/g, 284 ± 3 m^2 mesopore/g, and 280 ± 5 m^2 macropore/g. However, the surface area of RBS was just 2 m^2/g. The surface morphology of PBS and RBS, revealed by SEM observation (Figure 4.2 on page 59), also indicated that PBS had an enhanced porous structure compared with RBS. This may result in the much higher LEV adsorption capacity of PBS than that of RBS. Such results demonstrated that the pretreatment method in this work was successful in terms of enhancing surface area, porosity, and LEV adsorption capability of barley straw.

Table 5.4 Comparison of LEV adsorption capacity of adsorbents.

Adsorbents	q_m, mg/g	solution pH	Source
PBS	408 ± 5	6.88	This work
Charcoal	87	7.00	(Hattab 2010)
Kaolin	0.26	7.00	(Hattab 2010)
Goethite	1.03	6.00	(Qin et al. 2014)
Iron-pillared montmorillonite	48.61	7.00	(Liu et al. 2015)
Graphene oxide	256.6	not given	(Dong et al. 2016)

In addition, the LEV adsorption capacity of PBS was compared with other adsorbents reported in literature, and the results are presented in Table 5.4. The maximum LEV adsorption capacity of PBS obtained by the adsorption experiment in this work was 408 ± 5 mg/g at a pH of 6.88, and such value was much higher than that of goethite (1.0 mg/g at pH = 6.00) (Qin et al. 2014), Fe-P-Montmorillonite (48.6 mg/g at pH = 7.00) (Liu et al. 2015), kaolin (0.26 mg/g at pH = 7.00), charcoal (87 mg/g at pH = 7.00) (Hattab 2010), and graphene oxide (256.6 mg/g) (Dong et al. 2016). In addition, the highest LEV adsorption capacities reported in literature were observed at a relatively neutral pH, but PBS in this work showed high LEV adsorption capacity at a broad pH range (2.47-9.60). This demonstrated that PBS had a high LEV adsorption capacity and a promising potential for removal of LEV from the real sewage of waste water treatment plant (WWTP). The results again demonstrated that the pretreatment method applied in this work significantly enhanced the LEV adsorption capacity of barley straw from liquid phases. Such method may be transferrable to pretreat other lignocellulosic biomass for removal of LEV.

5.7 Adsorption of Levofloxacin on Pretreated Barley Straw at Low Levofloxacin Concentrations

To investigate the LEV adsorption capacity of PBS in the real water environment, the adsorption experiments were further conducted at low LEV concentrations. Due to the limit of the HPLC used in this work, the initial LEV concentrations were ranged from 1 mg/L to 10 mg/L. 5.0 ± 0.1 mg PBS particles were mixed with a 50.0 mL LEV solution at 298.15 ± 0.50 K for 168 h as those aforementioned in the Section of 3.6. All experiments were conducted in triplicate. The equilibrium solutions were 6.88 ± 0.03. As illustrated in Figure 5.18, the results demonstrated the high LEV adsorption capacity of PBS even as the LEV concentrations were lower than 1 mg/L. The corresponding removal efficiencies were higher than 89%.

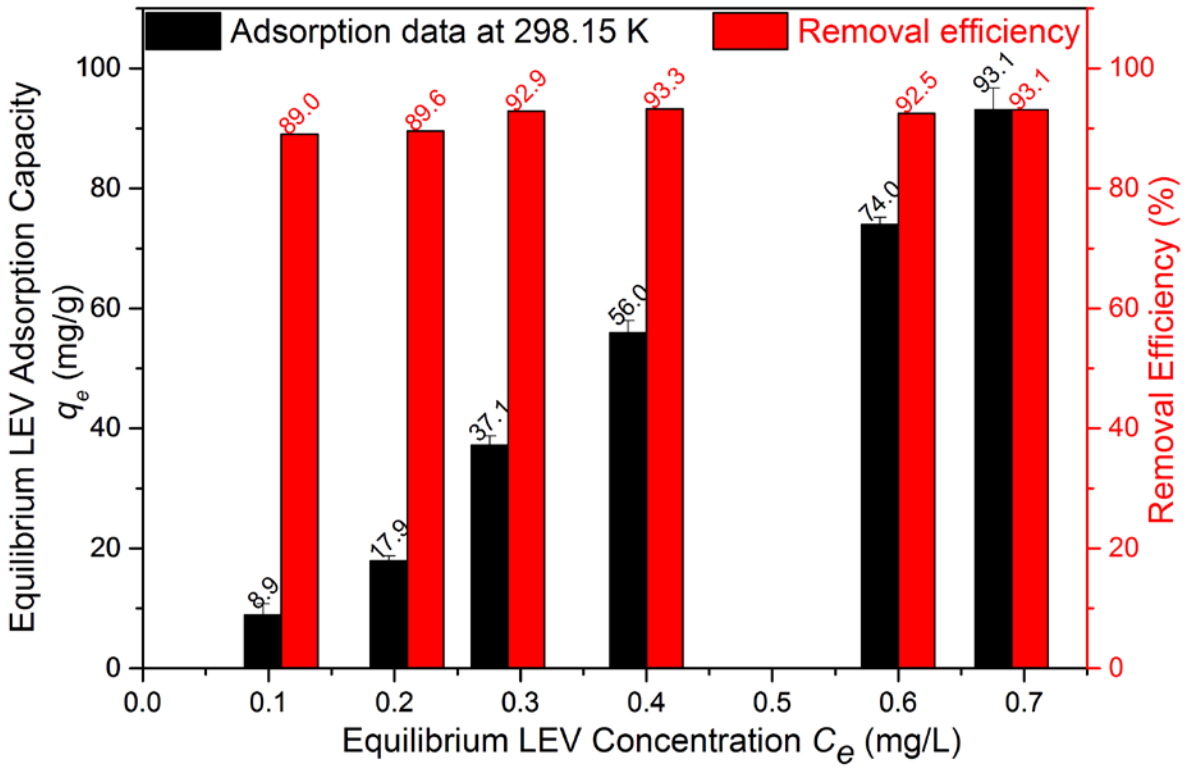

Figure 5.18 Adsorption of LEV on PBS at low LEV concentrations.

50.0 ± 0.5 mL LEV solution, 5.0 ± 0.1 mg PBS, pH 6.88 ± 0.03, and 298.15 ± 0.50 K. Error bars represent standard deviation.

5.8 Chapter Summary

As one of the emerging contaminants, LEV was efficiently removed by the adsorbent PBS. The adsorption kinetics was investigated at different temperatures and LEV concentrations, the kinetic data were well fitted by the pseudo-second-order kinetic model. Based on the *Arrhenius* equation, the activation energy was determined to be 45.9 kJ/mol, which suggested the adsorption of LEV on PBS mainly through chemical adsorption. The effect of solution pH on LEV removal was studied, and desorption of LEV loaded on PBS was also examined. PBS demonstrated high LEV adsorption capacities in a wide range of solution pH (2.47-9.60). The experimental maximum LEV adsorption capacity of PBS (408 ± 5 mg LEV/g at pH 6.88 and 298.15 K) was much higher than that of RBS and the reported adsorbents. The elevated ionic strength slightly decreased the LEV adsorption capacity of PBS. The adsorption equilibrium isotherms at different solution pH and temperatures were fairly well fitted by the *Langmuir-Freundlich* model, and revealed that the adsorption of LEV on PBS was an endothermic process. Furthermore, the site energy and its distribution of PBS for LEV adsorption were estimated. The weighted mean and standard deviation of the distribution were employed to depict the interaction strength between the adsorbent and adsorbate, and the adsorption heterogeneity. The π-π electron-donor-acceptor (EDA) interaction between the π^* aromatic C=C of adsorbent PBS and the π^* carbon atom in the benzene ring attached to fluorine of LEV was proposed as one of the major adsorption mechanisms. Such interaction was investigated by the C *K*-edge XANES. Elevated temperature increased the static dipole polarizability. Thus, the π-π EDA interaction between the aromatic adsorbent PBS and the adsorbate LEV with benzene ring was strengthened. This was reflected by the increase in weighted mean of site energy distribution. In addition, hydrogen bond may also play a role. Further investigation on the adsorption mechanisms is necessary.

CHAPTER 6 ADSORPTION OF NORFLOXACIN ON PRETREATED BARLEY STRAW

The aforementioned research demonstrated that PBS had a much higher LEV adsorption capacity than the reported adsorbents, and EDA interactions may be the dominant forces. Whether this material can effectively remove other antibiotics from water is worthy to be investigated. Among the antibiotics, norfloxacin (1-Ethyl-6-fluoro-4-oxo-7-(1-piperazinyl)-1,4-dihydro-3-quinolinecarboxylic acid, NOR) is a so-called second generation FQ, which acts by inhibiting bacterial DNA gyrase enzyme for DNA replication (Jia et al. 2012). The molecular structure of NOR (Pei et al. 2011) is presented in Figure 6.1, which is different from the molecular structure of LEV (Figure 5.1 on page 69). As another emerging environmental micropollutant, NOR is discharged into the environment via different sources. Waste streams containing NOR originate from residential areas, hospitals, production facilities, and animal farms. However, the average removal efficiency of NOR obtained from 52 wastewater treatment plants, which utilized a variety of removal processes such as a two activated sludge process with a nitrification tank, an extended aeration tank, rotating biological contactors, and a pure oxygen activated sludge reactor, was only 68% (Van Doorslaer et al. 2014). There is a need to effectively remove NOR to protect water security. Moreover, quantitative data of NOR adsorption by PBS as a function of the crucial operation parameters such as pH, temperature, and time in terms of engineering application were not available before this work, and adsorption energy and mechanisms of NOR need to be further investigated which are important to contribute to the science of adsorption. This work provided information and data to address the above aspects and contributed to fill in the respective knowledge gaps.

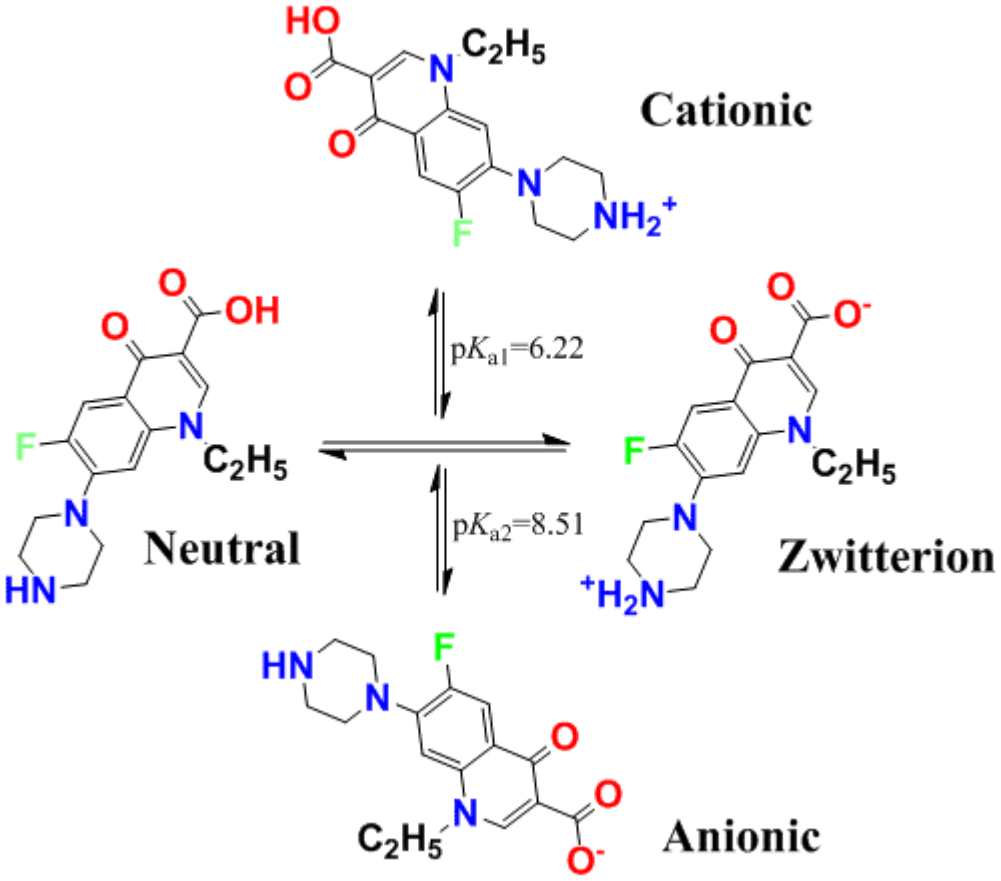

Figure 6.1 Molecular structure of NOR.

In this chapter, PBS was used as an adsorbent for NOR removal from artificial wastewater at various solution pH and temperatures. The effect of solution pH on NOR adsorption, which influenced the speciation of NOR molecules and the surface charge of PBS, was investigated. In addition, the adsorption behaviors, including adsorption kinetics, equilibrium, and adsorption energy with respect to the temperature, were also explored. Furthermore, the percentage of adsorption site, having site energies greater than or equal to a specific value of E^*, was estimated. These respective researches are critical to understand the adsorption mechanism and develop advanced technology for treating the pharmaceuticals-contaminated water.

6.1 Adsorption Kinetics

6.1.1 Effect of Contact Time

Figure 6.2a presents the effect of contact time on the adsorption of NOR by PBS at different initial NOR concentrations. Consistent with the adsorption of LEV on PBS, a rapid adsorption of NOR was observed at the first 12 h, then a slower adsorption followed, until the equilibrium was reached. The removal ratio of NOR by PBS, determined by the decrease of NOR concentration at equilibrium to the initial concentration of NOR, was 92% at a lower NOR concentration of 10 mg/L, and then decreased to 77% and 48% as the NOR concentration was continuously increased to 40 and 80 mg/L. However, the corresponding values of equilibrium adsorption capacity increased to 310 and 384 mg/g, respectively. The results demonstrated that the NOR removal ratio also highly depended on the initial NOR concentration if the rest conditions were kept constant.

The kinetic data were well fitted by the pseudo-second-order kinetic model as well. The fitting parameters with values of coefficient of determination (R^2) and residue sum of square (*RSS*) are presented in Figure 6.2b and Table 6.1. Moreover, calculated from $kq_{e,cal}^2$, the initial rate of NOR adsorption on PBS increased from 3.20 to 37.67 and 57.80 mg/(g·h) as the initial concentration was increased from 10 to 40 and 80 mg/L. This may also be explained as follows: as the initial concentration of NOR was increased, the equilibrium adsorption capacity q_e increased, which indicated the enhanced driving force (q_e-q_t), and therefore the initial rate increased.

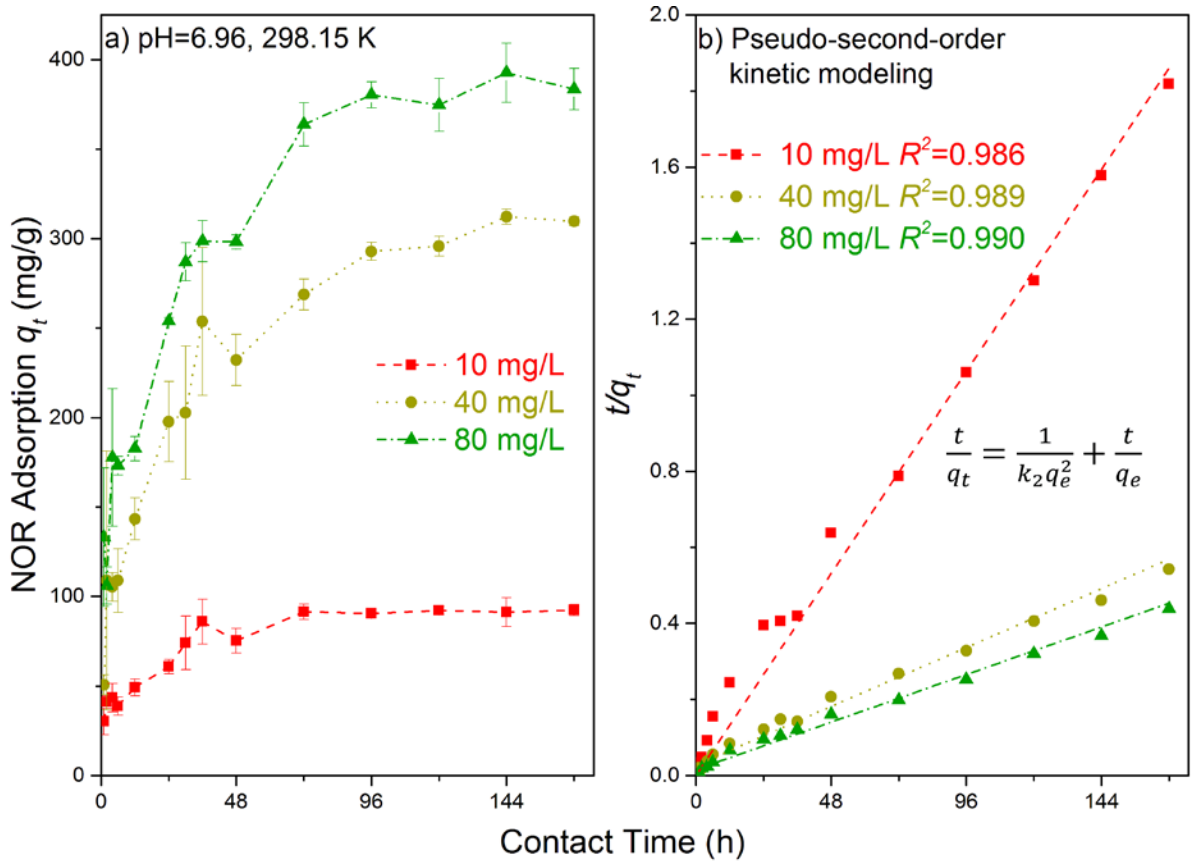

Figure 6.2 Kinetic analysis of NOR adsorption on PBS at different initial concentrations: a) effect of contact time; b) pseudo-second-order kinetic modeling.

50.0 ± 0.5 mL NOR solution, 5.0 ± 0.1 mg PBS, pH 6.96 ± 0.07, and 298.15 ± 0.50 K. Error bars represent the standard deviation.

Table 6.1 Kinetic parameters for the adsorption of NOR on PBS at 298.15 K.

Experimental			Pseudo-second-order kinetic model				
T, K	C_0, mg/L	q_e, mg/g	$q_{e,cal}$, mg/g	k, g/(mg·h)	$kq_{e,cal}^{2}$ *, mg/(g·h)	R^2	RSS, $(mg/g)^2$
298.15	10	92	90	3.92×10^{-4}	3.20	0.986	9390
298.15	40	310	310	3.92×10^{-4}	37.67	0.989	15722
298.15	80	384	384	3.92×10^{-4}	57.80	0.990	29699

* $kq_{e,cal}^{2}$ the initial rate of NOR adsorption on PBS mg/(g·h)

6.1.2 Analysis of Activation Energy

The adsorption kinetic experiments of NOR on PBS were conducted with respect to temperature (C_0 = 100 mg/L and pH 6.96 ± 0.07) in order to determine the activation energy, and the kinetic data are plotted in Figure 6.3a. As the temperature was increased from 298.15 K to 308.15 and 318.15 K, the equilibrium NOR adsorption capacity of PBS increased from 349 mg/g to 359 and 387 mg/g, respectively. These values were slightly lower than the LEV adsorption capacities of PBS at the same conditions.

Figure 6.3b displays the fitting curves of the pseudo-second-order kinetic model for NOR adsorption on PBS with respect to temperature. The pseudo-second-order kinetic model again well fitted the kinetic data with high values of coefficient of determination (R^2 > 0.999), as listed in Table 6.2. The obtained values of $q_{e,cal}$ and k at 298.15, 308.15, and 318.15 K were 355, 362, and 397 mg/g, and 5.60×10^{-4}, 6.93×10^{-4}, and 9.85×10^{-4} g/(mg·h), respectively, which were slightly lower than those of LEV adsorption on PBS. The initial rate of NOR adsorption on PBS (calculated from kq_e^2) was 70.37 mg/(g·h) (298.15 K). This may be due to the well-developed porous structure (revealed by the results of SEM and high specific surface area 1314 ± 10 m^2/g) and modified functional groups of PBS. Moreover, the initial rate of NOR adsorbed on PBS increased from 70.37 mg/(g·h) to 90.91 and 155.04 mg/(g·h) with increase in the temperature from 298.15 K to 308.15 and 318.15 K. Temperature may affect the adsorption kinetics: 1) as temperature was increased, the equilibrium adsorption capacity q_e increased, therefore the adsorption driving force ($q_e - q_t$) enhanced; 2) the adsorption rate constant k increased with increase in temperature. The influence of temperature on adsorption rate constant k can be quantified by the *Arrhenius* equation.

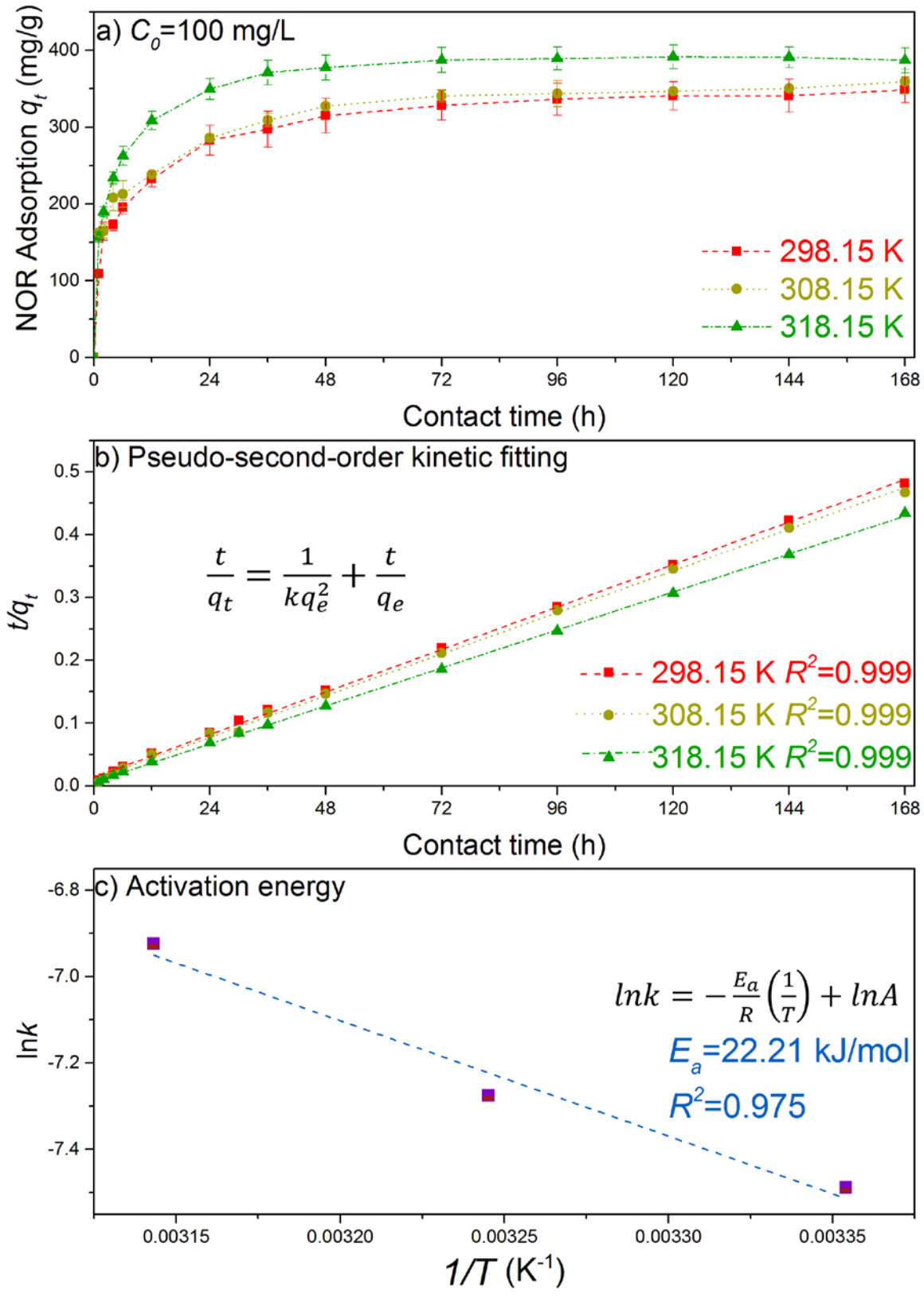

Figure 6.3 Kinetic analysis of NOR adsorption on PBS at different temperatures: a) effect of contact time; b) pseudo-second-order kinetic fitting; c) calculation of activation energy. 50.0 ± 0.5 mL NOR solution (C_0 = 100 mg/L), 5.0 ± 0.1 mg PBS, and pH 6.96 ± 0.07. Error bars represent standard deviation.

Table 6.2 Kinetic parameters for the adsorption of NOR on PBS at different temperatures.

Experimental			Pseudo-second-order kinetic model				
T, K	C_0, mg/L	q_e, mg/g	$q_{e,cal}$, mg/g	k, g/(mg·h)	$k \cdot q_{e,ca}^2$, mg/(g·h)	R^2	RSS, $(mg/g)^2$
298.15	100	349	355	5.60×10^{-4}	70.37	0.999	7736
308.15	100	359	362	6.93×10^{-4}	90.91	0.999	13951
318.15	100	387	397	9.85×10^{-4}	155.04	0.999	3148

Again, by incorporating the known values of rate constant k at 298.15, 308.15, and 318.15 K into the linearized *Arrhenius* equation (Eq. (2.3), Chapter 2, and page 33), the activation energy was determined to be 22.21 kJ/mol (Figure 6.3c). The energy of activation for physical adsorption was usually no more than 1 kcal/mol (equivalent to 4.2 kJ/mol) (Smith 1970, Unuabonah et al. 2007). The obtained value of activation energy 22.21 kJ/mol in this work also suggested that NOR may be primarily adsorbed by PBS via chemical adsorption.

6.2 Adsorption Equilibrium

6.2.1 Effect of Solution pH

6.2.1.1 Norfloxacin Equilibrium Adsorption on Pretreated Barley Straw in a Wide Range of Solution pH

The equilibrium NOR adsorption capacities q_e of PBS at various solution pH (2.67 ± 0.06 ~ 10.50 ± 0.13) are presented in Figure 6.4. Similar to the adsorption of LEV on PBS, as the equilibrium solution pH was increased from 2.67 ± 0.06 from 6.96 ± 0.07, q_e increased from 307 ± 2 mg/g to 396 ± 19 mg/g, and then decreased to 287 ± 6 mg/g at 10.50 ± 0.13. The highest NOR adsorption 396 ± 19 mg/g was achieved at pH 6.96 ± 0.07. As a result, pH 6.96 ± 0.07 was chosen as the equilibrium solution pH for the isotherm studies. Although NOR adsorption varied with the tested pH, the results demonstrated that high NOR adsorption

capacities of PBS were achieved in a wide range of pH 2.67-10.50. Both the adsorption of LEV and NOR by PBS achieved the highest adsorption capacities in a pH range of zwitterion at the tested conditions.

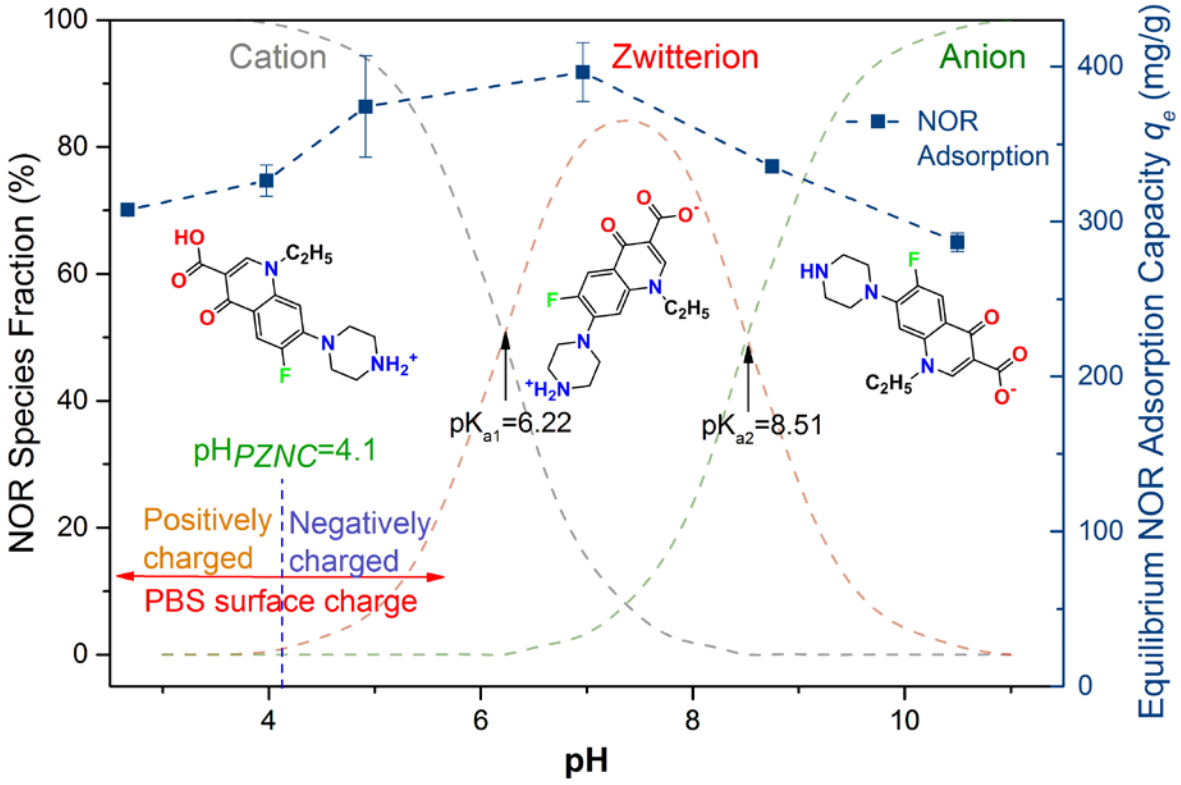

Figure 6.4 Effect of solution pH on NOR adsorption by PBS.
50.0 ± 0.5 mL, 73 mg/L NOR solution, 5.0 ± 0.1 mg PBS, contact time 168 h, and 298.15 ± 0.50 K. Error bars represent the standard deviation.

As presented in Figure 5.6 on page 76, the value of point of zero net charge (PZNC) of PBS was determined to be 4.10. Therefore, PBS was positively charged when solution pH was lower than 4.10, otherwise negatively charged (pH > 4.10). In addition, similar to LEV, NOR also had two values of dissociation constant via its tertiary amine group (pK_{a2} = 8.51) and carboxyl group (pK_{a1} = 6.22), and it can be positively charged (pH < 6.22), negatively charged (pH > 8.51), and zwitterionic (pH 6.22-8.51) (Pei et al. 2011). As illustrated in Figure 6.4, NOR had more positively charged groups than negatively charged groups at pH 4.10-6.96, while PBS was negatively charged. Thus, NOR cations could be bonded to PBS via electrostatic

attraction. As a result, the adsorption of NOR on PBS increased as solution pH was increased. Moreover, during adsorption process, the values of solution pH decreased from initial pH values 4.08 and 5.04 to final values 3.98 and 4.91, which indicated that positively charged groups of NOR (i.e., tertiary amine) might exchange with protons of acidic functional groups of PBS such as carboxyl groups.

At pH < 4.10 and pH > 8.51, NOR molecules and PBS surface had the same net charge and could repel each other. Again, if the pH-dependent electrostatic attraction was the major mechanism, adsorption of NOR on PBS was expected to be significantly depressed. However, the q_e values at acidic pH 2.67 ± 0.06 and basic pH 10.50 ± 0.13 were 307 ± 2 and 287 ± 6 mg/g, respectively, and variation of NOR adsorption capacity in the pH range (2.67-10.50) was lower than 27.5% using the highest q_e (396 ± 19 mg/g) value achieved at pH 6.96 as a reference. The results indicated that the pH-dependent electrostatic attraction between NOR and PBS influenced the adsorption process of NOR on PBS, but it may not be the principal mechanism. This is similar to LEV adsorption. Other adsorption mechanism could be the dominant one, which needs to be further investigated.

The FTIR results of RBS, pure NOR, PBS without NOR, and PBS loaded with NOR are illustrated in Figure 6.5. As mentioned in the Section of 5.2.1.1, two troughs representing hydroxyl O-H stretching (3712 cm^{-1}) and carboxylic O-H bond stretching (2978 cm^{-1}) were observed on the FTIR spectrum of PBS. However, after adsorption of NOR, the intensity of the aforementioned two troughs reduced on the spectrum of PBS loaded with NOR. Such results demonstrated that the hydroxyl and carboxyl groups may participate in the adsorption of NOR on PBS. The aromatic C-H bending (783 cm^{-1}) (Pawlak and Pawlak 1997) appeared on the spectra of RBS, PBS, and PBS loaded with NOR. Lignin, which has aromatic groups, is one of the major components of RBS. After the pretreatment, these groups still existed.

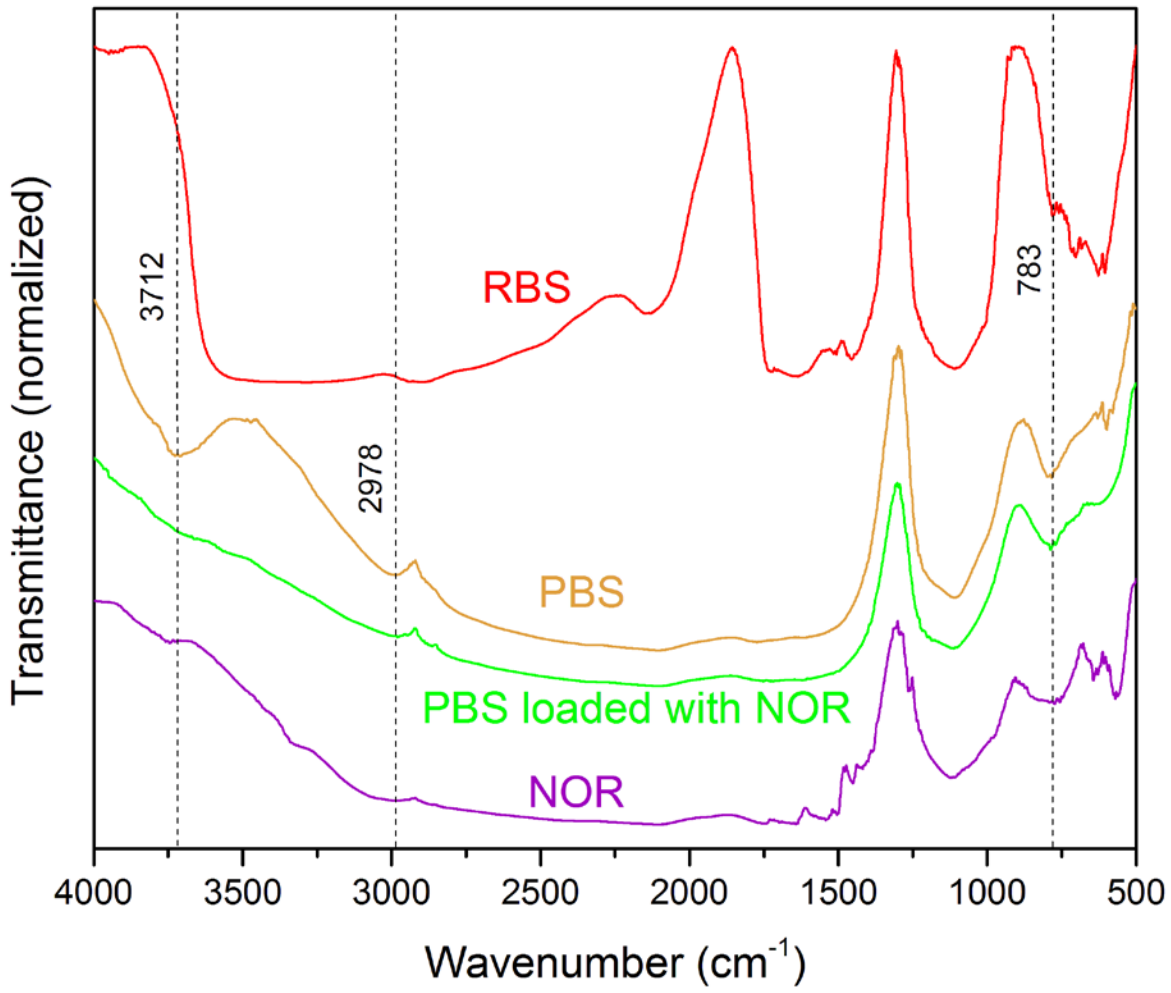

Figure 6.5 FTIR spectra of RBS, pure NOR, PBS, and PBS loaded with NOR (q_e = 396 ± 19 mg/g).

It has been reported that as the number of associated rings increased, the aromatic rings on adsorbent surface could be strong π-electron-donors due to the occurrence of quadrupole moment (Keiluweit and Kleber 2009, Zhu and Pignatello 2005). In addition, revealed by the FTIR spectra, carboxyl and hydroxyl groups were introduced to PBS. The surface-associated carboxyl groups ($-COO^-$) and hydroxyl groups ($-O^-$) have been considered to serve as strong *n*-electron-donors (Chen et al. 2008). On the other hand, the benzene ring on NOR could work as a π-electron-acceptor due to the strong electron withdrawing ability of the fluorine group (Wang et al. 2010c). Thus, the benzene ring of NOR and the carboxyl, hydroxyl and aromatic groups of PBS might build the *n*-π and π-π electron-donor-acceptor (EDA) pairs. The

aforementioned EDA interactions have been proposed as the dominant driving forces in the adsorption of NOR (Wang et al. 2010c), hydroxyl- and amino-substituted aromatic compounds (Chen et al. 2008), and phenolic compounds (Lin and Xing 2008) by carbon nanotubes. Therefore, the significantly high NOR adsorption capacity of PBS in a wide pH range (2.67 ± 0.06 ~ 10.50 ± 0.13) may be interpreted by the occurrence of *n*-π and π-π EDA interactions, which is consistent to the adsorption of LEV on PBS. The occurrence of EDA interactions was further investigated in the Section of 6.4.

Moreover, the hydrogen bonds might be formed between the NOR molecules and the carboxyl and hydroxyl groups of PBS that were revealed by the FTIR spectra of PBS. There is no doubt that more work is required to assess the contribution of hydrogen bond in the PBS-NOR adsorption process, although H-bond was reported as an insignificant role in the adsorption of substituted aromatics and carbon nanotubes (Lin and Xing 2008). In addition, hydrophobic interaction has been reported in the adsorption of sulfonamide antibiotics on biochar (Zheng et al. 2013) and soil (Wegst-Uhrich et al. 2014), and such interaction could also play a role in the adsorption of NOR on PBS. In a real aqueous environmental system, multiple bonding mechanisms are expected to simultaneously operate. The actual mechanisms of NOR adsorption by PBS require further investigations, such as the existences and binding strengths of EDA interactions (e.g., *n*-π and π-π EDA interactions), H-bond, hydrophobic interaction, and other interactions.

6.2.1.2 Norfloxacin Adsorption Isotherms of Pretreated Barley Straw and Raw Barley Straw

The NOR adsorption isotherms of PBS and RBS at pH 6.97 and 298.15 K are illustrated in Figure 6.6. The results demonstrated that PBS had a much higher NOR adsorption capacity than RBS, which indicated that PBS had more binding sites available for NOR adsorption. The *Langmuir-Freundlich* model successfully fitted the adsorption isotherms with high values of R^2. The obtained q_m, b, and n values of PBS and RBS were 356 and 54 mg/g, 1.10 and 0.00152

L/mg, and 1.04 and 2.07, respectively. Moreover, the corresponding values of residue sum of squares (*RSS*) were 2594 and 221 $(mg/g)^2$.

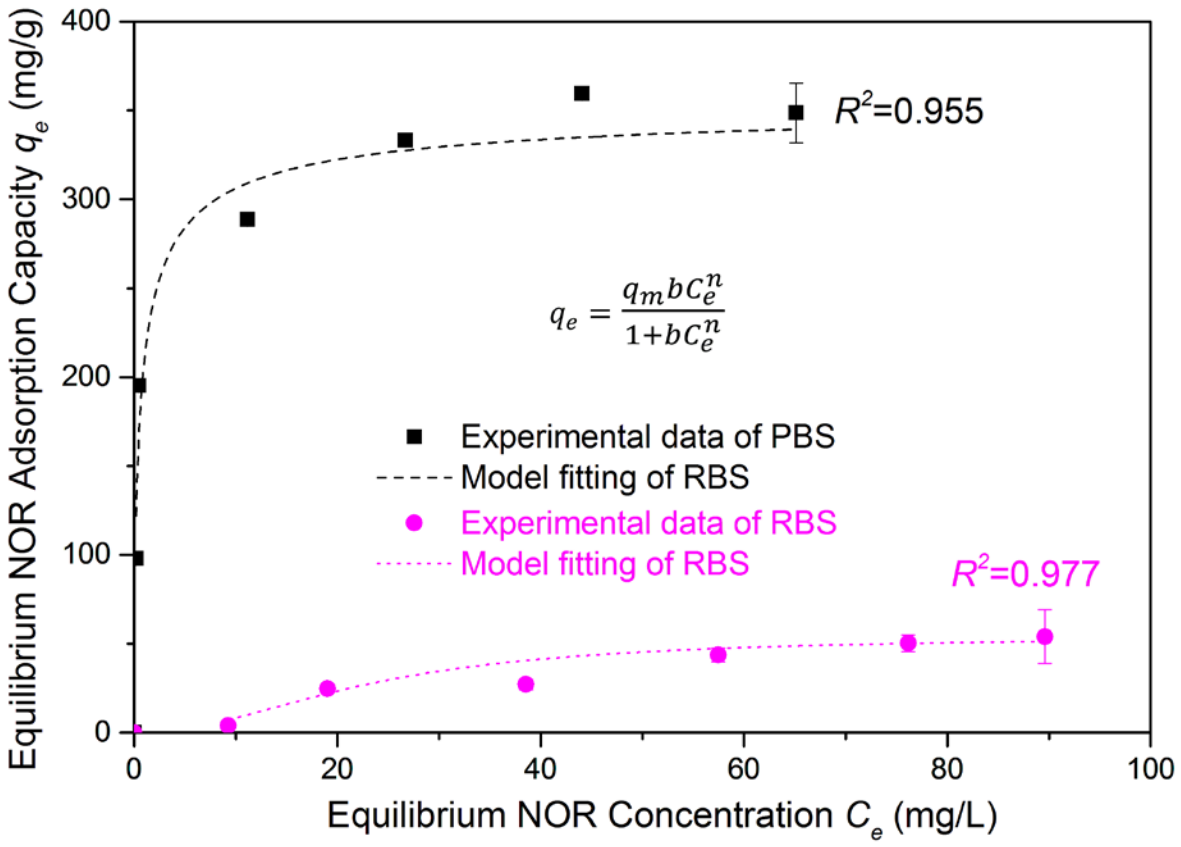

Figure 6.6 NOR adsorption isotherms of PBS and RBS.
50.0 ± 0.5 mL NOR solution, 5.0 ± 0.1 mg PBS/RBS, contact time 168 h, pH 6.96 ± 0.07, and 298.15 ± 0.50 K. Error bars represent the standard deviation.

In addition, it has been documented that BET surface area was important in the adsorption of aromatic compounds on activated carbon and carbon nanotubes (Shen et al. 2015, Wang et al. 2010a). In this work, PBS had a much higher q_m value (356 mg/L) and BET surface area (1314 ± 10 m^2/g) than RBS (56 mg/L and 1.8 m^2/g). Such comparisons indicated that the higher the value of BET surface area, the higher the value of q_m at the tested conditions in this work. The results again demonstrated that the pretreatment method applied in this work successfully improved the adsorption capacity of barley straw for NOR from liquid phases.

6.2.1.3 Approximate Site Energy and Its Distribution

Determined by Eq. (2.9) (Chapter 2 and page 35), the site energy E^* values of PBS and RBS are plotted as a function of the equilibrium NOR adsorption capacity q_e in Figure 6.7. As the amount of NOR adsorbed on the adsorbents increased, the E^* values dramatically decreased. Such results revealed that the high-energy adsorption sites on PBS/RBS were first occupied by NOR molecules, and the low-energy adsorption sites were then occupied. This was consistent to the adsorption of NOR on carbon nanotubes (Wang et al. 2010c) and LEV on PBS. Furthermore, the values of site energy E^* of NOR adsorbed on PBS were much higher than those of RBS.

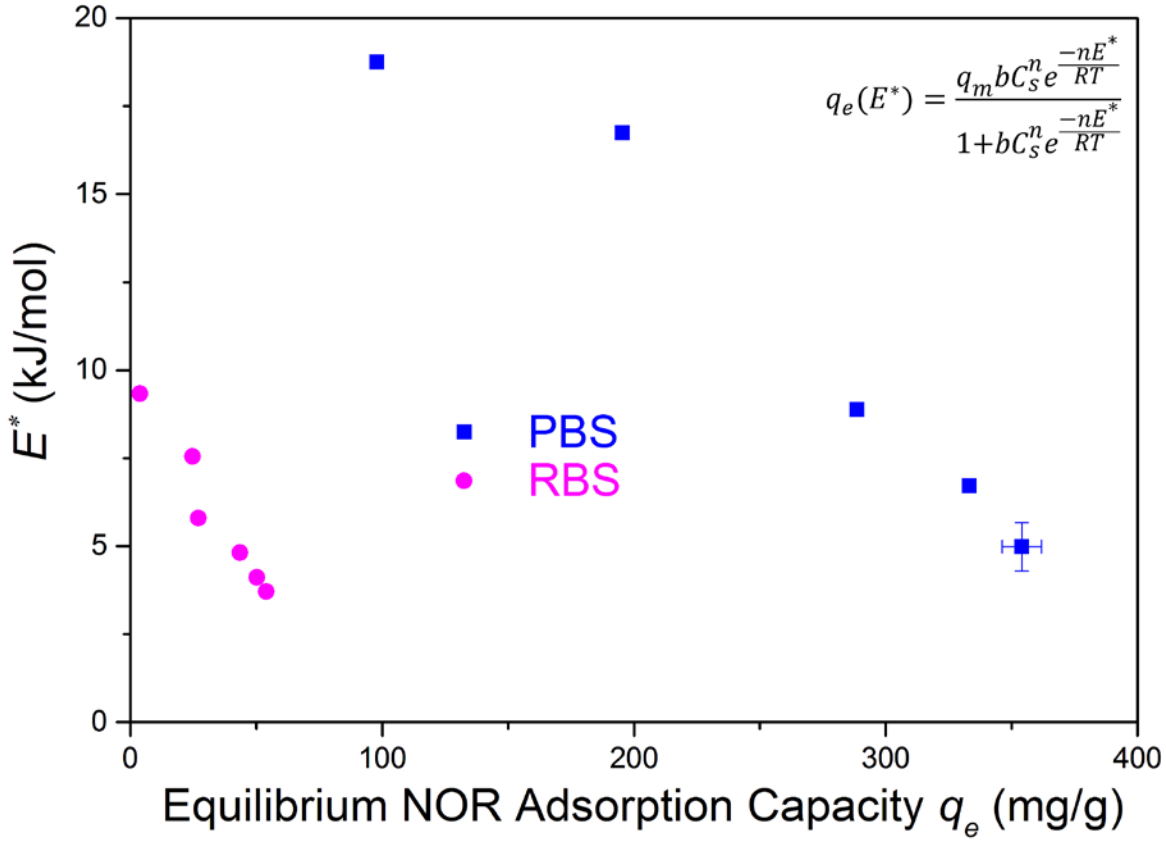

Figure 6.7 Site energy versus equilibrium NOR adsorption capacities of PBS and RBS. 50.0 ± 0.5 mL NOR solution, 5.0 ± 0.1 mg PBS/RBS, contact time 168 h, pH 6.96 ± 0.07, and 298.15 ± 0.50 K. Error bars represent the standard deviation.

Figure 6.8 displays the site energy distributions of NOR adsorption on PBS and RBS based on the *Langmuir-Freundlich* model. The weighted mean of site energy distribution was determined to depict the interaction strength between the adsorbents and adsorbate, and the surface energy heterogeneity of the adsorbents was described by the width of the distribution (Carter et al. 1995).

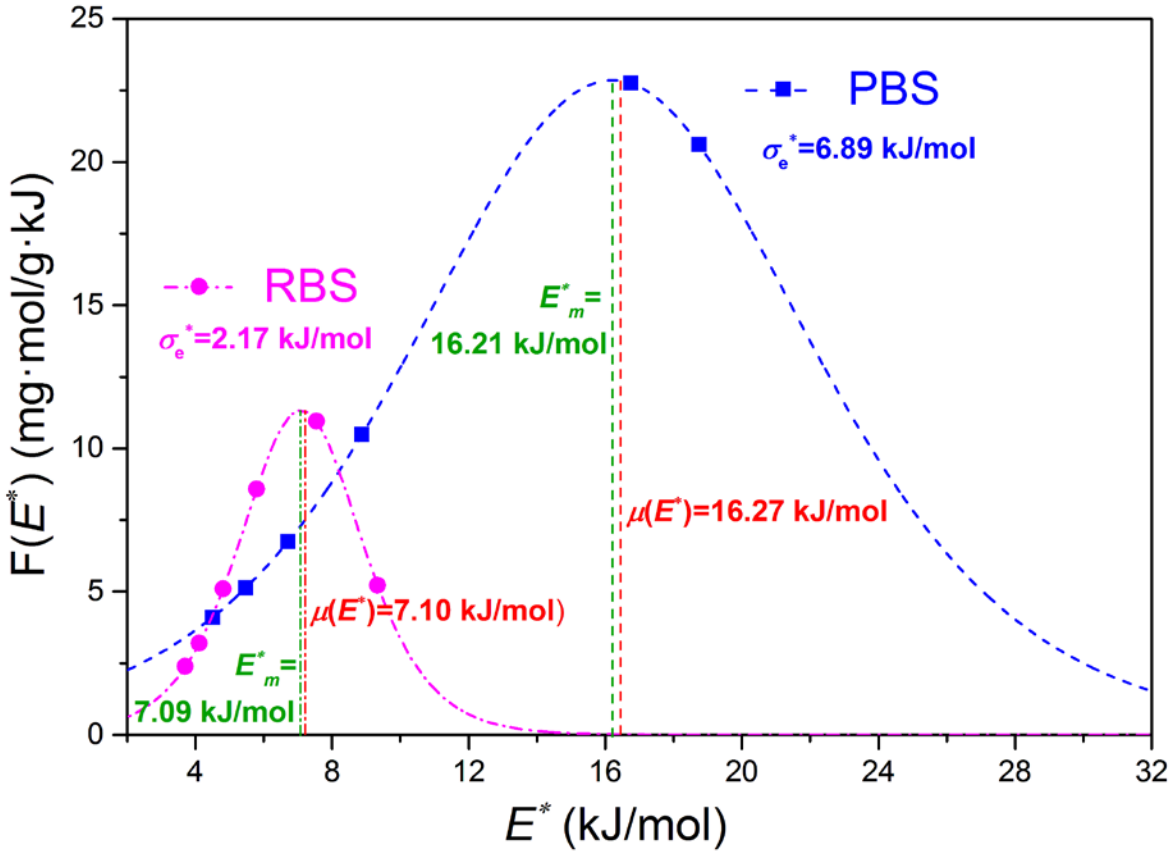

Figure 6.8 Site energy distribution curves of PBS (blue dashed line) and RBS (pink dashed with dots line). The data points represent the results obtained at the specific experimental conditions ■ PBS and ● RBS.
50.0 ± 0.5 mL NOR solution, 5.0 ± 0.1 mg PBS/RBS, contact time 168 h, pH 6.96 ± 0.07, and 298.15 ± 0.50 K.

The weighted mean values $\mu(E^*)$ of site energy distributions of PBS and RBS were given in Figure 6.8. As mentioned before, it has been documented that the higher the value of weighted mean, the stronger the adsorption affinity (Carter et al. 1995). PBS had a much higher

value of weighted mean (16.27 kJ/mol) than RBS (7.10 kJ/mol), which demonstrated that PBS had a much stronger adsorption affinity for NOR molecules than RBS, and thus PBS was more favorable for the adsorption reaction than RBS. Such result may be interpreted by the occurrence of *n*-π and π-π EDA interactions, and hydrogen bond between the benzene ring of NOR (π-electron-acceptor) and the carboxyl, hydroxyl and aromatic groups of PBS (*n*- and π-electron-donors).

Evidenced by the site energy distribution curves (Figure 6.8), PBS and RBS also revealed energetical heterogeneities for adsorption of NOR. Determined by Eq. (2.19) (Chapter 2 and page 37), the σ_e^* value of PBS (6.89 kJ/mol) was higher than that of RBS (2.17 kJ/mol), which indicated the stronger energetical heterogeneity of PBS for NOR adsorption. Again, as discussed before, generally, the heterogeneity of adsorption sites for carbonaceous adsorbents originated from the defect structures, as well as the crosslinking and disordered arrangement of various carbon structure (Cerofolini and Cerofolini 1980). In addition, the heterogeneity of adsorption sites could also be derived from the grafted functional groups (chemical composition heterogeneity), especially oxygen-containing functional groups (Yoon et al. 2006). In this work, PBS was made from barley straw with H_3PO_4 impregnation and microwave heating. The BET surface area of PBS was 1314 ± 10 m^2/g, while the surface area of RBS was just 1.8 m^2/g. The surface morphology of PBS and RBS, revealed by SEM, also indicated that PBS had an enhanced porous structure compared with RBS. Moreover, as illustrated in the FTIR spectra (Figure 6.5), the oxygen-containing functional groups (e.g., -COOH and –OH) were induced to PBS after pretreatment. As a result, the specific structure and diverse functional groups may contribute to the enhanced energetical heterogeneity of PBS.

Furthermore, according to the site energy distribution $F(E^*)$ plotted in Figure 6.8, the percentage (P) of binding sites whose site energy is greater than or equal to a specific value of E^* could be determined by Eq. (2.21) (Chapter 2 and page 37). For example, in the case of RBS,

the value of $P(E_m^*$ = 7.09 kJ/mol, the mode of site energy distribution), was determined to be 50%, which meant that 50 percent of binding sites had site energies greater than or equal to 7.09 kJ/mol.

6.2.2 Effect of Solution Temperature

It is well-known that temperature affects the adsorption process. The adsorption behaviors of NOR on PBS including isotherms and adsorption energy with respect to temperature remain largely unknown. These respective researches are critical to understand the adsorption mechanism and to develop advanced technologies to treat the pharmaceuticals-contaminated water.

6.2.2.1 Norfloxacin Adsorption Isotherms at Different Solution Temperatures

The NOR adsorption isotherms of PBS with respect to temperature (298.15, 308.15, and 308.15 K) are illustrated in Figure 6.9. As the temperature was increased, the equilibrium NOR adsorption capacities of PBS increased. This indicated that the adsorption of NOR on PBS was an endothermic process, which was consistent with the adsorption of LEV on PBS in this work and NOR on carbon nanotubes (Wang et al. 2010c). In addition, the experimental equilibrium data were well fitted by the *Langmuir-Freundlich* model (Eq. (2.4), Chapter 2, and page 34), and the obtained model parameters with coefficient of determination (R^2) and residual sum of squares (*RSS*) are presented in Table 6.3. The values of *n*, indicative of the surface site heterogeneity of the adsorbent, at 298.15, 308.15, and 318.15 K were 0.64, 0.77, and 0.83, respectively. It has been documented that the lower the value of "*n*", the stronger the heterogeneity (Cerofolini and Rudziński 1997), therefore, such *n* values demonstrated a weaker heterogeneity at a higher temperature. Discussion in the regards was made together with the results of site energy distribution in the later part of this section.

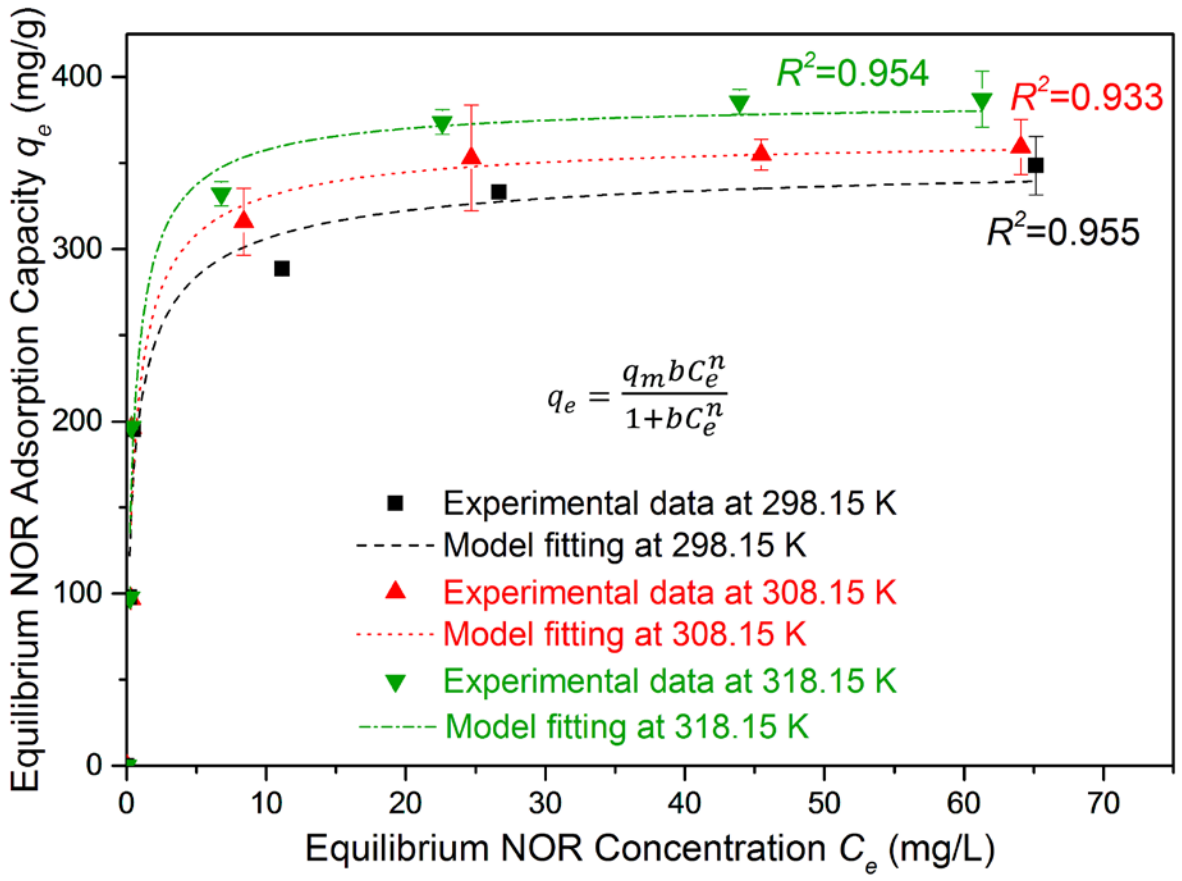

Figure 6.9 NOR adsorption isotherms of PBS at different temperatures.

50.0 ± 0.5 mL NOR solution, 5.0 ± 0.1 mg PBS, and pH 6.96 ± 0.07. Error bars represent standard deviation.

Table 6.3 Fitting results of the *Langmuir-Freundlich* model for NOR adsorption on PBS at different temperatures.

Temperature, K	q_m, mg/g	b, L/mg	n	R^2	*RSS*, $(mg/g)^2$
298.15 ± 0.50	356	1.42	0.64	0.955	2394
308.15 ± 0.50	367	1.53	0.77	0.933	3982
318.15 ± 0.50	387	1.78	0.83	0.954	3335

6.2.2.2 Approximate Site Energy and Its Distribution

Again, by incorporating the values of C_e into Eq. (2.9) (Chapter 2 and page 36), the adsorption site energy E^* was determined. Then, it was plotted against the equilibrium NOR

adsorption corresponding to the different temperatures in Figure 10a. As NOR loading increased, the adsorption site energy achieved at all solution temperatures dramatically decreased. Such result again revealed that at the same temperature, the high-energy adsorption sites on PBS were first occupied by NOR molecules at low concentrations, then the low-energy adsorption sites.

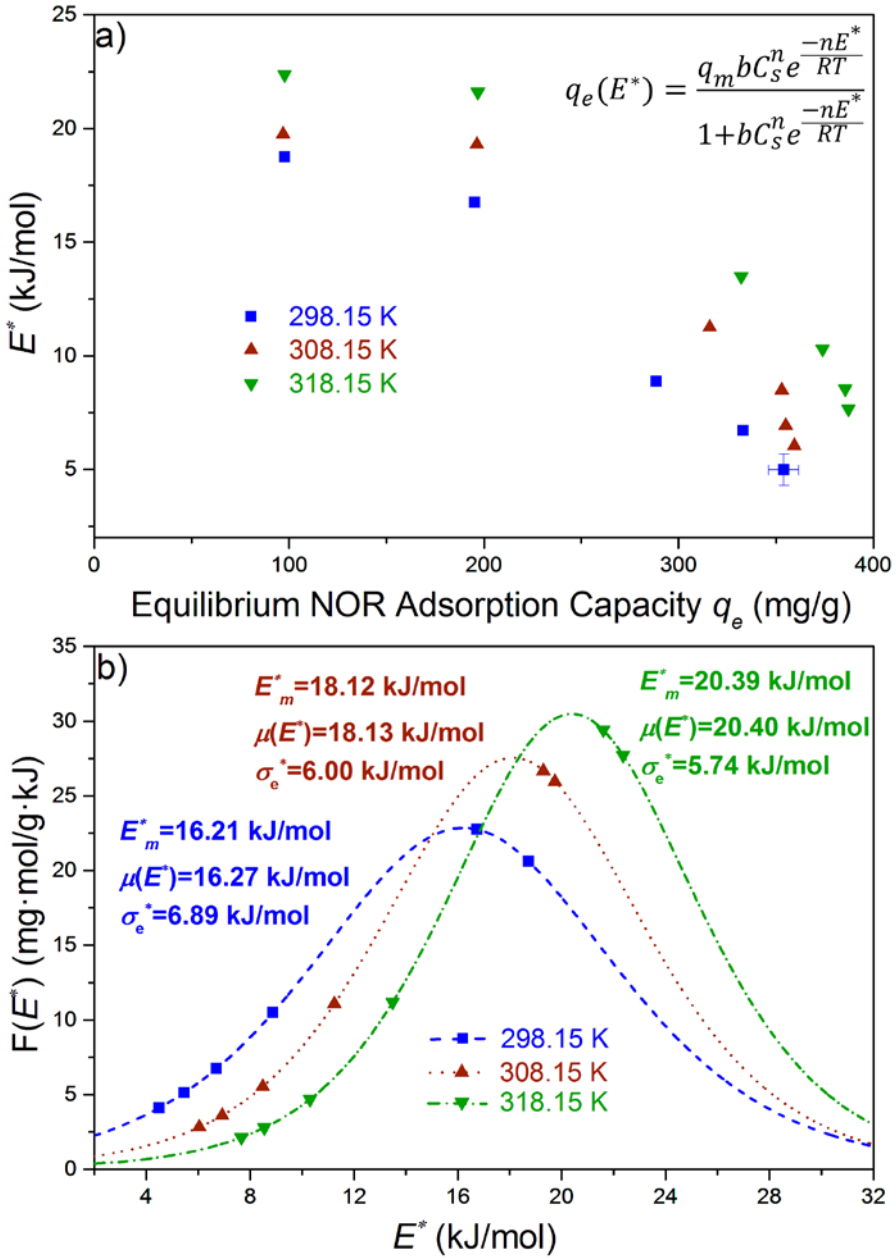

Figure 6.10 Site energy and its distribution of PBS for NOR adsorption with respect to temperature: a) dependence of site energy E^* on NOR loading; b) site energy distribution. Error bars represent standard deviation.

Based on the *Langmuir-Freundlich* modeling, the site energy distribution curves of PBS for NOR adsorption at different temperatures are illustrated in Figure 6.10b. Calculated by Eq. b(2.16) (Chapter 2 and page 36), the weighted mean of site energy distribution at 318.15 K (20.40 kJ/mol) was slightly higher than that of 298.15 K (16.27 kJ/mol) and 308.15 K (18.13 kJ/mol), which indicated the slightly stronger EDA interactions at 318.15 K. As a result, 318.15 K was more favorable for the adsorption reaction, which was consistent with the adsorption of LEV on PBS. This could also be interpreted by the increasing static dipole polarizability of the benzene ring of NOR (π-electron-acceptor) and the carboxyl, hydroxyl and aromatic groups of PBS (*n*- and π-electron-donors) with increase in temperature, which was discussed in the adsorption of LEV on PBS (Chapter 6 and pages 88-89).

Furthermore, the values of maximum NOR adsorption capacity q_m of PBS increased with increase in weighted mean of site energy distribution. This could be explained: as the temperature was increased, the site energy increased, and more binding sites were activated and available for NOR adsorption, as a result, the NOR adsorption capacity of PBS was improved.

As discussed in the Section of 6.2.1.3, PBS demonstrated the energetical heterogeneity for adsorption of NOR, and the energetical heterogeneity could be depicted by the standard deviation (σ_e^*) of site energy distribution. Given in Figure 6.10b, the σ_e^* values of PBS at 298.15 K, 308.15 K and 318.15 K were 6.89 kJ/mol, 6.00 kJ/mol and 5.74 kJ/mol, respectively. Therefore, the obtained values of "*n*" from the *Langmuir-Freundlich* model and σ_e^* determined from site energy distribution both demonstrated the consistent result that at the tested temperatures, the higher the temperature, the lower the heterogeneity. It can be interpreted as follows. EDA interactions (*n*-π, and π-π interaction) were proposed as one of the primary forces in the adsorption of NOR on PBS. Such interactions were the attractive forces between electron-rich (donors, i.e., PBS) and electron-deficient (acceptors, i.e., NOR) entities. Thus, the

electronic density heterogeneity of the adsorbent surface contributed to the energetical surface heterogeneity of the adsorbent which was reflected by the standard deviation of site energy distribution. Increasing temperature weakened the electronic density heterogeneity of the adsorbent surface, particularly for carbonaceous materials such as activated carbon (Fujiwara et al. 1991, Kaneko 1997), and thus narrowed the dispersion of EDA interactions of the adsorbent with the adsorbate. Such result was consequently reflected by the slightly decrease of standard deviation of the distribution as solution temperature was increased.

Furthermore, based on the site energy distribution $F(E^*)$, the percentage (P) of binding sites (the site energy of which were greater than or equal to a specific value of E^*) was estimated by Eq. (2.21) (Chapter 2 and page 37). Determined by Eq. (2.21), the value of $P(E_m^*$ =16.21 kJ/mol) at 298.15 K was 50.0%, which meant that 50 percentage of binding sites had site energies greater than or equal to 16.21 kJ/mol. The P value of the weighted mean of the distribution, $\mu(E^*)$ (16.27 kJ/mol at 298.15 K), was 49.6%.

6.3 Desorption of Norfloxacin Adsorbed on Pretreated Barley Straw

Desorption experiments were conducted immediately after adsorption equilibrium (168 h) at the same temperature and in the same vials as those for adsorption experiments. The residual NOR solutions (the initial concentrations were 40, 60, and 80 mg/L) were removed from the vials by a SOCOREX Acura 835 micropipette (1-10 mL). Then, the same volume of 50 mL ethylenediaminetetraacetic acid disodium salt dihydrate (EDTA, 100 mg/L) solutions were added to each vial containing the adsorbents loaded with NOR. The amount of NOR adsorbed on PBS were 333, 359, and 378 mg/g, respectively. The solution pH was adjusted to a value of 2.00 in order to obtain a higher desorption efficiency (determined by the ratio of the amount of NOR released from the adsorbent at the equilibrium of desorption to the amount of initially loaded NOR on the adsorbent). The vials were then shaken at 150 rpm for 168 h in the dark.

The desorption efficiencies of PBS samples loaded with 333, 359, and 378 mg NOR/g were (25 ± 3)%, (30 ± 3)%, and (39 ± 3)%, respectively. Although these values were higher than those of LEV adsorbed on PBS, they were still much lower than those of nickel adsorbed on RBS (Thevannan et al. 2010) and $Au(CN)_2$ adsorbed on the crab shells in which ion exchange and electrostatic attraction were proposed as the predominant mechanisms (Niu 2002). The strong binding of NOR by PBS once again indicated that π-π EDA interaction, the bonding strength of which could be larger than that of hydrogen bond, and comparable to inner- and outer-sphere complex formation (Keiluweit and Kleber 2009), may be one of the major adsorption mechanisms. In addition, the result supported that the pH-dependent electrostatic attraction was not the principal mechanism. Considering that the achieved desorption efficiency was low, other methods, such as oxidation and thermal treating in a microwave furnace, may be employed to improve the desorption efficiency. More in depth desorption investigations would form an area of future research.

6.4 Electron-Donor-Acceptor Interactions Characterized by X-ray Absorption Near Edge Structure Spectroscopy

The electronic structures of PBS, NOR, and PBS loaded with NOR were studied by the X-ray absorption near-edge structure (XANES) spectroscopy using a scanning transmission X-ray microscope (STXM) beamline at the Canadian Light Source. The corresponding C 1s *K*-edge XANES spectra are presented in Figure 6.11a. The resonance peaks at energy levels of 285.67 and 288.09 eV on the spectrum of PBS corresponded to C 1s →π* C=C of aromatic C and carboxylic C (Chen et al. 2014a, Heymann et al. 2011), respectively. There were resonance peaks at 284.92, 285.98, and 286.58 eV observed on the NOR spectrum, which have been attributed to the carbon atoms in benzene ring attached to hydrogen (C=C*-H) (Kuznetsova et al. 2001), nitrogen (C=C*-N) (Stöhr 1992), and fluorine (C=C*-F) (Brzhezinskaya et al. 2009,

Plaschke et al. 2005), respectively. The peak at 288.54 eV of NOR represented C 1s →π* C=O transition of carboxylic C (Lu et al. 2013). Comparing the spectra of PBS, NOR, and PBS loaded with NOR, blue shifts of the peaks were observed from 285.67 and 288.09 eV of the spectrum of PBS to 285.82 and 288.24 eV of the spectrum of PBS loaded with NOR, which was also observed in the C *K*-edge XANES spectra of LEV adsorption on PBS (Figure 5.17 on page 97). Such blue shifts meant the higher energy value of photon resonance for excitation, and that the carbon atoms of aromatic π*(C=C) and carboxylic π*(C=O) of NOR loading on PBS had partial-positive charges with less electron densities (Kuznetsova et al. 2001).

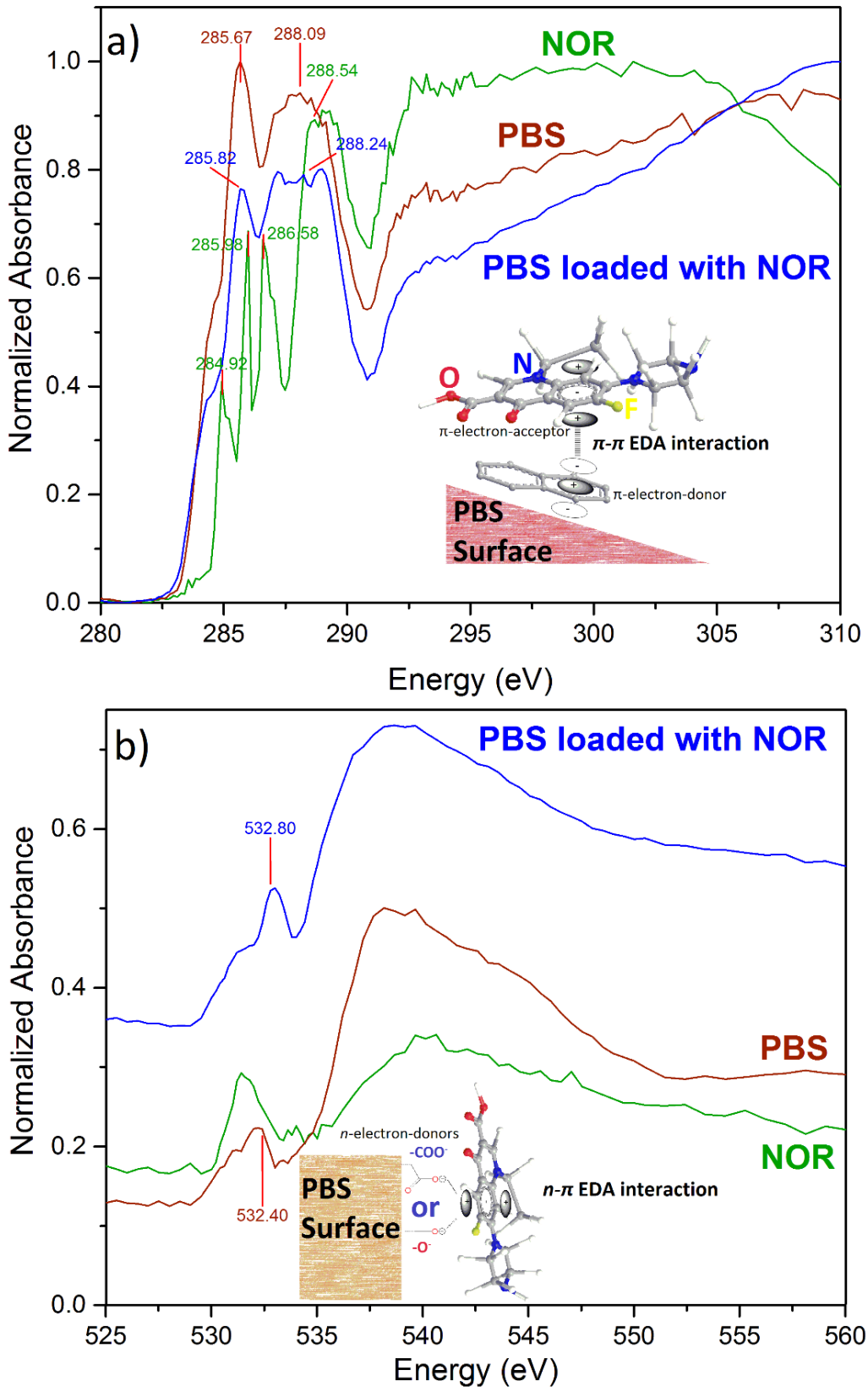

Figure 6.11 XANES spectra of PBS, NOR, and PBS loaded with NOR (q_e = 349 ± 17 mg/g): a) C 1s *K*-edge XANES spectra; b) O 1s *K*-edge XANES spectra.

50.0 ± 0.5 mL NOR solution (C_0 = 100 mg/L), 5.0 ± 0.1 mg PBS, pH 6.96 ± 0.07, and 298.15 ± 0.50 K.

Furthermore, the O 1s *K*-edge spectra of PBS, NOR, and PBS loaded with NOR are illustrated in Figure 6.11b. The peak representing O 1s O-C=O at 532.40 eV (Calborean et al. 2015) of the spectrum of PBS blue shifted to 532.80 eV of the spectrum of PBS loaded with NOR. The results of C 1s and O 1s XANES spectra demonstrated that the surface-associated electron-rich carboxylic groups (-COO^-) and aromatic groups of PBS served as *n*-electron-donors and π-electron-donors (Okbinoğlu 2014). This may be explained as follows: the functional groups of PBS (e.g., carboxyl and hydroxyl) were polar groups and can be polarized, surface sites close to the polarized edge sites or defects of graphene sheets could serve as electron-rich-(*n* or π)-donors, as informed in adsorption of benzene on charcoal and of polycyclic aromatic hydrocarbons on soot (Kubicki 2006, Zhu et al. 2005, Zhu and Pignatello 2005); on the other hand, the carbon atom that is bonded to the fluorine (C=C*-F) within a benzene ring of NOR has been reported to work as a π-electron-acceptor due to the strong electron withdrawing ability of F (Keiluweit and Kleber 2009, Wang et al. 2010c); therefore, the proposed EDA interactions (*n*-π and π-π) between the polarizable PBS (carboxyl and aromatic groups, *n*- or π-electron-donors) and NOR (carbon atom in benzene ring attached to F, π-electron-acceptor) became reasonable. The EDA interactions (*n*-π and π-π) between the adsorbates (e.g., norfloxacin (Wang et al. 2010c), naphthalene and atrazine (Shen et al. 2015)) and heterogeneous adsorbents (such as lignin (Wang et al. 2007) and humic substances (Zhu et al. 2004)) have been reported to play the predominant role. Therefore, such interactions were also proposed as one of the dominant mechanisms in the adsorption of NOR on PBS. In a real aquatic system, mechanisms like EDA interactions, hydrogen bond, electrostatic attraction, and hydrophobic interaction may simultaneously work in the adsorption of NOR on PBS, which needs to be further investigated.

6.5 Comparison of Norfloxacin Adsorption Capacity of PBS with Other Adsorbents

The experimentally obtained NOR adsorption capacity of PBS (396 ± 19 mg/g) was much higher than that of RBS (54 ± 15 mg/g) and adsorbents in literature, such as carbon nanotubes (<150 mg/g at pH 6.8-7.2 and room temperature) (Peng et al. 2012, Wang et al. 2010c), iron-doped activated alumina (7 mg/g at pH 6.5 and 298.15 K), and lotus stalk-based activated carbon (295 mg/g at pH 5.5 and 298.15 K) (Liu et al. 2011). The results demonstrated that PBS was also effective for NOR adsorption and had a promising potential for removal of antibiotics in aquatic systems.

6.6 Chapter Summary

In this chapter, as another model of antibiotics, NOR was efficiently removed by the adsorbent PBS. The experimentally achieved NOR adsorption capacity of PBS was 396 ± 19 mg/g at pH 6.96 ± 0.07, which was much higher than that of RBS and the reported adsorbents. High NOR adsorption capacities of PBS were achieved in a wide pH range from 2.67 ± 0.06 to 10.50 ± 0.13. As such, the EDA interactions (such as *n*-π and π-π) that was not significantly affected by the moderate solution pH, between the polarizable PBS (carboxyl and aromatic groups, as *n*- and π-electron-donors) and NOR (carbon atom in benzene ring attached to F, as a π-electron-acceptor), were proposed as one of the major forces and characterized by C and O *K*-edge XANES. In addition, hydrogen bond could also play a role in the adsorption. The adsorption kinetics and equilibrium isotherms with respect to temperature were investigated using the pseudo-second-order kinetic model and *Langmuir-Freundlich* model, respectively. According to the *Arrhenius* equation, the activation energy was determined to be 22.21 kJ/mol. The adsorption mechanism was investigated by the analysis of site energy and its distribution. The results of the activation energy, site energy distribution, and XANES supported that

chemical adsorption was the dominant mechanism in the adsorption of NOR on PBS, and that the EDA interactions played an important role. As a critical operating parameter, temperature affected the adsorption process as follows: i) the adsorption rate constant *k* increased with increase in temperature which led to the increase of NOR adsorption rate; ii) the adsorption of NOR on PBS was an endothermic process, more binding sites were activated and available for NOR adsorption at a higher temperature, therefore, the corresponding NOR adsorption capacity of PBS enhanced; iii) the promoted temperature enhanced the static dipole polarizability, as a result, the EDA interactions of PBS with NOR were strengthened, which was reflected by the increasing weighted mean of site energy distribution as temperature was increased; vi) the increasing temperature weakened the electronic density heterogeneity of the adsorbent surface, and thus narrowed the dispersion of EDA interactions of PBS with NOR, which was consequently reflected by the slightly decrease of the standard deviation of the distribution as temperature was increased, in the tested temperature range (298.15 K-318.15 K), the higher the temperature, the lower the energetical heterogeneity. Furthermore, the percentage of adsorption sites, the site energy of which are greater than or equal to a specific energy E^*, was estimated.

CHAPTER 7 ADSORPTION OF NICKEL ON PRETREATED BARLEY STRAW AND IMPACT OF NICKEL ON LEVOFLOXACIN ADSORPTION

In addition to pharmaceuticals-containing wastewater, large quantities of nickel wastewater are generated and discharged into the environment. Nickel-containing wastewater is associated with several diseases (e.g., dermatitis, nausea, chronic bronchitis, gastrointestinal distress, and lung cancer) and thus threatens human health (Flores-Garnica et al. 2013, Sharma and Singh 2013). Furthermore, the discharged nickel ions may pose another health threat as they coexist with antibiotics (e.g., LEV) in diverse aquatic systems. There is a need to effectively remove nickel ions from water bodies and streams to ensure the adequately treated effluent quality for various uses and to protect human health.

7.1 Adsorption of Nickel on Adsorbents Based on Barley Straw

It is well known that solution pH affects charge state of adsorbent and speciation of adsorbate, and therefore the adsorption process. As presented in the former chapters of this dissertation (Figure 5.6 on page 76), the value of point of zero net charge (PZNC) of PBS was determined to be 4.1. Thus, the surface of PBS was positively charged (solution pH < 4.1), otherwise negatively charged at pH higher than that. To ensure that the surface of PBS becomes negatively charged, the solution pH has to be higher than 4.1. In addition, the fact that nickel precipitation occurs at solution pH 8 and above should be considered (Cayllahua et al. 2009). As such, effect of solution pH on the adsorption of nickel (Ni^{2+}) by PBS was first examined at pH 5.0 ± 0.1 and 7.0 ± 0.1 (C_0 = 1000 mg/L), respectively. Adsorption experiments were run for 5 hours to ensure that the adsorption equilibrium was reached, which was consistent to the previous work (Thevannan et al. 2010). Each of the experiments was performed in duplicate.

The achieved equilibrium nickel adsorption capacity 55.8 mg/g at pH 7.0 was higher than 29.3 mg/g at pH 5.0.

In the adsorption process, nickel ions exchanged with protons of the acidic functional groups on PBS and were adsorbed via electrostatic attraction, which was evidenced by the fact that protons were released into the solution, therefore the solution pH decreased during the process of nickel adsorption. As a result, to maintain a constant value of solution pH, it had to be instantly automatically adjusted by the SCHOTT titrator via adding 0.1 M sodium hydroxide. Thus, electrostatic attraction between the negatively charged surface of PBS and positively charged nickel ions, was suggested to dominant the adsorption process. The solution pH 7.0 resulted in a more negatively charged surface of PBS, therefore stronger adsorption affinity (electrostatic interaction), which enhanced the nickel adsorption capacity of PBS.

As such, the nickel adsorption isotherm of PBS was determined at pH 7.0 ± 0.1 with equilibrium nickel concentrations from 1.7 mg/L to 932 mg/L. Each of the experiments was performed in duplicate. The equilibrium nickel adsorption data of PBS and RBS are presented in average value with standard deviation and illustrated in Figure 7.1. The model of *Langmuir-Freundlich* (Sips 1948) was used to fit the experimental data, and the regressed parameters of the model are listed in Table 7.1. The experimental data of PBS and RBS were also well fitted by the *Langmuir-Freundlich* model with high values of coefficients of determination R^2 ($\geq$ 0.980). Compared with RBS, the *b* value of PBS was again much higher than that of RBS indicating the higher binding energy of PBS with nickel ions than that of RBS. In addition, the q_m value of PBS obtained from the *Langmuir-Freundlich* modeling (59.5 ± 3.0 mg/g) was much higher than that of RBS (6.8 ± 1.3 mg/g). It demonstrated that after H_3PO_4 modification, more binding sites on RBS are available for nickel adsorption as well.

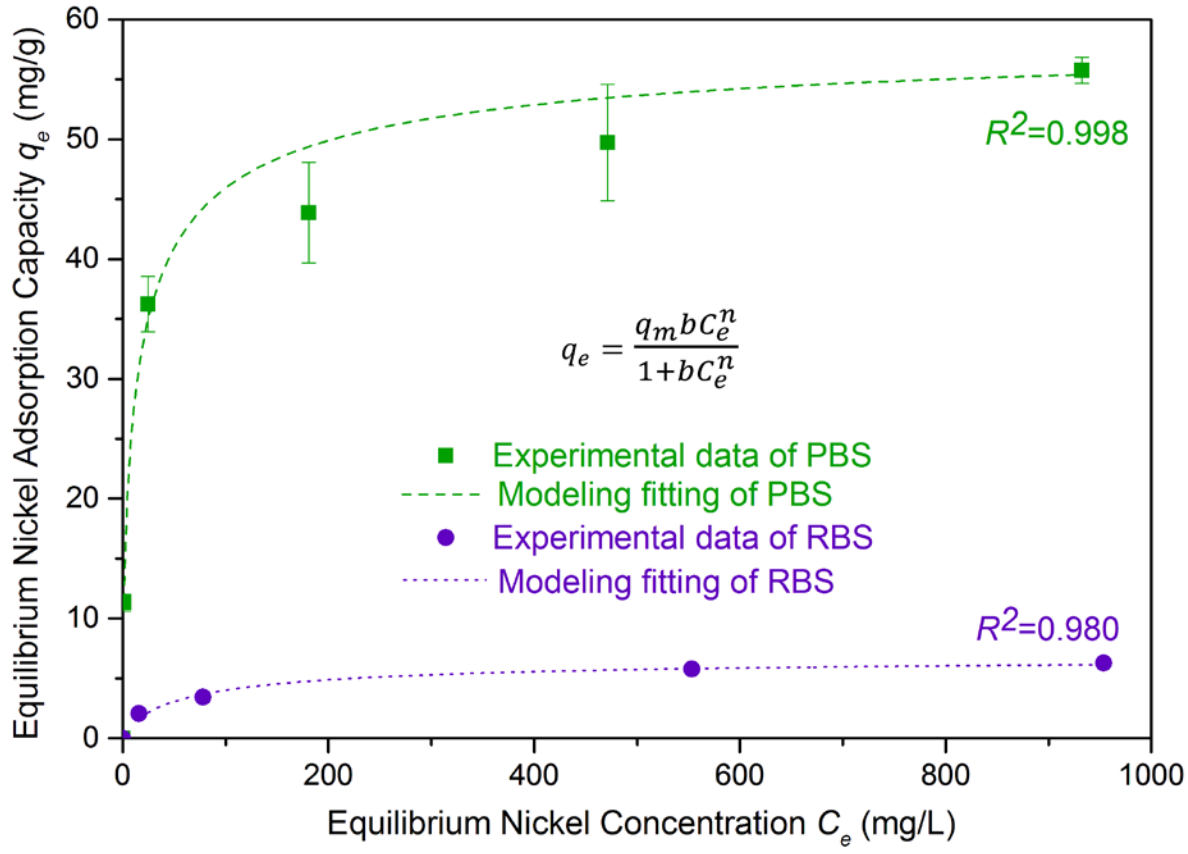

Figure 7.1 Nickel adsorption isotherms of PBS and RBS.

300 ± 2 mL nickel solution, 600 ± 2 mg PBS or RBS, 298.15 ± 0.50 K, and pH 7.0 ± 0.1. Error bars represent the standard deviation.

Table 7.1 The *Langmuir-Freundlich* modeling results of nickel adsorption on PBS and RBS.

Equation	Parameters	PBS	RBS
$q_e = \frac{q_m b C_e^n}{1 + b C_e^n}$	q_m, mg/g	59.5 ± 3.0	6.8 ± 1.3
	b, L/mg	0.196 ± 0.019	0.034 ± 0.039
	n	0.619 ± 0.085	0.808 ± 0.378
	R^2	0.998	0.980
	RSS^*, $(mg/g)^2$	46.29	0.24

* *RSS* residual sum of squares $(mg/g)^2$.

Previous FTIR analyses of PBS and RBS indicated that carboxyl groups were created on PBS. The proton dissociation constants (pK_a) of carboxyl group is 3.5-4.5 (Buffle et al. 1988,

Roberts 1992). This may lead to that the PZNC of PBS (4.1) was lower than that of RBS (5.9), which demonstrated that PBS had more acidic groups to bind nickel ions than RBS. In addition, the specific surface area of PBS was determined to be 1314 ± 10 m^2/g, while that of RBS was just 1.8 m^2/g. The surface morphology of PBS and RBS characterized by scanning electron microscopy also demonstrated that PBS had an enhanced porous structure compared with RBS. The well-developed pores of PBS facilitated nickel ions effectively accessing the functional groups on PBS. As a result, the significantly enhanced nickel adsorption capacity of PBS could be mainly contributed by the aforementioned acidic functional groups and porous structure of PBS.

7.2 Site Energy and Its Distribution

Figure 7.2a displays the site energy E^* as a function of the equilibrium nickel adsorption capacity q_e. Consistent with the adsorption of LEV and NOR on PBS, E^* of PBS and RBS for nickel dramatically decreased as nickel loading increased, which also revealed that nickel ions first occupied the high-energy adsorption sites of PBS and RBS, then spread to the low-energy adsorption sites.

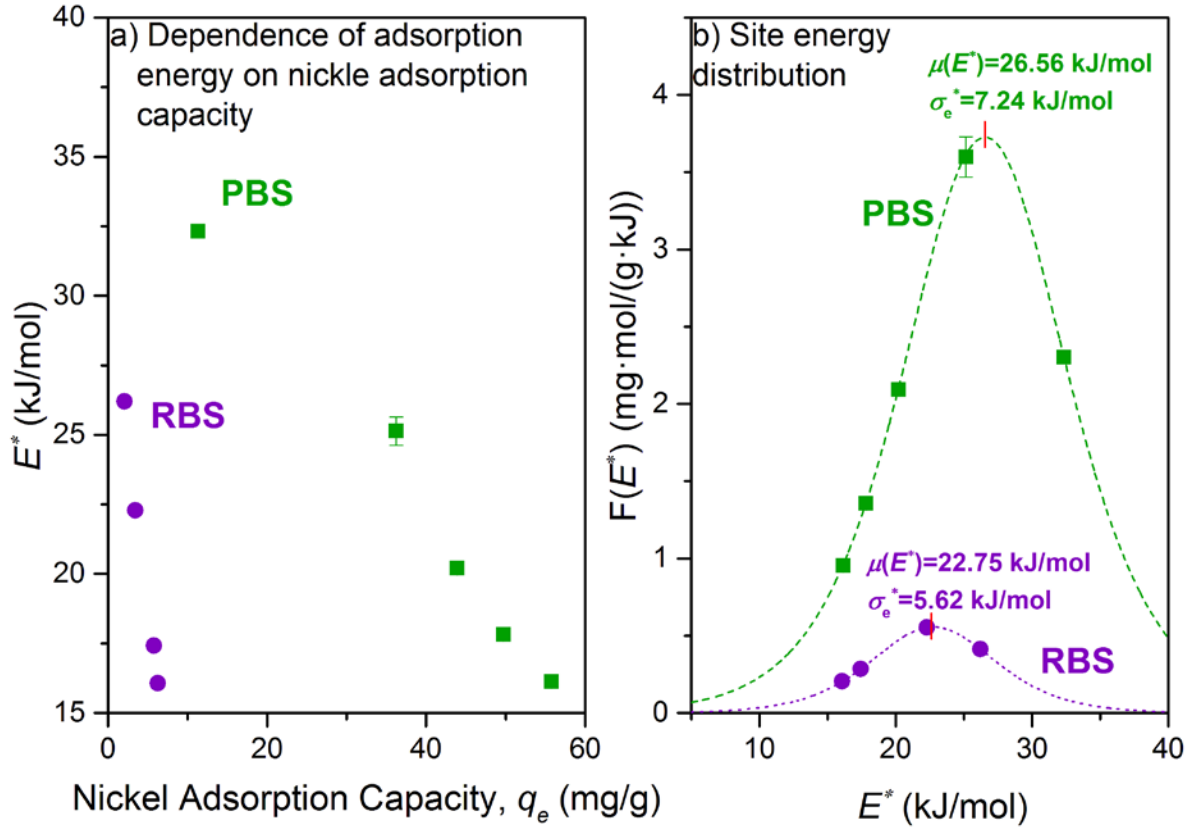

Figure 7.2 Site energy (a) and its distributions (b) of PBS and RBS for nickel adsorption.

The site energy distributions of PBS and RBS for nickel adsorption are plotted in Figure 7.2b. Reflected by the much bigger area under the distribution curve of PBS than that of RBS, PBS again showed a higher maximum nickel adsorption capacity than RBS, which was also confirmed by the experimental data. It again demonstrated that the pretreatment method successfully enhanced the nickel adsorption capacity of RBS.

As illustrated in Figure 7.2b, there was an overall right shift of site energy of PBS compared with that of RBS, reflecting the overall increase in site energy of PBS. Again, determined by Eq. (2.16) (Chapter 2 and page 36), PBS had a higher weighted mean of site energy distribution (26.56 kJ/mol) than RBS (22.75 kJ/mol), which indicated the stronger adsorption affinity of PBS for nickel ions (Carter et al. 1995). Thus, in addition to adsorption of LEV and NOR, PBS was more favorable for adsorption of nickel than RBS as well. This

could be attributed to the increased number of oxygen-containing functional groups of PBS, especially carboxyl groups having higher affinity for nickel ions (Shen et al. 2015).

Moreover, both PBS and RBS revealed site energy heterogeneity for adsorption of nickel ions, evidenced by the site energy distribution curves in Figure 7.2b. The standard deviation σ_e^* of the distribution was again applied to characterize the energetical heterogeneity of the adsorbents in this chapter. Through Eqs. (2.17), (2.18) and (2.19) (Chapter 2 and page 37), the σ_e^* values of PBS and RBS for nickel adsorption were determined to be 7.24 and 5.62 kJ/mol, respectively. The slightly higher σ_e^* value of PBS than that of RBS indicated the slightly stronger heterogeneity of PBS than that of RBS, which was consistent with the NOR adsorption on PBS and RBS. Similar to discussion in the Section of 6.2.1.3, such result might be due to the collective effects of the specific porous structure and diverse functional groups of PBS. However, the actual mechanisms need to be further investigated.

7.3 Desorption of Nickel Adsorbed on Pretreated Barley Straw

Desorption experiments were conducted at pH 2.0 ± 0.1. Desorption efficiency of the nickel loaded on PBS, the ratio of nickel eluted from PBS loaded with nickel to the initially loaded nickel, was determined to be 91.1%. The results indicated that higher electronegativity value H^+ ions (EN. H^+ is 2.20) were able to replace Ni^{2+} ions (EN. Ni^{2+} is 1.91) (Ewecharoen et al. 2009), and that ion exchange played an important role in the nickel adsorption on PBS. Niu et al. achieved 100% elution of $Au(CN)_2^-$ from the acid washed crab shells and proved that the adsorption was mainly through electrostatic attraction (Niu 2002). The slightly lower desorption efficiency (91.1%) in this work implied that other mechanisms might also be involved in the adsorption of nickel on PBS. It has been reported that metal ions can be bonded to carboxyl groups through chelation (Nakamoto 2008). The carboxyl groups of PBS may play an important multi-roles that significantly enhanced the nickel adsorption capacity of PBS than

that of RBS. The nickel adsorption mechanism was further investigated by the X-ray analyses in the following section.

7.4 X-ray Analyses of Nickel Adsorption on Pretreated Barley Straw

The X-ray fluorescence (XRF) spectra of PBS after exposure to nickel solutions are illustrated in Figure 7.3a, and show that the intensity of the peaks for nickel (K_α and K_β) increased as the amounts of nickel adsorbed on PBS was increased. The XRF results again confirmed that nickel ions were adsorbed on PBS. Figure 7.3b displays XRF spectra of PBS loaded with nickel (q_e = 35.8 mg/g) and PBS after desorption. The results clearly demonstrated that most of adsorbed nickel (~90%) was eluted from PBS at solution pH 2.0, which verified that the majority of nickel adsorption was reversible by lowering the solution pH to 2.0.

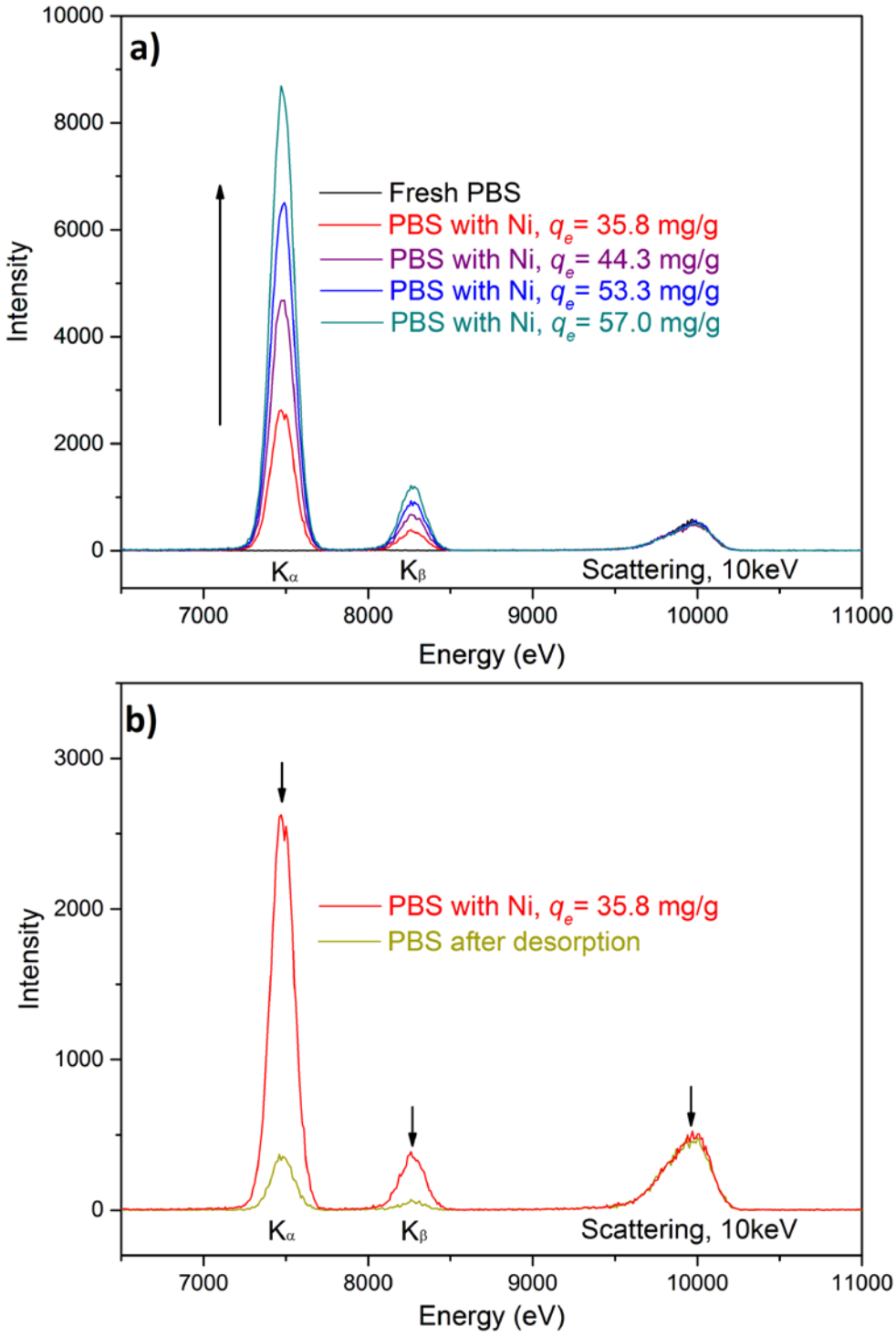

Figure 7.3 XRF spectra of nickel adsorbed on PBS (a) and after desorption (b).

In order to further investigate the adsorption mechanism, X-ray absorption spectroscopy (XAS) was used to characterize the chemical state and the environment of Ni atom. X-ray absorption near edge structure (XANES) spectroscopy could provide information about the

coordination geometry and oxidation state of the metal, whereas extended X-ray absorption fine structure (EXAFS) spectroscopy contains information about the backscattering atoms, coordination numbers (*CN*), and atomic distance (*r*) (Ewecharoen et al. 2009).

Figure 7.4 displays the results of normalized Ni *K*-edge XANES spectra of PBS loaded with Ni (curve a) in comparison with that of $NiSO_4$ (curve b, the valence of nickel is +2) and metallic Ni foil (curve c, the valence of nickel is 0) which were used as references in order to verify whether the valence of adsorbed nickel is the same as that of Ni(II) of nickel sulfate (nickel solution was prepared by dissolving $NiSO_4 \cdot 6H_2O$ into water in this work). The close absorption edge position of Ni adsorbed by PBS and $NiSO_4$ clearly indicated that the oxidation state of Ni adsorbed by PBS was Ni(II), which suggested that the oxidation state of Ni unchanged during the adsorption process of nickel on PBS. Such result was different from the adsorption of Cr(VI) from aqueous solution on polypyrrole wrapped oxidized multi-walled carbon nanotubes, in which Cr(VI) was partially reduced to Cr(III) (Bhaumik et al. 2016).

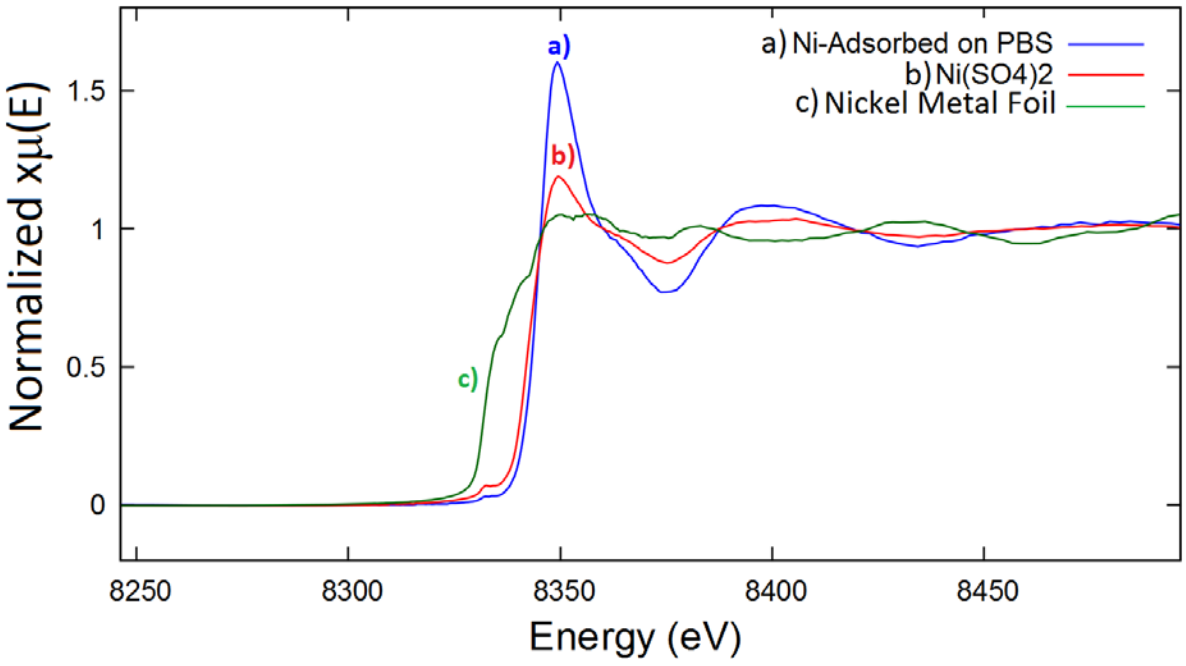

Figure 7.4 Ni *K*-edge XANES spectra: a) Ni adsorbed on PBS (blue, pH = 7.0 and q_e = 35.8 mg/g); b) $NiSO_4$ (red); c) nickel foil (green).

The k^2-weighted EXAFS spectra and the corresponding *Fourier* transforms into *R*-space of Ni adsorbed on PBS, $NiSO_4$ (nickel solution was prepared by dissolving $NiSO_4 \cdot 6H_2O$ into water in this work), and $Ni(CH_3COO)_2$ (as reference of Ni-C crystal structure) samples are illustrated in Figure 7.5. The fitting results and structural parameters are listed in Table 7.2. The main features of Ni adsorbed on PBS in Figure 7.5b (peaks 1 and 2) matched well with those from $NiSO_4 \cdot 6H_2O$. However, the rests (peaks 3 and 4) were closer to $Ni(CH_3COO)_2$. Peak 1 and 2 of Ni adsorbed on PBS could be well fitted by first oxygen shell of $NiSO_4$ (Beevers and Lipson 1932) or $NiCO_3$ (Pertlik 1986) at an atomic distance of 2.043 ± 0.013 Å with a coordination number (*CN*) of 6, and both the values of *R*-factor, representing the relative error of the crystallographic model fitting results to the experimental data, were 0.008. It indicated that Ni was surrounded by six oxygen atoms after adsorbed on PBS. The peaks 3 and 4 that were fitted by those of $Ni(CH_3COO)_2$, implied that the adsorbed Ni(II) might be bonded to the carboxyl groups on PBS. The result was in accordance with adsorption of copper ion on soil in which copper was suggested to be bonded to six oxygen atoms of the organic matter of soil (Graouer-Bacart et al. 2013). Thus, the interactions between the adsorbent PBS and adsorbate nickel could be proposed: pH-dependent electrostatic attraction and/or cation exchange dominated the adsorption, which was supported by release of proton and higher desorption efficiency (91.1%) at pH 2.0; and chelation between nickel and carboxyl groups of PBS might also exist though being insignificant, which could explain the small amount of undesorbed nickel on PBS. For aqueous environmental systems, multiple bonding mechanisms are expected to operate simultaneously. The actual mechanisms of nickel adsorption by PBS need further investigation.

Table 7.2 Structural parameters obtained from the EXAFS analysis of nickel adsorbed on PBS.

Nickel Samples	Shell	*CN*	*r* (Å)	*r* (Å)XRD	σ^2 (Å^2)
$NiSO_4 \cdot 6H_2O$	Ni-O	6	2.036 ± 0.012	2.016 (Beevers and Lipson 1932)	0.0040
$NiCO_3$ (Pertlik 1986)	Ni-O	6	--	2.076	--
	Ni-C	6	--	2.932	--
Ni-adsorbed on PBS	Ni-O	6	2.043 ± 0.013	-	0.0065

--: not given in literature.

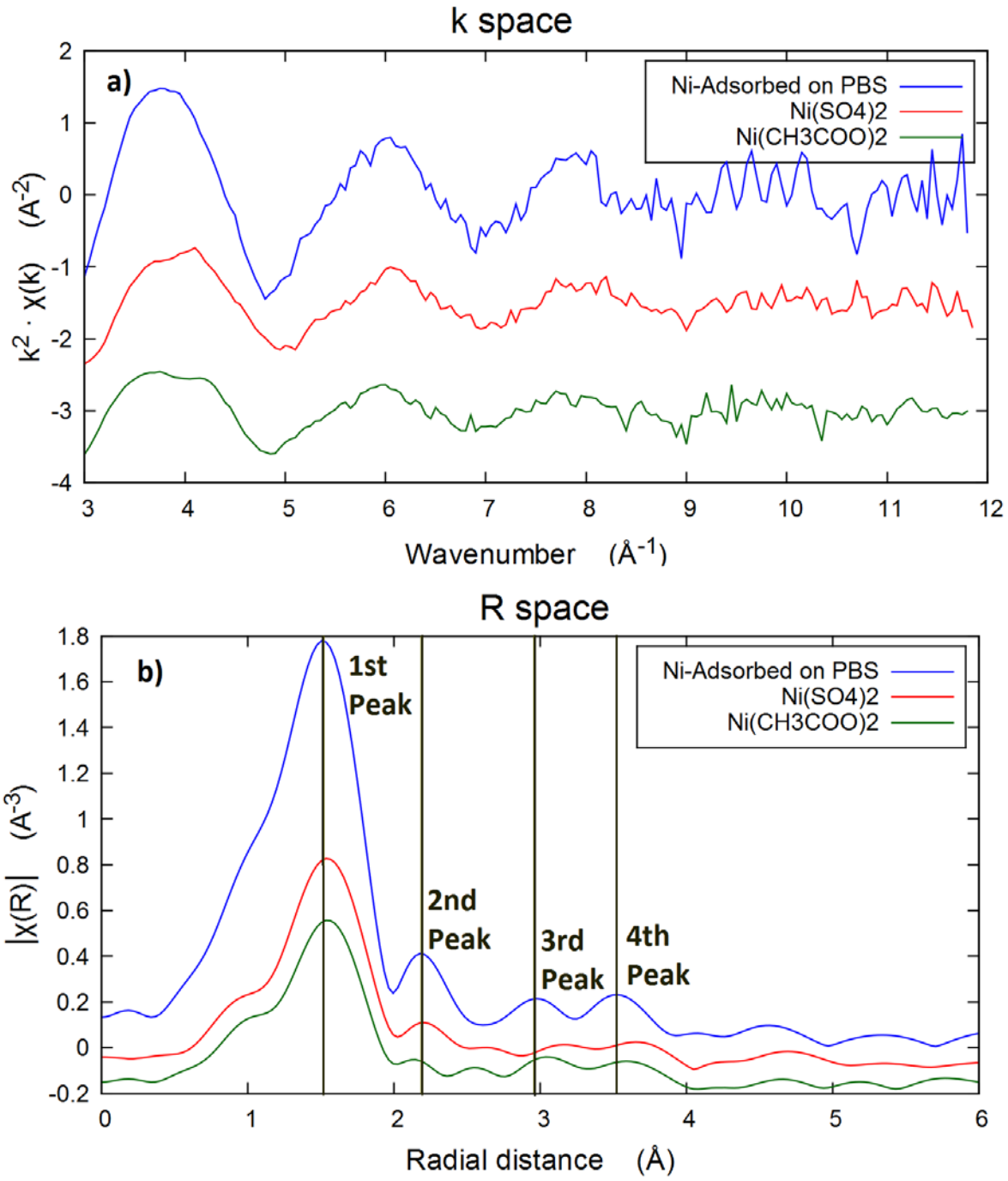

Figure 7.5 k^2-weighted EXAFS spectra (a) and their *Fourier* transforms (b) of Ni adsorbed on PBS (q_e = 35.8 mg/g), $NiSO_4$, and $Ni(CH_3COO)_2$.

7.5 Comparison of Nickel Adsorption Capacity of Pretreated Barley Straw with Other Adsorbents

For further comparison, the nickel adsorption capacity of PBS (q_m, obtained from *Langmuir-Freundlich* fitting) and other adsorbents reported in literature are summarized in Table 7.3. Nickel adsorption capacity of PBS determined in this work was higher than that of RBS, activated carbon from lignin (14 mg/g) (Gao et al. 2013), Bofe clay (1.9 mg/g) (Vieira et al. 2010), zeolite (26.8 mg/g) (Quintelas et al. 2013), aerobic activated sludge (24.3 mg/g) (Liu et al. 2012), lignocellulosic bagasse (2.8 mg/g) (Krishnani et al. 2009), Irish peat moss (21.1 mg/g) (Sen Gupta and Bhattacharyya 2008), magnetic porous Fe_3O_4-MnO_2 (55.6 mg/g) (Zhao et al. 2016), and close to the graphene oxide membranes (62.3 mg/g) (Tan et al. 2015). Although the activated carbon made from sugarcane bagasse pith had a higher nickel adsorption capacity (140.8 mg/g) (Krishnan et al. 2011), the preparation was placed in a muffle furnace maintained at 673.15 K for 1 h, then kept at 873.15 K for 2 h, which costed much more energy and time. The treatment of RBS in this work (9 min in microwave) is energy- and time-saving, and relatively low-cost.

Table 7.3 Comparison of nickel adsorption capacity of PBS with adsorbents reported in literature.

Adsorbents	pH	q_m, mg/g	Source
Pretreated barley straw	7.0	59.5 ± 3.0	This work
Raw barley straw	7.0	6.8 ± 1.3	This work
Activated carbon from lignin	6.4	14.0	(Gao et al. 2013)
Gamma irradiation activated carbon	3.9	55.7	(Ewecharoen et al. 2009)
Bofe clay	5.3	1.9	(Vieira et al. 2010)
Zeolite	6.0	26.8	(Quintelas et al. 2013)
Activated carbon from sugarcane bagasse pith	6.5	140.8	(Krishnan et al. 2011)
Aerobic activated sludge	7.0	24.3	(Liu et al. 2012)
Lignocellulosic bagasse	5.8	2.8	(Krishnani et al. 2009)
Irish peat moss	5.7	21.1	(Sen Gupta and Bhattacharyya 2008)
Graphene oxide membranes	5.7	62.3	(Tan et al. 2015)
Magnetic porous Fe_3O_4-MnO_2	7.7	55.6	(Zhao et al. 2016)

7.6 Impact of Nickel on Levofloxacin Adsorption by Pretreated Barley Straw

Effect of nickel on LEV adsorption by PBS at different solution pH (4.0 ± 0.1, 7.0 ± 0.1, and 9.0 ± 0.1) are illustrated in Figure 7.6. Addition of Ni(II) suppressed the adsorption of LEV on PBS at the tested three pH values, which may be due to the competition of the cation Ni^{2+} for the negatively charged adsorption sites of PBS. This result was consistent to the adsorption

of NOR on montmorillonite in the presence of Cu at pH 4.5 (Pei et al. 2011). However, the actual mechanism (e.g., the formation of ternary complexes between LEV, nickel and PBS) should be further investigated.

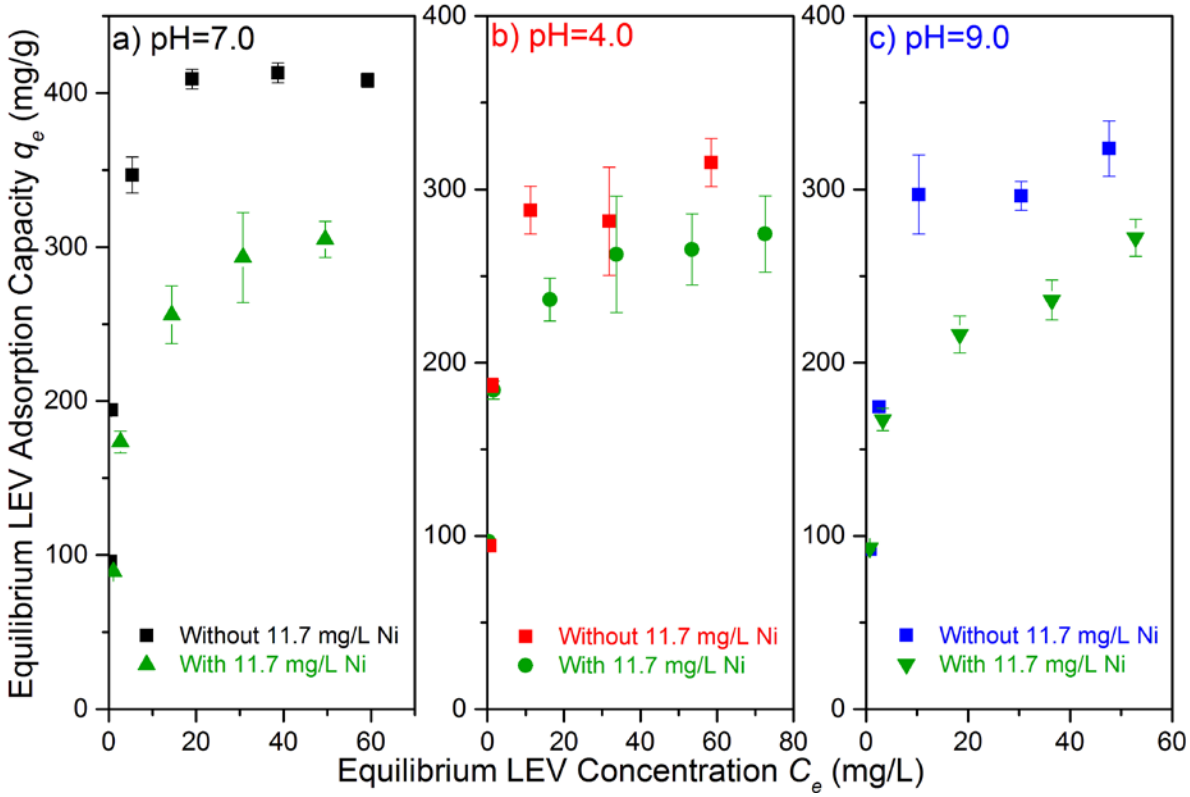

Figure 7.6 Effect of nickel on LEV adsorption by PBS at different solution pH.

50.0 ± 0.5 mL, LEV solution, 5.0 ± 0.1 mg PBS, contact time 168 h, and 298.15 ± 0.50 K. Error bars represent the standard deviation.

7.7 Chapter Summary

The adsorbent (PBS) made from raw barley straw with H_3PO_4 impregnation and microwave heating had a significantly enhanced nickel adsorption capacity almost six times that by RBS. Solution pH played an important role during the nickel adsorption process. The release of proton during adsorption and higher desorption efficiency (91.1%) at pH 2.0 indicated that electrostatic attraction dominated the adsorption. Furthermore, XAS studies (XANES and EXAFS) demonstrated that the adsorbed Ni remained the oxidation state (II)

during the adsorption process and associated with 6 oxygen atoms from water or the functional groups on PBS (such as carboxyl groups) at a distance of 2.043 ± 0.013 Å. For the first time, the approximate adsorption site energy distributions based on the *Langmuir-Freundlich* model was determined for nickel adsorption on PBS. The results revealed that the high-energy adsorption sites on PBS were first occupied, then nickel adsorption spread to the low-energy adsorption sites. The pretreatment of H_3PO_4 impregnation with microwave heating influenced the energetical heterogeneity and adsorption affinity of adsorbents for nickel. With a higher degree of heterogeneity and a higher value of weighted mean (therefore higher adsorption affinity), PBS was more favorable than RBS for nickel adsorption. Moreover, because nickel may co-exist with antibiotics in aquatic systems, the effect of nickel on the adsorption of LEV by PBS was also studied. The results demonstrated that Ni(II) slightly suppressed the LEV adsorption on PBS at the tested pH values (4.0, 7.0, and 9.0).

CHAPTER 8 APPLICATION OF PRETREATED BARLEY STRAW IN ETHANOL DEHYDRATION

The aforementioned work demonstrated that PBS had a high surface area and hydrophilic groups such as carboxyl and hydroxyl groups, it is of interest to investigate whether this adsorbent can be applied to diversified systems for the purpose of separation and purification. For that end, PBS was investigated on its capability to remove water from water-ethanol mixture in order to produce fuel grade ethanol. Bioethanol is a readily available, clean fuel made from plant-based feedstocks, such as sugar cane, potato, cassava, and corn. It has been considered to reduce the climate relevant greenhouse gas emissions (United Nations Environment Programme 2009). In 2014, 24.57 billion gallons of fuel ethanol were produced in the world. But the recent drop in oil prices still challenges the ethanol industry (Renewable Fuels Association 2015). Lowering the cost of ethanol production is essential.

In the industrial production of bioethanol, the conversion of carbohydrates to bioethanol through fermentation only generates a low concentration of ethanol. The end fermentation broth contains 5-15 *wt*% ethanol mixed with other organics and water. Separation of ethanol from the fermentation broth is conventionally done by a distillation process to produce ethanol with a maximum concentration of 95.5 *wt*% due to the formation of an azeotropic mixture (Simo et al. 2009). Therefore, additional methods are needed to further break the azeotropic point and produce anhydrous ethanol. There are a number of methods available for this purpose, such as azeotropic distillation, vacuum distillation, extractive distillation, chemical dehydration, membrane, and adsorption (Chang et al. 2006, Kumar et al. 2010, Ladisch and Dyck 1979). Among these methods, the adsorption process using zeolite has been popularly applied in the ethanol industry due to its relatively low energy consumption and ability to produce a very dry product. However, problems still exist. Regeneration of the water saturated adsorbent zeolites requires temperature up to 473.15 K (Simo et al. 2009). In addition, the transient thermal waves

that were produced during regeneration create unwanted by-products such as carbonyl sulfide (COS) (Lin et al. 2012). Furthermore, disposal of exhausted molecular sieve zeolites must be done in consideration of environmental risk. In the past decades, research has been done using cost effective cellulose and starch biomass materials, such as corn (Ladisch and Dyck 1979, Quintero and Cardona 2009), cassava starch pearls (Kim et al. 2011), canola meal (Tajallipour et al. 2013), starch (Sun et al. 2013), sweet potato (Wang et al. 2010b), and palm stone and oak (Al-Asheh et al. 2004), for drying ethanol vapor. Water adsorption occurs when a water molecule interacts with polar groups such as hydroxyl group on the surface of adsorbent (Kim et al. 2011, Liu et al. 2010, Quintero and Cardona 2009). Use of biomass materials requires lower regeneration temperature (no higher than 383.15 K) and is environment-friendly, which reveals the great potential for drying ethanol.

However, most of the researches using biomass materials to dry ethanol vapor still require energy. In order to further reduce the energy consumption in ethanol purification, attempts were made to directly remove water from ethanol-water liquid at room temperature instead of operating in vapor phase. It has been reported that RBS was able to selectively remove water from ethanol aqueous solution at room temperature and to concentrate ethanol (Sun et al. 2007). The obtained water capacity of barley straw was much higher than that of the aforementioned biomass materials tested in ethanol vapor dehydration. The results showed the great potential of RBS or the like for drying ethanol aqueous solution at room temperature. However, similar to the adsorption of nickel by RBS (Thevannan et al. 2010), there is a challenge that RBS is not stable when contacting with aqueous solution since the release of organic compounds from RBS into the liquid phase (measured as total organic carbon, TOC). Such issue needs to be addressed before this technology could be applied in industrial purification of bio-alcohols.

In this chapter, PBS was applied as an adsorbent to selectively remove water and to purify ethanol from aqueous solutions. The adsorption capacities of PBS in single (only water or

ethanol) and binary (mixtures of water and ethanol) systems were evaluated. The effect of contact time between the adsorbent and the adsorbates was also investigated. To compare with the adsorbents reported in literature, the unit of adsorption capacity was converted from mg/g to mol/g.

8.1 Adsorption of Water and Ethanol on Pretreated Barley Straw

To address the issue of TOC release from RBS in the process of ethanol dehydration, TOC release of PBS in a single system (only water or ethanol) was first investigated. The water and ethanol adsorption capacities and the water to ethanol adsorption ratio of PBS were also determined with a comparison with RBS.

The TOC release of RBS into water were measured to be 229 ppm (34.4 ± 0.9 mg TOC release/g dry RBS) while that of PBS was significantly reduced to 6 ppm (0.9 ± 0.2 mg TOC release/g dry PBS). It was observed that the solution of RBS turned yellow during the adsorption process. Organics were released into the solution. On the contrary, the solution of PBS was nearly colorless and transparent.

In addition, PBS had a higher water adsorption capacity (0.63 ± 0.02 mol/g dry PBS) than RBS (0.50 ± 0.01 mol/g dry PBS). Furthermore, PBS had a lower adsorption of ethanol (0.13 ± 0.01 mol/g) than water, and maintained a water to ethanol adsorption ratio of 4.85 similar to that of RBS (5.00).

Table 8.1 Comparison of water and ethanol adsorption capacity of PBS with the reported adsorbents.

Adsorbents	Water adsorption, mol/g	Ethanol adsorption, mol/g	Adsorption ratio	TOC release, mg/g	Source
PBS	0.63 ± 0.02	0.13 ± 0.01	4.85 ± 0.30	0.9 ± 0.2	This work
RBS	0.50 ± 0.01	0.10 ± 0.00	5.00 ± 0.10	34.4 ± 0.9	This work
RBS	0.43 ± 0.01	0.10 ± 0.01	4.31 ± 0.17	--	(Sun et al. 2007)
Wheat straw	0.22 ± 0.02	0.07 ± 0.03	3.22 ± 1.46	--	(Sun et al. 2007)
Acid washed crab shells	0.019 ± 0.001	0.024 ± 0.001	0.79 ± 0.08	--	(Sun et al. 2007)
Zeolites	0.004	--	--	--	(Carmo and Gubulin 1997)
Cassava shred	0.24	--	--	--	(Okewale et al. 2013)
Canola meal	0.12	--	--	--	(Ranjbar et al. 2013b)

--: not given in literature.

Given in Table 8.1, the water adsorption capacity of PBS was higher than that of RBS in this work, raw barley straw (0.43 ± 0.01 mol/g), wheat straw (0.22 ± 0.02 mol/g) and acid washed crab shells (0.019 ± 0.001 mol/g) (Sun et al. 2007), zeolites (0.004 mol/g) (Carmo and Gubulin 1997), canola meal (0.12 mol/g) (Ranjbar et al. 2013a), and Cassava shred (0.24 mol/g) (Okewale et al. 2013). The water adsorption capacity of RBS in the previous work of Sun et al.

(Sun et al. 2007) was lower than that of RBS in this work, which indicated that the source of barley straw also affected the water adsorption capacity. Such effect needs to be further investigated.

The results revealed that PBS has successfully reduced TOC release compared with RBS, which enhanced the stability of RBS. PBS demonstrated a better potential for industrial application in selectively adsorbing water from ethanol-water mixtures than RBS, which was further investigated as follows.

8.2 Effect of Contact Time

The adsorption of water and ethanol on PBS in single systems (water or ethanol) at different times are illustrated in Figure 8.1. The results indicated that adsorption of water by PBS was very fast and reached over 97% of the equilibrium adsorption capacity in the first 30 minutes. The water adsorption equilibrium of PBS was achieved within 1 h. However, adsorption of ethanol on PBS was relatively low and slow, which achieved about 80% of the equilibrium adsorption capacity in the first 30 min and took 2 h to reach equilibrium. The achieved equilibrium water and ethanol adsorption capacities of PBS were 0.64 ± 0.02 and 0.17 ± 0.01 mol/g, respectively.

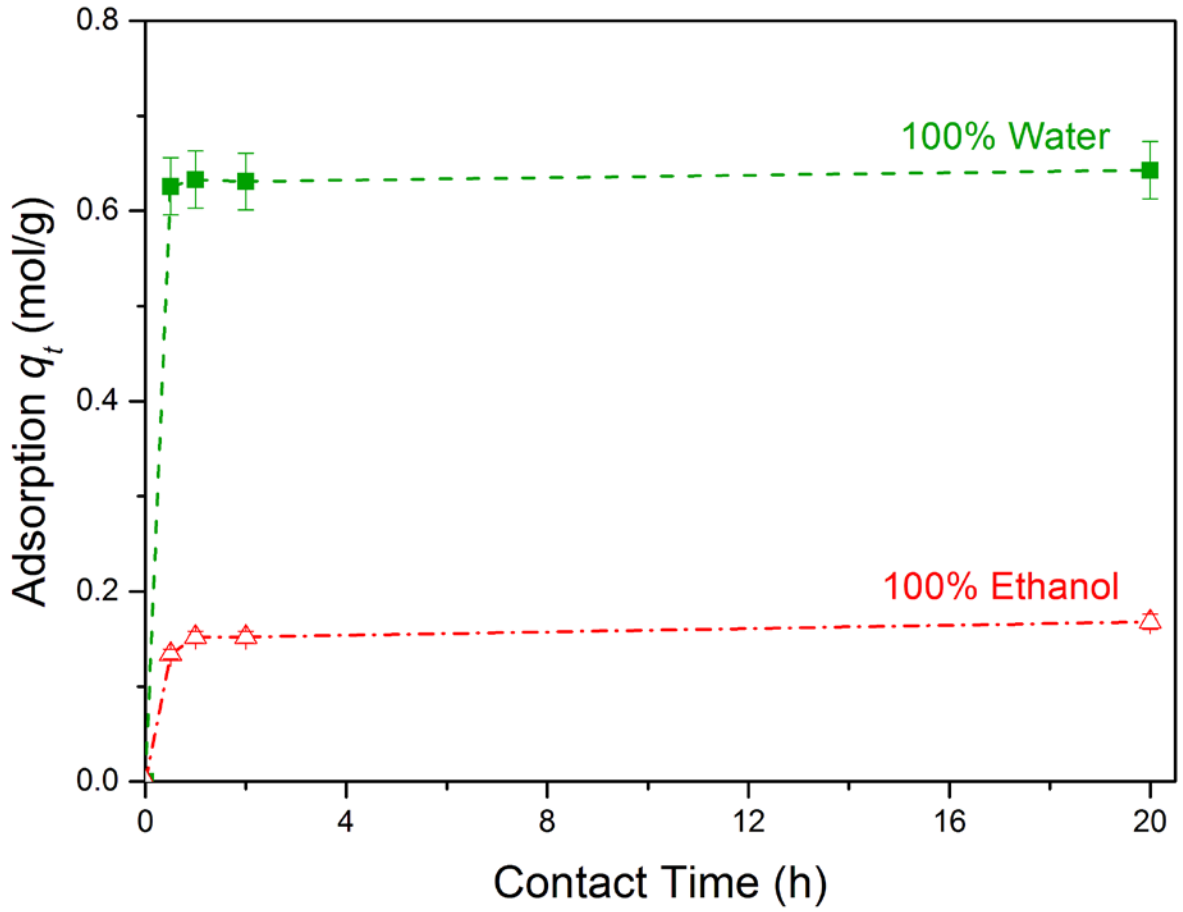

Figure 8.1 Effect of time on adsorption of water and ethanol by PBS.

30.0 ± 0.1 g solution of water or ethanol, 0.20 ± 0.01 g PBS, and 298.15 ± 0.50 K. Error bars represent the standard deviation.

In order to selectively remove water from ethanol, it is important to evaluate the ratio of water to ethanol adsorption of PBS at different time. The results revealed that the maximum molar ratio of water to ethanol adsorption was obtained at 0.5 h, being 4.68 (mol/mol). As time elapsed, the ratio dropped down. It could be due to that water molecules were adsorbed faster than ethanol molecules because the molecular size of water is 0.28 nm which is smaller than that of ethanol 0.44 nm (Carmo and Gubulin 1997). As a result, water adsorption on PBS approached equilibrium before ethanol on PBS, and with the time elapsed, more ethanol molecules were adsorbed, which caused the ratio of adsorbed water to ethanol decreased.

The higher adsorption capacity of PBS for water than ethanol might be due to that water molecule had a higher polarity than ethanol. Such higher polarity of water molecules could

lead to a stronger interaction with the polar groups of PBS. Moreover, the micropore structure of PBS could work as a molecular sieve to separate water from ethanol.

8.3 Concentration of Ethanol from Ethanol-Water Mixture

To examine the capability of PBS to selectively remove water from ethanol-water mixture at 298.15 ± 0.5 K, batch adsorption experiments were done in ethanol-water mixtures initially containing 78 *wt*% ethanol, and the experimental data are illustrated in Figure 8.2. PBS increased the concentration of ethanol from 78 *wt*% to 89 *wt*% within 0.5 h, while RBS from 78 *wt*% to 83 *wt*%. The results demonstrated that PBS obtained in this work not only enhanced the stability of barley straw by successfully reducing the release of TOC, but also had a higher water adsorption selectivity which concentrated ethanol to a higher purity compared with RBS during the dynamic adsorption process.

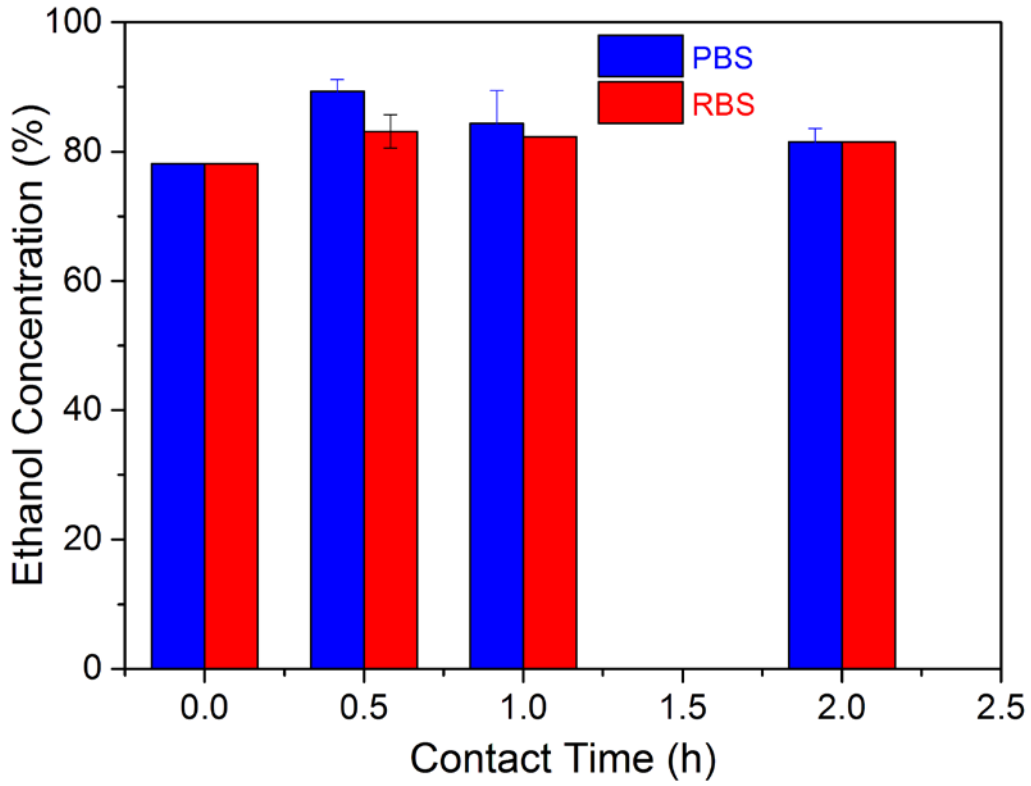

Figure 8.2 Concentration of ethanol from ethanol-water mixture versus time

30.0 ± 0.1 g water-ethanol mixture (ethanol 78 *wt*%), 0.20 ± 0.01 g PBS or RBS, and 298.15 ± 0.50 K. Error bars represent the standard deviation.

It was also observed that with increase in contact time, ethanol concentration in the presence of PBS decreased to 82 *wt*% at 2 h, which was similar to that of RBS. As mentioned before, ethanol has a bigger molecular size, and takes longer time to diffuse and be adsorbed by PBS. At 1 h and over, adsorption of water reached saturation (equilibrium) while adsorption of ethanol continued, thus, ethanol concentration in the mixtures decreased. Such result indicated that utilization of PBS in ethanol dehydration could be optimized by a dynamic system control. In summary, PBS demonstrated the potential of dehydrating ethanol-water mixture to achieve the high purity ethanol.

8.4 Chapter Summary

The results of water and ethanol adsorption experiments indicated that PBS not only demonstrated a significantly reduced TOC release and enhanced stability, but also had a higher water adsorption capacity (0.63 ± 0.02 mol/g) and a close water to ethanol adsorption ratio (4.85) comparing with those of RBS (0.50 ± 0.01 mol/g and 5.00). PBS also had a higher water adsorption selectivity during the dynamic adsorption process and was able to concentrate ethanol to a higher purity. Importantly, utilization of PBS in ethanol concentration can be optimized by a dynamic system control in order to achieve a higher concentration of ethanol. In addition, the water adsorption capacity of PBS was much higher than the reported adsorbents in literature. As such, PBS also showed the potential for application in purifying ethanol from water. The results again demonstrated the pretreatment method applied in this work could successfully enhance the stability of biomass materials. Moreover, how to further improve the water adsorption capacity should be considered in future work.

CHAPTER 9 CONCLUSIONS, ORIGINAL CONTRIBUTIONS, AND RECOMMENDATIONS FOR FUTURE WORKS

9.1 Conclusions and Original Contributions

1. Pretreated barley straw with a high adsorption capacity and an enhanced stability, was successfully made from raw barley straw with 5% (*w/v*) H_3PO_4 impregnation and 9 min 700W microwave heating. Revealed by the results of SEM and BET surface area, PBS had a well-developed porous structure and high surface area. Importantly, the TOC release of PBS was decreased to 0.9 ± 0.2 mg/g that was over 38 times lower than that of RBS (34.4 ± 0.9 mg/g), indicating the enhanced stability of PBS. The pretreatment method may be transferrable to modify other agricultural byproducts for wide applications.
2. Levofloxacin was effectively removed from aqueous solution by PBS in a wide range of solution pH (2.47-9.60). Adsorption of LEV on PBS was an endothermic process. The experimental LEV adsorption capacity of PBS (408 ± 5 mg/g at pH 6.88 and 298.15 K) was much higher than that of the reported adsorbents. The elevated ionic strength slightly decreased the LEV adsorption capacity of PBS. Based on the above results together with the analyses of activation energy (45.9 kJ/mol), C *K*-edge XANES, FTIR, and site energy distribution, the LEV adsorption was mainly through chemical adsorption, and π-π EDA interaction, and hydrogen bond could be one of the dominant mechanisms.
3. Norfloxacin was efficiently removed from aqueous solution by PBS in a wide pH range (2.67-10.50). Adsorption of NOR on PBS was an endothermic process. The experimental NOR adsorption capacity of PBS (396 ± 19 mg/g at pH 6.96 and 298.15 K) was much higher than that of adsorbents in literature. The analyses of adsorption

kinetics, C and O *K*-edge XANES, and site energy distribution suggested that such adsorption process was also mainly by chemisorption, and π-π and *n*-π EDA interactions, and hydrogen-bond could be one of the primary forces.

4. Nickel adsorption capacity was significantly enhanced by PBS (59.5 ± 3.0 mg/g), almost six times that by RBS (10.2 ± 2.0 mg/g). Solution pH played an important role. XAS studies (XANES and EXAFS) demonstrated that the adsorbed Ni remained the same oxidation state (II) as $NiSO_4$, and it was associated with 6 oxygen atoms from water or the functional groups of PBS (e.g., carboxyl groups) at an atomic distance 2.043 ± 0.013 Å.
5. Ni(II) slightly suppressed the adsorption of LEV on PBS at the tested pH values (4.0, 7.0, and 9.0), which might be due to the competition between LEV and the cationic Ni(II) for the negatively charged adsorption sites of PBS.
6. Water security is an important part of sustainability. Water pollution and scarcity directly affect environment, economy, and society. Treatment of antibiotics/nickel containing wastewater contributed to the sustainable development.
7. PBS also had a higher water adsorption capacity (0.63 ± 0.02 mol/g) and a close water to ethanol adsorption ratio (4.85) comparing with those of RBS (0.50 ± 0.01 mol/g and 5.00). Furthermore, utilization of PBS in ethanol concentration can be optimized by a dynamic system control in order to achieve a higher concentration of ethanol.

9.2 Recommendations for Future Works

- PBS demonstrated high adsorption capacities for LEV and NOR, representatives of FQ antibiotics, whether PBS works for other antibiotics (e.g., *β*-lactams, sulfonamides, and tetracyclines) needs to be investigated.

- Although the adsorption kinetics in this work was investigated by the pseudo-second-order kinetic model that is based on chemical reaction, the mass transfer in the adsorption process should be studied.
- π-π and *n*-π EDA interactions, and hydrogen-bond were proposed as one of the dominant mechanisms in the adsorption of FQ antibiotics on PBS. However, in a real aquatic system, mechanisms like EDA interactions, electrostatic attraction, and hydrophobic interaction may simultaneously work in the adsorption of FQ antibiotics on PBS. Thus, further investigations on the binding strengths of EDA interactions, electrostatic attraction, hydrophobic interaction, and other interactions are required.
- The desorption efficiencies of PBS samples loaded with antibiotics were far from the satisfactory level. Other methods, such as oxidation and thermal treating in a microwave furnace, may be employed to improve the desorption efficiency. More in depth desorption investigations would form an area of future research.
- Due to the limit of the HPLC used in this work, the initial concentrations of antibiotics were in ppm level (mg/L), while most of the reported antibiotic concentrations in water bodies and water streams were at ppb level (μg/L) and even at ppt level (ng/L). More works should be done at such low concentrations.
- The presence of Ni(II) slightly suppressed the adsorption of LEV on PBS at the tested pH values (4.0, 7.0, and 9.0) in this work. The mechanisms such as the interaction of PBS-LEV-nickel should be further investigated.
- PBS demonstrated higher adsorption capacities for water and ethanol and a slightly lower selectivity than RBS. How to further improve the selectivity should be considered.
- H_3PO_4 was used in the production of PBS, the recycle and reuse of the residue H_3PO_4 solution need to be investigated to fulfill the requirement of sustainability. In addition,

continuing reducing the MW energy used in the pretreatment process could form an area of future research.

PUBLICATIONS

Journal Publications:

(1) Yan, B.; Niu, C. H.*; Wang, J. Analyses of levofloxacin adsorption on pretreated barley straw with respect to temperature: Kinetics, π-π electron-donor-acceptor interaction and site energy distribution. *Environ. Sci. Technol.* **2017**, *51* (14), 8048-8056.

(2) Yan, B.; Niu, C. H.* Modeling and site energy distribution analysis of levofloxacin sorption by biosorbents. *Chem. Eng. J.* **2017**, *307*, 631-642.

(3) Yan, B.; Niu, C. H.*; Wang, J. Kinetics, electron-donor-acceptor interactions and site energy distribution analyses of norfloxacin adsorption on a heterogeneous adsorbent at various temperature. *Chem. Eng. J.* **2017**, *330*, 1211-1221.

(4) Yan, B.; Niu, C. H.*; Feng, R. F. Site energy distribution and X-ray analyses of nickel loaded on heterogeneous adsorbents. *Ind. Eng. Chem. Res*. **2017**, *56* (29), 8283-8291.

(5) Yan, B.; Niu, C. H.* Pre-trteating biosorbents for purification of ethanol from aqueous solution. *Int. J. Green Energy* **2017**, *14* (3), 245-252.

(6) Yan, B.; Niu, C. H.* Adsorption behavior of norfloxacin and site energy distribution based on the *Dubinin-Astakhov* isotherm. **2017**. Submitted to *Sci. Total Environ.*

Conference Presentations:

(1) Yan, B.; Niu, C. H.* "Pretreatment and characterization of barley straw for ethanol dehydration" in the 65th Canadian Chemical Engineering Conference. Calgarly, AB, Oct 4-7, 2015.

(2) Yan, B.; Niu, C. H.* "Modeling and site energy distribution analysis of levofloxacin sorption by biosorbents" in the 66th Canadian Chemical Engineering Conference. Quebec City, QC, Oct 16-19, 2016.

(3) Dhabhai, R.; Mahaninia, M.; Yan, B.; Niu, C. H.*; and Dalai, A. K. "Drying of nitrogen in a pressure swing adsorption process using canola meal biosorbent" in the 66th Canadian Chemical Engineering Conference. Quebec City, QC, Oct 16-19, 2016.

(4) Yan, B.; Niu, C. H.* "Adsorption of antibiotics on heterogeneous adsorbents based on barley straw" in the 67th Canadian Chemical Engineering Conference. Edmonton, AB, Oct 22-25, 2016.

NOMENCLATURE

b adsorption equilibrium constant $(L/mg)^{-n}$

C_0 initial adsorbate concentration (mg/L)

C_e equilibrium adsorbate concentration (mg/L)

C_s maximum solubility of adsorbate in water (mg/L)

E adsorption energy refers to the difference between the adsorbate and the solvent (water) for a given adsorption site (kJ/mol)

E^* difference of adsorption energy at C_e and C_s (kJ/mol)

E_m^* mode of the site energy distribution curve (kJ/mol)

E_s value of the adsorption energy corresponding to $C_e = C_s$ (kJ/mol)

F Statistic a value obtained from an ANOVA test or a regression analysis to find out if the means between two populations are significantly different

$F(E)$ site energy frequency distribution over a range of energies (dimensionless)

$F(E^*)$ site energy distribution over a range of energies (mg·mol/(g·kJ))

k pseudo-second-order rate constant (g/(mg·h))

n indicator of surface site heterogeneity of the adsorbent (dimensionless)

p-value a value used to determine the significance, a small p-value (typically ≤ 0.05) indicates the strong statistical significance

$P(E^*)$ percentage of adsorption site, the site energy of which are above E^*

q_e experimental equilibrium adsorption capacity (mg/g)

$q_{e,cal}$ equilibrium adsorption capacity obtained from the kinetic model (mg/g)

$q_h(E,C_e)$ energetically homogeneous isotherm $(mol^2/(g·kJ))$

q_m maximum adsorption capacity (mg/g)

q_t amount of adsorption at time t (mg/g)

R gas constant (8.314 J/(mol·K))

R^2 coefficient of determination

R-factor the relative error of the crystallographic model fitting results to the experimental data

T temperature (K)

X_1 independent variable, H_3PO_4 impregnation concentration

X_2 independent variable, microwave radiation time

Y dependent variable, value of specific surface area

Greek letters

σ_e^* standard deviation, indicative of energetical heterogeneity of the adsorbent (kJ/mol)

$\mu(E^*)$ weighted mean of site energy distribution, indicative of the strength of adsorption affinity (kJ/mol)

ABBREVIATIONS

AAS atomic absorption spectroscopy

ANOVA analysis of variation

BET *Brunauer-Emmett-Teller*

BJH *Barrett-Joyner-Halenda*

CAS conventional activated sludge

EDA electron-donor-acceptor

EDTA ethylenediaminetetraacetic acid disodium salt dihydrate

EXAFS extended X-ray absorption fine structure

FQ fluoroquinolone

FTIR *Fourier* transform infrared spectroscopy

GAC granular activated carbon

HPLC high performance liquid chromatography

IS ionic strength

LEV levofloxacin

MBR membrane bioreactor

MF microfiltration

MRA multiple regression analysis

NF nanofiltration

NOR norfloxacin

PAC powdered activated carbon

PBS pretreated barley straw

PZNC point of zero net charge

RBS raw barley straw

RMSE root-mean-square error

RO reverse osmosis

RSM response surface methodology

RSS residual sum of squares $((mg/g)^2)$

SEM scanning electron microscopy

SRT sludge retention time

SS sum of the squared deviations

STXM scanning transmission X-ray microscopy

TGA thermogravimetric analysis

TOC total organic carbon

UF ultrafiltration

WWTP wastewater treatment plant

XANES X-ray absorption near-edge structure

XAS X-ray absorption spectroscopy

XRF X-ray fluorescence

REFERENCES

Adam, A.M.A., Salman, M., Sharshar, T. and Refat, M.S. (2013) Chemical and physical studies on the reaction mechanism of charge-transfer complexes between narcotic drugs and electronic acceptors. International Journal of Electrochemical Science 8(1), 1274-1294.

Ahmed, M.J. and Theydan, S.K. (2014) Fluoroquinolones antibiotics adsorption onto microporous activated carbon from lignocellulosic biomass by microwave pyrolysis. Journal of the Taiwan Institute of Chemical Engineers 45(1), 219-226.

Ait Lahcen, A. and Amine, A. (2017) Mini-Review: Recent advances in electrochemical determination of sulfonamides. Analytical Letters. DIO: 10.1080/00032719.2017.1295977

Al-Asheh, S., Banat, F. and Al-Lagtah, N. (2004) Separation of ethanol-water mixtures using molecular sieves and biobased adsorbents. Chemical Engineering Research and Design 82(7), 855-864.

Alexy, R., Kümpel, T. and Kümmerer, K. (2004) Assessment of degradation of 18 antibiotics in the Closed Bottle Test. Chemosphere 57(6), 505-512.

Ambrose, P.G., Owens, R.C., Quntilian, R. and Nightingale, C.H. (1997) New generations of quinolones: With particular attention to levofloxacin. Connecticut Medicine 61(5), 269-272.

Appelbaum, P.C. and Hunter, P.A. (2000) The fluoroquinolone antibacterials: Past, present and future perspectives. International Journal of Antimicrobial Agents 16(1), 5-15.

Bandara, J., Nadtochenko, V., Kiwi, J. and Pulgarin, C. (1997) Dynamics of oxidant addition as a parameter in the modelling of dye mineralization (orange II) via advanced oxidation technologies. Water Science and Technology 35(4), 87-93.

Beevers, C.A. and Lipson, H. (1932) The Crystal structure of nickel sulphate hexahydrate, $NiSO_4 \cdot 6H_2O$. Zeitschrift für Kristallographie - Crystalline Materials 83(1-6), 123-135.

Bhaumik, M., Agarwal, S., Gupta, V.K. and Maity, A. (2016) Enhanced removal of Cr(VI) from aqueous solutions using polypyrrole wrapped oxidized MWCNTs nanocomposites adsorbent. Journal of Colloid and Interface Science 470, 257-267.

Białk-Bielińska, A., Maszkowska, J., Mrozik, W., Bielawska, A., Kołodziejska, M., Palavinskas, R., Stepnowski, P. and Kumirska, J. (2012) Sulfadimethoxine and sulfaguanidine: Their sorption potential on natural soils. Chemosphere 86(10), 1059-1065.

Blokhina, S.V., Sharapova, A.V., Ol'khovich, M.V., Volkova, T.V. and Perlovich, G.L. (2016) Solubility, lipophilicity and membrane permeability of some fluoroquinolone antimicrobials. European Journal of Pharmaceutical Sciences 93, 29-37.

Blundell, S.A., Guet, C. and Zope, R.R. (2000) Temperature dependence of the polarizability of sodium clusters. Physical Review Letters 84(21), 4826-4829.

Boparai, H.K., Joseph, M. and O'Carroll, D.M. (2011) Kinetics and thermodynamics of cadmium ion removal by adsorption onto nano zerovalent iron particles. Journal of Hazardous Materials 186(1), 458-465.

Bouyarmane, H., El Hanbali, I., El Karbane, M., Rami, A., Saoiabi, A., Saoiabi, S., Masse, S., Coradin, T. and Laghzizil, A. (2015) Parameters influencing ciprofloxacin, ofloxacin, amoxicillin and sulfamethoxazole retention by natural and converted calcium phosphates. Journal of Hazardous Materials 291, 38-44.

Box, G.E.P. and Wilson, K.B. (1951) On the experimental attainment of optimum conditions. Journal of the Royal Statistical Society B 13, 1-45.

Brzhezinskaya, M.M., Muradyan, V.E., Vinogradov, N.A., Preobrajenski, A.B., Gudat, W. and Vinogradov, A.S. (2009) Electronic structure of fluorinated multiwalled carbon nanotubes studied using x-ray absorption and photoelectron spectroscopy. Physical Review B 79(15), 155439.

Bu, Q., Wang, B., Huang, J., Deng, S. and Yu, G. (2013) Pharmaceuticals and personal care products in the aquatic environment in China: A review. Journal of Hazardous Materials 262, 189-211.

Buffle, J., Chalmers, R.A., Masson, M.R. and Midgley, D. (1988) Complexation reactions in aquatic systems: An analytical approach, E. Horwood.

Bunmahotama, W., Hung, W.N. and Lin, T.F. (2015) Predicting the adsorption of organic pollutants from water onto activated carbons based on the pore size distribution and molecular connectivity index. Water Research 85, 521-531.

Calborean, A., Martin, F., Marconi, D., Turcu, R., Kacso, I.E., Buimaga-Iarinca, L., Graur, F. and Turcu, I. (2015) Adsorption mechanisms of l-Glutathione on Au and controlled nano-patterning through Dip Pen Nanolithography. Materials Science and Engineering C 57, 171-180.

Carabineiro, S.A.C., Thavorn-amornsri, T., Pereira, M.F.R., Serp, P. and Figueiredo, J.L. (2012) Comparison between activated carbon, carbon xerogel and carbon nanotubes for the adsorption of the antibiotic ciprofloxacin. Catalysis Today 186(1), 29-34.

Carmo, M.J. and Gubulin, J.C. (1997) Ethanol-water adsorption on commercial 3A zeolites: Kinetic and thermodynamic data. Brazilian Journal of Chemical Engineering 14(3), 217-244.

Carter, M.C., Kilduff, J.E. and Weber, W.J. (1995) Site energy distribution analysis of preloaded adsorbents. Environmental Science & Technology 29(7), 1773-1780.

Cayllahua, J.E.B., de Carvalho, R.J. and Torem, M.L. (2009) Evaluation of equilibrium, kinetic and thermodynamic parameters for biosorption of nickel(II) ions onto bacteria strain, Rhodococcus opacus. Minerals Engineering 22(15), 1318-1325.

Cerofolini, G.F. (1974) Localized adsorption on heterogeneous surfaces. Thin Solid Films 23(2), 129-152.

Cerofolini, G.F. and Cerofolini, M. (1980) Heterogeneity, allostericity, and hysteresis in adsorption of water by proteins. Journal of Colloid and Interface Science 78(1), 65-73.

Cerofolini, G.F. and Rudziński, W. (1997) Studies in surface science and catalysis. Rudziński, W., Steele, W.A. and Zgrablich, G. (eds), pp. 1-103, Elsevier.

Ch. Teas, S. Kalligeros, F. Zanikos, S. Stournas, E. Lois and Anastopoulos, G. (2001) Investigation of the effectiveness of absorbent materials in oil spills clean up. Desalination 140(3), 259-264.

Chang, H., Yuan, X.G., Tian, H. and Zeng, A.W. (2006) Experimental investigation and modeling of adsorption of water and ethanol on cornmeal in an ethanol-water binary vapor system. Chemical Engineering & Technology 29(4), 454-461.

Chen, C., Dynes, J.J., Wang, J., Karunakaran, C. and Sparks, D.L. (2014a) Soft X-ray spectromicroscopy study of mineral-organic matter associations in pasture soil clay fractions. Environmental Science & Technology 48(12), 6678-6686.

Chen, C., Dynes, J.J., Wang, J. and Sparks, D.L. (2014b) Properties of Fe-organic matter associations via coprecipitation versus adsorption. Environmental Science & Technology 48(23), 13751-13759.

Chen, G.C., Shan, X.Q., Wang, Y.S., Wen, B., Pei, Z.G., Xie, Y.N., Liu, T. and Pignatello, J.J. (2009) Adsorption of 2,4,6-trichlorophenol by multi-walled carbon nanotubes as affected by Cu(II). Water Research 43(9), 2409-2418.

Chen, W., Duan, L., Wang, L. and Zhu, D. (2008) Adsorption of hydroxyl- and amino-substituted aromatics to carbon nanotubes. Environmental Science & Technology 42(18), 6862-6868.

Conkle, J.L., Lattao, C., White, J.R. and Cook, R.L. (2010) Competitive sorption and desorption behavior for three fluoroquinolone antibiotics in a wastewater treatment wetland soil. Chemosphere 80(11), 1353-1359.

Dafale, N.A., Semwal, U.P., Agarwal, P.K., Sharma, P. and Singh, G.N. (2015) Development and validation of microbial bioassay for quantification of levofloxacin in pharmaceutical preparations. Journal of Pharmaceutical Analysis 5(1), 18-26.

Daghrir, R. and Drogui, P. (2013) Tetracycline antibiotics in the environment: A review. Environmental Chemistry Letters 11(3), 209-227.

Davis, J.A. and Leckie, J.O. (1978) Surface ionization and complexation at the oxide/water interface II. Surface properties of amorphous iron oxyhydroxide and adsorption of metal ions. Journal of Colloid and Interface Science 67(1), 90-107.

De la Cruz, N., Giménez, J., Esplugas, S., Grandjean, D., de Alencastro, L.F. and Pulgarín, C. (2012) Degradation of 32 emergent contaminants by UV and neutral photo-fenton in domestic wastewater effluent previously treated by activated sludge. Water Research 46(6), 1947-1957.

Deblonde, T., Cossu-Leguille, C. and Hartemann, P. (2011) Emerging pollutants in wastewater: A review of the literature. International Journal of Hygiene and Environmental Health 214(6), 442-448.

Derylo-Marczewska, A., Jaroniec, M., Gelbin, D. and Seidel, A. (1984) Heterogeneity effects in single-solute adsorption from dilute solutions on solids. Chemica Scripta 24(4-5), 239-246.

Dmitrienko, S.G., Kochuk, E.V., Apyari, V.V., Tolmacheva, V.V. and Zolotov, Y.A. (2014) Recent advances in sample preparation techniques and methods of sulfonamides detection: A review. Analytica Chimica Acta 850, 6-25.

Do, D.D. (1998) Adsorption analysis: Equilibria and kinetics, Imperial College Press.

Dong, S., Sun, Y., Wu, J., Wu, B., Creamer, A.E. and Gao, B. (2016) Graphene oxide as filter media to remove levofloxacin and lead from aqueous solution. Chemosphere 150, 759-764.

Donowitz, G.R. and Mandell , G.L. (1988) Beta-lactam antibiotics. New England Journal of Medicine 318(8), 490-500.

Ewecharoen, A., Thiravetyan, P., Wendel, E. and Bertagnolli, H. (2009) Nickel adsorption by sodium polyacrylate-grafted activated carbon. Journal of Hazardous Materials 171(1-3), 335-339.

Feng, R., Dolton, W., Igarashi, R., Wright, G., Bradford, M. and McIntyre, S. (2010) Commissioning of the VESPERS beamline at the Canadian Light Source. AIP Conference Proceedings 1234(1), 315-318.

Feng, R., Gerson, A., Ice, G., Reininger, R., Yates, B. and McIntyre, S. (2007) VESPERS: A beamline for combined XRF and XRD measurements. AIP Conference Proceedings 879(1), 872-874.

Fink, L., Dror, I. and Berkowitz, B. (2012) Enrofloxacin oxidative degradation facilitated by metal oxide nanoparticles. Chemosphere 86(2), 144-149.

Flores-Garnica, J.G., Morales-Barrera, L., Pineda-Camacho, G. and Cristiani-Urbina, E. (2013) Biosorption of Ni(II) from aqueous solutions by Litchi chinensis seeds. Bioresource Technology 136, 635-643.

Food and Drug Administration (2008) Bioterrorism and Drug Preparedness/UCM133684. http://www.fda.gov/downloads/Drugs/EmergencyPreparedness/BioterrorismandDrugPreparedness/UCM133684 (accessed 2016.03.05).

Food and Drug Administration (2012) Estimate of antibacterial drug sales for use in humans. http://www.fda.gov/Drugs/DrugSafety/InformationbyDrugClass/ucm261160.htm (accessed 2017.04.26).

Food and Drug Administration (2013) 2011 Summary report on antimicrobials sold or distributed for use in food-producing animals.

https://www.fda.gov/downloads/forindustry/userfees/animaldruguserfeeactadufa/ucm338170 (accessed 2017.04.26).

Foster, R. and Fyfe, C.A. (1966) Electron-donor-acceptor complex formation by compounds of biological interest II. The association constants of various 1,4-dinitrobenzene-phenothiazine drug complexes. Biochimica et Biophysica Acta (BBA) - Biophysics including Photosynthesis 112(3), 490-495.

Ftouni, H., Sayen, S., Boudesocque, S., Dechamps-Olivier, I. and Guillon, E. (2012) Structural study of the copper(II)–enrofloxacin metallo-antibiotic. Inorganica Chimica Acta 382, 186-190.

Fujiwara, Y., Nishikawa, K., Iijima, T. and Kaneko, K. (1991) Simulation of small-angle X-ray scattering behaviour of activated carbon fibres adsorbing water. Journal of the Chemical Society, Faraday Transactions 87(17), 2763-2768.

Gao, L., Shi, Y., Li, W., Liu, J. and Cai, Y. (2015) Occurrence and distribution of antibiotics in urban soil in Beijing and Shanghai, China. Environmental Science and Pollution Research 22(15), 11360-11371.

Gao, Y., Li, Y., Zhang, L., Huang, H., Hu, J., Shah, S.M. and Su, X. (2012) Adsorption and removal of tetracycline antibiotics from aqueous solution by graphene oxide. Journal of Colloid and Interface Science 368(1), 540-546.

Gao, Y., Yue, Q., Gao, B., Sun, Y., Wang, W., Li, Q. and Wang, Y. (2013) Preparation of high surface area-activated carbon from lignin of papermaking black liquor by KOH activation for Ni(II) adsorption. Chemical Engineering Journal 217, 345-353.

Gaunt, P.N. and Piddock, L.J.V. (1996) Ciprofloxacin resistant Campylobacter spp. in humans: An epidemiological and laboratory study. Journal of Antimicrobial Chemotherapy 37(4), 747-757.

Graouer-Bacart, M., Sayen, S. and Guillon, E. (2013) Macroscopic and molecular approaches of enrofloxacin retention in soils in presence of Cu(II). Journal of Colloid and Interface Science 408, 191-199.

Gu, C. and Karthikeyan, K.G. (2005) Sorption of the antimicrobial ciprofloxacin to aluminum and iron hydrous oxides. Environmental Science & Technology 39(23), 9166-9173.

Hattab, A.M. (2010) Adsorption of some fluoroquinolones on selected adsorbents, Master Dissertation, An - Najah National University, Nablus, Palestine.

Heymann, K., Lehmann, J., Solomon, D., Schmidt, M.W.I. and Regier, T. (2011) C 1s K-edge near edge X-ray absorption fine structure (NEXAFS) spectroscopy for characterizing functional group chemistry of black carbon. Organic Geochemistry 42(9), 1055-1064.

Hickey, J.P. and Passino-Reader, D.R. (1991) Linear solvation energy relationships: "rule of thumb" for estimation of variable values. Environmental Science & Technology 25(10), 1753-1760.

Ho, Y.-S. (2006) Second-order kinetic model for the sorption of cadmium onto tree fern: A comparison of linear and non-linear methods. Water Research 40(1), 119-125.

Homem, V. and Santos, L. (2011) Degradation and removal methods of antibiotics from aqueous matrices: A review. Journal of Environmental Management 92(10), 2304-2347.

Hoseinzadeh Hesas, R., Wan Daud, W.M.A., Sahu, J.N. and Arami-Niya, A. (2013) The effects of a microwave heating method on the production of activated carbon from agricultural waste: A review. Journal of Analytical and Applied Pyrolysis 100, 1-11.

Hunter, C.A., Lawson, K.R., Perkins, J. and Urch, C.J. (2001) Aromatic interactions. Journal of the Chemical Society, Perkin Transactions 2 (5), 651-669.

Hunter, C.A. and Sanders, J.K.M. (1990) The nature of π-π interactions. Journal of the American Chemical Society 112(14), 5525-5534.

International Union of Pure and Applied Chemistry (1991) Manual on Catalyst Characterization. Pure and Applied Chemistry 63(9), 1227-1246.

Jagtoyen, M. and Derbyshire, F. (1993) Some considerations of the origins of porosity in carbons from chemically activated wood. Carbon 31(7), 1185-1192.

Jagtoyen, M. and Derbyshire, F. (1998) Activated carbons from yellow poplar and white oak by H_3PO_4 activation. Carbon 36(7-8), 1085-1097.

Jia, A., Wan, Y., Xiao, Y. and Hu, J. (2012) Occurrence and fate of quinolone and fluoroquinolone antibiotics in a municipal sewage treatment plant. Water Research 46(2), 387-394.

Jones, O.A.H., Voulvoulis, N. and Lester, J.N. (2001) Human pharmaceuticals in the aquatic environment: A review. Environmental Technology 22(12), 1383-1394.

Kaneko, K. (1997) Studies in Surface Science and Catalysis. W. Rudziński, W.A.S. and Zgrablich, G. (eds), pp. 679-714, Elsevier.

Katsuura, K. and Inagaki, N. (1975) Studies on the thermal degradation of phosphorus-containing polymers. VIII Relation between the thermal reaction of flame-retardant cellulose and its flammability. Textile Research Journal 2, 103-107.

Keen, O.S. and Linden, K.G. (2013) Degradation of antibiotic activity during UV/H_2O_2 advanced oxidation and photolysis in wastewater effluent. Environmental Science & Technology 47(22), 13020-13030.

Keiluweit, M. and Kleber, M. (2009) Molecular-level interactions in soils and sediments: The role of aromatic π-systems. Environmental Science & Technology 43(10), 3421-3429.

Khan, G.A., Berglund, B., Khan, K.M., Lindgren, P.-E. and Fick, J. (2013) occurrence and abundance of antibiotics and resistance genes in rivers, canal and near drug formulation facilities: A study in pakistan. PLoS ONE 8(6), e62712.

Kim, Y., Hendrickson, R., Mosier, N., Hilaly, A. and Ladisch, M.R. (2011) Cassava starch pearls as a desiccant for drying ethanol. Industrial & Engineering Chemistry Research 50(14), 8678-8685.

Klamerth, N., Malato, S., Maldonado, M.I., Agüera, A. and Fernández-Alba, A.R. (2010) Application of photo-fenton as a tertiary treatment of emerging contaminants in municipal wastewater. Environmental Science & Technology 44(5), 1792-1798.

Košutić, K., Dolar, D., Ašperger, D. and Kunst, B. (2007) Removal of antibiotics from a model wastewater by RO/NF membranes. Separation and Purification Technology 53(3), 244-249.

Kovalova, L., Siegrist, H., von Gunten, U., Eugster, J., Hagenbuch, M., Wittmer, A., Moser, R. and McArdell, C.S. (2013) Elimination of micropollutants during post-treatment of hospital wastewater with powdered activated carbon, ozone, and UV. Environmental Science & Technology 47(14), 7899-7908.

Koyuncu, I., Arikan, O.A., Wiesner, M.R. and Rice, C. (2008) Removal of hormones and antibiotics by nanofiltration membranes. Journal of Membrane Science 309(1), 94-101.

Krishnan, K.A., Sreejalekshmi, K.G. and Baiju, R.S. (2011) Nickel(II) adsorption onto biomass based activated carbon obtained from sugarcane bagasse pith. Bioresource Technology 102(22), 10239-10247.

Krishnani, K.K., Meng, X.G. and Dupont, L. (2009) Metal ions binding onto lignocellulosic biosorbent. Journal of Environmental Science and Health, Part A: Toxic/Hazardous Substances & Environmental Engineering 44(7), 488-499.

Kubicki, J.D. (2006) Molecular simulations of benzene and PAH interactions with soot. Environmental Science & Technology 40(7), 2298-2303.

Kumar, S., Singh, N. and Prasad, R. (2010) Anhydrous ethanol: A renewable source of energy. Renewable and Sustainable Energy Reviews 14(7), 1830-1844.

Kümmerer, K., Al-Ahmad, A. and Mersch-Sundermann, V. (2000) Biodegradability of some antibiotics, elimination of the genotoxicity and affection of wastewater bacteria in a simple test. Chemosphere 40(7), 701-710.

Kuznetsova, A., Popova, I., Yates, J.T., Bronikowski, M.J., Huffman, C.B., Liu, J., Smalley, R.E., Hwu, H.H. and Chen, J.G. (2001) Oxygen-containing functional groups on single-wall carbon nanotubes: NEXAFS and vibrational spectroscopic studies. Journal of the American Chemical Society 123(43), 10699-10704.

Ladisch, M.R. and Dyck, K. (1979) Dehydration of ethanol: New approach gives positive energy balance. Science 205(4409), 898-900.

Lan, Y.K., Chen, T.C., Tsai, H.J., Wu, H.C., Lin, J.H., Lin, I.K., Lee, J.F. and Chen, C.S. (2016) Adsorption behavior and mechanism of antibiotic sulfamethoxazole on carboxylic-functionalized carbon nanofibers-encapsulated ni magnetic nanoparticles. Langmuir 32(37), 9530-9539.

Leal, R.M.P., Alleoni, L.R.F., Tornisielo, V.L. and Regitano, J.B. (2013) Sorption of fluoroquinolones and sulfonamides in 13 Brazilian soils. Chemosphere 92(8), 979-985.

Li, D., Yang, M., Hu, J., Zhang, Y., Chang, H. and Jin, F. (2008) Determination of penicillin G and its degradation products in a penicillin production wastewater treatment plant and the receiving river. Water Research 42(1), 307-317.

Lin, D. and Xing, B.S. (2008) Adsorption of phenolic compounds by carbon nanotubes: Role of aromaticity and substitution of hydroxyl groups. Environmental Science & Technology 42(19), 7254-7259.

Liu, D., Tao, Y., Li, K. and Yu, J. (2012) Influence of the presence of three typical surfactants on the adsorption of nickel (II) to aerobic activated sludge. Bioresource Technology 126, 56-63.

Liu, F.F., Zhao, J., Wang, S. and Xing, B.S. (2016) Adsorption of sulfonamides on reduced graphene oxides as affected by pH and dissolved organic matter. Environmental Pollution 210, 85-93.

Liu, M.K., Liu, Y.K., Bao, D.D., Zhu, G., Yang, G.H., Geng, J.F. and Li, H.T. (2017) Effective removal of tetracycline antibiotics from water using hybrid carbon membranes. Scientific Reports 7, 43717.

Liu, W., Zhang, J., Zhang, C. and Ren, L. (2011) Sorption of norfloxacin by lotus stalk-based activated carbon and iron-doped activated alumina: Mechanisms, isotherms and kinetics. Chemical Engineering Journal 171(2), 431-438.

Liu, Y.W., Tang, T., Chung, T.W., Huang, C. and Lin, Y.S. (2010) Equilibrium isotherms of water and ethanol vapors on immobilized starch sorbents. Journal of Chemical & Engineering Data 55(12), 5807-5811.

Liu, Y., Dong, C., Wei, H., Yuan, W. and Li, K. (2015) Adsorption of levofloxacin onto an iron-pillared montmorillonite (clay mineral): Kinetics, equilibrium and mechanism. Applied Clay Science 118, 301-307.

Locatelli, M., Ciavarella, M.T., Paolino, D., Celia, C., Fiscarelli, E., Ricciotti, G., Pompilio, A., Di Bonaventura, G., Grande, R., Zengin, G. and Di Marzio, L. (2015) Determination of ciprofloxacin and levofloxacin in human sputum collected from cystic fibrosis patients using microextraction by packed sorbent-high performance liquid chromatography photodiode array detector. Journal of Chromatography A 1419, 58-66.

Lu, J., Lei, Y., Lau, K.C., Luo, X., Du, P., Wen, J., Assary, R.S., Das, U., Miller, D.J., Elam, J.W., Albishri, H.M., El-Hady, D.A., Sun, Y.-K., Curtiss, L.A. and Amine, K. (2013) A nanostructured cathode architecture for low charge overpotential in lithium-oxygen batteries. Nature Communications 4, 2383.

Luo, Y., Guo, W., Ngo, H.H., Nghiem, L.D., Hai, F.I., Zhang, J., Liang, S. and Wang, X.C. (2014) A review on the occurrence of micropollutants in the aquatic environment and their fate and removal during wastewater treatment. Science of The Total Environment 473-474, 619-641.

Malamis, S. and Katsou, E. (2013) A review on zinc and nickel adsorption on natural and modified zeolite, bentonite and vermiculite: Examination of process parameters, kinetics and isotherms. Journal of Hazardous Materials 252-253, 428-461.

Manes, M. and Hofer, L.J.E. (1969) Application of the Polanyi adsorption potential theory to adsorption from solution on activated carbon. The Journal of Physical Chemistry 73(3), 584-590.

Martínez-Alcalá, I., Guillén-Navarro, J.M. and Fernández-López, C. (2017) Pharmaceutical biological degradation, sorption and mass balance determination in a conventional activated-sludge wastewater treatment plant from Murcia, Spain. Chemical Engineering Journal 316, 332-340.

Marzo, A. and Dal Bo, L. (1998) Chromatography as an analytical tool for selected antibiotic classes: A reappraisal addressed to pharmacokinetic applications. Journal of Chromatography A 812(1), 17-34.

McDermott, M.T. and McCreery, R.L. (1994) Scanning tunneling microscopy of ordered graphite and glassy carbon surfaces: Electronic control of quinone adsorption. Langmuir 10(11), 4307-4314.

McDermott, M.T., McDermott, C.A. and McCreery, R.L. (1993) Scanning tunneling microscopy of carbon surfaces: Relationships between electrode kinetics, capacitance, and morphology for glassy carbon electrodes. Analytical Chemistry 65(7), 937-944.

Miao, X.S., Bishay, F., Chen, M. and Metcalfe, C.D. (2004) Occurrence of antimicrobials in the final effluents of wastewater treatment plants in Canada. Environmental Science & Technology 38(13), 3533-3541.

Milewska-Duda, J. and Duda, J. (1997) Hard coal surface heterogeneity in the sorption process. Langmuir 13(5), 1286-1296.

Moore, B.C., Cannon, F.S., Metz, D.H. and Demarco, J. (2003) GAC pore structure in Cincinnati during full-scale treatment/reactivation. Journal American Water Works Association 95(2), 103-112.

Moore, B.C., Cannon, F.S., Westrick, J.A., Metz, D.H., Shrive, C.A., DeMarco, J. and Hartman, D.J. (2001) Changes in GAC pore structure during full-scale water treatment at Cincinnati: A comparison between virgin and thermally reactivated GAC. Carbon 39(6), 789-807.

Murphey, R. and Pardalos, P.M. (2002) Cooperative control and optimization, Kluwer Academic Publishers, Netherlands.

Muzzarelli, R.A.A. (1973) Natural chelating polymers: Alginic acid, chitin, and chitosan, Pergamon Press, New York.

Nakamoto, K. (2008) Infrared and raman spectra of inorganic and coordination compounds: Part A: Theory and applications in inorganic chemistry, Wiley.

Näslund, J., Hedman, J.E. and Agestrand, C. (2008) Effects of the antibiotic ciprofloxacin on the bacterial community structure and degradation of pyrene in marine sediment. Aquatic Toxicology 90(3), 223-227.

Newville, M. (2001) IFEFFIT : Interactive XAFS analysis and FEFF fitting. Journal of Synchrotron Radiation 8(2), 322-324.

Nguyen, T.T., Bui, X.T., Luu, V.P., Nguyen, P.D., Guo, W. and Ngo, H.H. (2017) Removal of antibiotics in sponge membrane bioreactors treating hospital wastewater: Comparison

between hollow fiber and flat sheet membrane systems. Bioresource Technology 240, 42-49.

Niu, H. (2002) Biosorption of Anionic Metal Species, PhD Dissertation, Mcgill University, Montreal, Canada.

Okbinoğlu, T.N. (2014) Electronic structure of sulfur-nitrogen containing compounds : Correlations with theory and chemical reactivity, PhD Dissertation, University of British Columbia, Vancouver, Canada.

Okewale, A.O., Foo, K.Y., Hameed, B.H., Babayemi, K.A. and Olalekan, A.P. (2013) Adsorption isotherms and kinetics models of starchy adsorbents on uptake of water from ethanol-water systems. International Journal of Applied Science and Technology 3(1), 35-42.

Oller, I., Malato, S. and Sánchez-Pérez, J.A. (2011) Combination of advanced oxidation processes and biological treatments for wastewater decontamination: A review. Science of The Total Environment 409(20), 4141-4166.

Ou, H., Tan, W., Niu, C.H. and Feng, R. (2015) Enhancement of the stability of biosorbents for metal-ion adsorption. Industrial & Engineering Chemistry Research 54(23), 6100-6107.

Owens Jr, R.C. and Ambrose, P.G. (2000) Clinical use of the fluoroquinolones. Medical Clinics of North America 84(6), 1447-1469.

Pan, B., Qiu, M., Wu, M., Zhang, D., Peng, H., Wu, D. and Xing, B.S. (2012) The opposite impacts of Cu and Mg cations on dissolved organic matter-ofloxacin interaction. Environmental Pollution 161, 76-82.

Pawlak, Z. and Pawlak, A.S. (1997) A Review of infrared spectra from wood and wood components following treatment with liquid ammonia and solvated electrons in liquid ammonia. Applied Spectroscopy Reviews 32(4), 349-383.

Pei, Z.G., Shan, X.Q., Zhang, S.Z., Kong, J.J., Wen, B., Zhang, J., Zheng, L.R., Xie, Y.N. and Janssens, K. (2011) Insight to ternary complexes of co-adsorption of norfloxacin and Cu(II) onto montmorillonite at different pH using EXAFS. Journal of Hazardous Materials 186(1), 842-848.

Peng, B., Chen, L., Que, C., Yang, K., Deng, F., Deng, X., Shi, G., Xu, G. and Wu, M. (2016) Adsorption of antibiotics on graphene and biochar in aqueous solutions induced by π-π interactions. Scientific Reports 6, 31920.

Peng, H., Pan, B., Wu, M., Liu, Y., Zhang, D. and Xing, B. (2012) Adsorption of ofloxacin and norfloxacin on carbon nanotubes: Hydrophobicity- and structure-controlled process. Journal of Hazardous Materials 233-234, 89-96.

Peng, X., Tan, J., Tang, C., Yu, Y. and Wang, Z. (2008) Multiresidue determination of fluoroquinolone, sulfonamide, trimethoprim, and chloramphenicol antibiotics in urban waters in China. Environmental Toxicology and Chemistry 27(1), 73-79.

Peng, X., Wang, Z., Kuang, W., Tan, J. and Li, K. (2006) A preliminary study on the occurrence and behavior of sulfonamides, ofloxacin and chloramphenicol antimicrobials in wastewaters of two sewage treatment plants in Guangzhou, China. Science of The Total Environment 371(1), 314-322.

Pérez, S., Eichhorn, P. and Aga, D.S. (2005) Evaluating the biodegradability of sulfamethazine, sulfamethoxazole, sulfathiazole, and trimethoprim at different stages of sewage treatment. Environmental Toxicology and Chemistry 24(6), 1361-1367.

Pertlik, F. (1986) Structures of hydrothermally synthesized cobalt(II) carbonate and nickel(II) carbonate. Acta Crystallographica Section C 42(1), 4-5.

Petrie, B., Barden, R. and Kasprzyk-Hordern, B. (2015) A review on emerging contaminants in wastewaters and the environment: Current knowledge, understudied areas and recommendations for future monitoring. Water Research 72, 3-27.

Petrovic, M., Radjenovic, J. and Barcelo, D. (2011) Advanced oxidation processes (AOPs) applied for wastewater and drinking water treatment: Elimination of pharmaceuticals. The Holistic Approach to Environment 1(2), 63-74.

Plaschke, M., Rothe, J., Altmaier, M., Denecke, M.A. and Fanghänel, T. (2005) Near edge X-ray absorption fine structure (NEXAFS) of model compounds for the humic acid/actinide ion interaction. Journal of Electron Spectroscopy and Related Phenomena 148(3), 151-157.

Polk, R.E. (1989) Drug-drug interactions with ciprofloxacin and other fluoroquinolones. The American Journal of Medicine 87(5), S76-S81.

Pouretedal, H.R. and Sadegh, N. (2014) Effective removal of Amoxicillin, Cephalexin, Tetracycline and Penicillin G from aqueous solutions using activated carbon nanoparticles prepared from vine wood. Journal of Water Process Engineering 1, 64-73.

Pulicharla, R., Das, R.K., Brar, S.K., Drogui, P., Sarma, S.J., Verma, M., Surampalli, R.Y. and Valero, J.R. (2015) Toxicity of chlortetracycline and its metal complexes to model microorganisms in wastewater sludge. Science of The Total Environment 532, 669-675.

Qin, X., Liu, F., Wang, G., Weng, L. and Li, L. (2014) Adsorption of levofloxacin onto goethite: Effects of pH, calcium and phosphate. Colloids and Surfaces, B: Biointerfaces 116, 591-596.

Qu, X.L., Lin, X. and Zhu, D. (2008) Site-specific adsorption of 1,3-dinitrobenzene to bacterial surfaces: A mechanism of n-[pi] electron-donor-acceptor interactions. Journal of Environmental Quality 37(3), 824-829.

Quintelas, C., Pereira, R., Kaplan, E. and Tavares, T. (2013) Removal of Ni(II) from aqueous solutions by an Arthrobacter viscosus biofilm supported on zeolite: From laboratory to pilot scale. Bioresource Technology 142, 368-374.

Quintero, J.A. and Cardona, C.A. (2009) Ethanol dehydration by adsorption with starchy and cellulosic materials. Industrial & Engineering Chemistry Research 48(14), 6783-6788.

Radjenović, J., Petrović, M. and Barceló, D. (2009) Fate and distribution of pharmaceuticals in wastewater and sewage sludge of the conventional activated sludge (CAS) and advanced membrane bioreactor (MBR) treatment. Water Research 43(3), 831-841.

Ranjbar, Z., Sun, N., Niu, C.H. and Dalai, A. (2013a) Adsorption of water and ethanol by canola meal in batch liquid system, pp. 1-10, Canadian Society for Bioengineering, University of Saskatchewan, Saskatoon, SK, Canada.

Ranjbar, Z., Tajallipour, M., Niu, C.H. and Dalai, A.K. (2013b) Water removal from ethanol vapor by adsorption on canola meal after protein extraction. Industrial & Engineering Chemistry Research 52(40), 14429-14440.

Ravel, B. and Newville, M. (2005) ATHENA, ARTEMIS, HEPHAESTUS: Data analysis for X-ray absorption spectroscopy using IFEFFIT. Journal of Synchrotron Radiation 12(4), 537-541.

Renewable Fuels Association (2015) Going global-2015 Ethanol industry outlook, pp. 4, 12, Washington DC, USA.

Rivera-Utrilla, J., Gómez-Pacheco, C.V., Sánchez-Polo, M., López-Peñalver, J.J. and Ocampo-Pérez, R. (2013) Tetracycline removal from water by adsorption/bioadsorption on activated carbons and sludge-derived adsorbents. Journal of Environmental Management 131, 16-24.

Roberts, G.A.F. (1992) Chitin Chemistry, Macmillan.

Ross, D.L. and Riley, C.M. (1990) Aqueous solubilities of some variously substituted quinolone antimicrobials. International Journal of Pharmaceutics 63(3), 237-250.

Sahu, J.N., Acharya, J. and Meikap, B.C. (2010) Optimization of production conditions for activated carbons from Tamarind wood by zinc chloride using response surface methodology. Bioresource Technology 101(6), 1974-1982.

Seidel, A. and Carl, P.S. (1989) The concentration dependence of surface diffusion for adsorption on energetically heterogeneous adsorbents. Chemical Engineering Journal 44(1), 189-194.

Sen Gupta, S. and Bhattacharyya, K.G. (2008) Immobilization of Pb(II), Cd(II) and Ni(II) ions on kaolinite and montmorillonite surfaces from aqueous medium. Journal of Environmental Management 87(1), 46-58.

Sharma, R. and Singh, B. (2013) Removal of Ni (II) ions from aqueous solutions using modified rice straw in a fixed bed column. Bioresource Technology 146, 519-524.

Shen, X., Guo, X., Zhang, M., Tao, S. and Wang, X. (2015) Sorption mechanisms of organic compounds by carbonaceous materials: Site energy distribution consideration. Environmental Science & Technology 49(8), 4894-4902.

Shi, X., Fu, H., Li, Y., Mao, J., Zheng, S. and Zhu, D. (2011) Impact of coal structural heterogeneity on the nonideal sorption of organic contaminants. Environmental Toxicology and Chemistry 30(6), 1310-1319.

Simo, M., Sivashanmugam, S., Brown, C.J. and Hlavacek, V. (2009) Adsorption/Desorption of Water and Ethanol on 3A Zeolite in Near-Adiabatic Fixed Bed. Ind. Eng. Chem. Res. 48(20), 9247-9260.

Sing, K.S.W. (1985) Reporting physisorption data for gas/solid systems with special reference to the determination of surface area and porosity (Recommendations 1984), p. 603.

Sipma, J., Osuna, B., Collado, N., Monclús, H., Ferrero, G., Comas, J. and Rodriguez-Roda, I. (2010) Comparison of removal of pharmaceuticals in MBR and activated sludge systems. Desalination 250(2), 653-659.

Sips, R. (1948) On the structure of a catalyst surface. Journal of Chemical Physics 16(5), 490-495.

Smith, J.M. (1970) Chemical engineering kinetics, McGraw-Hill, New York.

Snowberger, S., Adejumo, H., He, K., Mangalgiri, K.P., Hopanna, M., Soares, A.D. and Blaney, L. (2016) Direct Photolysis of Fluoroquinolone Antibiotics at 253.7 nm: Specific Reaction Kinetics and Formation of Equally Potent Fluoroquinolone Antibiotics. Environmental Science & Technology 50(17), 9533-9542.

Snyder, S.A., Adham, S., Redding, A.M., Cannon, F.S., DeCarolis, J., Oppenheimer, J., Wert, E.C. and Yoon, Y. (2007) Role of membranes and activated carbon in the removal of endocrine disruptors and pharmaceuticals. Desalination 202(1), 156-181.

Solum, M.S., Pugmire, R.J., Jagtoyen, M. and Derbyshire, F. (1995) Evolution of carbon structure in chemically activated wood. Carbon 33(9), 1247-1254.

Sousa, I., Claro, V., Pereira, J.L., Amaral, A.L., Cunha-Silva, L., de Castro, B., Feio, M.J., Pereira, E. and Gameiro, P. (2012) Synthesis, characterization and antibacterial studies of a copper(II) levofloxacin ternary complex. Journal of Inorganic Biochemistry 110, 64-71.

Stackelberg, P.E., Gibs, J., Furlong, E.T., Meyer, M.T., Zaugg, S.D. and Lippincott, R.L. (2007) Efficiency of conventional drinking-water-treatment processes in removal of pharmaceuticals and other organic compounds. Science of The Total Environment 377(2), 255-272.

Stöhr, J. (1992) NEXAFS Spectroscopy, Springer, New York.

Sturini, M., Speltini, A., Maraschi, F., Profumo, A., Pretali, L., Irastorza, E.A., Fasani, E. and Albini, A. (2012) Photolytic and photocatalytic degradation of fluoroquinolones in untreated river water under natural sunlight. Applied Catalysis B: Environmental 119–120, 32-39.

Suarez, S., Lema, J.M. and Omil, F. (2009) Pre-treatment of hospital wastewater by coagulation–flocculation and flotation. Bioresource Technology 100(7), 2138-2146.

Sun, C.L., Chang, C.T., Lee, H.H., Zhou, J., Wang, J., Sham, T.K. and Pong, W.F. (2011) Microwave-assisted synthesis of a core-shell MWCNT/GONR heterostructure for the

electrochemical detection of ascorbic acid, dopamine, and uric acid. ACS Nano 5(10), 7788-7795.

Sun, J., Wang, W., Wang, P., Lv, H., Luo, X. and Gao, H. (2013) Characterization of a compound starch-based adsorbent for alcohol-water azeotrope dehydration. Adsorption Science & Technology 31(9), 829-844.

Sun, N., Okoye, C., Niu, C.H. and Wang, H. (2007) Adsorption of water and ethanol by biomaterials. International Journal of Green Energy 4(6), 623-634.

Sun, Y., Yang, S., Chen, Y., Ding, C., Cheng, W. and Wang, X. (2015) Adsorption and desorption of U(VI) on functionalized graphene oxides: A combined experimental and theoretical study. Environmental Science & Technology 49(7), 4255-4262.

Tajallipour, M., Niu, C. and Dalai, A. (2013) Ethanol dehydration in a pressure swing adsorption process using canola meal. Energy & Fuels 27(11), 6655-6664.

Tan, F., Sun, D., Gao, J., Zhao, Q., Wang, X., Teng, F., Quan, X. and Chen, J. (2013) Preparation of molecularly imprinted polymer nanoparticles for selective removal of fluoroquinolone antibiotics in aqueous solution. Journal of Hazardous Materials 244–245, 750-757.

Tan, P., Sun, J., Hu, Y., Fang, Z., Bi, Q., Chen, Y. and Cheng, J. (2015) Adsorption of Cu^{2+}, Cd^{2+} and Ni^{2+} from aqueous single metal solutions on graphene oxide membranes. Journal of Hazardous Materials 297, 251-260.

Tang, Y., Guo, H., Xiao, L., Yu, S., Gao, N. and Wang, Y. (2013) Synthesis of reduced graphene oxide/magnetite composites and investigation of their adsorption performance of fluoroquinolone antibiotics. Colloids and Surfaces A: Physicochemical and Engineering Aspects 424, 74-80.

Teas, C., Kalligeros, S., Zanikos, F., Stournas, S., Lois, E. and Anastopoulos, G. (2001) Investigation of the effectiveness of absorbent materials in oil spills clean up. Desalination 140(3), 259-264.

Thevannan, A., Mungroo, R. and Niu, C.H. (2010) Biosorption of nickel with barley straw. Bioresource Technology 101(6), 1776-1780.

Tien, C. (1994) Adsorption calculations and modeling, Butterworth-Heinemann.

Turel, I. (2002) The interactions of metal ions with quinolone antibacterial agents. Coordination Chemistry Reviews 232(1-2), 27-47.

Uivarosi, V. (2013) Metal complexes of quinolone antibiotics and their applications: An update. Molecules 18(9), 11153.

United Nations Environment Programme (2009) Towards sustainable production and use of resources: Assessing biofuels, p. 22, United Nations Environment Programme.

United Nations. Statistical Division and United Nations. Deparment for Economic Social Information and Policy Analysis (1997) Glossary of environment statistics, United Nations.

University of Massachusetts (2012) Analysis of total organic carbon, Amherst, MA, U.S.

Unuabonah, E.I., Adebowale, K.O. and Olu-Owolabi, B.I. (2007) Kinetic and thermodynamic studies of the adsorption of lead (II) ions onto phosphate-modified kaolinite clay. Journal of Hazardous Materials 144(1–2), 386-395.

Uwaydah, M., Mokhbat, J.E., Karam-Sarkis, D., Baroud-Nassif, R. and Rohban, T. (2006) Penicillin-resistant Streptococcus pneumoniae in Lebanon: The first nationwide study. International Journal of Antimicrobial Agents 27(3), 242-246.

Van Doorslaer, X., Dewulf, J., Van Langenhove, H. and Demeestere, K. (2014) Fluoroquinolone antibiotics: An emerging class of environmental micropollutants. Science of The Total Environment 500-501, 250-269.

Vieira, M.G., Neto, A.F., Gimenes, M.L. and da Silva, M.G. (2010) Sorption kinetics and equilibrium for the removal of nickel ions from aqueous phase on calcined Bofe bentonite clay. Journal of Hazardous Materials 177(1-3), 362-371.

Vieno, N.M., Härkki, H., Tuhkanen, T. and Kronberg, L. (2007) Occurrence of pharmaceuticals in river water and their elimination in a pilot-scale drinking water treatment plant. Environmental Science & Technology 41(14), 5077-5084.

Vijaikumar, S., Subramanian, T. and Pitchumani, K. (2008) Zeolite encapsulated nanocrystalline CuO: A redox catalyst for the oxidation of secondary alcohols. Journal of Nanomaterials 2008, 7.

Volesky, B. (2007) Biosorption and me. Water Research 41(18), 4017-4029.

Waheed ul Hasan, S. and Ani, F.N. (2014) Review of limiting issues in industrialization and scale-up of microwave-assisted activated carbon production. Industrial & Engineering Chemistry Research 53(31), 12185-12191.

Wallis, S.C., Gahan, L.R., Charles, B.G., Hambley, T.W. and Duckworth, P.A. (1996) Copper(II) complexes of the fluoroquinolone antimicrobial ciprofloxacin: Synthesis, X-ray structural characterization, and potentiometric study. Journal of Inorganic Biochemistry 62(1), 1-16.

Wan, Y., Bao, Y. and Zhou, Q. (2010) Simultaneous adsorption and desorption of cadmium and tetracycline on cinnamon soil. Chemosphere 80(7), 807-812.

Wang, S. and Wang, H. (2015) Adsorption behavior of antibiotic in soil environment: A critical review. Frontiers of Environmental Science and Engineering 9(4), 565-574.

Wang, X., Cook, R., Tao, S. and Xing, B. (2007) Sorption of organic contaminants by biopolymers: Role of polarity, structure and domain spatial arrangement. Chemosphere 66(8), 1476-1484.

Wang, X., Liu, Y., Tao, S. and Xing, B. (2010a) Relative importance of multiple mechanisms in sorption of organic compounds by multiwalled carbon nanotubes. Carbon 48(13), 3721-3728.

Wang, Y., Gong, C., Sun, J., Gao, H., Zheng, S. and Xu, S. (2010b) Separation of ethanol/water azeotrope using compound starch-based adsorbents. Bioresource Technology 101(15), 6170-6176.

Wang, Y., Lu, J., Wu, J., Liu, Q., Zhang, H. and Jin, S. (2015) Adsorptive removal of fluoroquinolone antibiotics using bamboo biochar. Sustainability 7(9), 12947.

Wang, Z., Yu, X., Pan, B. and Xing, B. (2010c) Norfloxacin sorption and its thermodynamics on surface-modified carbon nanotubes. Environmental Science & Technology 44(3), 978-984.

Wegst-Uhrich, S.R., Navarro, D.A.G., Zimmerman, L. and Aga, D.S. (2014) Assessing antibiotic sorption in soil: A literature review and new case studies on sulfonamides and macrolides. Chemistry Central Journal 8, 5-5.

Worch, E. (2012) Adsorption technology in water treatment: Fundamentals, processes, and modeling, De Gruyter.

Wormser, G.P. and Keusch, G.T. (1979) Drugs five years later: Trimethoprim-sulfamethoxazole in the united states. Annals of Internal Medicine 91(3), 420-429.

Wu, D., Pan, B., Wu, M., Peng, H., Zhang, D. and Xing, B.S. (2012) Coadsorption of Cu and sulfamethoxazole on hydroxylized and graphitized carbon nanotubes. Science of The Total Environment 427-428, 247-252.

Xie, X.P., Meng, Z.L., Jiang, J.C., Sun, K. and Lu, X.C. (2013) Preparation and characterization of activated carbon from eucalyptus sawdust with phosphoric acid. Journal of Northeast Forestry University 41, 116-119.

Yamashita, N., Yasojima, M., Nakada, N., Miyajima, K., Komori, K., Suzuki, Y. and Tanaka, H. (2006) Effects of antibacterial agents, levofloxacin and clarithromycin, on aquatic organisms. Water Science and Technology 53(11), 65-72.

Yang, K. and Xing, B. (2010) Adsorption of Organic Compounds by Carbon Nanomaterials in Aqueous Phase: Polanyi Theory and Its Application. Chemical Reviews 110(10), 5989-6008.

Yang, R.T. (2003) Adsorbents: Fundamentals and applications, Willy Press.

Yasojima, M., Nakada, N., Komori, K., Suzuki, Y. and Tanaka, H. (2006) Occurrence of levofloxacin, clarithromycin and azithromycin in wastewater treatment plant in Japan. Water Science and Technology 53(11), 227-233.

Yiruhan, Wang, Q.J., Mo, C.H., Li, Y.W., Gao, P., Tai, Y.P., Zhang, Y., Ruan, Z.L. and Xu, J.W. (2010) Determination of four fluoroquinolone antibiotics in tap water in Guangzhou and Macao. Environmental Pollution 158(7), 2350-2358.

Yoon, T.H., Benzerara, K., Ahn, S., Luthy, R.G., Tyliszczak, T. and Brown, G.E. (2006) Nanometer-scale chemical heterogeneities of black carbon materials and their impacts on PCB sorption properties: Soft X-ray spectromicroscopy study. Environmental Science & Technology 40(19), 5923-5929.

Zelmanov, G. and Semiat, R. (2008) Iron(3) oxide-based nanoparticles as catalysts in advanced organic aqueous oxidation. Water Research 42(1), 492-498.

Zhanel, G.G., Ennis, K., Vercaigne, L., Walkty, A., Gin, A.S., Embil, J., Smith, H. and Hoban, D.J. (2012) A Critical Review of the Fluoroquinolones. Drugs 62(1), 13-59.

Zhao, J., Liu, J., Li, N., Wang, W., Nan, J., Zhao, Z. and Cui, F. (2016) Highly efficient removal of bivalent heavy metals from aqueous systems by magnetic porous Fe_3O_4-MnO_2: Adsorption behavior and process study. Chemical Engineering Journal 304, 737-746.

Zheng, H., Wang, Z., Zhao, J., Herbert, S. and Xing, B. (2013) Sorption of antibiotic sulfamethoxazole varies with biochars produced at different temperatures. Environmental Pollution 181, 60-67.

Zhu, D., Hyun, S., Pignatello, J.J. and Lee, L.S. (2004) Evidence for π-π electron donor-acceptor interactions between π-donor aromatic compounds and π-acceptor sites in soil organic matter through pH effects on sorption. Environmental Science & Technology 38(16), 4361-4368.

Zhu, D., Kwon, S. and Pignatello, J.J. (2005) Adsorption of single-ring organic compounds to wood charcoals prepared under different thermochemical conditions. Environmental Science & Technology 39(11), 3990-3998.

Zhu, D. and Pignatello, J.J. (2005) Characterization of aromatic compound sorptive interactions with black carbon (charcoal) assisted by graphite as a model. Environmental Science & Technology 39(7), 2033-2041.

Zorita, S., Mårtensson, L. and Mathiasson, L. (2009) Occurrence and removal of pharmaceuticals in a municipal sewage treatment system in the south of Sweden. Science of The Total Environment 407(8), 2760-2770.